F-105F TRANSONIC BUFFET STUDY AND EFFECT OF MANEUVERING FLAPS

Milton Margolin
Jung G. Chung

FOREWORD

This report, FHR 3649-1, presents the results of a flight investigation and a wind tunnel test of the high subsonic-transonic buffet phenomena using the F-105F two-place fighter-bomber as the reference aircraft. The effects of a maneuvering flap on increasing the normal force prior to buffet onset and on reducing the buffet intensity at high load factors were tested. The report was prepared by the Republic Aviation Division of the Fairchild Hiller Corporation, Farmingdale, New York, under Air Force Contract F33657-68-C-1057. The work was administered under the direction of the Air Force System Command, Flight Dynamics Laboratory, with Mr. Lawrence W. Rogers, FDMM, as Project Monitor.

The work reported here was performed during the period from 2 April 1968 to April 1969. This report was submitted by the authors in April 1969.

No recommendations are included in this report.

The authors acknowledge the contributions of the following members of the Republic Aviation Division to the project: Messrs. A. Milligan and A. Montamagno, who supervised the design and modification of the 1/22-scale F-105F model; Mr. J. Guarino, who supervised the instrumentation of the F-105F airplane; Mr. E. Schwarz, on-site Project Engineer; and Mr. D. Williams, who directed the flight test program and flight data reduction. The contributions of Messrs. R. Taylor and E. Ray of the NASA Langley in directing the wind tunnel test program are also acknowledged.

Publication of this report does not constitute Air Force approval of the report's findings or conclusions. It is published only for the exchange and stimulation of ideas.

for PHILIP P. ANTONATOS
Chief, Flight Mechanics Division

ABSTRACT

A flight test investigation was made using a Republic F-105F aircraft to obtain data related to high subsonic-transonic buffet and the effects of utilizing a maneuvering flap. Flight tests were made at nominal altitudes of 25,000 feet and 35,000 feet. At each altitude, data was collected at three Mach numbers from level flight to maximum usable lift. A related investigation was made using a 1/22-scale model of the F-105F aircraft in the NASA Langley High-Speed Wind Tunnel. The wind tunnel tests were made at three Mach numbers (0.80, 0.85, and 0.90) and data was obtained from zero angle-of-attack to the strain gage balance limits.

Flight test results compare readily to wind tunnel data. The boundary layer profiles between flight test and wind tunnel are quite similar. The angles of attack at buffet onset are also comparable.

Selection of the leading edge flap and trailing edge flap deflection may be made on the basis of the greatest normal force coefficient at buffet onset, but the final criterion will be the level of buffet intensity apparent to the pilot. This level may be varied with the leading edge flap deflection.

Distribution of this abstract is unlimited.

CONTENTS

CONTENTS (Cont'd)

ILLUSTRATIONS

ILLUSTRATIONS (Cont'd)

ILLUSTRATIONS (Cont'd)

ILLUSTRATIONS (Cont'd)

ILLUSTRATIONS (Cont'd)

ILLUSTRATIONS (Cont'd)

ILLUSTRATIONS (Cont'd)

ILLUSTRATIONS (Cont'd)

LIST OF TABLES

LIST OF ABBREVIATIONS AND SYMBOLS

The list is divided into parts, similar to the presentation in the USAF Stability and Control DATCOM. These are: 1. ENGLISH SYMBOLS, 2. GREEK SYMBOLS, 3. CAPITAL-LETTER COEFFICIENTS AND DERIVATIVES, and 4. ABBREVIATIONS.

1. ENGLISH SYMBOLS

Symbol	Definition
A	Aspect ratio of surface, b^2/S
$\bar{a}_{x,y,z_B}$	Absolute acceleration along body axes, g
a_{x,y,z_B}	Measured acceleration along body axes, g
$a'_{x,y,z}$	Absolute acceleration along ground axes, g
b	Wing span
c	Chord of airfoil
c_a	Aileron average chord, 2.29 ft
$\bar{c}$	Mean aerodynamic chord
D	Drag force along stability axes, or wind axes
D_{ram}	Ram drag force along body axis
g	Gravitational acceleration, 32.16 ft/sec^2
H	Altitude, feet
i_H	Horizontal tail incidence, degrees
L	Total lift along stability axes, or wind axes
L/D	Lift-to-drag ratio
M	Mach number
ΔM_B	Wing bending moment fluctuations
ΔM_{Ha}	Aileron hinge moment fluctuations
M_P	Pitching moment
M_R	Rolling moment
M_Y	Yawing moment
n	Load factor
N	Normal force along body axes

Symbol	Definition
p	Static pressure
p_a	Ambient pressure
p_L	Local pressure
p_o	Ambient pressure at sea level, 2116.2 psf
p_T	Total pressure
p_{T_2}	Total pressure in inlet duct
p_{T_7}	Total pressure at engine turbine discharge
$p_{T_{10}}$	1) Total pressure at exhaust duct exit 2) Total pressure at ejector exit
p_{t_e}	Total pressure at ejector exit
q	Dynamic pressure
q_c	Pitot gage pressure
S	1) Wing area, 385 ft^2 2) Area
S_a	Aileron area per side, 15.446 ft^2
T	1) Temperature 2) Thrust
T_{gross}	Gross thrust
T_{net}	Net thrust
V	Velocity
W	Weight
X	Axial force

2. GREEK SYMBOLS

Symbol	Definition
α	Angle of attack positive nose up
β	Angle of side slip positive nose left
δ	Pressure ratio p/p_o
δ_{fuel}	Fuel density (specific gravity)
δ_{LE}	Leading edge flap deflection
δ_{TE}	Trailing edge flap deflection
γ	Angle of flight path with horizontal reference
ϕ	Angle of roll

3. CAPITAL LETTER COEFFICIENTS AND DERIVATIVES

Symbol	Definition
C_A	Axial force coefficient
ΔC_{BM}	Coefficient of wing bending moment fluctuations, $\Delta C_{BM} = \frac{WSG}{\frac{1}{2} q Sb\sqrt{\delta}}$
C_D	Drag force coefficient
ΔC_{H_a}	Coefficient of aileron hinge moment fluctuations, $\Delta M_{H_a} / (qS_a c_a \sqrt{\delta})$
C_L	Lift force coefficient
C_ℓ	Rolling moment coefficient
C_m	Pitching moment coefficient
C_N	Normal force coefficient
C_n	Yawing moment coefficient
C_p	Pressure coefficient, $(p_L - p_a)/q$
C_X	Axial force coefficient
C_Y	Side force coefficient
dH/dt	Rate of climb
dV/dt	Absolute axial acceleration
dW/dt	Fuel flow

4. ABBREVIATIONS

Symbol	Definition
A/B	Afterburner
a.c.	Aerodynamic center
av	Average
c.g.	Center of gravity
c.p.	Center of pressure
F.S.	Fuselage station
H.L.	Hinge line
L.E.	Leading edge
MAC	Mean aerodynamic chord
max	Maximum
MRP	Military rated power
min	Minimum
W.L.	Water line
W.S.	Wing station
WUTL	Wind up turn to the left, flight maneuver
NASA	National Aeronautics and Space Administration
NACA	National Advisory Committee for Aeronautics
RM	Research memorandum
TN	Technical note
B.L.	Buttock line station
T.E.	Trailing edge
WSG	Wing strain gage bending moment fluctuation, inch-pound

SECTION I
INTRODUCTION

The objective of the test program reported herein was the evaluation of maneuvering flaps as a means of increasing the lift of a high performance aircraft at the onset of Mach buffet and decreasing the level of buffet intensity so that the total maneuvering range of the aircraft is increased. The results of this evaluation are presented in this report.

Buffeting is defined as aerodynamically induced high frequency structural vibration of one or more components of an aircraft. The origin of Mach buffeting lies in the fluctuating pressures of unstable airflows associated with local shock induced boundary layer separation on the wing surfaces at high subsonic-transonic speeds and low lift conditions. The resulting random flow field downstream of the shock excites buffet vibrations on the aft surfaces of the airplane which promote sonic fatigue and other serious structural problems.

SECTION II
TEST PROGRAM

1. GENERAL

A test program has been conducted to evaluate the use of leading and trailing edge flaps as a means of increasing the total maneuvering range of an aircraft by increasing the lift at the onset of Mach buffet and decreasing the level of buffet intensity. The program was conducted by flight tests of an F-105F aircraft and by wind tunnel tests of a 1/22-scale F-105F model (Figure 1). The flight testing was performed first, in its entirety, to provide the means for correlating wind tunnel test data with flight test data.

The F-105F aircraft was selected because of its trailing edge flap design which incorporates chord extension with flap deflection (Figure 2). For simulation of the NASA maneuvering flap concept, the flap gap was sealed by fairings (Figures 3 through 7). Extensive flight test data in the high subsonic-transonic range is available on this aircraft. This includes buffet studies performed in 1958 (Reference 1) and wing pressure distribution measurements (Reference 2). An instrumented F-105F aircraft (AF 62-4414) was on flight test status at Eglin Air Force Base, Florida, and required only minor additions to perform this test program. A 1/22-scale model of the F-105F aircraft was available and was amenable to modification to simulate the various desired flight configurations. Furthermore, a substantial amount of wind tunnel data exists on the basic aerodynamic characteristics of the F-105 family of aircraft. Table I presents comparative data for the full-scale F-105F aircraft and the 1/22-scale model. These characteristics are summarized for dynamic motion studies in Reference 3.

2. FLIGHT TEST PROGRAM

a. Flight Test Summary

The flight test of the maneuvering flap configurations on the government loaned F-105F aircraft (AF 62-4414) was conducted at Eglin Air Force Base, Florida, during the period from 22 May to 4 June 1968. During this period, eighty buffet flight runs were made in nine flights. A century series safety chase aircraft was provided on seven of the nine flights. All flights are summarized in Table II. The seven basic configurations for the leading edge flap and the trailing edge flap settings are the first seven configurations given in Table III. Data was obtained at two altitudes - 25,000 feet and 35,000 feet - and three Mach numbers - 0.80, 0.85, and 0.90.

b. Flight Maneuver and Configuration

The basic maneuver was a wind-up turn to the left in which the load factor increased with angle of bank. Increases in load factor are accompanied by increases in induced drag. In order to maintain constant speed at a constant power setting, the wind-up turn maneuver was performed in a descending spiral. Gradual horizontal tail power was applied to minimize pitch accelerations during the maneuver. Lateral and directional control was avoided during the data collection period. During the latter part of the test program, entry into the test pattern was made at zero gravity to increase the data collection in the low angle of attack range. This aided the definition of the background vibrations and the onset of Mach buffet measured during the test program.

Data runs were made at the highest altitude and the highest Mach number first during each flight, since these runs required the maximum time to reach their specified test conditions. During the exploratory flight (Flight 367 in Table II), the runs were made at the lower Mach numbers first, since power was more critical in establishing the flight test pattern at this test condition.

Trailing edge flap deflections were increased as the program progressed to minimize the effect of loose parts in the flap structure. This increase is displayed in Table II, column 8. The fairings which sealed the flap gap were fastened with rivets. Reduction of the fairing thickness as the trailing edge flap deflection decreases would require removal of fairing skins and re-opening of the flap structure to remove the rivet ends which fall as the rivets are drilled out.

Leading edge flap settings were varied during the test flight. The flap setting was recorded on the second gage of hole No. 2 of the photorecorder. The basic airplane with flaps undeflected was the final test configuration on flight number 374.

Speed brakes were not applied during the data collection period. Their positions are recorded on the first gage of hole No. 2 of the photorecorder. No external stores were carried.

The fuel levels and the fuel sequencing were monitored by records logged by the radio operator and by fuel gages on the photorecord. The fuel level in the internal tank in the bomb bay was reported by the pilot. The fuel remaining in the forward, main, and aft fuel tanks was recorded on hole Nos. 13, 18, and 23, respectively. The fuel used was recorded by hole No. 4. At this location, counter No. 3 records the fuel used by the engine and counter No. 4 records the fuel used by the afterburner. These records are used to determine the aircraft weight and center of gravity at the test conditions. The fuel remaining is reported in column 4 of Table II.

c. Buffet Definition

Particular emphasis was placed on defining buffet qualitatively by recording the pilot's sensations as the load factor increased. To aid this determination, pilot sensations were recorded on the radio log by the radio operator, a light was lit on the photopanel (light No. 5), and a blip was recorded on channel one (1) of the oscillograph record. These sensations of buffet are sensed as normal acceleration fluctuations by the pilot. The flight maneuvers were performed into and through buffet onset to maximum usable lift, and the maximum load factor of 6.0 g was never exceeded.

Maximum load factors for the deflected trailing edge flap positions are presented in Table IV against flight altitude and calibrated airspeed. At 35,000 feet altitude, flight runs for buffet intensity may be performed to the maximum lift capability of the wing. At 25,000 feet altitude, the maximum load factor is restricted to the structural capability of the present flap design. In all cases, a load factor of greater than 3.0 can be attained with the trailing edge flaps deflected.

Table II presents a summary of the pilot comments during the buffet run. The normal acceleration at the start of the run is recorded as 1g (level flight) or zero g in a push-over. The zero-g entry was initiated with flight 371. The normal acceleration at buffet onset, light buffet, moderate buffet, and heavy buffet were obtained from the radio log. Circled values indicate that the records may not be clean due to the use of lateral or directional controls during the test run.

These normal acceleration levels were converted to airplane angles of attack and normal force coefficients and shown on the presentations for the aileron hinge moment fluctuations, the wing bending moments, and the trailing edge pressure measurements. Both the flight test data and the wind tunnel test results are correlated in this manner. This correlation of the qualitative results to the quantitative results of the flight test and wind tunnel instrumentation are reviewed in subsection 4.

d. Power Effects

The effect of air spillage around the engine inlets on the wing airflow characteristics was investigated on two configurations at an altitude of 25,000 feet. Flight test calibration data was available for two engine power settings; namely, military rated power (MRP) and idle power. Afterburner power has not been completely calibrated for use in these test runs. Configurations 1 and 2 in Table III were flight tested at these two engine settings at Mach numbers of 0.85 and 0.90. Generally, the effect of air spillage was to increase the buffet intensity, as evidenced by the aileron hinge moment fluctuations.

3. WIND TUNNEL TEST PROGRAM

a. Wind Tunnel Test Summary

The wind tunnel tests of the maneuvering flap configuration on the government owned 1/22-scale model of the F-105F aircraft was conducted in two test periods at the NASA Langley 7- by 10-foot High Speed Wind Tunnel facility. The first test period (test 845) was from 11 October to 16 October 1968. The second test period (test 850) was from 9 December to 16 December 1968. During these two periods, 53 test runs were made. These runs are summarized in Tables V and VI. The 13 configurations tested are summarized in Table III. Each configuration was tested at three Mach numbers - 0.80, 0.85, and 0.90 - to the limits of the NASA 815A balance.

b. Wind Tunnel Test Schedule

The wind tunnel test programs are presented in Tables V and VI for test numbers 845 and 850 at the NASA Langley 7- by 10-foot High Speed Wind Tunnel facility. The test dates are given in column 1. The other columns list the starting time of the test run, the test run number, and the reference data point numbers.

The test configuration is given in the fifth column. The basic wing-body configuration was varied by leading edge flap deflections, trailing edge flap deflections, and aileron deflections. The boundary layer rake was located aft of the trailing edge on most of the runs but was removed when the horizontal tail was added to the configuration. The trailing edge gap was not sealed on one test configuration used on run Nos. 1, 2, and 3 of test 850 in Table VI. All configurations were tested at three Mach numbers - 0.80, 0.85, and 0.90.

Most of the configurations were tested in pitch at zero sideslip. The maximum angle of attack was limited by the normal force load limit on the NASA 815A six-component strain gage balance. Pitch runs at a constant 6° yaw were limited by the rolling moment limit of the balance. The maximum angle of attack attained in each run is given in column 7 of Table VI.

The transition grit was placed at the 30% chord line of the wing and the horizontal tail top and bottom surfaces. The effect of variations in the location of this grit was made on the first test (845), runs 17, 19, and 20.

The tunnel test conditions are given by the test section static pressure, stagnation pressure, and temperature. The Mach number was determined by the ratio of static to stagnation pressure.

c. Buffet Definition

Particular emphasis was placed on establishing quantitative definitions of the buffet intensity as the lift increased for correlation with the flight test data. The aileron hinge moment vibrations may be more sensitive to the buffet onset, but wing bending moment fluctuations provide the greater utility because of the large library of model data available for comparison and evaluation. The rapid build-up of buffet intensity after onset provides similar lift and angle of attack values for both the fluctuations of the aileron hinge moment and the wing bending moment. No related reference data is available for the comparison of the aileron hinge moment fluctuation amplitudes with the normal accelerations measured at the aircraft center of gravity or the pilot's seat.

The flight test records present the strain-gage records as wavy lines on the oscillograph paper. Maximum peak-to-peak values were used as a measure of the buffet magnitude. Electrical techniques were used at the NASA Langley facility which provide the root-mean-square value or the standard deviation. The integration time for each data point was 40 seconds.

The positioning of the 1/22-scale F-105F model in a minimum air flow turbulence station in the NASA tunnel was determined by Messrs. R. Taylor and E. Ray for this test program. This low air turbulence level is required to prevent tunnel turbulence from masking the vibration levels at the onset of buffet. A three-foot sting extension was used to position the model at this station.

4. INSTRUMENTATION

a. General

The primary measurements made were for buffet intensity levels and their manner of variation with angle of attack. Buffet is evidenced by the fluctuations of the strain gage output and the change in the pressures over the aft wing surfaces. Other buffet indicators included accelerometers which quantitively related the pilot's sensations to measured data. Visual evidence of in-flight buffet was obtained by taking motion pictures of the airflow patterns revealed by tufts placed on the upper surface of the right wing. These patterns were recorded by a 16 mm motion picture camera located on the right surface of the vertical stabilizer (fin) near the tip. In the wind tunnel model tests, a shaking of the model on the sting can be observed.

Auxiliary measurements of the aircraft are made to define the flight conditions, the flight configuration, attitude, and flight path. The engine thrust was analyzed from pressure measurements in the engine ducts and from fuel flow and temperature measurements. The aircraft weight and center of gravity was determined by the fuel sequencing, fuel used, and fuel remaining.

Auxiliary measurements of the test section were made to determine the test section operating conditions and records were kept of the test configurations.

b. Flight Test Instrumentation

Flight test data was recorded at five locations during the data collection run. The locations were: 1) the flight card record kept by the pilot, 2) the radio log maintained by the base flight test monitor, 3) the film record of the photopanel on board the aircraft, 4) the oscillograph record of the instrumentation output on board the aircraft, and 5) the film record of the right wing upper surface air flow field made by the camera mounted on the right side of the fin. The main purpose of the flight test operations was to provide qualitative and quantitative data on buffet intensity with airplane angle of attack or load factor. To define the test, the flight data includes: 1) the flight conditions, 2) the engine operating conditions, 3) the aircraft weight and balance, 4) the flight configuration, 5) the flight attitude and accelerations, 6) the airflow field, 7) the buffet parameters, and 8) correlation marks on the various records to document the relative time of the events.

The basic reference record is the oscillograph trace record. A 36-channel CEC oscillograph was operated at 4.0 inches per second during the data collection period. Thus, during a 30-second test run, 10 feet of oscillograph record was made. Calibration records were taken after each run. At 0.2 second per channel, 7.6 seconds are required for calibration, or 2.533 feet of record. On this basis, 15 feet of oscillograph record is made on each data collection period. At 15 test runs per flight, 225 feet of records were made and the remaining footage from a full 400-foot roll is used for ground calibration operations before and after the flight.

The second onboard recorder was the 28-hole photorecorder operated at one frame per second. This device used 35 mm film to record most of the flight conditions, engine operation parameters, and the fuel measurements.

The third onboard recorder was the 16 mm motion picture camera - a Flight Research Engineering Corporation, Model III, with a 1-inch lens, a rotating shutter 36° open and an aperture of f/11, operated at 5 frames per second. This camera was mounted on the right side of the fin near the tip. The tufts mounted on the upper surface of the right wing panel were photographed in flight by this camera. A light flashed onto the film at the start of each test run to separate the segments of test data.

The flight test instruments are tabulated in Tables VII and VIII for the photopanel and the oscillograph, respectively. Table VII for the photopanel tabulates the location of the instrument by its hole number, the name of the instrument, the date the instrument was calibrated, the number of the calibration curve, and the figure number in this report for the calibration curve. Table VIII for the oscillograph tabulates the location of the channel trace by its reference channel number, the item recorded, and the galvanometer type used. The date the item was calibrated, the figure number in this report of the calibration curve, and the flight test reference number of the calibration curve are also included.

The instrumentation was divided into sections according to the purpose for which it was selected. The flight conditions were defined by measurements recorded by the photopanel. These include the altitude, airspeed, and outside total air temperature. The engine operation parameters were recorded by the photopanel. These include the engine rotor speeds, pressures in the intake, burner, and exhaust ducts, and the cooling air mass. The fuel temperatures were also recorded. For weight and balance analysis of the aircraft, the photopanel recorded the fuel used and the fuel remaining. A radio log record was also maintained of the fuel remaining as reported by the pilot prior to entering the test run pattern.

The flight configuration was set on the ground by the project engineer. The positions of the leading edge flaps and the speed brakes were recorded by the photopanel. The control surface positions were recorded by the oscillograph. The flight attitude and the accelerations along the body axes were recorded by the photopanel and the oscillograph. The photopanel recorded the roll attitude and the normal acceleration at the center of gravity.

The 16 mm camera on the fin recorded the airflow field over the upper surface of the right wing panel. On the first three flights, a 10 mm lens was used with a f/11 opening. On flights 370 and later, a 1-inch lens was used with an f/8 opening for better definition of the tufts.

All the buffet parameters were recorded on the oscillograph. Accelerometers were placed at the wing tips and under the pilot's seat. The hinge moments were recorded for the horizontal stabilizer and the ailerons. The left wing bending moment was recorded for loads outboard of the main landing gear well. Wing surface pressures were recorded at two chord stations and three wing stations for a total of twelve pressure measurement stations on the trailing edge flap and aileron surfaces. A pitot rake was installed at the trailing edge of wing station 105 to measure the boundary layer pressures above the wing surface.

All four of the records taken during the data collection period were correlated by time and event markers. At the start of each run, the pilot pressed a "freeze" button on the control stick which caused a 3-second freeze mark to be made on channel 1 of the oscillograph, lighted the number 5 lamp on the photopanel, and a lamp in the fin tip camera. The actuation of the "freeze" button produced an audible tone in the cockpit which was heard by the radio operator and logged by a check mark to evidence that such an action was taken.

As each photo was taken by the photorecorder, a 0.05 second blip was produced on channel 1 of the oscillograph. An oscillograph record number was produced every 2 seconds on the top edge of the record. A record of the oscillograph recorder number was made at the same time. The initial and final oscillograph record number on each test run was reported by the pilot to the radio operator and recorded in the radio log.

The fin camera recorded the tuft pattern over the upper surface of the right wing at 5 frames per second.

(1) Flight Test Configuration

The flight test configuration of the two-place F-105F airplane during the data collection run was clean with zero lateral and direction control deflection and speed brakes closed. The trailing edge flap was kept at the deflection set on the ground. The leading edge flap deflection was varied in accordance with the flight test schedule.

The trailing edge flap gaps were sealed by metal covers which fitted under the spoilers on the wing top surface and which were fastened to the trailing edge of the main wing panel on the bottom surface. The configuration at 7.5° trailing edge flap deflection is shown on Figure 5 for the top surface and on Figure 6 for the bottom surface. The rivet pattern and step caused by the top surface fairing is shown on Figure 7. The lower surface fairing was fastened to the main wing panel; the positive air pressure and spring action of the fairing was relied upon to keep the gap sealed. The configuration for the 15.0° trailing edge flap deflection is shown in Figure 3 for the top surface and in Figure 4 for the bottom surface. An additional fairing strip was placed under the spoiler due to increased gap as the flap was deflected beyond the initial 7.5° position. The bottom flap gap cover remained unchanged. The flap movement may be noted in Figure 4 by the lighter shading behind the trailing edge of the flap gap seal.

(2) Surface and Boundary Layer Survey

Surface pressures were measured at two chord stations (85% and 95% chord) and at three span stations (W.S. 95, 135, and 175). The reference pressure was the ambient pressure at altitude as determined by the aircraft. The reference pressure chamber was located in the main wing panel, therefore, pressure leads from the pressure taps on the flap and aileron surfaces were routed to the chamber. These leads are shown in Figure 4 on the bottom surface of the left wing trailing edge flap. Figures 8 and 9 are photographs showing more detail. The details of the plumbing and wiring for wing station 125 are shown in Figures 10 and 11. Similar details for wing station 95 are shown in Figure 12.

Details of the static pressure ports on the left wing upper surface at wing stations 95, 135, and 175 are shown in Figures 13, 14, and 15. The static pressure ports on the lower surface are shown in Figures 16, 17, and 18. The pressure ports on the flaps consisted of holes drilled in thin tubing faired into the surface. The pressure ports on the aileron were placed within the structure.

Stagnation pressures were measured above the flap trailing edge at wing station 105 by four tubes installed parallel to the plane of symmetry and spaced 1 inch apart in a vertical plane. This rake assembly is shown in Figure 19 and the plumbing detail is shown in Figures 10 and 16. Spanwise flow over these pressure orifices causes a reduction in the measured total pressure.

(3) Wing Bending

The wing bending moment was measured by strain gages attached to the center of the front spar covers outboard of the landing gear well. Stress paths at and inboard of the landing gear well area do not provide clear wing bending moment patterns due to the wing structural design in this inboard area. The stress measured

at this gage station is most easily duplicated by the 1/22-scale F-105F aircraft model. Placement of the strain gages at the 50% chord near the wing-fuselage juncture would place them in a most undesirable position, since this is the location of the main landing gear well. Other positions near the leading edge of the wing panel are affected by the forward carryover structures to the air inlet structure.

Photographs of the strain gage installation on the top and bottom covers of the forward spar are shown as Figures 20 and 21. Wing bending measurements were recorded during flights 370 to 374 on oscillograph channel number 31.

(4) Right Wing Upper Surface Airflow

The airflow over the upper surface of the right wing panel was provided by a 16 mm film record of the motions of the tuft pattern placed on this surface. The tufts were formed from 300-pound load rated nylon line with 5-inch loops which were fastened to the wing surface with epoxy cement. A typical tuft installation is shown in Figure 22. Two photographs of the tuft installation pattern are shown in Figures 23 and 24. Although Figure 23 shows that the tufts near the gap sealer cover had been blown off, their locations can be noted by the black dots remaining on the surface. Figure 24 presents the view of the right wing as seen by the 16 mm camera located near the tip of the fin. The camera installation is shown in Figure 25.

c. Wind Tunnel Instrumentation

The wind tunnel test data was recorded at three locations during the data collection points. The test configuration schedule was set by the NASA Langley wind tunnel project engineer, Mr. Edward Ray, and was coordinated with the Fairchild-Hiller Corporation, Republic Aviation Division, program monitor, Mr. Milton Margolin. The test section conditions and the sting position were controlled from the control room adjacent to the test section and recorded by the operator. Once the conditions at the data collection point stabilized, the data was recorded on magnetic tape in the data collection room. An optional paper tape printout was used as a check on the individual output channels. The wing bending moment fluctuations were taped for power spectral density analysis at a later date. The main purpose of this wind tunnel program was to provide a basis for correlation of wind tunnel data with flight test data and, in this manner, to provide a vehicle for the prediction of flight test buffet characteristics at high subsonic Mach numbers from wind tunnel test results. To define the test, the wind tunnel data included: 1) the test section conditions, 2) the wind tunnel operating conditions, 3) the 1/22-scale model configuration, 4) the model attitude and the basis loads and moments, and 5) the buffet parameters.

The basic reference record is the magnetic tape record of the 50 channels of output data. The other data is being retained at NASA Langley for reference as required.

The wind tunnel instrumentation is tabulated in Table IX. This instrumentation is divided into sections according to the purpose for which it was selected. The test conditions were defined by the barometric pressure and the test section static pressure. The test configuration was set prior to test by the wind tunnel project engineer and communicated to the model mechanic. The model mechanic adjusted the model to the desired configuration and the final configuration was visually inspected prior to the test run.

The model attitude was set by a Kistler balance mounted in the forebody on NASA test 845 and by a Kistler balance mounted in the aft end of the sting assembly on NASA test 850. Angle of attack readings required correction for sting bending under the imposed airloads during the second test. The model was supported on a six-component strain gage balance which provided the loads and moments. The model sting was attached to a 3-foot extension and the assembly was connected to the main sting by a 6° elbow.

The NASA 815A Balance was installed by the Electro-Mechanical Instrumentation Branch at the Langley Research Center. Fairchild-Hiller provided the spacer blocks and blueprints for the location of the balance. The final drilling and tapping for the balance pins were accomplished at Langley.

Installation of the strain gages at the 50% chord and 0.125 semi-span location on the top and bottom of the left wing was performed at NASA Langley. This installation for the measurement of wing bending was not similar to the gage installation on the F-105F airplane but it was compatible with previous NASA buffet study procedures. A magnetic tape record was kept of the wing bending moment fluctuations for power spectral density analysis as required at some future date.

SECTION III
TEST PROCEDURE

1. GENERAL

The test procedures in the two parts of the test program consisted of the following. The flight test procedures include flight test scheduling, research test run pattern, and post-flight review. The wind tunnel test procedures include configuration scheduling, test data collection, and model inspection after the test run.

2. FLIGHT TEST PROCEDURE

The flight test scheduling considered that sequence of configuration which would provide rapid collection of the more critical data based on 1) time to attain the given test configuration and conditions and 2) the time required to modify the aircraft to the subsequent test configurations. The research test run considered the test maneuvers which would permit data collection at progressively increasing load factors with minimum pitch rates. The post-flight review included 1) the pilot debriefing with respect to methods of improving the data collection quality and 2) examination of the flight records for checking on the proper operation of the recording equipment.

A review of the seven basic flight test configurations shows that the leading edge flap can be controlled accurately in flight (Table III). A similar accuracy in positioning cannot be achieved with the trailing edge flap. Sealing of the trailing edge flap gap does not permit closure of the flap without damage to the flap gap seal covers. Because of this condition, the trailing edge flaps were set on the ground and their settings were not changed during the flight.

The trailing edge flap deflections were increased (rather than decreased) as the flight test program progressed. This permitted additions to be made to the flap gap cover thickness. These operations required less aircraft modification time during flap configuration changes. Raising the flaps would have involved removal of material from the gap cover, and opening and reclosing of the main flap skins to remove rivet ends, a process involving a considerably longer time.

The flight test mission was integrated with the flight test activity at Eglin Air Force Base. Missions were scheduled in order of priority and the flights were flown as determined by weather conditions and the availability of a century series chase aircraft.

All flights were tracked by radar. The test aircraft was monitored by a century series chase aircraft. Radio contact was maintained with the Fairchild Hiller Corporation base operations and the test progress was logged.

The research test runs were made at an altitude of 35,000 feet and the test pattern was repeated at 25,000 feet. The first point at each altitude was at the highest Mach number. The basic test maneuver was a wind-up turn to the left with a split-S recovery and pull-up to the following test run. Altitude departures were held to 3000 feet and Mach number departures were held to 0.03. The average research run took 25 seconds. Lateral and direction controls were not used during the data collection period and, if such controls were required, the run was terminated.

The start of a data collection period was signaled by a 3-second operation of the freeze button by the pilot. This placed an offset on the trace of channel 1 in the oscillograph. An audible tone was generated in the pilot's compartment which was also heard by the radio operator monitoring the flight. Qualitative sensations of the pilot were recorded by a 0.4-second signal on the freeze button which signaled the buffet intensity build-up from 1) buffet onset, 2) moderate buffet, and 3) the end of the research test run at the maximum allowable load factor. Use of the freeze button was also noted by the lighting of the number 5 lamp on the photopanel.

After the flight, the aircraft was examined on the flight apron for missing tufts and aircraft damage, if any. The photorecorder and the oscillograph records were removed for development. The oscillograph records were generally available for review in 2 hours and the films were available in 2 days. Further comments were obtained from the pilot to clarify entries in the radio log.

3. WIND TUNNEL TEST PROCEDURE

The wind tunnel program was scheduled in consideration of the sequence of model and sting configuration changes which would minimize the change time while allowing the maximum collection of data. The checkout of the model instrumentation was one of the more time-consuming operations. The root-mean-square integration for the buffet intensity required 40 seconds per integration for each data point.

The NASA Langley high speed 7- by 10-foot tunnel is a closed, single-return wind tunnel, which operates with atmospheric stagnation pressure. The tunnel is powered by a 14,000-horsepower variable speed electrical-drive system, which turns the single 18-blade, fixed pitch, 28.5-foot diameter fan at speeds up to 490 rpm. A set of countervanes downstream of the fan removes the airstream rotation imparted by the fan. The tunnel is cooled by an air-exchange system which introduces filtered atmospheric air into the diffuser and exhausts a like amount of heated tunnel air. A two-part noise-suppression system is installed. A sound-absorbing blanket surrounds the tunnel shell at the drive fan. Sound-absorbing baffles are installed in the airstream at either end of the drive section. A series of four turbulence-damping screens of 16-mesh wire cloth is installed in the settling chamber ahead of the entrance cone. This installation reduces the turbulence and airstream roughness to the low values required for reliable studies of buffeting phenomena.

The F-105F model was supported by the variable angle of attack sting system. The sting can be rotated through a total range of about 26°. The forward part of the sting, to which the model was attached, is mounted to the rearward part by means of a 6°-elbow which determines the relative angle between the two parts of the sting. This coupling was turned 90° so that angles of attack between 0 and 13° were obtained with a sideslip angle of -6°.

Originally, the program was closely scheduled between two priority tests. However, the time between the priority tests was too short, therefore, the test program was conducted in two parts: The runs at zero trailing edge flap deflection were made on NASA test 845 and the runs with the trailing edge flap deflected were made on NASA test 850.

The test program was scheduled to minimize the number of items removed, installed, and rechecked during each configuration change. A list of items to be accomplished was given to the model mechanics by the project engineer. Based on the data obtained during the preceding runs, the specific data gathering and transmitting channels were retraced for open or noisy circuits. Also, the monitor television camera coverage was rechecked.

The size of the screws used to attach the various items were small, special, and easily misplaced. To reduce search time during a model change, a set of screws was attached to each item for installation.

Model changes involving a trailing edge flap change require repositioning the boundary layer rake so that the relative position of the rake to the trailing edge flap remained constant. The trailing edge flap brackets were changed according to the configuration scheduled. Care was taken during these changes to ensure that the pressure leads were not opened from the flap static pressure ports to the pressure sensor above the test section. Care was also taken to ensure that the static pressure ports were not sealed during the plastering operation of smoothing the model contours. For this latter operation, the static pressure ports were covered with tape until the plastering operation had been completed. After all such operations, the pressure leads were checked for leaks by testing their ability to maintain a negative pressure. The pressure leads were checked for pressure response by blowing into them. A slow response to the change in pressure indicated a clogged pressure port or dirt in the pressure line.

Strain gages used for measuring moments and loads were checked for temperature effects, open circuits, and noisy circuits. Temperature effects often occur when the temperature over the length of the gage has an appreciable variation. An open circuit may occur anywhere in the gage or in its transmission circuit. A noisy circuit may be the result of poor contacts in the plugs and receptacles in the circuit.

The voltage of the power source used as a standard was checked. Variations in the voltage will cause current variations which may be erroneously interpreted. The Kistler angle of attack indicator is one instrument that has a separate power source whose voltage was monitored.

After setting up the test configuration and checking the data gathering and transmission circuits, the pressure orifices were taped and the gaps and extraneous opening were filled with plaster to the model basic contours. All personnel and loose material were cleared from the wind tunnel air flow area and the test section door was closed.

Wind-off records were taken over the pitch range of the test. These wind-off records formed the tare data which was used in correcting the measured data. The tunnel temperature must be in the operational range for these records to reduce temperature effects.

In this NASA facility, the control room monitor watches the test section temperature and Mach number. He informs the power control mechanics when the test section temperature should be lowered by the intake of outside air. The power mechanic adjusts the Mach number by the ratio of static pressure to total pressure in the test section. The model is monitored by a television receiver in the control room.

The Mach number in the test region was varied between 0.70 and 0.95. A gradient amounting to a Mach number change of less than 0.01 for a typical model length exists because the wall divergence is greater than that required to compensate for boundary-layer growth. The resulting longitudinal buoyancy force was accounted for in the data-reduction process and is small compared to the minimum drag values.

The buffet intensity is measured by departures of the average wing bending moment. Under constant conditions of lift and Mach number, these fluctuations are shown to be normally distributed. This indicates that buffeting is a particular type of a random process, a Gaussian process. For such a process, a natural value is the root-mean-square value or the standard deviation, σ. In the wind tunnel, this measure was obtained from the wing bending moment strain gage output by an electrical integration technique. Each data value was obtained by a 40-second integration. The NASA project engineer, Mr. E. Ray, performed this integration detail during the time the data collection was in progress.

Six selected data stations were monitored in the recording room. After the model pitch attitude was set by the test monitor, the data was observed on the monitor channels. When the data was stabilized, a record was made on both magnetic tape and paper tape. The balance limits were monitored at this station and verbal warnings were issued as the model attitude approaches the limit loads. The project engineer was also informed when observation of the paper tape output revealed possible malfunctions of the pressure output channels.

Cables were installed to handle up to 50 channels of data from the test section and the control room. Of these, 25 were used for ancillary data and test section monitoring. The channels used and the items recorded are given in Table IX.

The 815A balance limits to be observed are as follows:

815A Internal Strain Gage Balance Limits

Normal force	±500 lb
Axial force	50 lb
Pitching moment	±1500 in.-lb
Rolling moment	±300 in.-lb
Yawing moment	±240 in.-lb
Side force	±80 lb

After the runs were complete for a given model configuration, the model was inspected for missing, cracked, or warped parts. These model changes were noted when they occurred and rerun decisions made as necessary. When the model inspection showed no significant change, the recorded data was released for data reduction by the project engineer.

SECTION IV

DATA REDUCTION

1. GENERAL

The data from the various records are reduced to non-dimensional coefficients for comparison purposes. Normal and chordwise force data and aileron hinge moment data were plotted as a function of angle of attack in Figures 26, 27, and 28. These plots were examined for correlation between points of inflection of the normal and chordwise forces in Figures 29 and 30 and the indication of onset of buffet from the aileron hinge moment data in Figure 28. The chordwise and spanwise pressure distributions were plotted in Figures 31 and 32 from correlation with the trailing edge pressure divergence shown in Figure 33. The aileron hinge moment strain gage buffet indications in Figure 28 for onset of buffet were correlated with the trailing edge pressure divergence. The wing bending moment strain gage buffet indications were also correlated with these parameters in Figure 34.

The flight test records were analyzed manually from oscillograph and photopanel data. The wind tunnel data was taken from the results computed by the NASA-Langley performance program FSR 4420. The wing bending moment fluctuations were reduced to non-dimensional form by the general aerodynamic rolling moment constant and the square root of the ambient pressure ratio.

2. FLIGHT TEST DATA REDUCTION

The primary flight test measurements made were for buffet intensity levels and their manner of variation with angle of attack. For this purpose, the oscillograph records provided the major source of information. The buffet intensity levels reported by the pilot were correlated with the angle of attack on the aileron hinge moment fluctuations in Figure 28. Typical boundary layer pressure profiles before Mach buffet, near Mach buffet, and at a steady-state buffet are shown in Figure 35. Trailing edge pressure distributions, in the same order of presentation, are shown in Figures 31 and 32.

Reduction of the flight test records for the normal and axial force coefficients did not provide sufficient correlation with wind tunnel data. The main reasons for this situation were insufficient definition and the transient nature of the data. A stable flight condition was not held while the data was recorded. The data reduction procedure for the normal and axial force coefficients is reviewed in this presentation. The normal force coefficient resulting from such an analysis appears to be the more reliable term.

a. Force Data Reduction Procedure

A force data reduction procedure is presented below for the determination of the normal and axial force coefficients from flight test data. The data obtained from the flight test records include the following items:

Measured Data from Flight Test Records

Symbol	Item
T_{td}	Temperature, Engine Discharge Calibration Curve 10863030 Range: 30 to 750°C Location: Photopanel Hole No. 14
$p_{T_{td}}$	Total Pressure, Engine Discharge Calibration Curve 10663016 Range: 5 to 120 in. Hg Location: Photopanel Hole No. 10
p_{T_e}	Total Pressure, Ejector Exit Calibration Curve 10663018 Range: 5 to 120 in. Hg Location: Photopanel Hole No. 21
T_{ef}	Temperature, Engine Fuel Calibration Curve 10863031 Range: 0 to 100°C Location: Photopanel Hole No. 22
T_{17}	Temperature, Afterburner Fuel Calibration Curve 10863029 Range: 0 to 100°C Location: Photopanel Hole No. 17
V_i	Airspeed, Nose Boom, Knots Calibration Curve 10163022 Range: 0 to 700 knots Location: Photopanel Hole No. 2
H_i	Altitude, Feet Calibration Curve 10263028 Range: -1000 to 40000 ft Location: Photopanel Hole No. 3
T_a	Total Temperature of ambient air Calibration Curve 10463013 Range: -50 to 100°C Location: Photopanel Hole No. 11

Measured Data from Flight Test Records (Continued)

Symbol	Item
n_1	Rotor Speed, Low Pressure Side Calibration Curve 10563015 Range: 50 to 106% rpm Location: Photopanel Hole No. 8
n_2	Rotor Speed, High Pressure Side Calibration Curve 10563016 Range: 50 to 106% rpm Location: Photopanel Hole No. 7
Δp_{2L}	Total Pressure Loss, Left Intake Duct Calibration Curve 10763092 Range: -100 to 400 in. H_2O Location: Photopanel Hole No. 15
Δp_{2R}	Total Pressure Loss, Right Intake Duct Calibration Curve 10763091 Range: -100 to 400 in. H_2O Location: Photopanel Hole No. 19
Δp_{2C}	Total Pressure Differential, Center of Intake Duct Calibration Curve 10763093 Range: -100 to 400 in. H_2O Location: Photopanel Hole No. 20
Δp_{24}	Pressure Differential, Shroud Cooling Scoop Calibration Curve 10763094 Range: -100 to 400 in. H_2O Location: Photopanel Hole No. 24
p_{28}	Static Pressure, Shroud Cooling Scoop Calibration Curve 10263027 Range: -1000 to 40000 ft pressure altitude Location: Photopanel Hole No. 28
p_{27}	Total Pressure, Shroud Cooling Scoop Calibration Curve 10663017 Range: 5 to 120 in. Hg Location: Photopanel Hole No. 27
W_3	Fuel Quantity Used by Engine 0.141 gallon per count Location: Photopanel Hole No. 4, Counter No. 3
W_4	Fuel Quantity Used by Afterburner 0.47 gallon per count Location: Photopanel Hole No. 4, Counter No. 4

Measured Data from Flight Test Records (Continued)

Symbol	Item
A_{scs}	Effective Inlet Area of Shroud Cooling Scoop 0.201 sq ft
V_i	Indicated Airspeed, knots Location: Photopanel Hole No. 2
n_1	Low Pressure Rotor Speed, percent rpm Location: Photopanel Hole No. 8
n_2	High Pressure Rotor Speed, percent rpm Location: Photopanel Hole No. 7
p_{T_e}	Total Pressure, Ejector Exit, in. Hg Location: Photopanel Hole No. 21
Δp_{2R}	Total Pressure Loss, Right Intake Duct, in. H_2O Location: Photopanel Hole No. 19
W_4	Fuel Quantity used by Afterburner, count Location: Photopanel Hole No. 4 Counter No. 4
H_i	Indicated Altitude, ft Location: Photopanel Hole No. 3
T_a	Indicated Total Temperature of Ambient Air, °C Location: Photopanel Hole No. 11
$p_{T_{td}}$	Total Pressure, Engine Discharge, in. Hg Location: Photopanel Hole No. 10
Δp_{2L}	Total Pressure Loss, Left Intake Duct, in. H_2O Location: Photopanel Hole No. 15
T_{22}	Temperature, Engine Fuel, °C Location: Photopanel Hole No. 22
T_{17}	Temperature, Afterburner Fuel, °C Location: Photopanel Hole No. 17
W_3	Fuel Quantity Used by Engine, count Location: Photopanel Hole No. 4 Counter No. 3
Δp_{2C}	Total Pressure Differential, Center of Intake Duct, in. H_2O Location: Photopanel Hole No. 20
T_{td}	Temperature, Turbine Discharge, °C Location: Photopanel Hole No. 14

Measured Data from Flight Test Records (Continued)

Symbol	Item
dW_3/dt	Engine Fuel Flow Location: Photopanel Hole No. 5
dV/dt	Axial Acceleration Location: Oscillograph Channel No. 8 Calibration Curve 51263033 Location: Photopanel Hole No. 2 Time derivative of data
dH/dt	Rate of Climb Location: Photopanel Hole No. 3 Time derivative of data
$K_{a/c}$	F-105 Aircraft Number
K_{flight}	Test Flight Number
K_{run}	Test Run Number
W_o	Take-off Gross Weight, pounds
K_{hour}	Take-Off Time, hour
K_{min}	Take-Off Time, minutes
K_{day}	Take-Off Time, day
K_{month}	Take-Off Time, month
K_{year}	Take-Off Time, year
δ_{fuel}	Average Fuel Density, specific gravity Location: Refueling record
K_{osc}	Oscillograph Record Number Location: Top edge of oscillograph record
K_{pp}	Photopanel Frame Number Location: Photopanel counter 2

(1) Aircraft Drag Determination

The three general methods for determining airplane drag are reviewed in Reference 4 by Beeler, Bellman, and Saltzman of NACA. The stabilized flight method consists of a constant-altitude, fixed-throttle flight of sufficient duration to enable the aircraft to reach a stabilized speed. This can be difficult due to weight variations and atmospheric turbulence. The energy method allows some variations in speed and altitude but requires greater accuracies in measurements of the engine thrust, altitude, and flight speed. Angle of attack variations with altitude become an additional consideration. The accelerometer method permits integration of all aerodynamic, gravitational, momentum, and inertia forces on an airplane at any given instant, regardless of airplane attitude or acceleration. Application of this method requires the use of very sensitive longitudinal accelerometers and an accurate means of measuring angle of attack in addition to the customary research instruments.

The F-105F flight data reduction program reported herein is based on the energy method and requires a stabilized flight time period. The F-105F buffet test pattern presents excessive variations in the measured parameters for accurate drag analysis. The instrumentation is more accurate than that required for routine checking of production aircraft but is not sufficiently accurate for chordwise force determination at instantaneous flight conditions.

A procedure for computing the body force coefficients by the acceleration method is presented in the following paragraphs. This method has not been used on the flight test data. Preliminary analysis indicates that reasonable results can be obtained by this or a similar procedure.

Five sets of orthogonal axes are used to determine the components of the known forces and accelerations in a common axes system. These axes are referred to as the body axes, stability axes, wind axes, flight axes, and ground axes.

The body axes are fixed relative to the aircraft frame. The x-axis passes through the center of gravity and is positive forward parallel to the longitudinal axis. The y-axis passes through the center of gravity and is positive right and outboard normal to the aircraft plane of symmetry. The z-axis passes through the center of gravity and is positive downward and normal to the horizontal waterline plane.

The stability axes and the body axes have a common y-axis. The x-axis for the stability axis is normal to the y-axis and in the plane of the wind through the y-axis. The angle of attack is measured from the stability x-axis to the body x-axis. The z-axis is normal to the x- and y-axes.

The wind axes and the stability axes have a common z-axis. The x-axis for the wind axes is headed into the wind vector. The angle of sideslip is measured from the wind x-axis to the stability x-axis. This angle is positive when the wind comes from the right (starboard) side and the aircraft nose is pointed to the left of the wind.

The flight axes and the wind axes have a common x-axis. The x-axis is headed into the wind vector and lies along the aircraft flight path. The angle of bank is measured from the flight y-axis to the wind y-axis. This angle is positive when the right wing is down at low angles of attack and sideslip. This is not the angle of bank as measured in the aircraft.

The ground axes and the flight axes have a common y-axis. The x-axis is parallel to the ground plane and positive in the direction of flight. The y-axis is also parallel to the ground plane. The angle of climb is the angle between the ground x-axis and the flight x-axis (reference Figure 36).

Transformation of the axes to the body axes involves the known acceleration due to gravity and the unknown centrifugal force term. Summing of the forces along the airplane axes and equating them to the acceleration term yields the following equations:

$$W \bar{a}_x = T_{gross} - D_{ram} - C_X q S + W a_y' (\sin \alpha \sin \phi - \cos \alpha \sin \beta \cos \phi) - W (\cos \alpha \cos \beta \sin \gamma + \cos \alpha \sin \beta \sin \phi \cos \gamma + \sin \alpha \cos \phi \cos \gamma) \quad (1)$$

$$W \bar{a}_y = C_Y q S + W a_y' \cos \beta \cos \phi - W (\sin \beta \sin \gamma - \cos \beta \sin \phi \cos \gamma) \quad (2)$$

$$W \bar{a}_z = C_N q S + W a_y' (\sin \alpha \sin \beta \cos \phi - \cos \alpha \sin \phi) - W (\sin \alpha \cos \beta \sin \gamma + \sin \alpha \sin \beta \sin \phi \cos \gamma - \cos \alpha \cos \phi \cos \gamma) \quad (3)$$

Because the accelerometers are also affected by gravity:

$$\bar{a}_x = a_{x_B} - (\cos \alpha \cos \beta \sin \gamma + \cos \alpha \sin \beta \sin \phi \cos \gamma + \sin \alpha \cos \phi \cos \gamma) \quad (4)$$

$$\bar{a}_y = a_{y_B} - (\sin \beta \sin \gamma - \cos \beta \sin \phi \cos \gamma) \quad (5)$$

$$\bar{a}_z = a_{z_B} - (\sin \alpha \cos \beta \sin \gamma + \sin \alpha \sin \beta \sin \phi \cos \gamma - \cos \alpha \cos \phi \cos \gamma) \quad (6)$$

Combining these two sets of equations gives:

$$C_X = (T_{gross} - D_{ram} - W a_{x_B})/qS + (W/qS) a_y' (\sin \alpha \sin \phi - \cos \alpha \sin \beta \cos \phi) \quad (7)$$

$$C_Y = (W/qS) (a_{y_B} - a_y' \cos \beta \cos \phi) \quad (8)$$

$$C_N = (W/qS) (a_{z_B} - a_y' (\sin \alpha \sin \beta \cos \phi - \cos \alpha \sin \phi)) \quad (9)$$

The accelerations along the body axes are obtained from the oscillograph record (Table VIII, channels 8, 10, and 22). Since the aircraft is not in yaw, the side force is essentially zero. The lateral accelerations measured in flight are inputs from the centrifugal force and the angle of bank. A first approximation of the axial and normal force is:

$$C_X = (T_{gross} - D_{ram} - W a_{x_B})/qS + (W/qS) a_{y_B} (\sin \alpha \sec \beta \tan \phi - \cos \alpha \tan \beta) \quad (10)$$

$$C_N = (W/qS) (a_{z_B} - a_{y_B} (\sin \alpha \tan \beta - \cos \alpha \tan \phi)) \quad (11)$$

(2) Sample Computation for the Body Loads

A sample computation from the present flight test data reduction program is reviewed and recomputed with reference to the preceding analysis. The information from the performance program 9130, version 13, is given in Table X. The Flight Test Number 368, Run 2; Oscillograph Record 34, Photopanel Frame 16; was selected because the flight test analysis showed a negative drag coefficient and a negative profile drag coefficient.

The aircraft is flying at 34,685 feet pressure altitude, at an ambient pressure of 7.147 in. Hg (505.49 psf) and a true Mach number of 0.888. The reference dynamic pressure under these conditions is 279.02 psf and the reference aerodynamic force for an area of 385 sq ft (ref wing area for F-105F) is qS = 107424 lb. The true airspeed is 517.4 knots (869.2 fps).

The engine net thrust of 5011 lb was determined from the digital computer program. The program determined this thrust from the primary and secondary gross thrust of 7933 lb and 92 lb. The ram drag was 2780 lb for the primary engine ducts, 84 lb for the fin ducts, and 149 lb for the shroud cooling scoops. The aircraft was flying at Military Rated Power.

The aircraft weight of 36712 lb was determined from the take-off weight of 40692 lb, the fuel used, and the fuel flow. Based on this weight, the level flight lift coefficient was 0.34175 (W/qS).

The flight configuration was zero trailing edge flap deflection with 8° leading edge flap deflection. The speed brakes were closed. The zero control position was determined near the start of the run at oscillograph record number 28. The comparisons are tabulated below:

Control	(Chan)	Zero Position	Read Position	Change	Deflection
Stabilizer	(18)		7.15 in.		-20°
Aileron					
Right Wing	(32)	2.8 in.	2.6 in.	-0.20	-2.0°
Left Wing	(3)	8.55 in.	8.28 in.	-0.27	-3.0°
Spoiler					
Right Wing	(36)	2.0 in.	1.95 in.	-0.05	-1.0°
Left Wing	(2)	10.6 in.	10.6 in.	0.0	0.0

The zero position was assumed to be the entry condition. The stabilator position was determined directly from the trace deflection in Figure 37. The aileron positions were assumed to be zero, and the movement of the trace was used as the aileron movement. The motion was read from Figures 38 and 39 for the right and left ailerons, respectively. This same analysis was applied to the spoilers with reference to Figures 40 and 41.

The flight attitude and body accelerations were obtained from the oscillograph record. The roll attitude was given in hole No. 12 of the photopanel, and the normal acceleration at the center of gravity was given in hole No. 9 of the photopanel (Table VII). The angle of attack was read from channel 12 of the oscillograph. This trace was 7.86 inches from the bottom reference trace which corresponds to 8.2° angle of attack (Figure 42 for flight 368). The angle of sideslip was read from channel 20 of the oscillograph. This trace was 4.88 in. from the bottom reference trace at the start of the run and 4.88 in. at the photopanel frame 16 blip, therefore, it may be assumed that there was zero sideslip (Figure 43).

The accelerations measured at the center of gravity for the body x-axis, y-axis, and z-axis are read from oscillograph channels 8, 10, and 27, respectively. At the start of the run, the traces were measured from the bottom reference trace as 9.52 in., 8.76 in., and 4.26 in. At the photopanel frame 16 blip, these measurements were 9.55 in., 8.80 in., and 3.96 in. The acceleration at the pilot's seat was channel 27. This replaces channel 22 for the normal acceleration because the channel was inoperative. At the start of the run, the channel 22 trace measurement was 5.72 in., which was constant throughout this run. The axial acceleration exhibited a 0.03 in. change in the positive direction which, combined with a calibration constant of 0.727 and a calibration deflection measurement of 1.15 in. in the same direction, results in a 0.0216 g acceleration (Figure 44). The lateral acceleration exhibited a 0.062 g acceleration (Figure 45). The calibration constant was 1.386 g and the calibration deflection was 1.20 in. The normal acceleration at the pilot's seat results in 1.715 g using a calibration constant of 2.4 g and a calibration deflection of 1.01 in. (Figure 46).

Based on the load factor at the pilot's seat, the angle of bank was estimated:

$$\cos \phi = 1/a_{z_B} = 1/1.715 = 0.5830903$$

$\phi = 54.3$ deg. $\quad \alpha = 8.2$ deg.

$\sin \phi = 0.8124074 \quad \sin \alpha = 0.1421$

$\tan \phi = 1.39328 \quad \cos \alpha = 0.9899$

The axial and normal force coefficients are (by substituting values in Equations (10) and (11)) thus:

$$C_X = (5011. - 36712.\ (0.0216))/107424. + (0.34175)\ (0.062)\ (0.1421\ (1.3933) - 0.0)) = 0.04346 \quad (10)$$

$$C_N = (0.34175)\ (1.715 - 0.062\ (0.1421\ (0.0) - 0.9899\ (1.3933)) = 0.615319 \quad (11)$$

$$C_L = C_N \cos \alpha - C_X \sin \alpha = 0.6029 \quad (12)$$

$$C_D = C_X \cos \alpha + C_N \sin \alpha = 0.13046 \quad (13)$$

The drag coefficient is no longer negative and the profile drag coefficient becomes 0.0780 based on an induced drag factor of 0.14427 and a lift coefficient of 0.6029. The value of normal force is larger than the wind tunnel value of 0.58 at an angle of attack of 8.2° (Figure 26b).

b. Buffet Parameters

The primary flight test measurements made were for buffet intensity levels and their manner of variation with angle of attack. The angle of attack measurements in flight are accurate to about 0.5°. Figure 42 is the result of a ground calibration of the angle of attack indicator, which is a pivoted vane mounted on a nose boom. While this system is capable of measuring the vane position to within 0.1°, the flow angles registered by the vane do not necessarily represent the true angle of attack of the airplane because of the effects of pitching velocity, boom and fuselage bending, and upwash.

The measurements of the buffet intensity levels provided the determination of the angle of attack at the onset of Mach buffet. The qualitative references for the buffet intensity levels were from the pilot input. The values of angle of attack, normal force coefficient, aileron hinge moment fluctuations, normal accelerations felt at the pilot's seat, and other parameters were compared with the pilot event marks on the oscillograph traces.

The wing tip accelerometers were calibrated by inverting each one for a 1g negative reading and then holding the axis vertical for a zero-g reading. The results are shown in Figures 47 and 48. High frequency response galvanometers were used in the oscillograph to provide the wider trace deflections. Although the instrumentation on both wing tips was similar, the right wing had the greater vibrations (channel 24). This may be noted on the oscillograph sample traces presented in Figure 49.

The calibration curves for the 95% chord static pressure data are presented in Figures 50 through 54. The pressure transducer calibration curves of the 85% chord static pressure data are presented in Figures 55 through 60. For the twelve static pressure ports, the calibration curves for eleven of these are presented in these figures.

The calibration curves for the four total pressure tubes above the trailing edge of the flaps are presented in Figure 61.

c. Parameters on Photopanel

The calibration curves for the parameters presented on the photopanel are also presented. These include the flight test conditions in Figures 62 and 63. The curves for the tachometer are presented in Figures 64 and 65.

The inlet duct pressure calibration curves are shown in Figures 66 through 68. The curves for the turbine discharge pressure and temperature are presented in Figures 69 and 70. The correction factors for the absolute and differential pressure readings for the shroud cooling scoop are given in Figures 71 and 72.

The engine fuel temperature correction to the readings presented in the photopanel are presented in Figure 73.

3. WIND TUNNEL DATA REDUCTION

The primary wind tunnel test measurements made were for buffet intensity and its variation with angle of attack. For this purpose, the NASA Langley Research Center provided a root-mean-square integration of one buffet parameter for the test. Individual departures from the nominal value were available on tape for a power spectral density analysis of the 1/22-scale F-105F aircraft model.

The test data was reduced at NASA by their program FSR 4420. The wing bending moment was presented as a dimensional quantity. This was non-dimensionalized to a coefficient form:

WSG = Wing strain gage bending moment fluctuation, inch pounds

ΔC_{BM} = Coefficient of the Wing Bending Moment Fluctuations.

$$= (WSG)/(q \frac{Sb}{2}\sqrt{\delta})$$

q = Dynamic pressure, psf

S = Wing area = $385/(22^2)$ sq ft

b = Wing span = 35/22 ft

$\sqrt{\delta}$ = $(p/p_o)^{\frac{1}{2}}$

p = Ambient pressure

p_o = Sea level pressure, 2116.2 psf

These results are presented in Figure 34.

SECTION V

BASIC DATA PRESENTATION

1. GENERAL

The normal and the chordwise force data from the wind tunnel test of the 1/22-scale model of the F-105F aircraft is presented in Figures 26 and 27. The aileron hinge moment data from the full-scale F-105F flight test program is presented in Figure 28. The local slopes of the normal and the chordwise force data are presented in Figures 29 and 30 in order to amplify their points of inflection and correlate this position with the trailing edge pressure divergence in Figure 33 and the strain gage buffet indications for the aileron hinge moment in Figure 28, as well as the wing bending moments in Figure 34.

Typical pressure distributions chordwise and spanwise are presented in Figures 31 and 32 to illustrate the pressure patterns below Mach buffet, near Mach buffet, and above Mach buffet onset. Boundary layer pressures for these three cases are also presented in Figure 35. The 1/22-scale model had two chordwise pressure ports at wing station 95 which did not show a notable change in the pressure distribution as noted in the flight test data in Figure 74.

The trailing edge pressure variation at the outboard wing station from flight test can be compared in general with the wind tunnel data. This is the comparison of Figures 74a, b, and c with Figures 33a, b, and c. A notable similarity of angle of attack at buffet onset is apparent.

The trailing edge pressure variation was also presented against normal force coefficient as determined by the normal flight test data reduction technique. This presentation in Figure 75 may be compared to the root-mean-square displacement of the normal acceleration at the pilot's seat as presented in Figure 76a. Figure 76b presents this displacement against angle of attack.

2. BUFFET INDICATORS

Buffet onset in the high subsonic speed range can be recognized by the sharp rate of increase in buffet intensity with angle-of-attack (Ref. Figure 28). This increase in intensity does not continue its rate of build-up to maximum levels. The rate of build-up reduces rapidly after 2 or 3° increase in angle of attack after buffet onset. The evaluation of buffet intensity will not be attempted in this report until further study is made on the power spectral density of the buffet phenomena and the pilot's response to these frequency and amplitude modes.

The onset of Mach buffet is easily detectable from the output of the strain gage measuring the outboard aileron hinge moment vibration levels (Figure 28). This may not be related as easily to the fluctuations of the normal acceleration at the pilot's seat due to the aeroelastic and structural damping in the stress paths between the aileron and the pilot. The outboard aileron hinge moment measurement location is one of the most accessible for instrumentation, both in the wind tunnel and on the full-scale aircraft. Sufficient amplitude is available for correlation with pilot sensations for a given aircraft.

The pressure divergence at the outboard static pressure ports provides the earliest buffet indication because it is the pressures that impose the loads on the airframe. The transmission of this pressure change to the structural measurement system may be almost instantaneous, depending on the method of recording. Measurements at the static pressure ports are more time-consuming and expensive.

A buffet detection system sensing wing bending moment vibrations can determine the point of buffet onset as well as static pressure port or aileron hinge moment systems. The wing bending moment system, however, does not sense the intermediate reduction in the rate of growth of buffet intensity due to the low mass damping characteristics of the wing. As more aircraft become capable of continuous flights at high subsonic speeds, these variations in the rate of growth in buffet intensity will become subjects of intense study.

The boundary layer profile (Figure 35) shows that a rapid change in the boundary layer characteristics results from the Mach buffet phenomena. The flight test data apparently filled the gap between two probes in the wind tunnel test model. That is, the one nearest the edge of the trailing edge flap and the first probe above on the wind tunnel model appears to bracket the probes used in flight test.

A study of the effect of locating the boundary layer transition strip at various chord stations was made during the first series of runs in the NASA wind tunnel. For the test configuration, the transition strip was off on run 19, was placed at the 10% wing chord station on run 20, and on run 4, it was at the 30% chord station, which was the standard test location for this series. Figure 77 shows that locating the transition strip forward or leaving it off, decreases the angle of attack for the onset of Mach buffet slightly more than 1°. It may also be noted in the same figure that the buffet intensity also tends to increase as the transition strip is moved from 10% chord to the 30% chord station.

There seems to be a small range of angles of attack in the high subsonic speed range at which the onset of Mach buffet occurs; therefore, for the same angle of attack, the flap setting providing the best lift with a minimum drag penalty would be favored. The variation of the angle of attack at the onset of Mach buffet is presented in Figure 78 for various flap configurations. Increasing the trailing edge deflection angle has a tendency to cause the onset of buffet to occur at lower angles of attack. A leading edge flap deflection of 8°, combined with trailing edge deflections greater than 6°, will delay the onset of buffet to higher angles of attack.

The normal force coefficient at buffet onset increases with trailing edge flap deflection (Figure 79). This increase is greatest with the leading edge flap deflection angle of 8°. For trailing edge deflection angles greater than 12°, the data continues to exhibit increases in angle of attack and normal force coefficient at buffet onset.

The variation of normal force coefficient at buffet onset with Mach number is presented in Figure 80. Figure 80c, d shows the highest normal force coefficient at buffet onset, which were attained with an 8° leading edge flap deflection and the two trailing edge flap deflections.

The variation of angle of attack at buffet onset (Figure 81) shows an increase in angle of attack at buffet onset for the 8° leading edge flap deflection with 7.5° trailing edge flap deflection at speeds above Mach 0.86. This same characteristic is not shown for the 15° trailing edge flap deflection (Figure 81c, d). These curves indicate that the optimum trailing edge flap deflection is about 10° with an 8° leading edge flap deflection.

3. MANEUVERING FLAPS

A study of the use of flaps as maneuvering aids was made to further the progress toward providing greater lift for aircraft maneuvering in the high subsonic speed regime. A flap which will increase the lift capability of the aircraft without an attendant increase in buffet intensity is a maneuvering flap. One of the methods for attaining such a design is to incorporate features which will delay the onset of buffet to higher lift coefficients. One of the purposes of this study is to provide the basis for selecting features which will delay the onset of buffet.

Table XI presents a comparison of three configurations. The first configuration is the basic F-105F airplane with the flaps undeflected. The second configuration has the leading edge flaps deflected 8°. The third configuration adds to the second configuration by deflecting the trailing edge flaps 7.5°.

The criterion for selecting a particular leading and trailing edge flap configuration for a maneuvering flap is the buffet intensity to which the pilot is subjected. This criterion may be affected by the engine power setting (Figure 82), since air spillage around the inlets at the lower power settings will increase the air mass over and around the wing surface. The increase in air mass around the wing seems to increase the maximum coefficient of aileron hinge moment fluctuations. This indicates that the higher engine power levels seem better for lower buffet intensities.

The maximum coefficient of wing bending moment fluctuation is lower at the higher leading and trailing edge flap deflections (Figure 83). For the same normal load factor (Figure 79), or normal force coefficient, there is an apparent advantage to a 20° leading edge flap deflection, since it has the lower buffet intensity based on the wing bending moment.

The aileron hinge moment coefficient of buffet intensity (Figure 84) is not in agreement with the wing bending moment parameter. This parameter continues to favor the leading edge flap deflection of 8° and the trailing edge flap deflection of 15°. Since the wing bending stresses, which are passed through the structure are the most likely avenues for transmitting the stress to the pilot, the wing bending parameter is favored for the selection of the maneuvering flap geometry.

SECTION VI

CONCLUSIONS

The F-105F flight test program and the 1/22-scale model wind tunnel test of the same configurations have demonstrated that the use of leading edge flaps in conjunction with trailing edge flaps can delay the onset of Mach buffet to higher lift coefficients. This provides a higher usable load factor for high speed maneuvers. The use of a sealed or unsealed trailing edge flap gap does not materially affect the lift coefficient at buffet onset. An unsealed flap gap will reduce the flap design complexities.

Selection of the optimum leading edge flap and trailing edge flap deflection will be based not only on the normal force at buffet onset but also on the maximum buffet intensities transmitted to the pilot's seat. After selection of a configuration to delay buffet to the highest normal force practical, variations of the leading edge flap may be used to control the buffet intensities.

The point of buffet onset from flight test correlated reasonably well with the values in wind tunnel data. Buffet intensity correlation between flight test and wind tunnel data appears promising but requires further study because of position differences in the locations of the strain gages for measuring wing bending.

APPENDIX I

TABLES

TABLE I. F-105F AREAS AND DIMENSIONS

	Full-Scale	1/22-Scale
1. WING ASSEMBLY		
a. Basic Wing Data		
Area		
In wing chord plane	385.00 sq ft	.794 sq ft
Projected Area	384.274 sq ft	-
Span		
Along wing chord plane	35.000 ft (420.00 in.)	1.588 ft
Projected span	34.934 ft (419.208 in.)	-
Aspect Ratio		
In wing chord plane	3.182	3.182
Projected	3.176	-
Taper ratio	.467	.467
Sweepback of leading edge	48.09°	48.09°
Sweepback of trailing edge	33.34°	33.34°
Sweepback of $\frac{1}{4}$ chord line		
In wing chord plane	45.000°	45.00°
Projected	45.056°	
Dihedral	-3.500°	-3.5°
Incidence	0°	0°
Twist (geometric)	0°	0°
Wing Section		
Wing station 80.000	65A005.5	65A005.5
Wing tip (theoretical)	65A003.7	65A003.7
Root chord length		
(Theoretical, wing station 0)	15.000 ft (180.000 in.)	.6818 ft
Tip chord length (theoretical)	7.000 ft (84.000 in.)	.3182 ft
Longitudinal location of leading edge of theoretical root chord	F.S. 298.38 in.	13.563 in.
Longitudinal location of C/4 point of theoretical root chord	F.S. 343.38 in.	

TABLE I---Continued

	Full-Scale	1/22-Scale
Vertical location of theoretical root chord	W.L. 13.50 in.	.614 in.
Length of MAC (theoretical)	11.4848 ft (137.818 in.)	.522 ft (6.264 in.)
Longitudinal location of MAC leading edge (theoretical)	F.S. 401.108 in.	18.235 in.
Vertical location of MAC	W.L. 7.8672 in.	-
Lateral location of MAC	B.L. 92.099 in.	4.194 in.
Longitudinal location of C/4 point of MAC	F.S. 435.642 in.	19.802 in.

b. Flaps and Control Surfaces

(1) Slotted Trailing Edge Flaps

Type	Single slotted
Total area, both T.E. flaps	61.12198 sq ft
Location of outboard end	W.S. 147.000 (.70b/2)
Location of inboard end	W.S. 30.849 (.147b/2)
Flap span	9.679 ft (116.151 in.)
Average T.E. flap chord (streamwise)	.2605 c
Max deflection measured from wing chord plane normal to .82 c chordline	34.5°
Flap chord at outboard end	29.716 in. (.264c)
Flap chord at inboard end (theoretical)	41.475 in. (.256c)
Sweepback of .82 c line	36 deg, 28 min, 49 sec

TABLE I---Continued

	Full-Scale	1/22-Scale
(2) Leading Edge Flaps		
Total area, both leading edge flaps	22.815 sq ft	.0469 sq ft
Location of inboard end	W.S. 82.149 (.391 b)	
Location of outboard end	W.S.199.780 (.951b)	
Flap span, measured perpendicular to fuselage $\mathcal{L}$ (each side)	9.803 ft (117.636 in.)	.4455 ft
L.E. flap chord at W.S. 82.149, streamwise	11.55 in. (.08c)	.0429 ft
at W.S. 199.78, streamwise	16.38 in. (.185c)	.0633 ft
Average L.E. flap chord, streamwise	.125c	
Maximum deflection, normal to hinge line	0°,8°,20°	
Sweepback of L.E. flap hinge line	49 deg, 7 min,26 sec	
(3) Ailerons		
Type	Plain flap	
Total area aft of hinge line	15.446 sq ft	
Inboard end	W.S.147.25	
Outboard end	At Wing Tip	
Chord	.20c	
Maximum deflection (normal to hinge line)	±20°	
Sweepback of hinge line (on .80c)	36 deg,49 min, 8.4 sec	
Location of centroid of area	W.S.173.900 F.S. 581.130	

TABLE I---Continued

	Full-Scale	1/22-Scale
2. FUSELAGE		
a. Basic Data		
Length	66.940 ft (803.328 in.)	
Nose Location	F.S.26.328	
Width max (excluding fuselage bump)	4.375 ft (52.500 in.)	.1989 ft
Width max (including fuselage bump)	5.370 ft (64.440 in.)	
Maximum depth (excluding canopy)	6.748 ft (80.974 in.)	.2955 ft
Frontal area		
(excluding canopy)	29.05 sq ft	0.05103 sq ft
(including canopy)	30.47 sq ft	
Side area (excluding canopy)	366.376 sq ft	
Forward of .25 MAC	194.876 sq ft	
Aft of .25 MAC	171.500 sq ft	
Side area (including canopy)	383.357 sq ft	
Forward of .25 MAC	211.657 sq ft	
Aft of .25 MAC	171.700 sq ft	
Total plan area	284.252 sq ft	
Forward of .25 MAC	148.952 sq ft	
Aft of .25 MAC	135.300 sq ft	
Total volume (excluding canopy)	1342.100 cu ft	
Forward of .25 MAC	668.000 cu ft	
Aft of .25 MAC	674.100 cu ft	
Total volume (including canopy)	1384.000 cu ft	
Forward of .25 MAC	709.800 cu ft	
Aft of .25 MAC	674.200 cu ft	
b. Inlets	924 sq in.	

TABLE I---Continued

	Full-Scale	1/22-Scale
3. HORIZONTAL TAIL AREA		
Theoretical	96.487 sq ft	.18795 sq ft
Exposed	60.365 sq ft	.12556 sq ft
Span	17.394 ft (208.72 in.)	.7577 ft
Aspect ratio		
Theoretical	3.135	3.06
Exposed	2.494	2.47
Taper ratio		
Theoretical	.445	.456
Exposed	.532	.531
Sweepback of $\frac{1}{4}$ chord line	45°	45°
Dihedral	0°	0°
Incidence	7° nose-up 25° nose-down	
Twist	0°	0°
Airfoil section		
Root (theoretical)	65A006	65A006
Tip (theoretical)	65A004	65A004
Root chord		
Theoretical	7.678 ft (92.136 in.)	.3409 ft
Exposed (B.L. 30.74	6.423 ft (77.074 in.)	.2927 ft
Tip chord (theoretical)	3.417 ft (41.000 in.)	.1555 ft
Longitudinal location of hinge line	F.S. 690.000 in.	31.361 in.
Longitudinal location of leading edge of theoretical root chord	F.S. 612.606 in.	28.069 in.
Root $\frac{1}{4}$ chord point location	F.S. 635.640 in.	
MAC length		
Theoretical	5.820 ft (69.841 in)	.2595 ft
Exposed	5.073 ft (60.874 in.)	.2309 ft
MAC leading edge longitudinal location		
Theoretical	F.S. 663.681	30.30
Exposed	F.S. 684.223	31.091

TABLE I---Continued

	Full-Scale	1/22-Scale
MAC $\frac{1}{4}$ chord point longitudinal location		
Theoretical	F.S. 682.141	31.078
Exposed	F.S. 699.441	31.784
MAC lateral location		
Theoretical	B.L. 45.501 in.	.1659 ft
Exposed	B.L. 63.801 in.	.2241 ft
MAC vertical location	W.L. -19.00 in.	-.888 in.
l_{h_t} .18 MAC wing (theoretical) to .25 MAC tail (theoretical)	21.270 ft (255.240 in.)	
l_{h_t} .18 MAC wing (theoretical) to .25 MACtail (Exposed)	22.787 ft (273.440 in.)	

4. VERTICAL TAIL

a. Basic Data

Area	
Theoretical (above W.L.0)	107.962 sq ft
Exposed (above W.L. 38.000)	72.974 sq ft
Height (above W.L.0)	13.800 ft (165.603 in.)
Aspect ratio	
Theoretical	1.764
Exposed	1.553
Taper ratio	
Theoretical	.3028
Exposed	.3605
Sweepback of $\frac{1}{4}$ chord line	45 deg, 36 min
Root chord	NACA 65A005.46 (W.L. 38.00)
Theoretical (W.L.0)	12.009 ft. (144.112 in.)
Exposed (W.L. 38.000)	10.088 ft (121.058 in.)
Tip chord (theoretical)	3.637 ft) (43.645 in.) NACA 65A003.41

TABLE I---Continued

	Full-Scale	1/22-Scale
Longitudinal location of leading edge of root chord		
Theoretical (W.L. 0)	F.S. 535.201	
Exposed (W.L. 38.000)	F.S. 579.629	
Root $\frac{1}{4}$ chord point location		
Theoretical (W.L. 0)	F.S. 571.229	
Exposed (W.L. 38.000)	F.S. 609.894	
MAC length		
Theoretical	8.570 ft (102.838 in.)	
Exposed	7.368 ft (88.416 in.)	
MAC leading edge longitudinal		
Theoretical	F.S. 614.743	
Exposed	F.S. 642.537	
MAC $\frac{1}{4}$ chord point longitudinal location		
Theoretical	F.S. 640.452	
Exposed	F.S. 664.641	
MAC vertical location		
Theoretical	W.L. 68.033	
Exposed	W.L. 91.806	
l_{vt} .25 MAC wing (theoretical) to .25 MAC vertical tail (theoretical)	17.505 ft (210.060 in.)	
l_{vt} .25 MAC wing (theoretical) to .25 MAC vertical tail (exposed)	18.976 ft (227.712 in.)	
l_{vt} .18 MAC wing (theoretical) to .25 MAC vertical tail (exposed)	19.886 ft (238.636 in.)	
b. Rudder		
Type	Plain flap	
Total area aft of hinge line	11.879 sq ft	
Location of inboard end	W.L. 42.000	

TABLE I---Continued

	Full-Scale	1/22-Scale
Location of outboard end	W.L. 124.00	
Chord of inboard end	20.861 in. (.161c)	
Chord of outboard end	20.861 in. (.277c)	
Average chord	.219c	
Rudder span measured perpendicular to horizontal	6.833 ft (82.000 in.)	
Reference line		
Maximum rudder deflection	±32°	
Normal to hinge line		
Sweepback of hinge line	29 deg, 21 min, 28 sec	
5. VENTRAL FIN		
Area (exposed)	12.347 sq ft	
Overall length (from F.S. 541.134 to F.S. 724.482)	15.278 ft (183.348 in.)	
Span (from W.L. -38.500 to W.L. -61.226)	1.894 ft (22.726 in.)	
Aspect ratio	.3	
Centroid of ventral fin	F.S. 596.5 W.L. -43.9	
Distance from $\frac{1}{4}$ MAC point to centroid of ventral fin	13.405 ft (160.858 in.)	
6. LANDING GEAR		
Ground angle - ground line to fuselage centerline	1 deg, 36 min, 26 sec	
Longitudinal distance from nose wheel to main wheel measured along ground line	23.669 ft. 284.032 in.	

TABLE I---Continued

	Full-Scale	1/22-Scale
Nose wheel location	F.S.187.230	
Main wheel location (strut compressed)	F.S. 471.130	
Main wheel location in percent MAC	50.74	
Main wheel lateral location	BL 103.60	
Main wheel tread	17.267 ft 207.200 in.	

7. GEOMETRIC PARAMETERS

a. Trailing Edge Flaps

$$\frac{S_t}{S_w} = \frac{61.122}{385.000} \qquad .15875$$

b. Ailerons

$$\frac{S_a}{S_w} = \frac{15.370}{385.000} \qquad .03992$$

c. Horizontal tail

(1) Theoretical

$$\frac{S_{h_t}}{S_w} = \frac{96.4866}{384.274} \qquad .25109$$

$$\overline{V} = \frac{S_{h_t}}{S_w} \frac{l_t}{c} \qquad .46500$$

(2) Exposed

$$\frac{S_{h_t}}{S_w} = \frac{60.365}{384.274} \qquad .15708$$

$$\overline{V} = \frac{S_{h_t}}{S_w} \frac{l_t}{\overline{c}} \qquad .31165$$

TABLE I---Concluded

	Full-Scale	1/22-Scale
d. Vertical tail		
(1) Theoretical		
$\frac{S_{v_t}}{S_w}$	.28095	
$\overline{V} = \frac{S_{v_t}}{S_w} \frac{l_{v_t}}{b_w}$	.14372	
(2) Exposed		
$\frac{S_{v_t}}{S_w}$	.18990	
$\overline{V} = \frac{S_{v_t}}{S_w} \frac{l_{v_t}}{b_w}$	.10810	

TABLE II. F-105F FLIGHT TEST SUMMARY-BUFFET RESEARCH

Buffet Run	Date	Time	Fuel Remaining (lb)	Flight No.-Run	Power	L.E. Flap Deflection	T.E. Flap Deflection	$Mach_i$	Altitude (1000 ft)	Norm. Accel. Buffet: Start	Onset	Light	Mod	Heavy	Performance	Mach Variation	Altitude Variation (1000 ft)	Osc Record: Start	Finish
1	5/	0906	6500	367-1	MRP	8	0	.785	35	1			$3\frac{1}{2}$	-	Poor	.2		95	118
2	22	16	5800	-2				.835		1			$3\frac{1}{2}$	-		.01	10	120	135
3		22	5100	-3				.88		1		2	$2\frac{1}{2}$	3			10	140	259
4		27	4600	-4	MRP	20	0	.785	35	1		$2\frac{1}{2}$-3	-	-	Poor	.03	10	159	174
5		33	3900	-5				.835		1		$2\frac{1}{2}$	3	-				177	187
6	738 - #187 Chase	37	3600	-6				.88		1			3.5	-				193	
7		39	3500	-7	MRP	20	0	.785	25	1			$3\frac{1}{2}$	-				208	219
8		43	3000	-8				.835		1			5	-				222	242
9		48	2400	-9				.88		1				$4\frac{1}{2}$				242	258
10	5/	0806	6300	368-1	MRP	8	0	.88	35	1			3.2	-				9	26
11	23	11	5500	-2				.835		1			$3\frac{1}{2}$	-			13	27	44
12		16	5000	-3				.785		1			$3\frac{1}{2}$	-				44	62
13		18	4800	-4	MRP	8	0	.88	25	1			4	-				62	74
14		20	4500	-5				.835		1			(5)	-				78	89
15		22	4200	-6				.785		1			$4\frac{1}{2}$	-	Good			93	105
16		26	3700	-7	IDLE	8	0	.88	25	1			5	-		Good		111	129
17		29	3100	-8				.835		1			4.8	-				129	141
18	F-105 #173 chase	33	2800	-9				.785		1			5	-				147	153
19		35	2400	-10	MRP	20	0	.785	25	1			$4\frac{1}{2}$	-				163	169
20		38	2000	-11				.88		1			5	-				178	189
21		40	1800	-12				.835		1			5	-				193	205
22	5/	0915	6000	369-1	MRP	20	0	.785	34	1			3	-				9	25
23	24	21	5000	-2				.835	34	1			$3\frac{1}{2}$	-				34	48
24		33	3500	-3				.88	35	1			$3\frac{1}{2}$	-				49	63
25		38	2900	-4	MRP	0	0	.785	25	1			4	-				63	74
26		41	2500	-5				.835		1			4.4	-				78	89
27	F-104 #324 Chase	44	2200	-6				.88		1			5	-				94	104
28	5/	0955	6600	370-1	MRP	8	$7\frac{1}{2}$	.785	25	1			4	-				52	64
29	28	58	6000	-2				.835		1			(4.2)	-				70	85
30		1004	5200	-3				.88		1			4.5					90	100
31		07	5000	-4	MRP	20	$7\frac{1}{2}$	.785	25	1		4.2	-	-				106	118
32	TTA	11	4500	-5				.835		1			4.5	-				125	135
33		15	3800	-6				.88		1			4.5	-				139	156

TABLE II - Continued

Buffet Run	Date	Time	Fuel Remaining (lb)	Flight No.-Run	Power	L.E. Flap Deflection	T.E. Flap Deflection	$Mach_i$	Altitude (1000 ft)	Norm. Accel. Buffet: Start	Onset	Light	Mod	Heavy	Performance	Mach Variation	Altitude Variation (1000 ft)	Osc Record: Start	Finish
34	5/28	17	3400	370-7	IDLE	8	7½	.785	25	1			4.2	+				157	160
35	TTA	21	3200	-8				.835		1			4.2	+				175	188
36		25	2600	-9				.88		1			4.5					193	209
37	5/29		7200	371-1	A/B	8	15	.785	25	1	2.4	(3.2)	-	+				18	30
38			6700	-2				.835		1	(3.0)		-	+				31	43
39				-3				.88		1	(2.6)	-	-	+				44	57
40				-4	MRP	8	15	.785	25	1	2.4	-	-	+				58	71
41			6000	-5	MRP	20	15	.785	25	1	3.0		-	+	Poor			72	83
42			5800	-6	A/B	20	15	.785	25	1		3.2	-	+				84	95
43			5600	-7				.835		1	(3.0)	-	-	+				96	110
44			5400	-8				.88		1	(2.6)	-	-	+				111	123
45	TTA		5200	-9	MRP	8	15	.785	25	0	3.2	-	-	+				124	140
46			5100	-10	A/B	8	15	.835	25	0								141	154
47			4800	-11				.88		0								155	167
48				-12	MRP	20	15	.785	25	0		3.2						168	181
49			4500	-13	A/B	20	15	.835	25	0								182	196
50			4400	-14				.88		0	2.5							197	208
51	5/29	1603	6200	372-1	A/B	8	15	.785	35	0		2.3						10	25
52		05	5400	-2				.785		0	1.8	(2.6)						27	40
53		06	5000	-3				.835		0			3					42	62
54		07	4900	-4				.88		0			3					63	75
55	F-104 #324 chase	08	4600	-5	A/B	20	15	.785	35	0			(2)					77	89
56		10	4300	-6				.835		0			3.3					90	104
57		12	3800	-7				.835		0			3.2					105	123
58		14	3800	-8				.88		0		3.5						124	139
59		16	3500	-9	MRP	20	15	.785	35	0			2.8					140	154
60		17	3200	-10	MRP	8	15	.785	35	0			(2.6)					155	167
61	5/31	1006	6000	373-1	A/B	8	7½	.785	35	0				3.0				01	06
62		08	5200	-2				.835		0			3.4					09	14
63		10	5100	-3				.88		0			3.6					19	20

TABLE II ---Concluded

Buffet Run	Date	Time	Fuel Remaining (lb)	Flight No. -Run	Power	L.E. Flap Deflection	T.E. Flap Deflection	$Mach_1$	Altitude (1000 ft)	Norm. Accel. Buffet						Performance		Osc Record	
										Start	Onset	Light	Mod	Heavy		Mach Variation	Altitude Variation (1000 ft)	Start	Finish
64	5/31	1011	4800	373-4	A/B	20	$7\frac{1}{2}$	.785	35	0			3.1					22	25
65		13	4600	-5				.835		0			3.5					26	33
66		14	4400	-6				.88		0			3.6					34	38
67	F-104 #324 chase	15	4600	-7	MRP	8	$7\frac{1}{2}$	.785	35	0			3.0					42	46
68		17	3800	-8				.835		0			3.5					54	59
69		19	3000	-9	MRP	20	$7\frac{1}{2}$	.785	35	0			3.2					68	74
70		21	2500	-10				.835		0			3.5					84	94
71	6/4	0927	6200	374-1	A/B	8	$7\frac{1}{2}$	.785	25	0				4.3				55	67
72			6000	-2				.835		0				4.5				71	82
73		31	5400	-3				.88		0			4.8			To 372K		85	96
74	F-100 #729 chase		4900	-4	A/B	8	$7\frac{1}{2}$	.785	35	0	2.1		3.1						111
75			4600	-5				.835		0			3.5					116	126
76			4200	-6				.88		0			3.9					131	132
77			3600	-7	A/B	0	0	.785	35	0			4.0		Snapped at end			146	160
78			2600	-8				.835		0				3.9				166	
79			2300	-9				.88		0				3.9				183	195
80		48	2200	-10	MRP	0	0	.785	35	0								200	210

TABLE III. TEST CONFIGURATIONS

Configuration			Mach	Flight No.-Run					Test No.-Run		
	Flap Setting			25000 ft			35000 ft		GRIT		
No.	L.E.	T.E.	No.	Idle	MRP	A/B	MRP	A/B	@.30c	Other	β -6°
1	8°	0°	.8		368-6		368-3		845-6		845-1
			.85	368-9	368-5		368-2		845-5		845-16
			.9	368-8	368-4		368-1		845-4	845-19	845-17
			.95	368-7						845-20	
2	8°	7.5°	.8				373-7		850-21		
			.85	370-7	370-1			373-1	850-20		
			.9	370-8	370-2	373-8		373-2	850-19		
			.95	370-9	370-3			373-3			
3	8°	15°	.8		371-9		372-10		850-18		
			.85					372-1			
								372-2	850-17		
			.9			371-10		372-3	850-16		
			.95			371-11		372-4			
4	20°	0°	.8		368-10		369-1	369-1	845-9		
			.85		368-12		369-2		845-8		
			.9		368-11		369-3		845-7		
5	20°	7.5°	.80						850-6		850-9
			.85		370-4		373-9	373-4	850-5		850-8
			.90		370-5		373-10	373-5	850-4		850-7
			.95		370-6			373-6			
6	20°	15°	.80		371-12		372-9		850-15		850-12
			.85					372-5	850-14		850-11
								372-6			
			.90			371-13		372-7	850-13		850-10
			.95			371-14		372-8			
7	0°	0°	.8						845-3		
			.85		369-4		374-10	374-7	845-2		
			.9		369-5			374-8	845-1		
			.95		369-6			374-9			

TABLE III---Concluded

Configuration			Mach No.	Flight No.-Run					Test No.-Run		
No.	Flap Setting L.E.	T.E.		Idle	25000 ft MRP	A/B	MRP	A/B	GRIT @.30c	Other	β -6°
8*	8°	7.5°	.8								
			.85			374-1		374-4			
			.9			374-2		374-5			
			.95			374-3		374-6			
9*	20°	7.5°	.8						850-1		
			.85						850-3		
			.90						850-2		
10*	8°	7.5°	.8						850-24		
			.85						850-23		
			.9						850-22		
11*	8°	15°	.8						850-27		
			.85						850-26		
			.9						850-25		
12*	20°	15°	.8						850-30		
			.85						850-29		
			.90						850-28		
13*	20°	15°	.8						850-33		
			.85						850-32		
			.90						850-31		

*Notes on Configuration

8. T.E. Flap gap open
9. T.E. flap gap open
10. Uprigged ailerons, 10°
11. Uprigged ailerons, 10°
12. Tail on, $i_t = 0°$
13. Tail on, $i_t = -8°$

COMMENTS:

845-19 WT test, fuselage nose GRIT on, wing GRIT off
845-20 WT test, fuselage nose GRIT on, wing GRIT at 0.10c

TABLE IV. LOAD FACTOR LIMITATION FOR PARTIAL EXTENSION OF TRAILING EDGE FLAP

Aircraft Weight - 38000 pounds

Flap Deflected 7.5°

Mach	Altitude	Velocity (kcas)	Load Factor
0.80	25,000 ft	340	4.3 (C_{Lmax} @ 4.6)
0.85	25,000 ft	360	4.5 (C_{Lmax} @ 5.1)
0.90	25,000 ft	385	4.8 (C_{Lmax} @ 5.7)
0.80	35,000 ft	270	3.1 (C_{Lmax})
0.85	35,000 ft	290	3.5 ($C_L$max)
0.90	35,000 ft	310	3.9 ($C_L$max)

Flap Deflected 15°

0.80	25,000 ft	340	3.75 (C_{Lmax} @ 4.7)
0.85	25,000 ft	360	3.5 (C_{Lmax} @ 5.2)
0.90	25,000 ft	385	3.0 (C_{Lmax} @ 5.8)
0.80	35,000 ft	270	3.2 (C_{Lmax})
0.85	35,000 ft	290	3.7 (C_L max)
0.90	35,000 ft	310	4.1 (C_{Lmax})

TABLE V. TEST SCHEDULE - NASA LANGLEY 7 BY 10 FOOT WIND TUNNEL - TEST NO. 845

Date 1968	Time	Run No.	Points	Wing Body Configuration	Mach	Max Angle of Attack	Sideslip	Transition Grit	P_s	P_t	$\frac{P_s}{P_t}$	Temp (°F)	Notes
10/11	1815	1	12-29	$L_0F_0A_0R$	.90	13.4°	0	30%	1288	2136		120	T.E. flap gap closed; CP_{10}, CP_{20}, Bad
	1930	2	33-51		.85	16.7°	0	30%	1358	2182		115	
	2010	3	52-70		.80	16.3°	0	30%	1416	2138		115	
	2115	4	73-91	$L_8F_0A_0R$	.90	13.6°	0	30%	1289	2138		120	
	2200	5	92-110		.85	16.8°	0	30%	1355	2137		119	
	2218	6	111-121		.80	12.2°	0	30%	1417	2138		114	
10/14	0915	7	134-150	$L_{20}F_0A_0R$	.90	12.6°	0	30%	1286	2133		121	
	1010	8	151-168		.85	14.7°	0	30%	1355	2137		118	
		9	169-187		.80	18.7°	0	30%	1417	2137		118	CP_{18} loose, $CP_{10} + CP_{11}$ stopped
	1410	10	190-203	$L_{20}F_{7.5}A_0R$	.90	10.4°	0	30%					Data deleted for possible trailin edge gap discrepancy
		11	204-218		.85	11.4°	0	30%					
		12	219-234		.80	12.4°	0	30%					
	1600	13	237-254	$L_8F_{7.5}A_0R$	.80	14.6°	0	30%					
10/15	0830	14	268-277		.90	10.4	0	30%					
		15	278-287		.84	11.4°	0	30%					
		16	300-310	$L_8F_0A_0R$	.85	9.9°	-6°	30%	1356	2138		110	
		17	311-321		.90	10.1°	-6°	30%	1289	2137		120	
		18	333-343		.80	9.8°	-6°	30%	1417	2139		103	
		19	355-367		.90	13.6°	0	OFF	1289	2138		119	GRIT off wings
		20	370-382		.90	13.6°	0	10%	1289	2139		122	GRIT at 10% chord

TABLE VI. TEST SCHEDULE - NASA LANGLEY 7 BY 10 FOOT WIND TUNNEL - TEST NO. 850

Date 1968	Time	Run No.	Points	Wing/Body Configuration	Mach	Max Angle of Attack	Sideslip	Transition Grit	P_s	P_t	$\frac{P_s}{P_t}$	Temp (°F)	Notes
12/9	1550	1	11-24	$L_{20}F_{7.5}A_0RG$	.80	15°	0°	30%	1414	2134	.6619	112	T.E. Flap gap open
12/10	0900	2	36-44		.90	10°	0°	30%	1296	2150		97	
	0930	3	45-54		.85	11°	0°	30%	1364	2152	.6295	93	
	1010	4	57-65	$L_{20}F_{7.5}A_0R$	.90	11°	0°	30%	1294	2151	.5907	90	T.E. flap gap closed
	1030	5	66-75		.85	11°	0	30%	1363	2151	.6290	93	
	1050	6	76-88		.80	14°	0	30%	1424	2151	.6582	92	
	1230	7	100-108		.90	10°	-6°	30%	1293	2149	.5897	93	
	1300	8	109-119		.85	13°	-6°	30%	1363	2149		95	
	1330	9	120-131		.80	14°	-6°	30%	1422	2149		96	
12/10	1600	10	134-141	$L_{20}F_{15}A_0R$	.90	10°	-6°	30%	1293	2150		91	
12/11	0900	11	153-161		.85	10°	-6°	30%	1363	2151		97	
	0918	12	162-172		.80	13°	-6°	30%	1424	2153		94	
	1105	13	186-193		.90	10°	0	30%	1296	2153		95	
	1120	14	194-201		.85	10°	0	30%	1362	2151		96	
	1135	15	202-212		.80	13°	0	30%	1423	2150		97	
	1400	16	215-222	$L_8F_{15}A_0R$	.90	10°	0	30%	1291	2146		97	
	1413	17	223-231		.85	10°	0	30%	1362	2149		94	
	1426	18	232-243		.80	14°	0	30%	1421	2147		97	
12/12	1025	19	255-264	$L_8F_{7.5}A_0R$	.90	12°	0	30%	1293	2146		96	
	1050	20	265-279		.85	15°	0	30%	1361	2148	.6335	93	
	1110	21	280-294		.80	17°	0	30%	1420	2147	.6613	93	
12/13	0840	22	310-321	$L_8F_{7.5}A_{-10}R$	.906	12°	0	30%	1284	2133	.6008	97	
	0905	23	322-334		.85	15°	0	30%	1354	2135	.6344	97	
	0920	24	335-349		.80	17°	0	30%	1413	2136	.6614	97	
	1115	25	352-359	$L_8F_{15}A_{-10}R$	.90	10°	0	30%	1282	2131	.6016	104	
	1124	26	360-370		.85	12°	0	30%	1352	2133	.6333	100	
	1138	27	371-387		.80	15°	0	30%	1411	2133	.6612	100	
12/13	1430	28	406-413	$L_{20}F_{15}A_0T_0$	.90	10°	0	30%	1280	2128	.6016	103	T.E. galp gap closed
	1450	29	414-421		.85	9°	0	30%	1351	2132	.6337	101	
	1507	30	422-431		.80	12°	0	30%	1410	2132	.6617	101	
12/16		31	443-452	$L_{20}F_{15}A_0T_{-8}$	.90	10°	0	30%	1226	2105	.6018	106	
		32	453-462		.85	12°	0	30%	1336	2109	.6326	90	
		33	463-475		.80	14°	0	30%	1396	2109	.6612	86	

TABLE VII. FLIGHT TEST INSTRUMENTATION - PHOTOPANEL

Hole No.	Item	Calibration		Figure No.
		Date	Curve No.	
	FLIGHT TEST CONDITION			
2	Airspeed, knots	1-30-68	10163034	
	Airspeed, knots	5-13-68	10163025	62
3	Altitude, feet	1-23-68	10263028	
	Altitude, feet	5-17-68	10263029	63
11	Total temperature, outside air	1-11-68	10463013	
	ENGINE OPERATING CONDITION			
8	Tachometer, rotor speed, low pressure	1-23-68	10563015	
		5-16-68	10563017	64
7	Tachometer, rotor speed, high pressure	1-23-68	10563016	
		5-16-68	10563018	65
	Primary intake duct total pressure losses			
19	Right inlet	1-22-68	10763091	
		5-15-68	10763096	66
20	Center	1-22-68	10763093	
		5-15-68	10763097	67
15	Left inlet	1-22-68	10763092	
		5-15-68	10763095	68
1	Burner pressure	Not calibrated		
10	Total pressure, turbine discharge	1-23-68	10663016	
		5-14-68	10663019	69
14	Temperature, turbine discharge	1-23-68	10863030	
		5-14-68	10863032	70
27	Total pressure, shroud cooling scoop	5-14-68	10663020	71
28	Static pressure, shroud cooling scoop	5-13-68	10263030	
24	Differential pressure, shroud cooling scoop	5-15-68	10763098	72

TABLE VII---Concluded

Hole No.	Item	Calibration		Figure No.
		Date	Curve No.	
21	Total Pressure, ejector exit	1-23-68	10663018	
22	Temperature, engine fuel	1-22-68 5-16-68	10863031 10863033	73
17	Temperature, afterburner fuel	1-23-68	10863029	
	AIRCRAFT WEIGHT AND BALANCE			
	Fuel Quantity remaining			
13	Forward tank		Liquidometer	
18	Main tank		Liquidometer	
23	Aft tank		Liquidometer	
	Fuel quantity used			
4	by engine		Counter 3	
4	by afterburner		Counter 4	
5	Fuel flow, fuel system		No calibration	
	FLIGHT CONFIGURATION			
6-(1)	Speed brake position	1-30-68	110630031	
6-(2)	L.E. flap position	5-24-68	110630023	
	FLIGHT ATTITUDE AND ACCELERATION			
12	Roll attitude		No calibration	
9	Normal acceleration at center of gravity		No calibration	
	EVENT CORRELATION			
9a	Clock		No calibration	
Lamp 5	Freeze button operation		No calibration	
Lamp 7	Afterburner operation		No calibration	
C-2	Correlation counter		Counter 2	

TABLE VIII. FLIGHT TEST INSTRUMENTATION - OSCILLOGRAPH

Channel No.	Item	Calibration		Galvo Type	Figure No.
		Date	Curve No		
	FLIGHT CONFIGURATION				
18	Stabilator position	6-10-68	5-063165	312	37
	Aileron position				
32	Right wing	5-24-68	51063011	315	38
3	Left wing	5-24-68	51063034	315	39
	Spoiler Position				
36	Right wing	5-24-68	51063057	342	40
2	Left wing	5-24-68	51063087	342	41
	FLIGHT ATTITUDE AND ACCELERATIONS				
12	Angle of attack	5-22-68	50363020	315	42
20	Angle of sideslip	5-22-68	50363045	315	43
6	Pitch rate		No calibration		
	Accelerations at center- of gravity				
22	Normal	5-21-68	51263076	351	
8	Axial	5-13-68	51263033	351	44
10	Lateral	5-13-68	51263018	351	45
	BUFFET PARAMETERS				
27	Pilot accelerations, normal at seat	5-21-68	51263075	351	46
	Tip accelerations,				
24	Right wing	5-13-68	51263078	312	47
15	Left wing	5-13-68	51263077	312	48
	Hinge Moments,				
11	Stabilator		No calibration		
30	Right aileron		21000-in.-lb/ 100kΩ		
7	Left aileron		21000-in.-lb/ 100kΩ		
31	Bending moment, left wing		No calibration		

TABLE VIII---Concluded

Channel No.	Item	Calibration		Galvo Type	Figure No.
		Date	Curve No.		
	0.95 Chord station, left wing surface pressures				
17	W.S. 95 top	5-16-68	50663039	341	50
5	W.S. 95 bottom	5-17-68	50663043	341	51
21	W.S. 135 top	No calibration			
26	W.S. 135 bottom	5-16-68	50663046	315	52
28	W.S. 175 top	5-17-68	50663041	341	53
33	W.S. 175 bottom	5-17-68	50663047	341	54
	0.85 chord station, left wing surface pressures				
14	W.S. 95 top	5-16-68	50663040	341	55
9	W.S. 95 bottom	5-16-68	50663042	315	56
19	W.S. 135 top	5-16-68	50663044	312	57
25	W.S. 135 bottom	5-16-68	50663045	315	58
29	W.S. 175 top	5-17-68	50663038	341	59
34	W.S. 175 bottom	5-17-68	50663037	341	60
	Wing station 105, left wing Boundary layer rake above wing top surface				
4	1 inch above	5-17-68	50663036G	315	61
13	2 inch above			315	61
16	3 inch above			315	61
23	4 inch above	5-20-68	50663048	315	61
	EVENT CORRELATION				
1	Freeze button operation				
1	Photopanel frame		0.05 sec blip		
Top edge	counter number				

TABLE IX. WIND TUNNEL INSTRUMENTATION
NASA LANGLEY 7 BY 10 FOOT HIGH SPEED TUNNEL

Data Channel	Item
	TEST CONDITION
44	Barometric pressure
45	Static pressure in test section
	TEST ATTITUDE AND BODY LOADS
47	Pitch angle
46	Yaw angle (manual input)
33	Angle of attack, Kistler balance
1	Normal force
2	Axial force
3	Pitching moment
4	Rolling moment
5	Yawing moment
6	Side force
	BUFFET PARAMETERS
	Wing bending moment fluctuations
40	Root-mean-square integration gain setting
14	Root-mean-square value over a 40-second time interval
	0.95 chord station, left wing surface pressures
845 850	NASA Test Series
8 21	W.S. 95 top
12 9	W.S. 95 bottom
	0.85 chord station surface pressures
845 850	NASA test series
None 20	Left W.S. 95 top
11 10	Left W.S. 95 bottom
7 19	Left W.S. 135 top
10 8	Left W.S. 135 bottom
9 22	Right W.S. 175 top
13 11	Right W.S. 175 bottom

TABLE IX.---Concluded

Data Channel		Item
		Wing station 135, left wing boundary layer rake referenced to flap trailing edge
845	850	NASA Test Series
15	None	0.350 inch below
16	12	0.160 inch below
17	13	0.030 inch above
18	15	0.230 inch above
19	16	0.450 inch above
20	17	0.625 inch above
21	18	0.800 inch above
22	None	0.960 inch above
		REFERENCE NUMBERS
39		Time
37		Test number
38		Run number
34		Test data point number
35		Mode of test
48		Test batch number

TABLE X. RESULTS FROM FLIGHT TEST PERFORMANCE PROGRAM 9130 VERSION 13

Flight 368, Run 2, Oscillograph Record 34, Photopanel Frame 16
Date of Flight: 23 May 1968, Time 0811, MRP Power
Altitude: 35,000 feet, Target Mach 0.835, Take-off Weight 40692 lb

v_i	= 305.5 knots	Indicated airspeed
n_1	= 92.6% rpm	Low pressure rotor speed
n_2	= 99.05% rpm	High pressure rotor speed
p_{T_e}	= 7.85 in. Hg	Total pressure, ejector exit
Δp_{2R}	= 8.90 in. H_20	Pressure loss, right intake duct
W_4	= 177 count	Fuel used by afterburner
H_i	= 34,280 feet	Indicated altitude
T_{a_i}	= 9.8°C	Outside air total temperature
$p_{T_{td}}$	= 31.45 in. Hg	Total pressure, turbine discharge
Δp_{2L}	= 8.45 in. H_20	Pressure loss, left intake duct
T_{22}	= 1°C	Temperature, engine fuel
T_{17}	= -1°C	Temperature, afterburner fuel
W_3	= 3897 count	Fuel used by engine
Δp_{2C}	= 16.50 in. H_20	Pressure differential, center intake duct
T_{td}	= 620°C	Temperature, turbine discharge
dW_3/dt	= 20.0	Engine fuel flow
dV/dt	= 8.4400	Axial acceleration
dH/dt	= -200	Rate of climb
V_{i_c}	= 303.5 knots	Corrected airspeed
V_c	= 307.7 knots	Calibrated airspeed
H_{i_c}	= 34,283 feet	Corrected altitude
H_p	= 34,683 feet	Pressure altitude

TABLE X---Continued

$p_a/p_{a_{ic}}$	= 0.981	Pressure correction ratio
$p_{a_{ic}}$	= 7.284 in. Hg	Corrected ambient pressure
p_a	= 7.147 in. Hg	Ambient pressure
M_{ic}	= 0.870	Corrected Mach number
ΔM_{pc}	= 0.018	Mach number correction
M	= 0.888	True Mach number
$p_{T_{td}}$	= 31.55 in. Hg	Total pressure, turbine discharge, corrected
p_{T_e}	= 8.05 in. Hg	Total pressure, ejector exit, corrected
Δp_{2L}	= 0.62 in. Hg	Pressure loss, left intake duct, corrected
Δp_{2R}	= 0.64 in. Hg	Pressure loss, right intake duct, corrected
Δp_{2C}	= 1.15 in. Hg	Pressure loss, center intake duct, corrected
T_{td}	= 618°C	Temperature, turbine discharge, corrected
T_{ic}	= -14.8°C	Outside air total temperature, corrected
T_{ic}	= 258.2°K	Outside air total temperature, corrected
p_{Te}	= 1.13	Total pressure, ejector exit
$p_{T_{td}}$	= 4.41	Total pressure, turbine discharge
n_1	= 6648.42 rpm	Low pressure rotor speed
n_2	= 9151.71 rpm	High pressure rotor speed
Δp_{T2L}	= 0.09	Pressure Loss, left intake duct
Δp_{T2R}	= 0.09	Pressure loss, right intake duct
$p_{T_{td}}$ to p_{T_2}	= 2.81	Pressure differential
T_{td}/T_{to}	= 3.44	Temperature ratio

TABLE X---Continued

F_{n_o}	= 12566.27 lb	Corrected net thrust, sea level
W	= 36712 lb	Aircraft weight
dW_3/dt	= 1200. lb/hr	Engine fuel flow
V_t	= 517.4 knots	True airspeed
V_t/W_3	= .4311	Airspeed/fuel flow
dW_3/dt	= 3175	Corrected fuel flow
.941		RT2/RTO
255.0		Corrected airflow, lb/sec
243.5		Max. corrected airflow, lb/sec
5011.		Net thrust, total lb
-2672.		Required net thrust, lb
2780.		Primary ram drag, lb
84.		Secondary ram drag, lb
7933.		Gross thrust, primary, lb
92.		Gross thrust, secondary, lb
258.9		T_{to} °C Outside air total temperature, corrected
1.5		Normal load factor, a_{z_B}
8.7		Angle of attack, degrees
.34195		Lift coefficient at 1g level flight
-.02489		Drag coefficient
.01687		Induced drag coefficient
-.04177		Profile drag coefficient
351.0		Corrected fin duct ram drag, sea level
84.0		Fin duct ram drag
11.403		Total pressure shroud cooling scoop, in. Hg
9.928		Static pressure, shroud cooling scoop, in. Hg
1.149		Total/static, shroud cooling scoop, in. Hg
.4492		Mach, cooling scoop
19.32157		Corrected airflow, cooling scoop, sea level
5.5042		Corrected cooling scoop airflow
626.		Corrected cooling scoop ram drag
149.		Cooling scoop ram drag

TABLE X---Concluded

1.475	$p_T - p_S$, cooling scoop, in. Hg
11.403	p_T, shroud cooling scoop, in. Hg
9.928	p_S, shroud cooling scoop, in. Hg
11.931	p_T, nose boom
0.957	p_T/p_{T_o}, shroud cooling scoop

TABLE XI. BUFFET CHARACTERISTICS OF THREE F-105F CONFIGURATIONS

Configuration	1	2	3
Leading edge flap position	0°	8°	8°
Trailing edge flap position	0°	0°	7.5°
Onset of buffet			
Buffet at pilot's seat			
Angle of attack			
Pilot signal	9.5°	9.0°	12.0°
Accelerometer	6.5°	6.3°	8.0°
Normal force			
Pilot signal	0.83	0.61	0.74
Accelerometer	0.56	0.45	0.64
Aileron hinge moment			
Angle of attack	5.0°	6.2°	4.8°
Normal force	0.35	0.43	0.49
Trailing edge pressures			
Angle of attack (tunnel)	4.5°	8.0°	6.7°
Angle of attack (flight)	5.5°	7.0°	7.0°
Normal force (tunnel)	.31	.56	.63
Normal force (flight)	.5	.5	.64
Wing root bending			
Angle of attack (tunnel)	3.4°	6.3°	6.0°
Normal force (tunnel)	.23	.43	.57

APPENDIX II

ILLUSTRATIONS

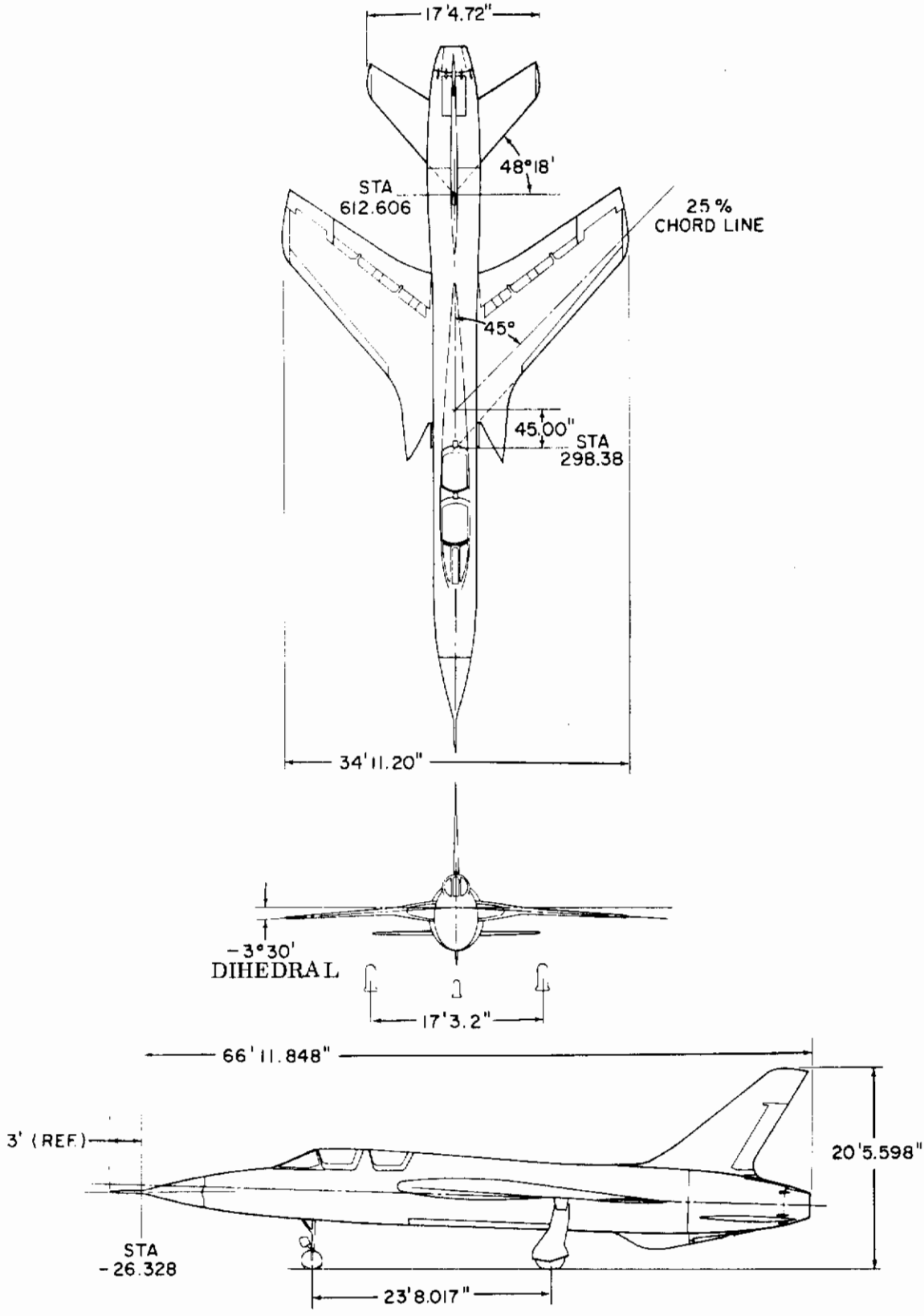

Figure 1. Three-View - F-105F Two-Place Fighter-Bomber

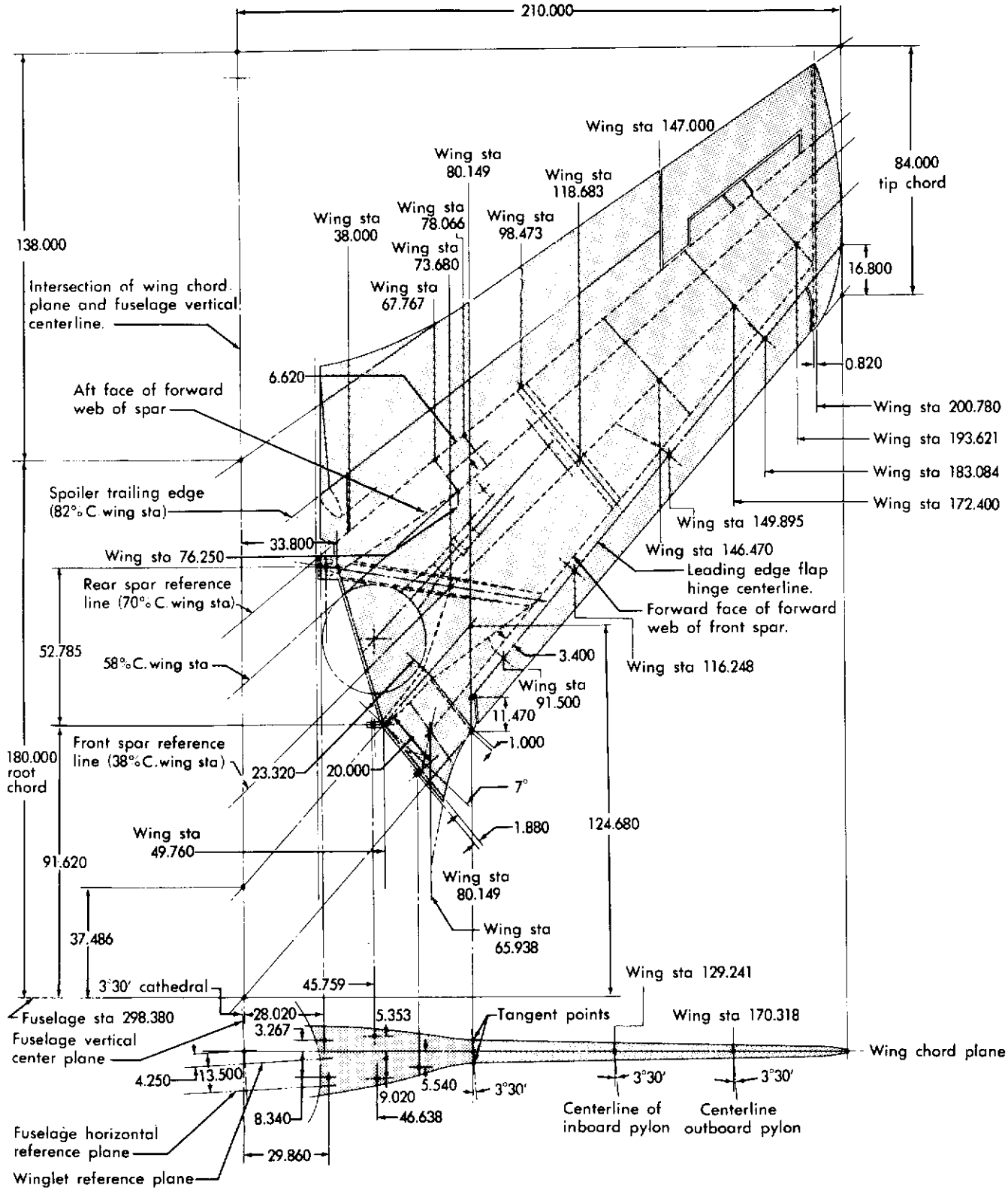

Figure 2. Plan View - Basic F-105F Wing

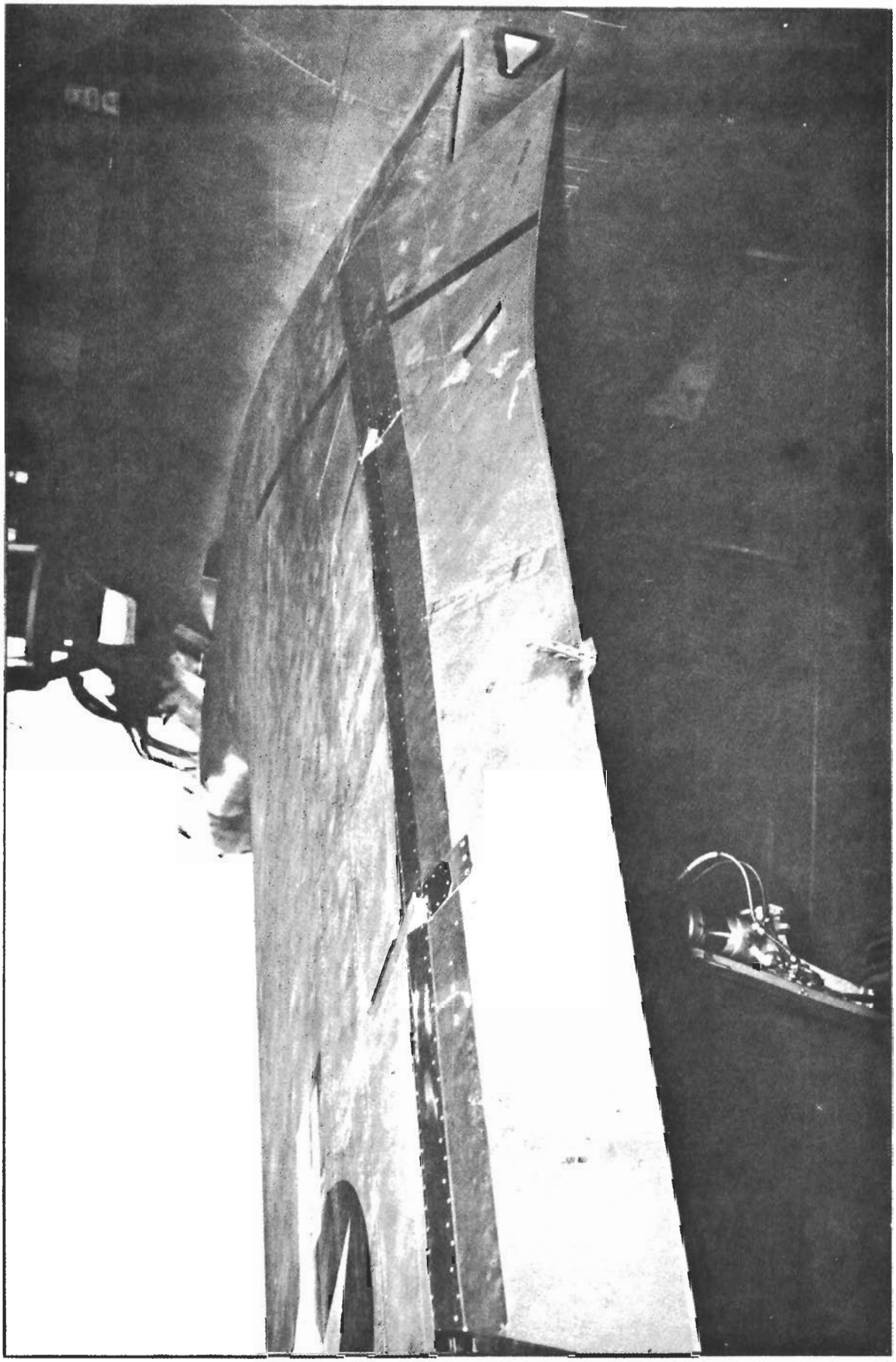

Figure 3. Left Wing Top Surface with Details of 15° Trailing Edge Flap Deflection and Flap Gap Seal Covers

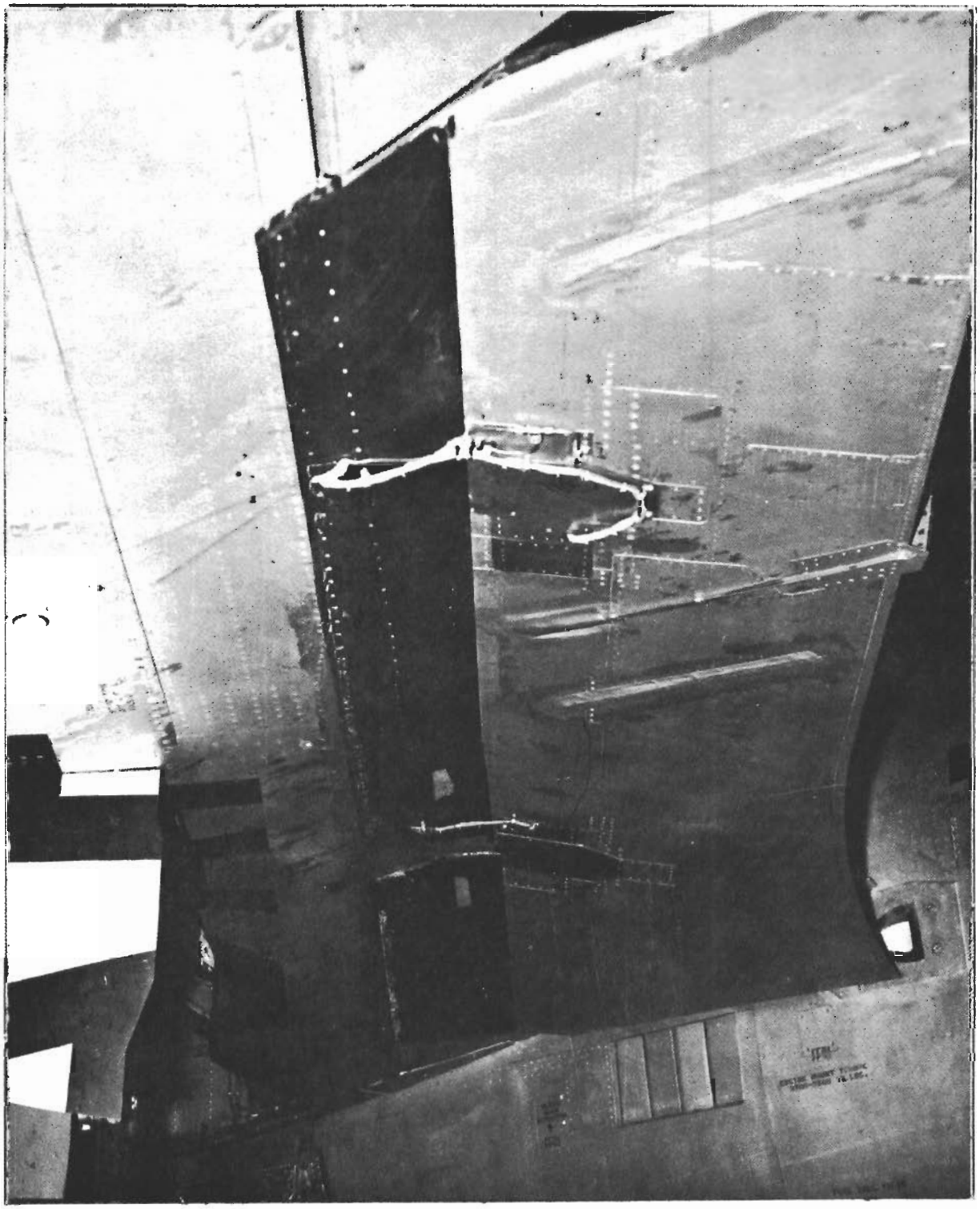

Figure 4. Left Wing Bottom Surface with Details of 15° Trailing Edge Flap Deflection and Flap Gap Seal Covers

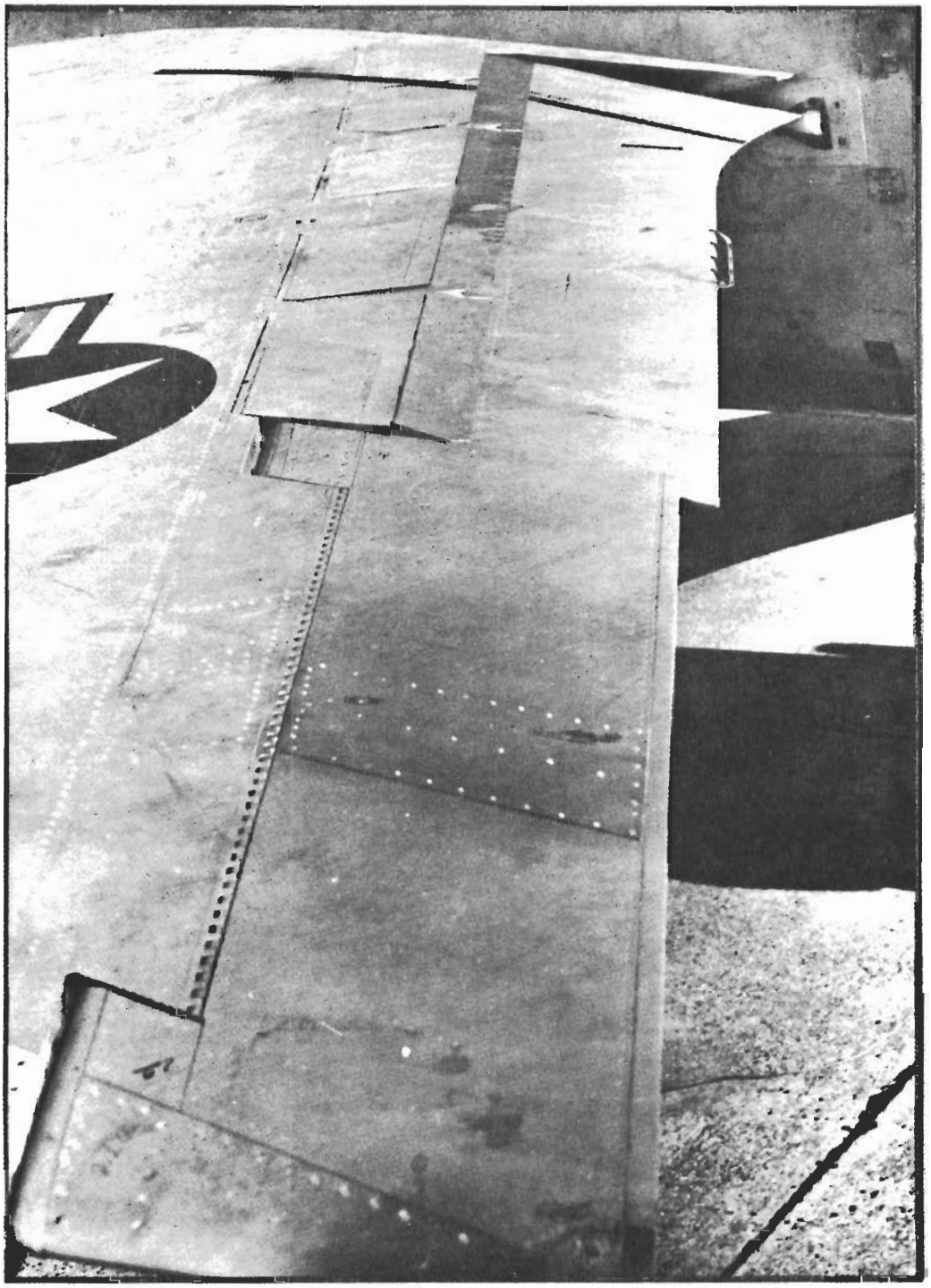

Figure 5. Left Wing Top Surface with Details of 7.5° Trailing Edge Flap Deflection and Flap Gap Seal Covers

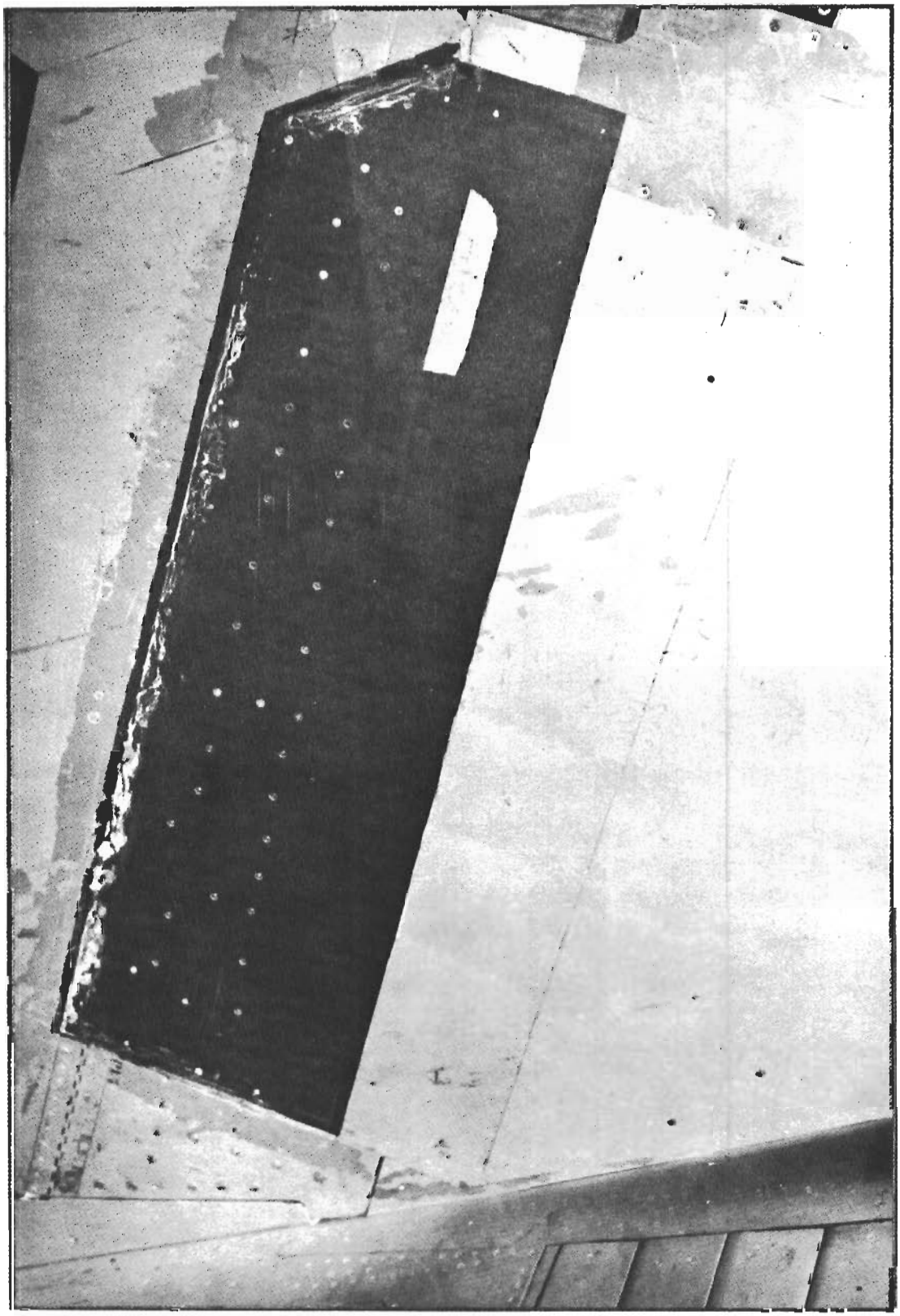

Figure 6. Left Wing Bottom Surface with Details of 7.5° Trailing Edge Flap Deflection and Flap Gap Seal Covers

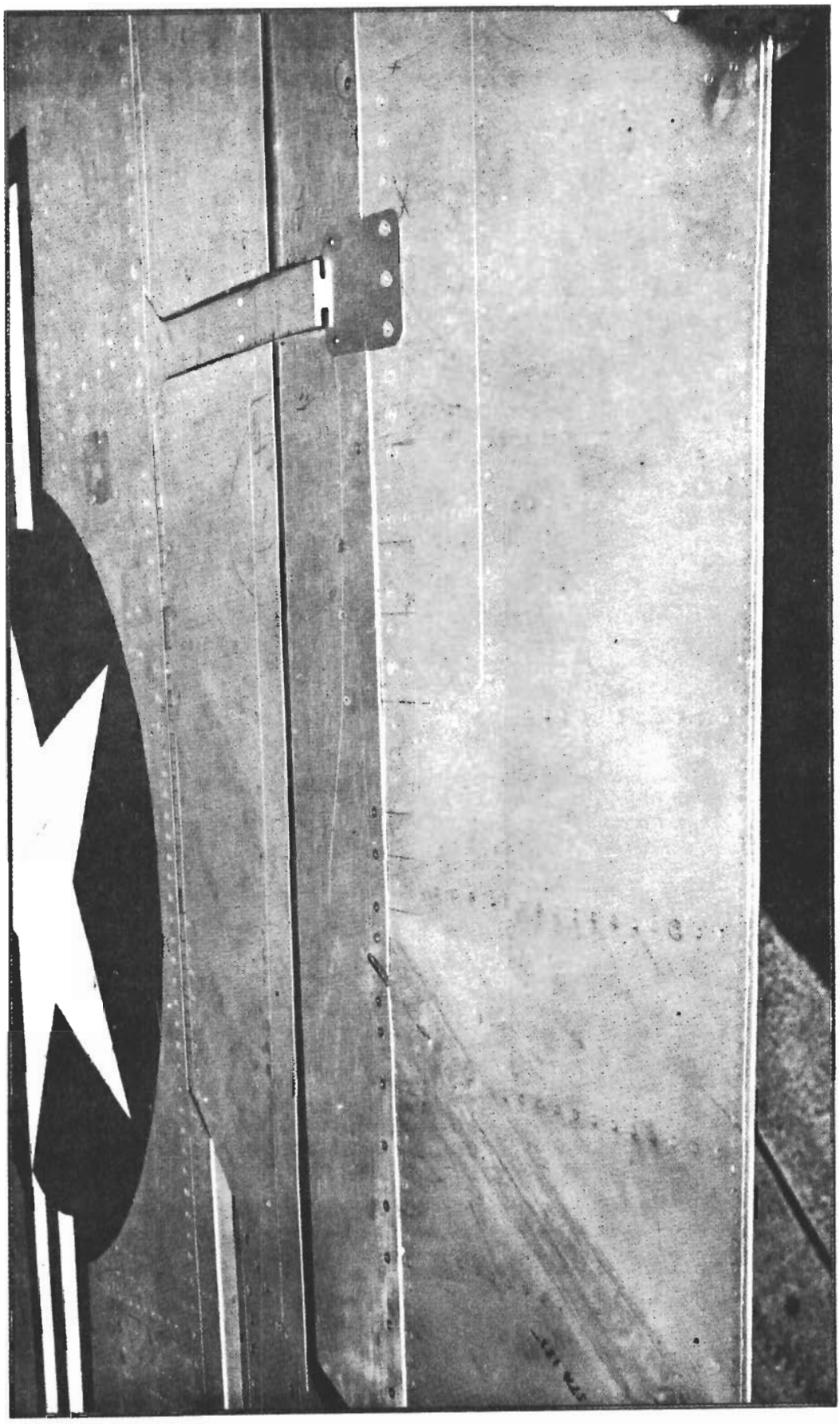

Figure 7. 7.5° Trailing Edge Flap Deflection with Details of Upper Surface Flap Gap Seal Cover

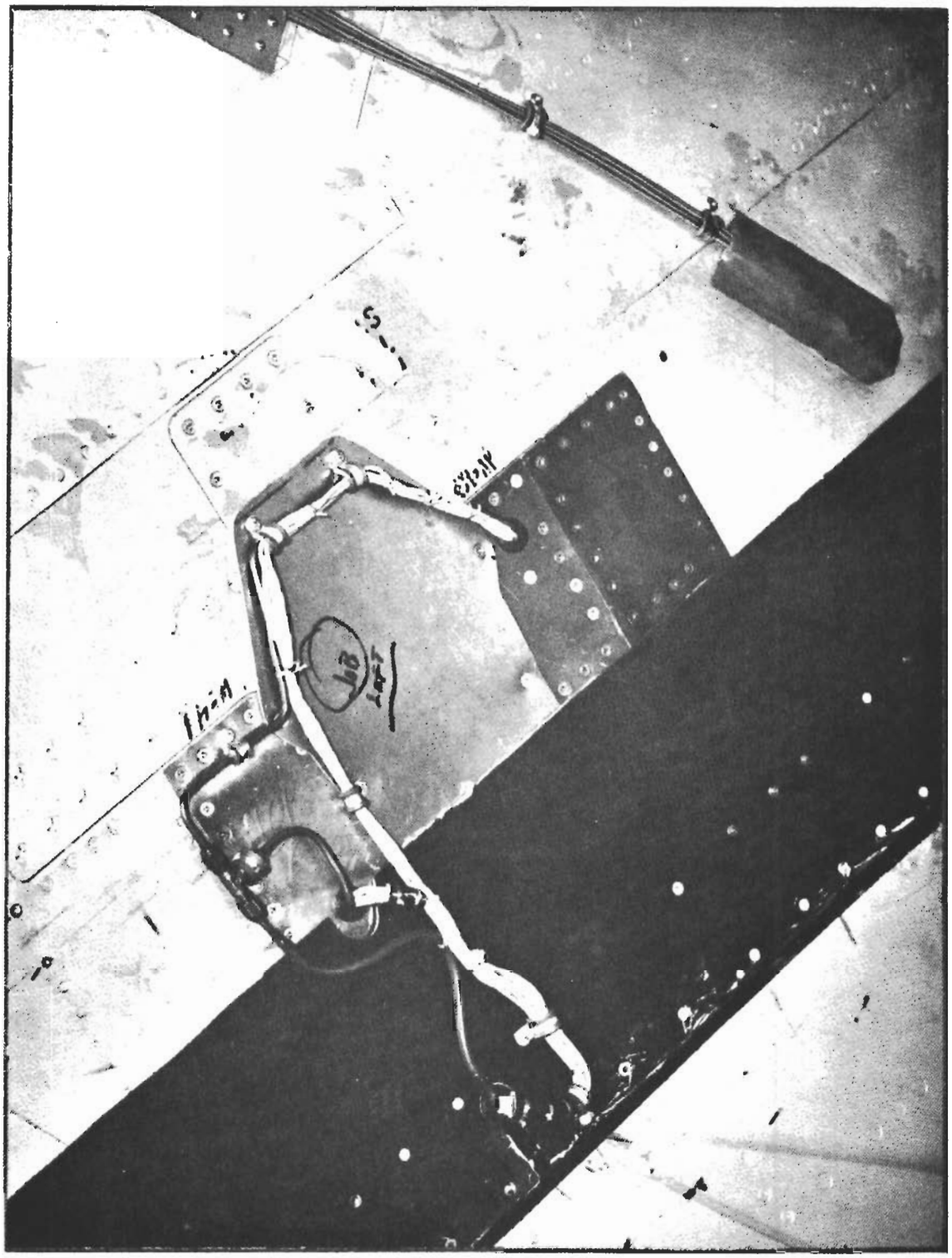

Figure 8. Installation Details of Pressure Instrumentation on Bottom Surface of Left Wing Near Wing Station 135

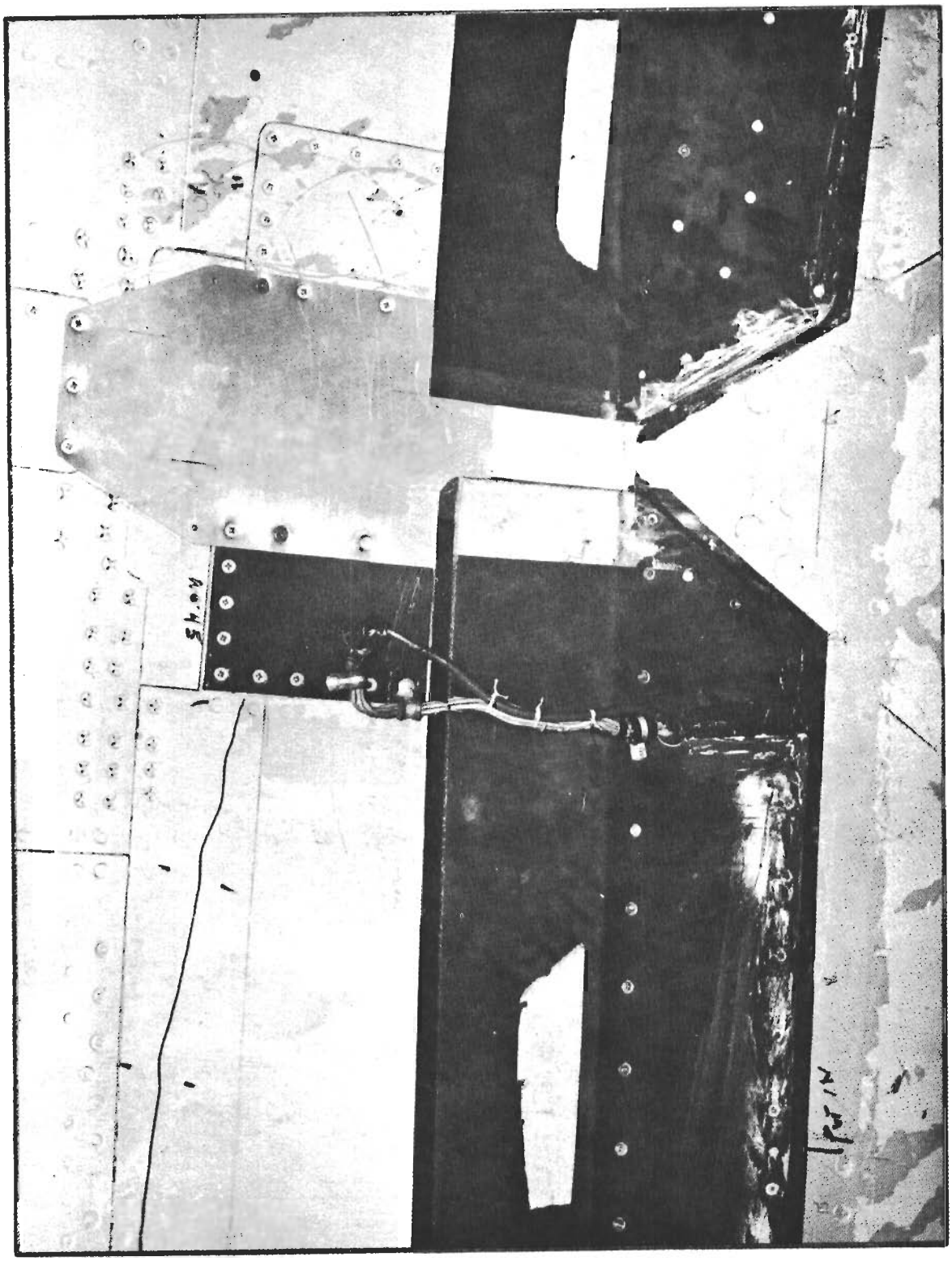

Figure 9. Installation Details of Pressure Instrumentation on Bottom Surface of Left Wing Near Wing Station 95

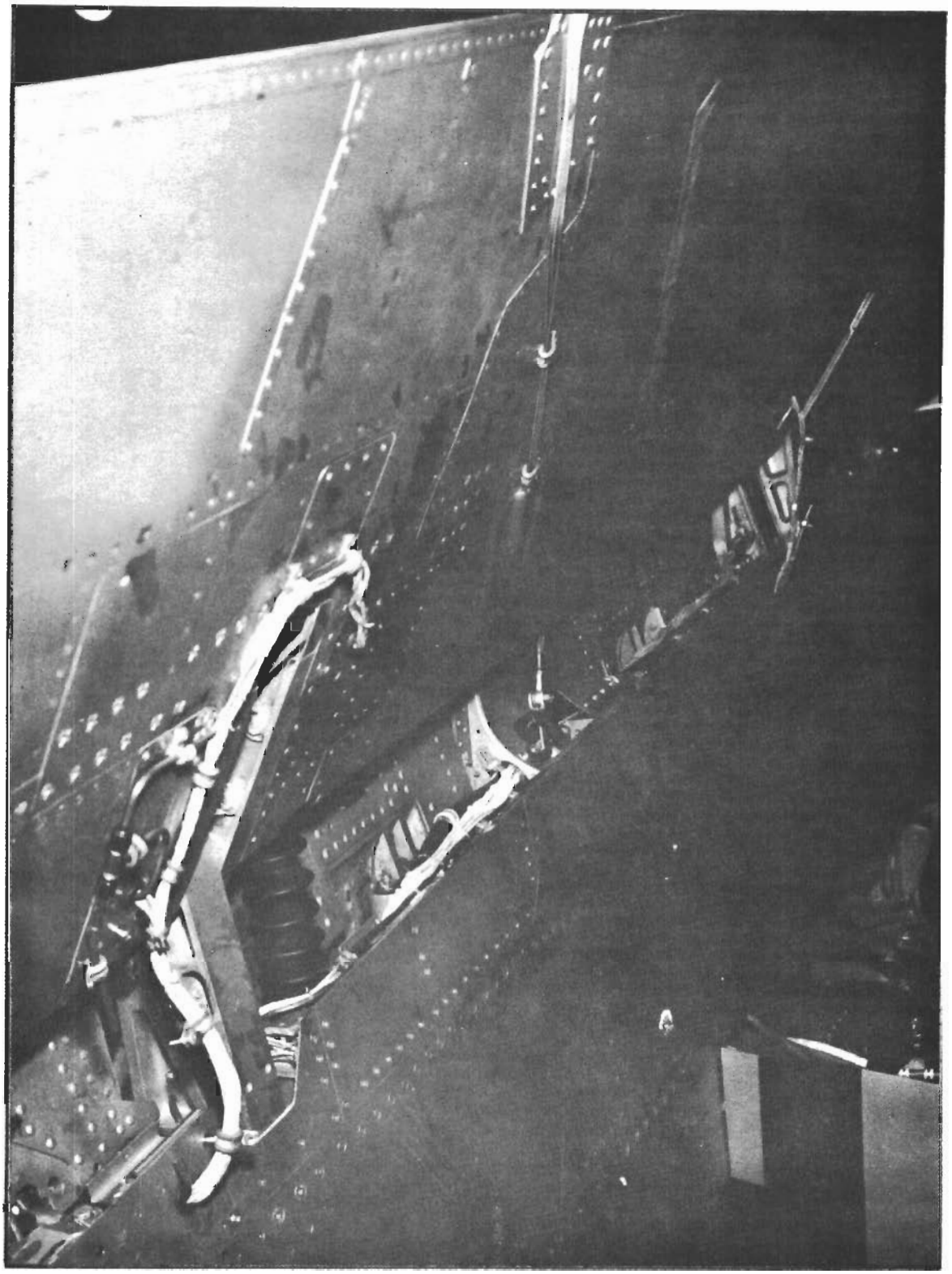

Figure 10. Plumbing and Wiring Details of Pressure Instrumentation on Bottom Surface of Left Wing Near Wing Station 125. Gap Seal Cover Off

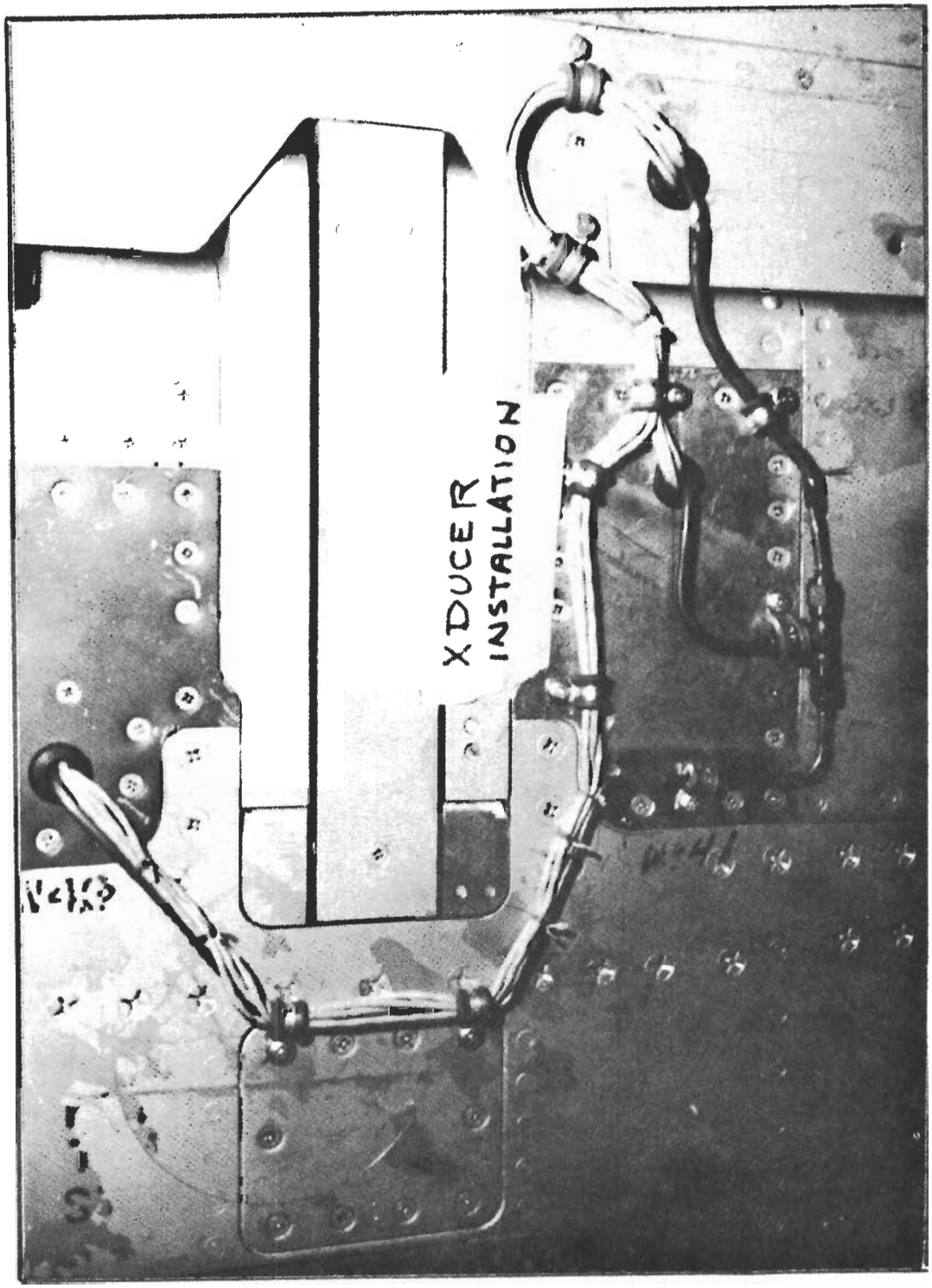

Figure 11. Plumbing and Wiring Details of Pressure Instrumentation on Bottom Surface of Left Wing Near Wing Station 125

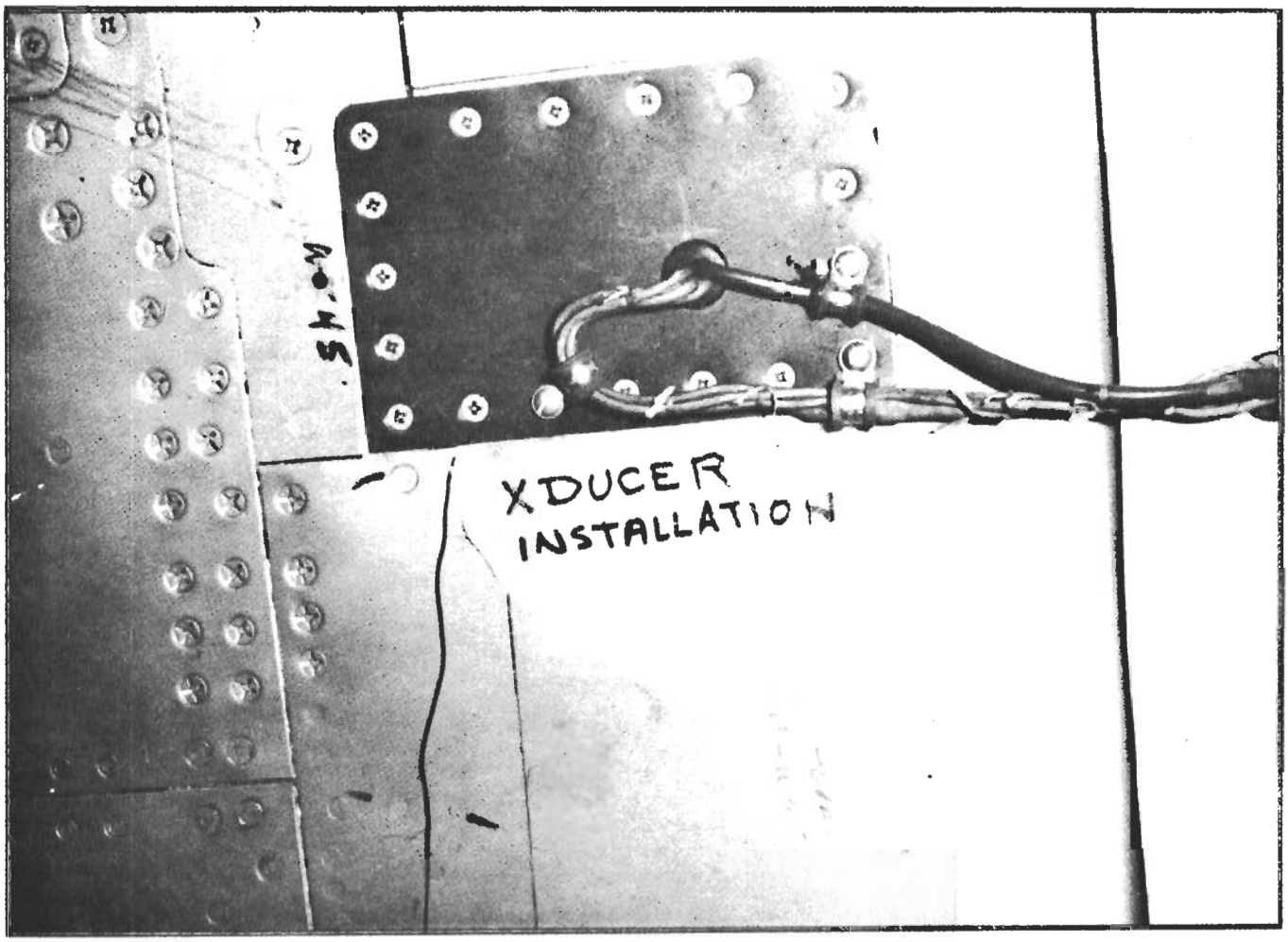

Figure 12. External Plumbing and Wiring Details of Pressure Instrumentation of Bottom Surface of Left Wing Near Wing Station 95

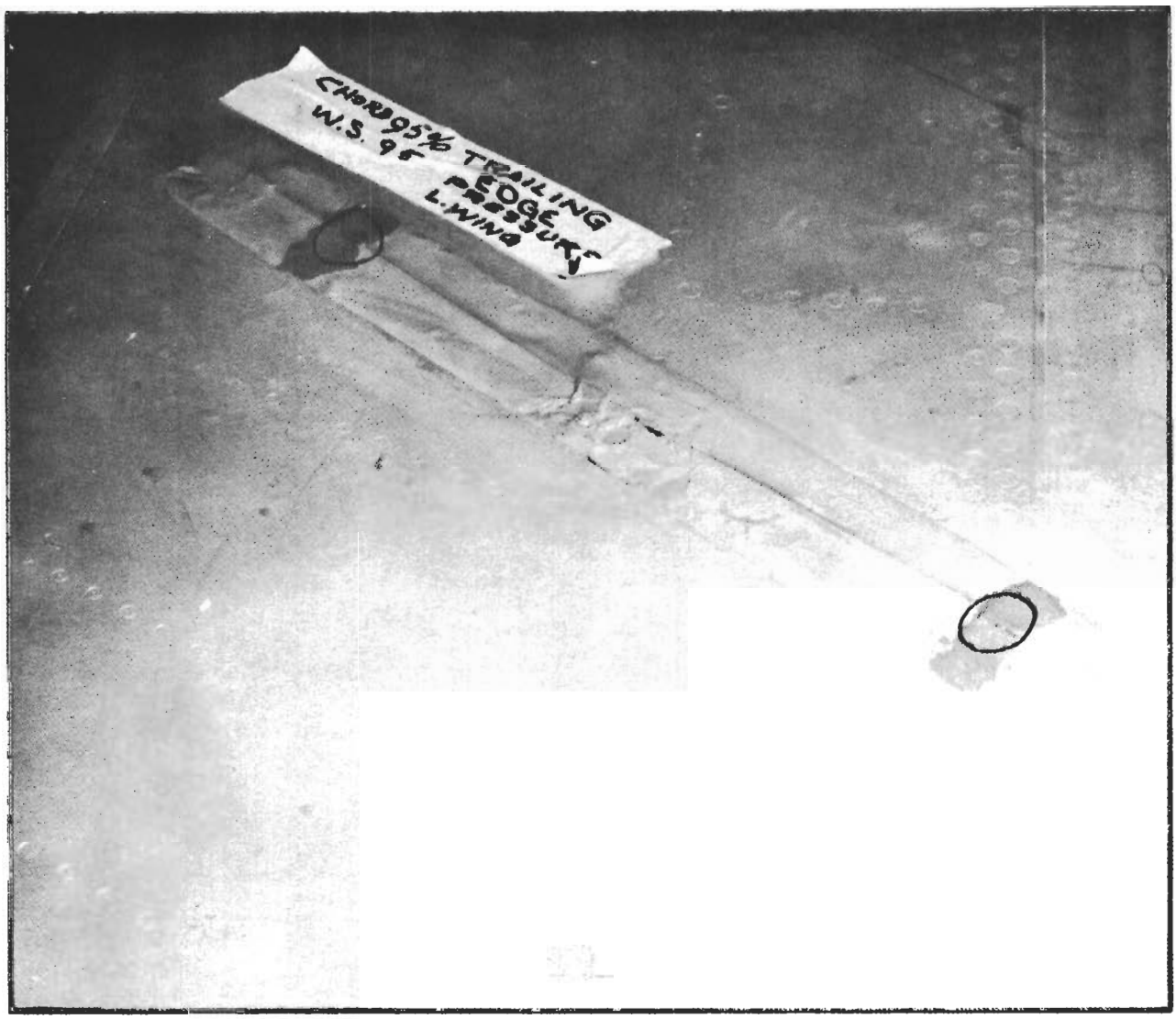

Figure 13. Static Pressure Ports on Top Cover of Left Wing Trailing Edge Flap Near Wing Station 95

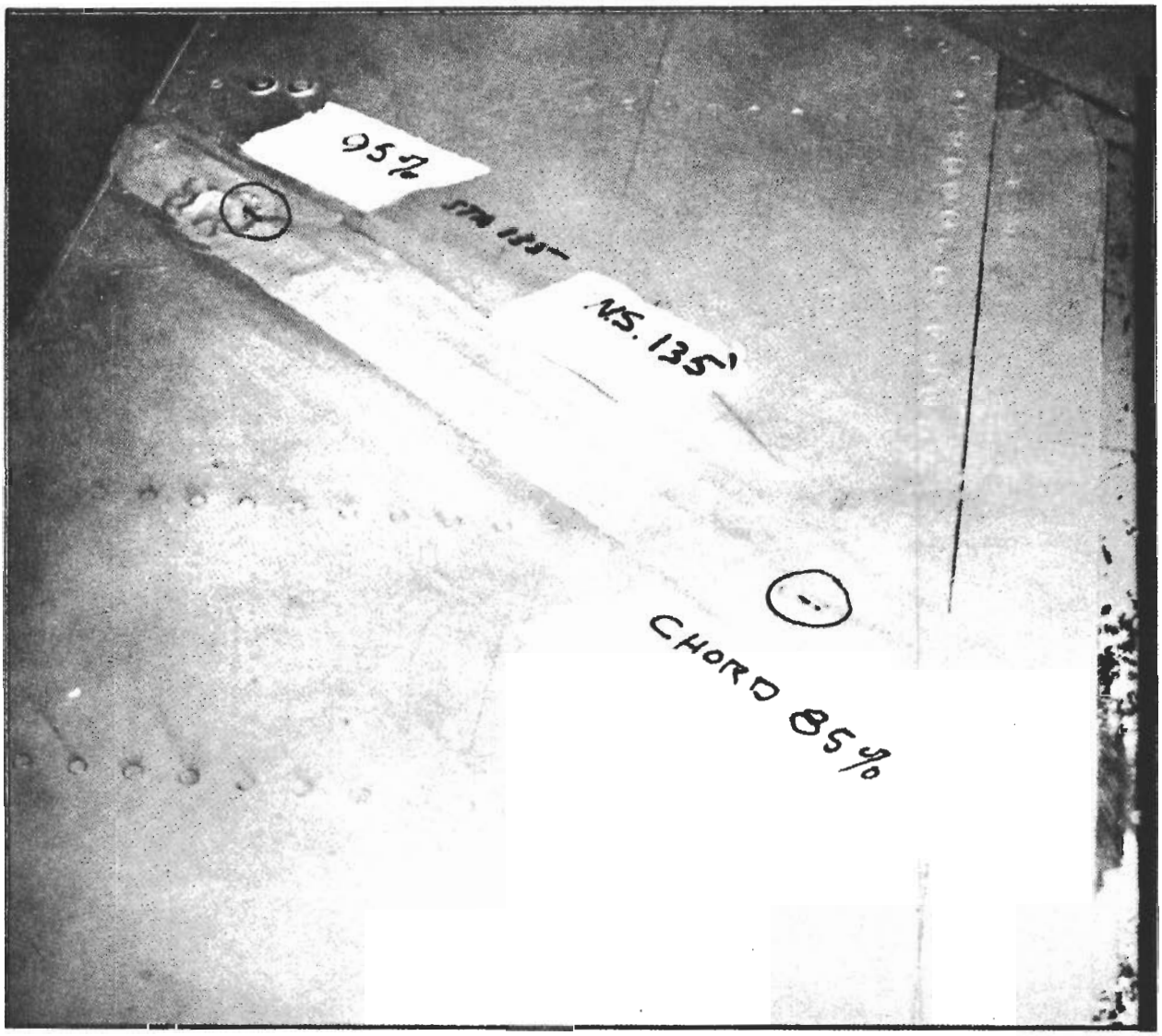

Figure 14. Static Pressure Ports on Top Cover of Left Wing Trailing Edge Flap Near Wing Station 135

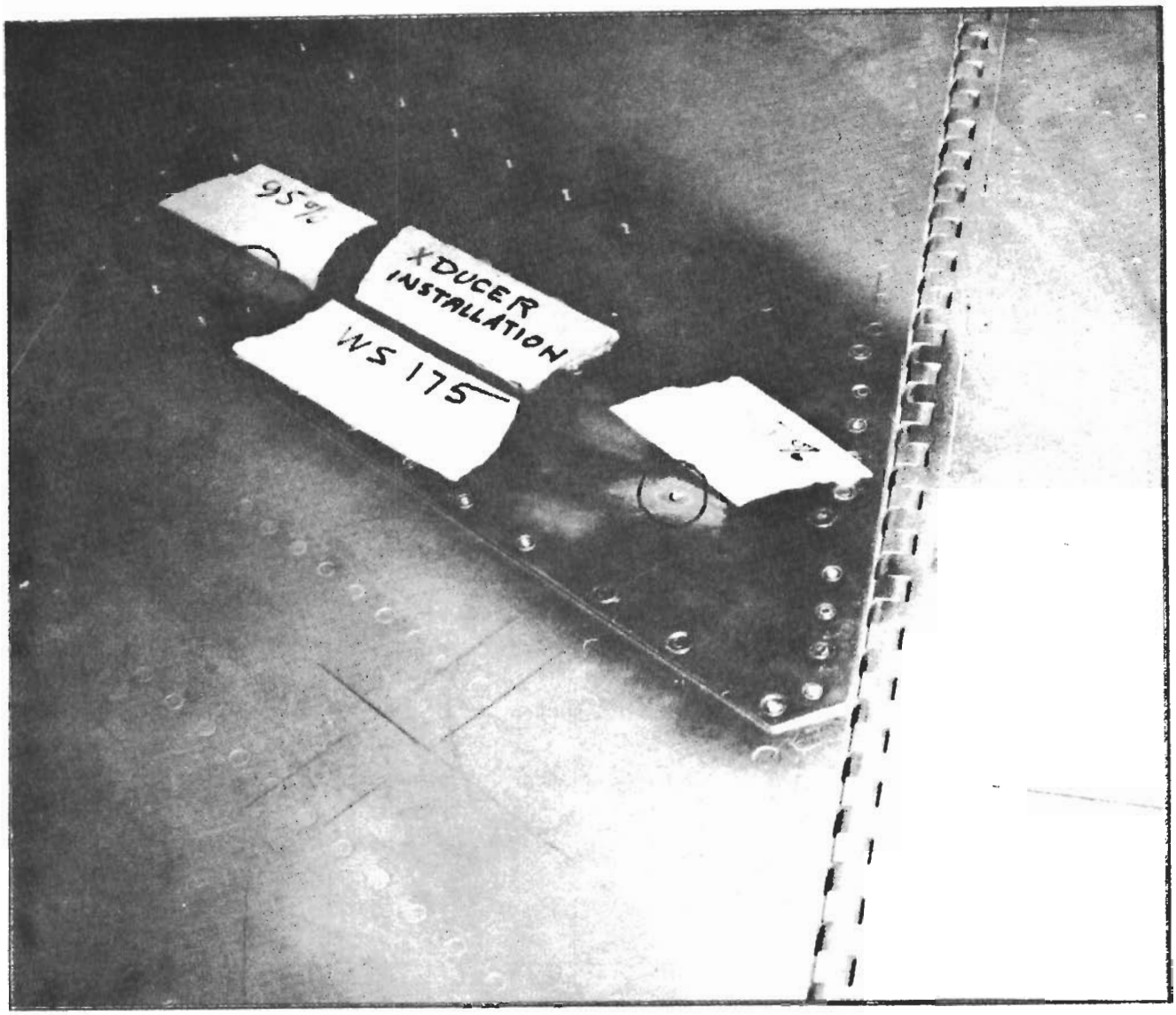

Figure 15. Static Pressure Ports on Top Cover of Left Wing Aileron Near Wing Station 175

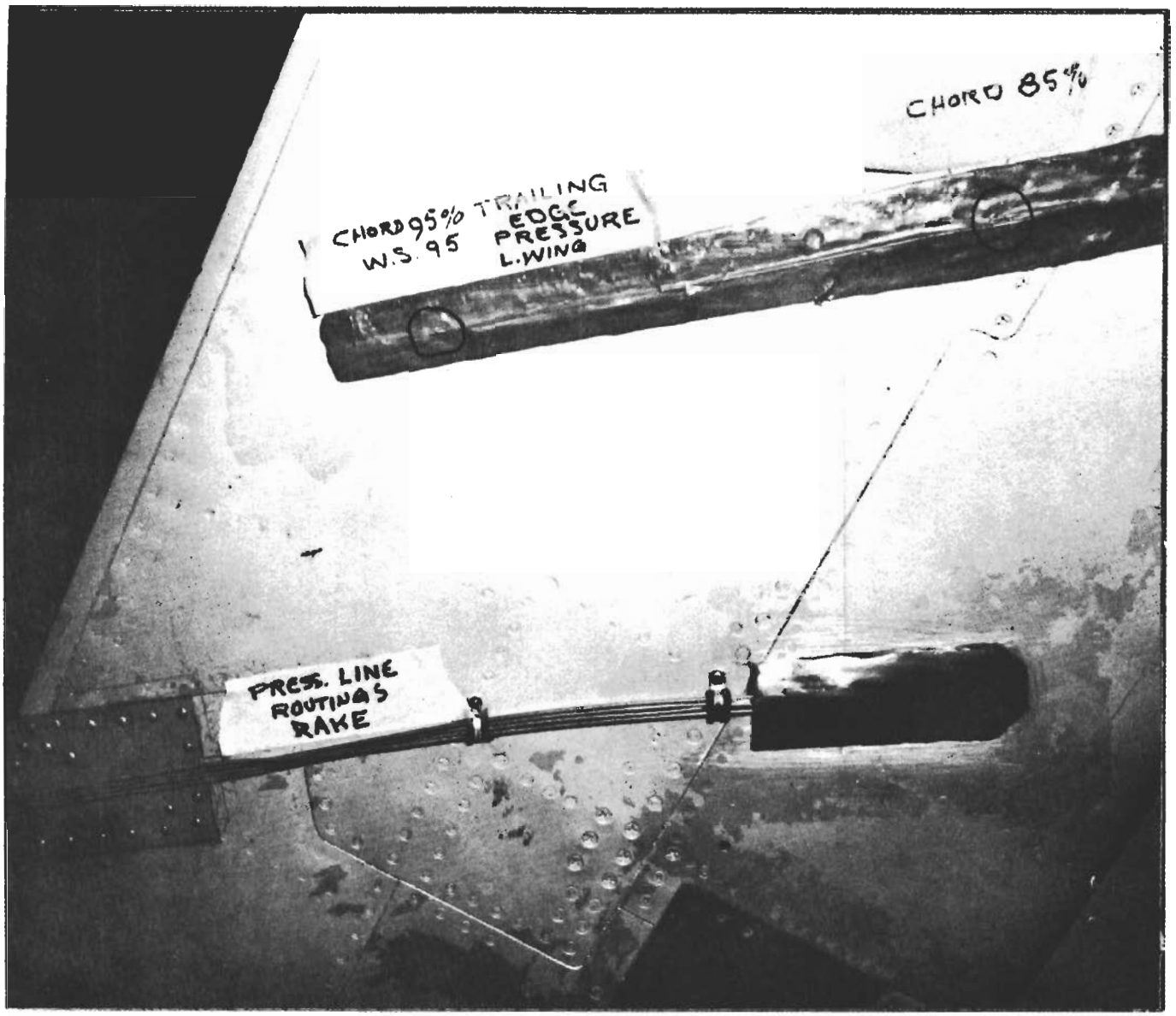

Figure 16. Static Pressure Ports on Bottom Cover of Left Wing Trailing Edge Flap Near Wing Station 95. Pressure Line Routings to Boundary Layer Rake also Shown

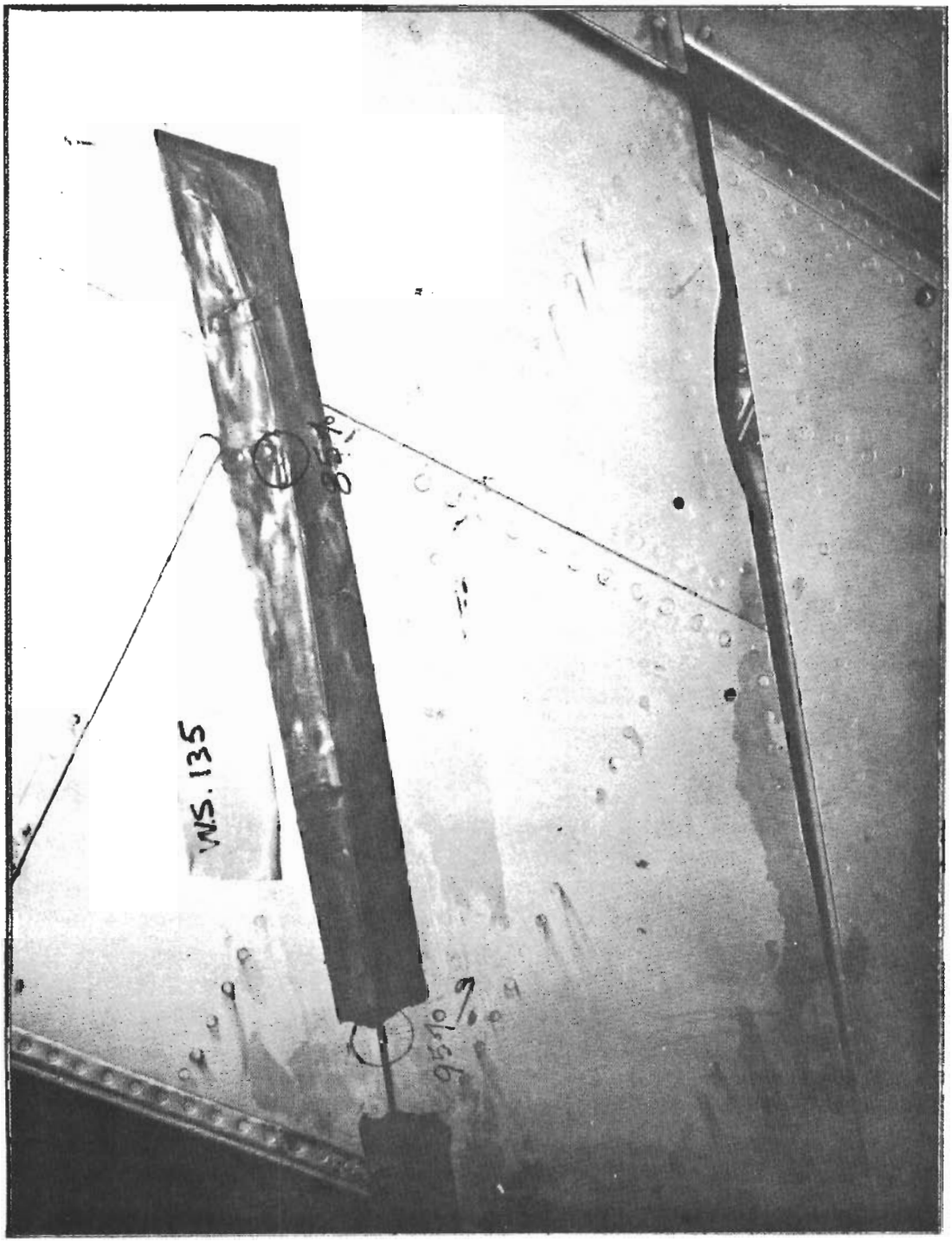

Figure 17. Static Pressure Ports on Bottom Cover of Left Wing Trailing Edge Flap Near Wing Station 135

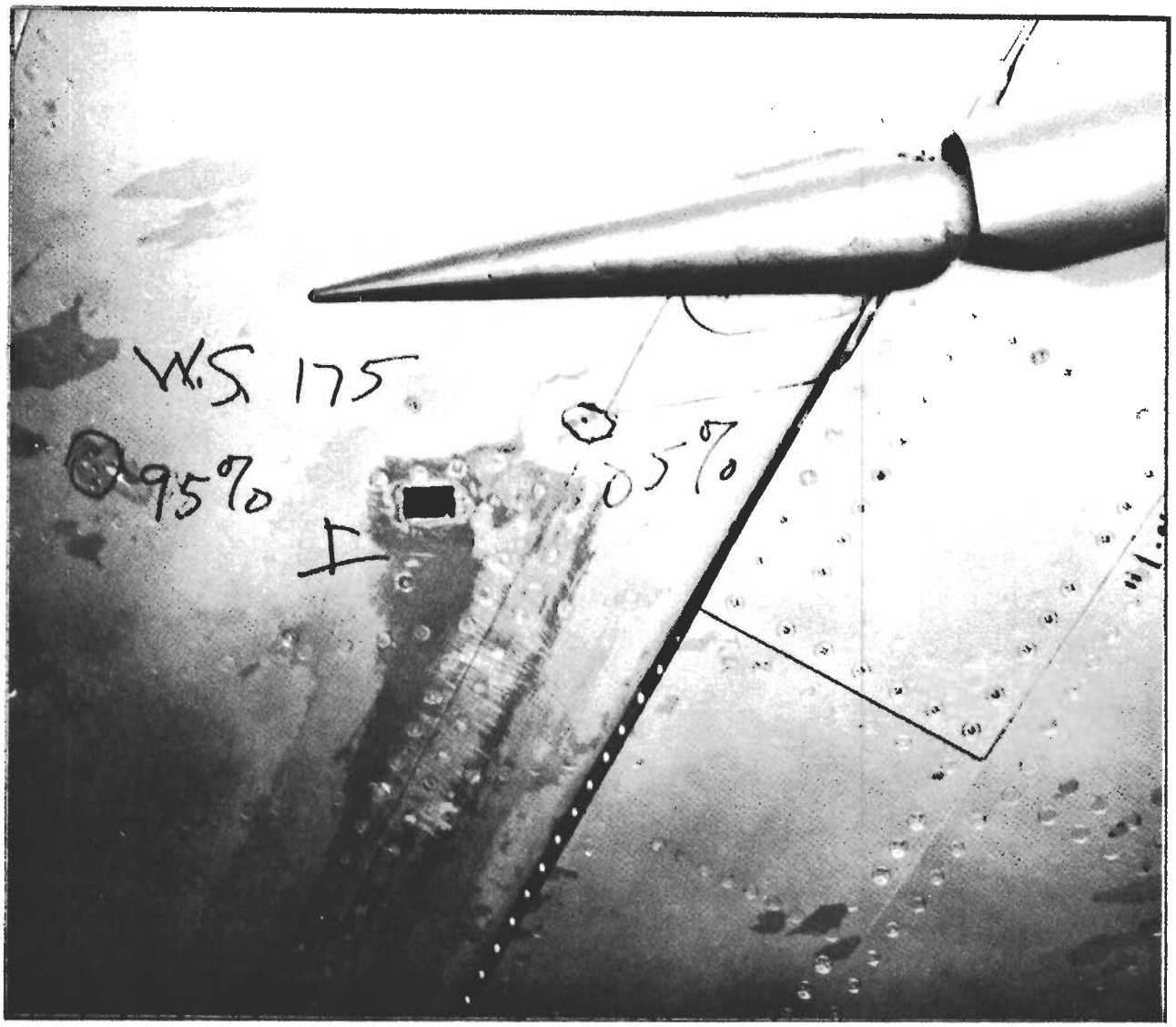

Figure 18. Static Pressure Ports on Bottom Cover of Left Wing Aileron Near Wing Station 175

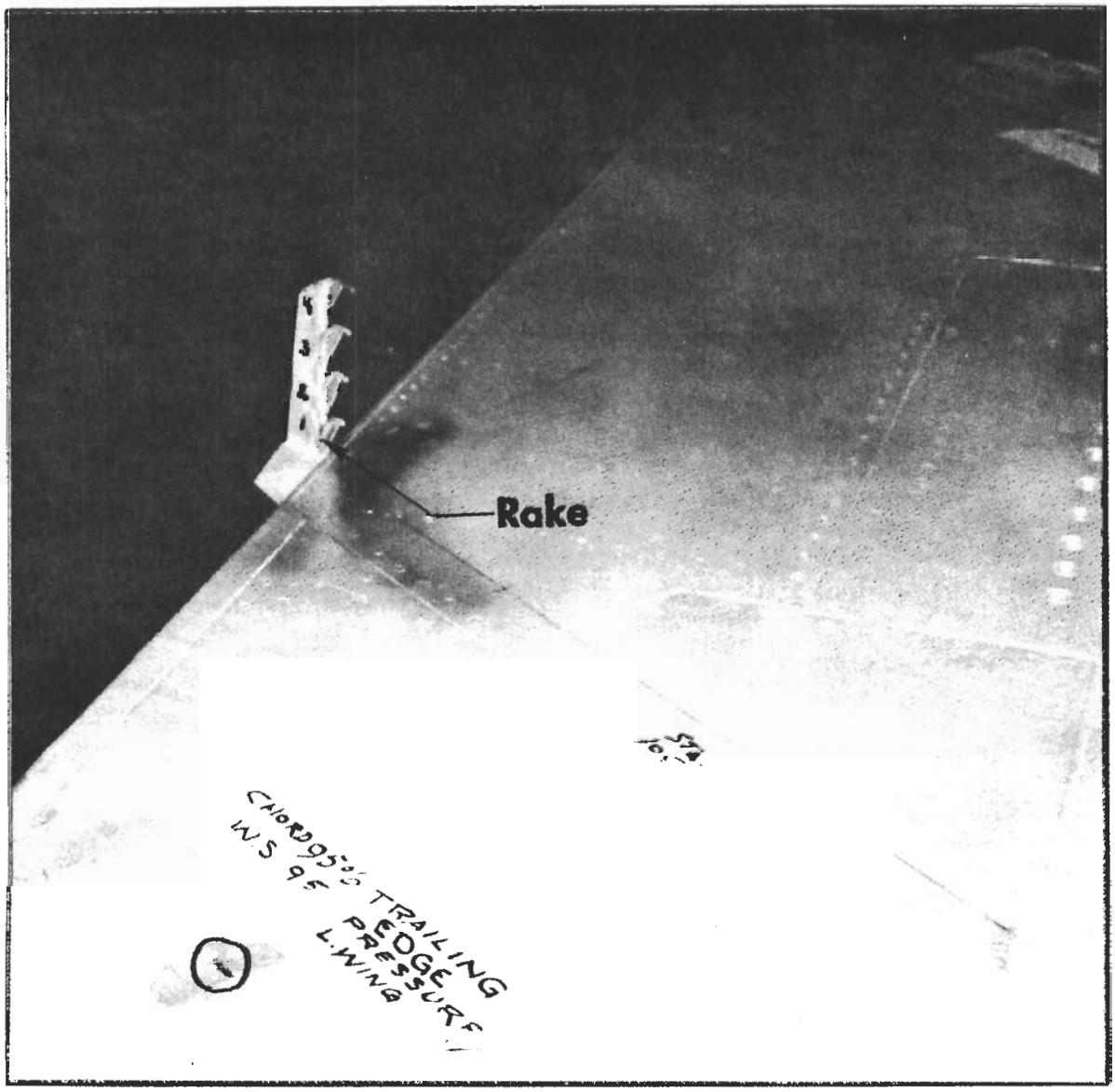

Figure 19. Boundary Layer Pressure Rake above Top Cover of Left Wing Trailing Edge Flap Near Wing Station 105. The Total Pressure Probes are 1, 2, 3, and 4 Inches above the Surface

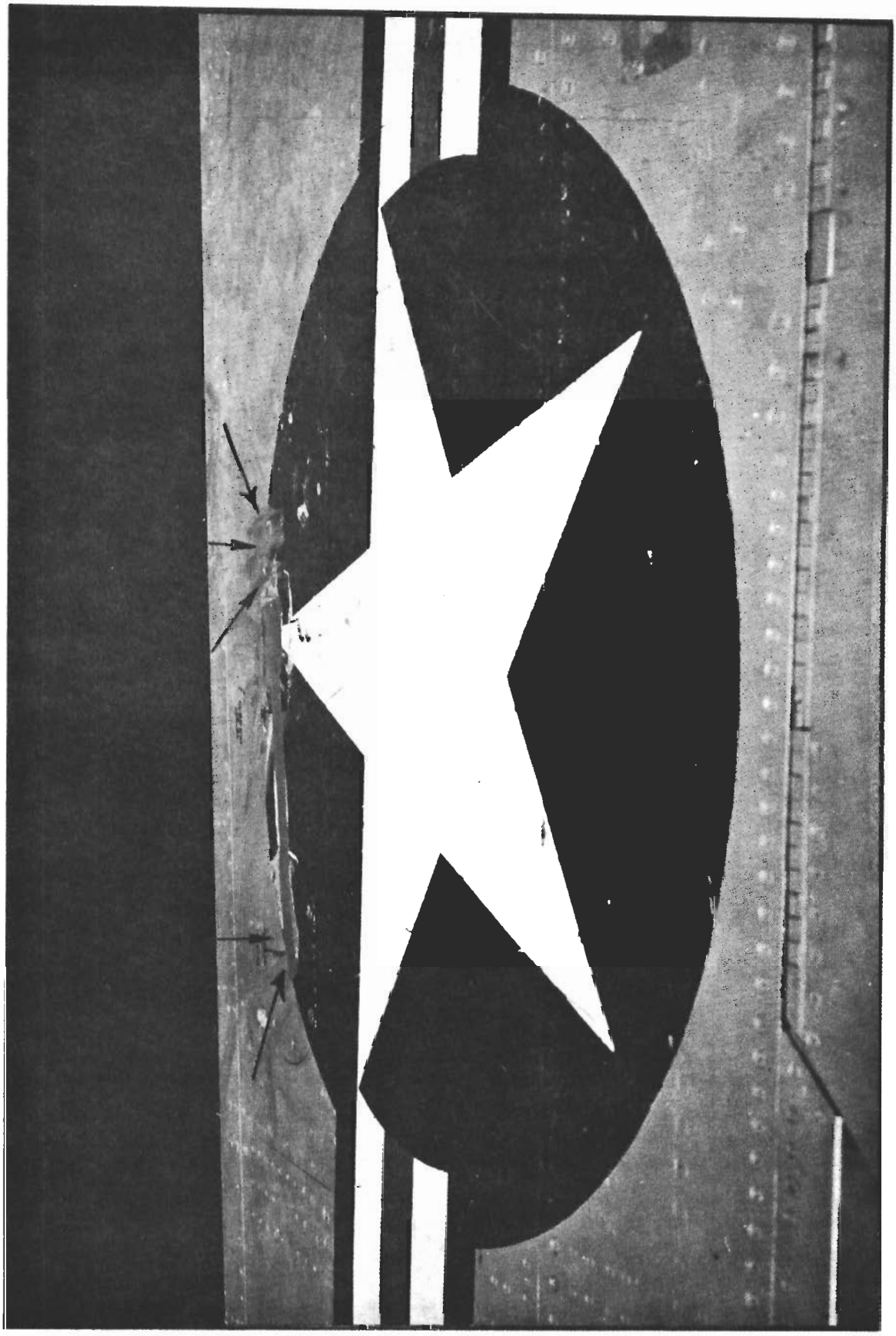

Figure 20. Strain Gage Installation for Measuring the Bending Moment of the Outer Portion of the Left Wing Panel. Top Cover

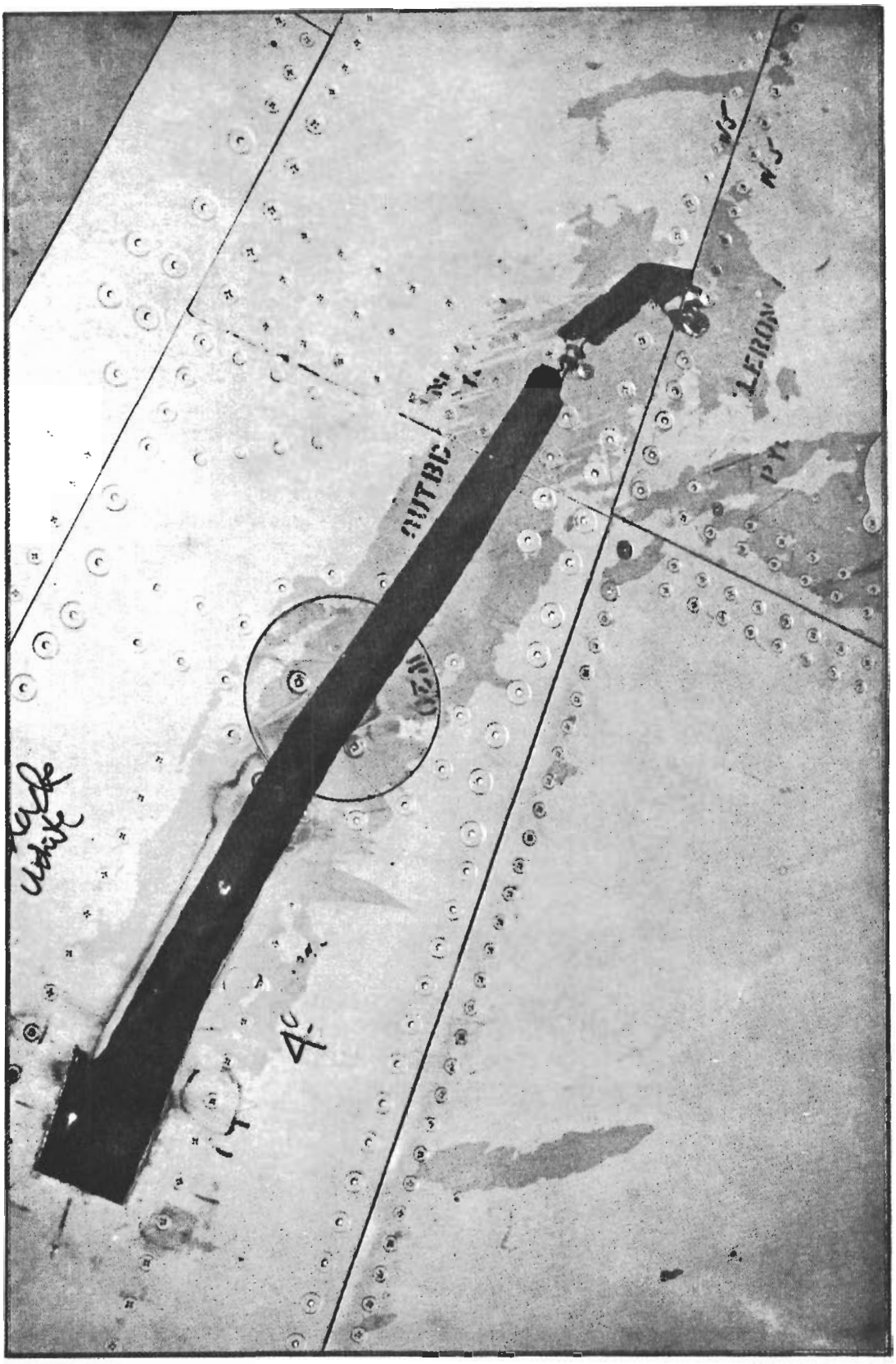

Figure 21. Strain Gage Installation on Left Wing Bottom Cover for Measuring the Bending Moment of the Outer Portion of the Panel

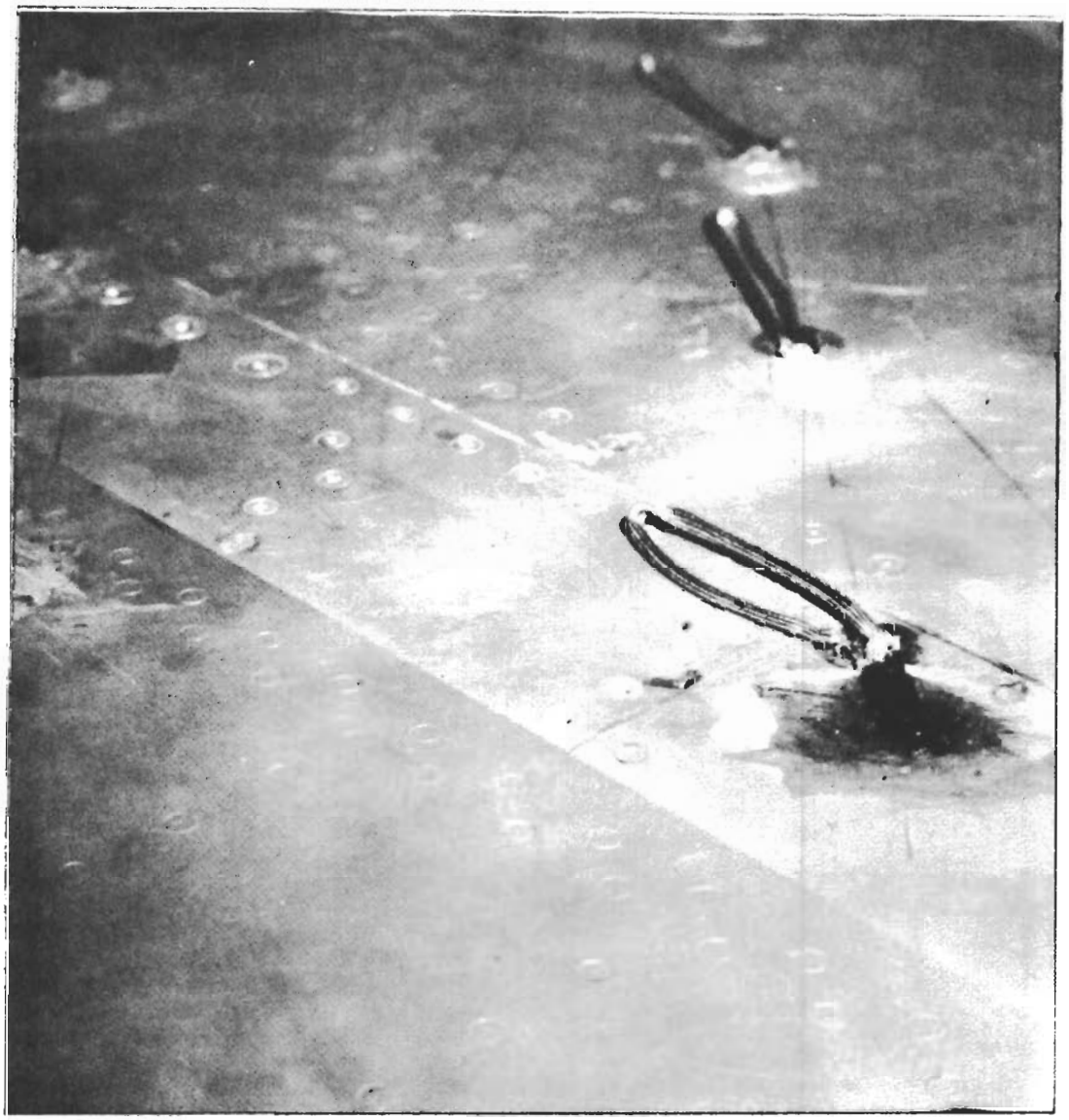

Figure 22. Tuft Installed on Top Cover of the Right Wing Epoxy Anchor and Loop Details

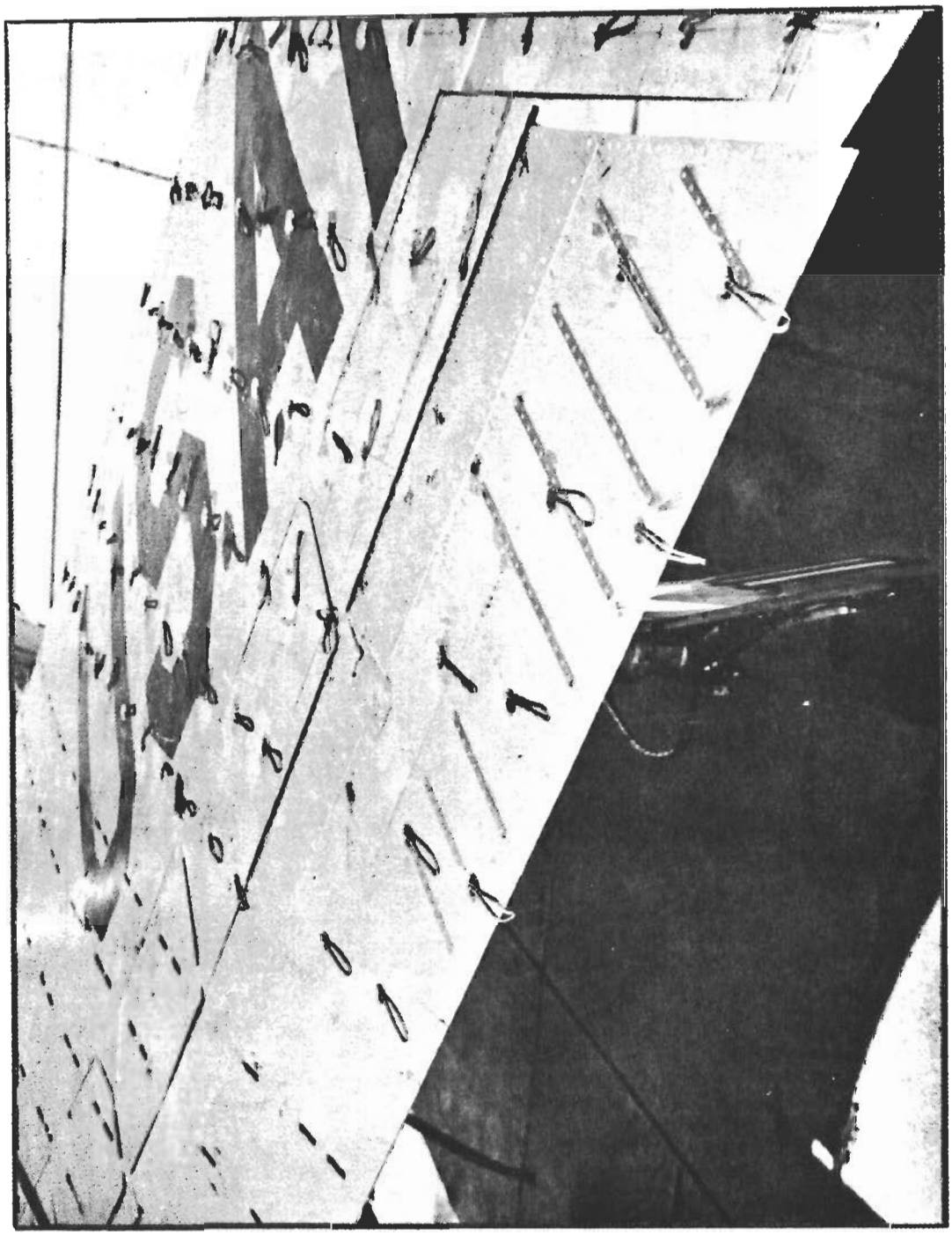

Figure 23. Tuft Installation Pattern on Top Cover of the Right Wing

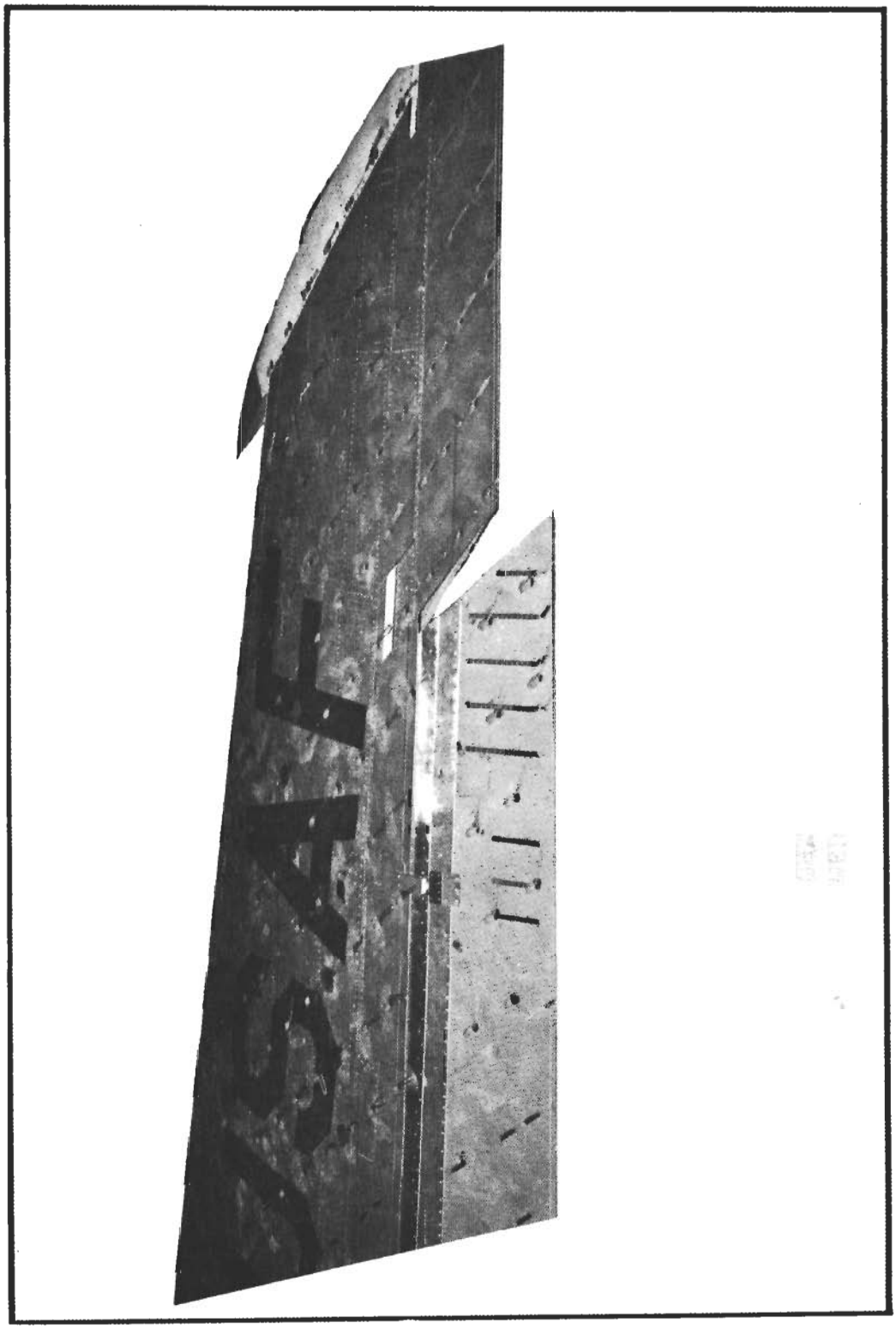

Figure 24. Tuft Installation Pattern on Top Cover of the Right Wing as Viewed by Vertical Stabilizer Fin Camera

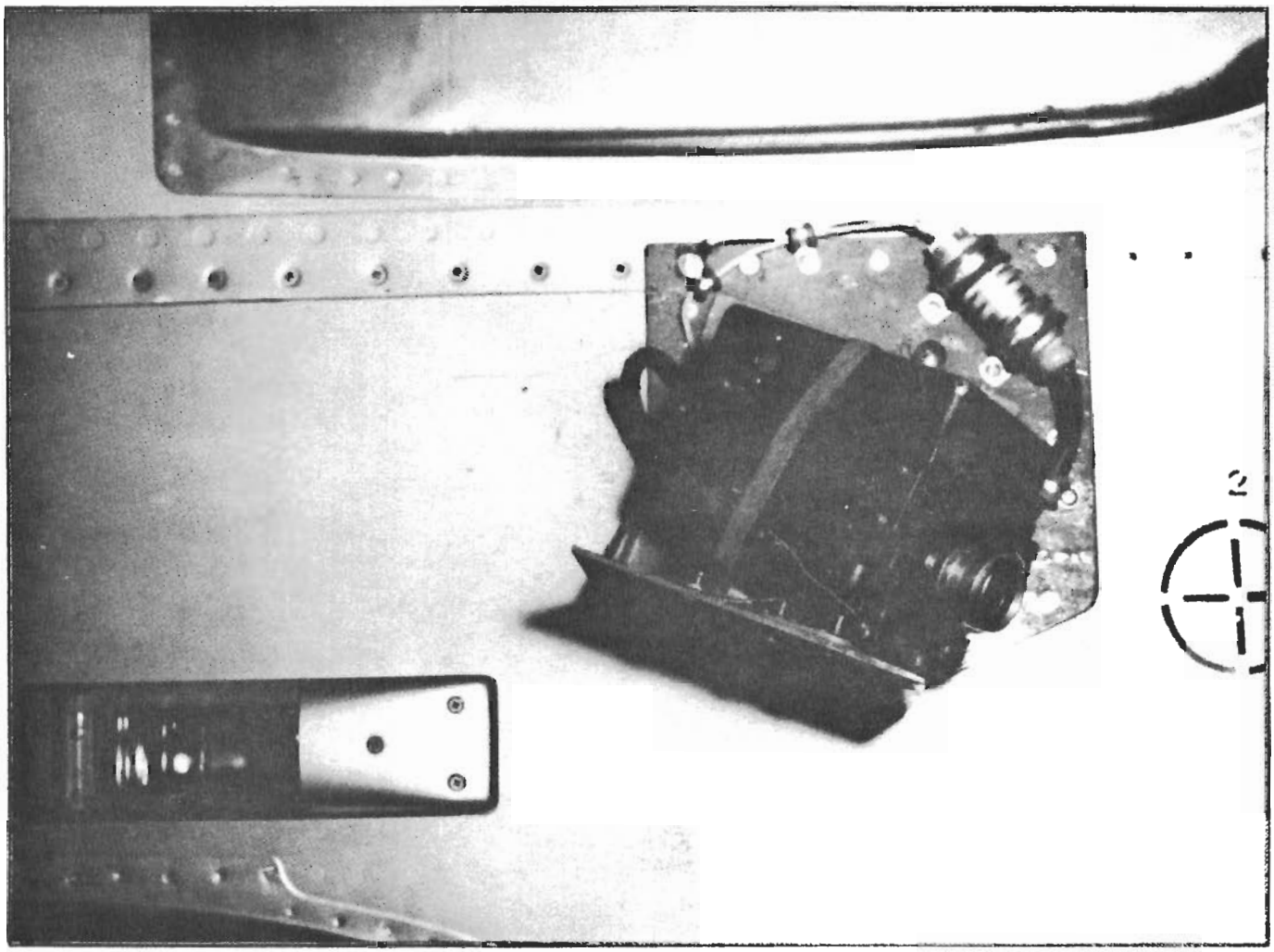

Figure 25. 16-mm Camera Installation on Vertical Stabilizer Fin Assembly

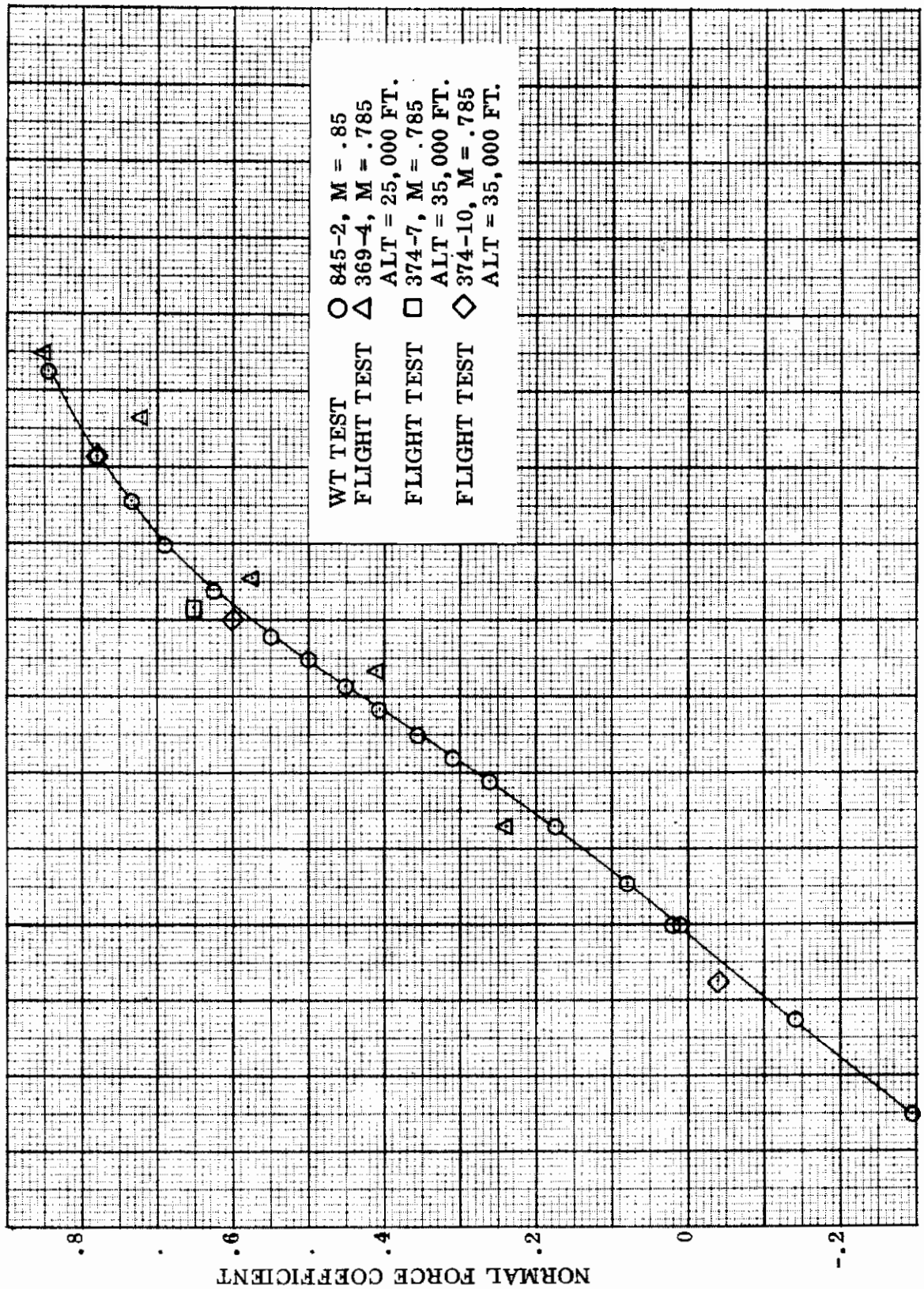

Figure 26. Variation of Normal Force Coefficient with Angle of Attack
(a) Leading Edge Flap and Trailing Edge Flap Undeflected

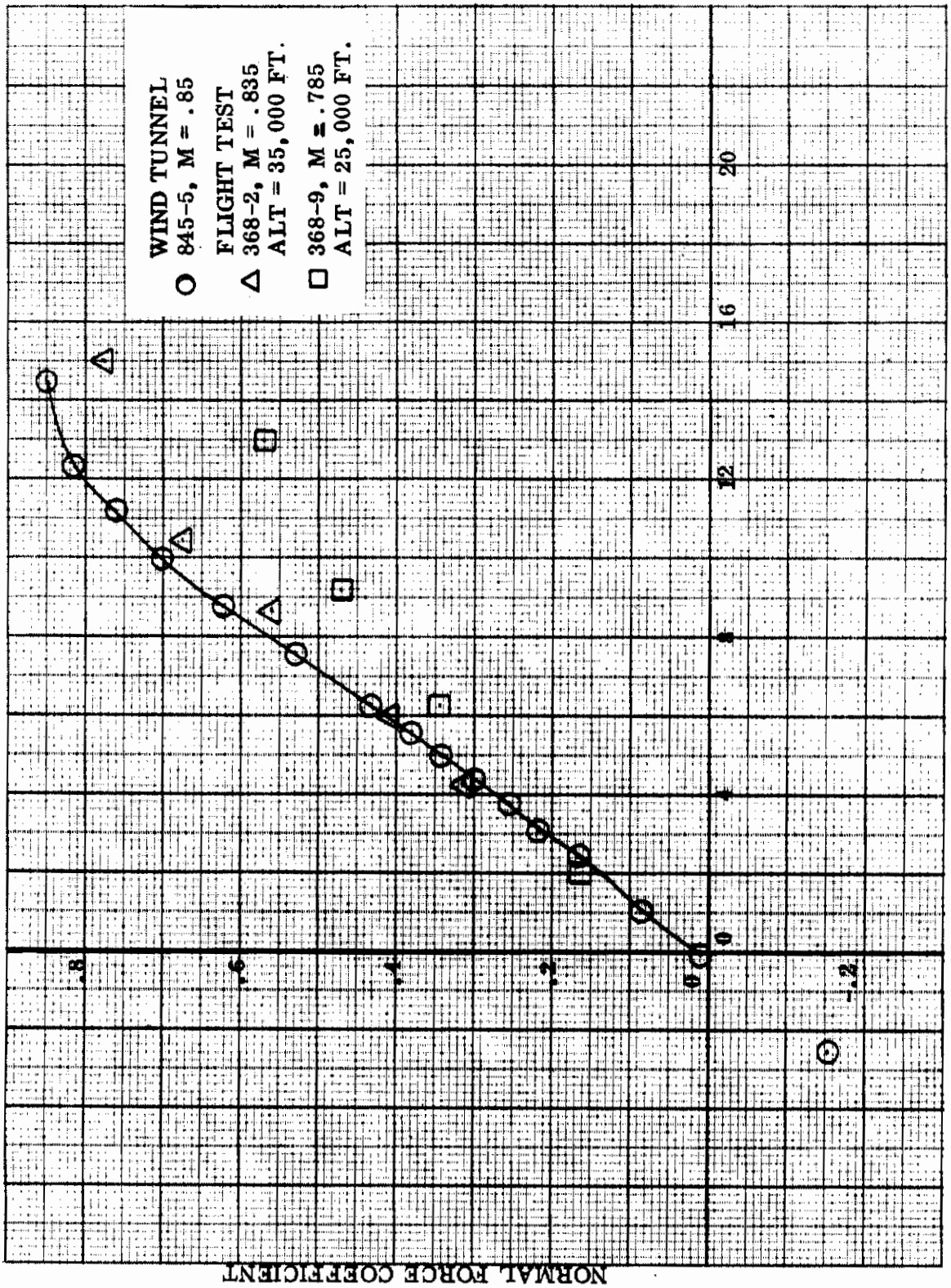

Figure 26. - - - Continued
(b) Leading Edge Flap 8°, Trailing Edge Flap Undeflected

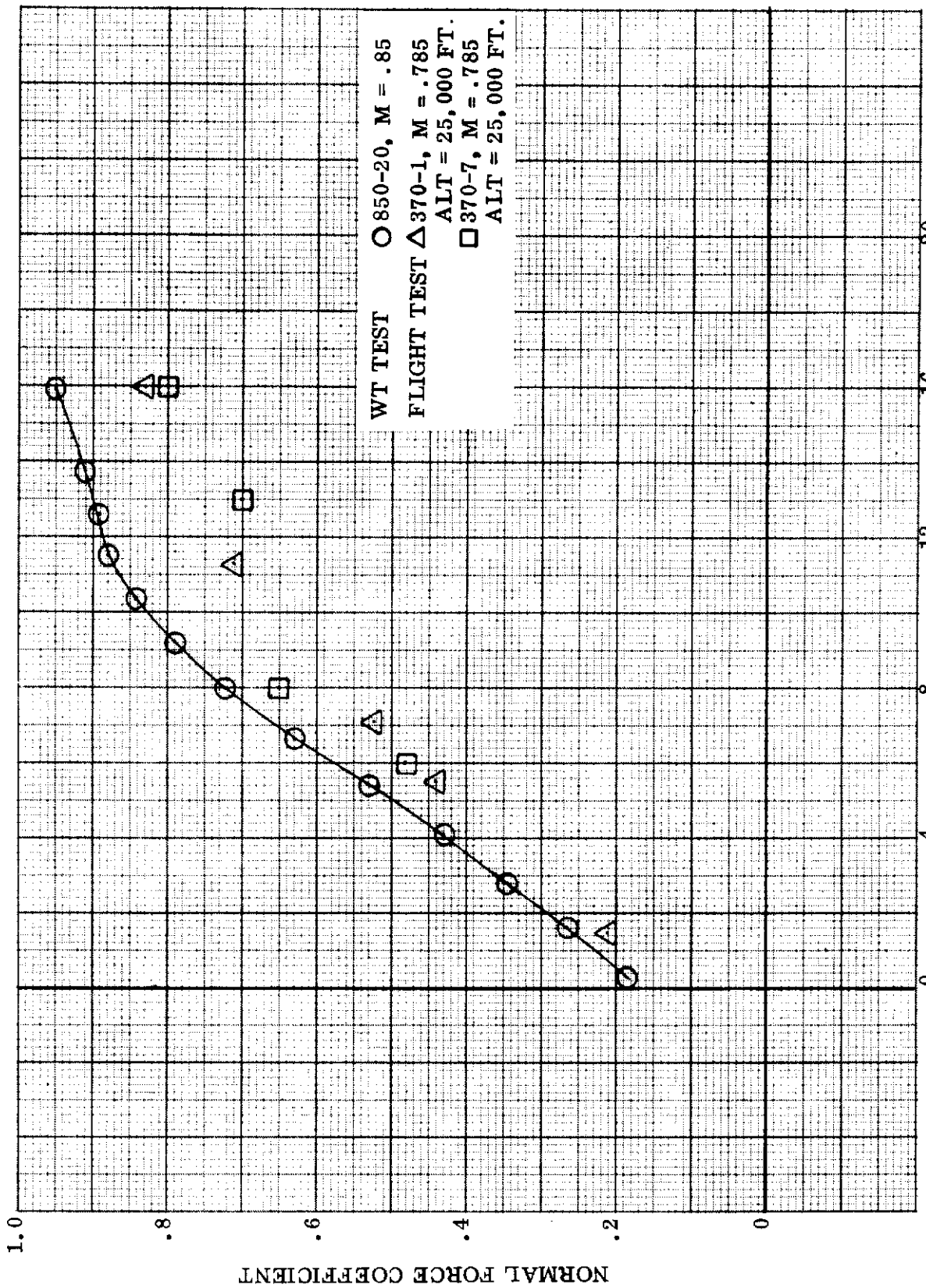

Figure 26. - - - Continued
(c) Leading Edge Flap 8°, Trailing Edge Flap 7.5°.

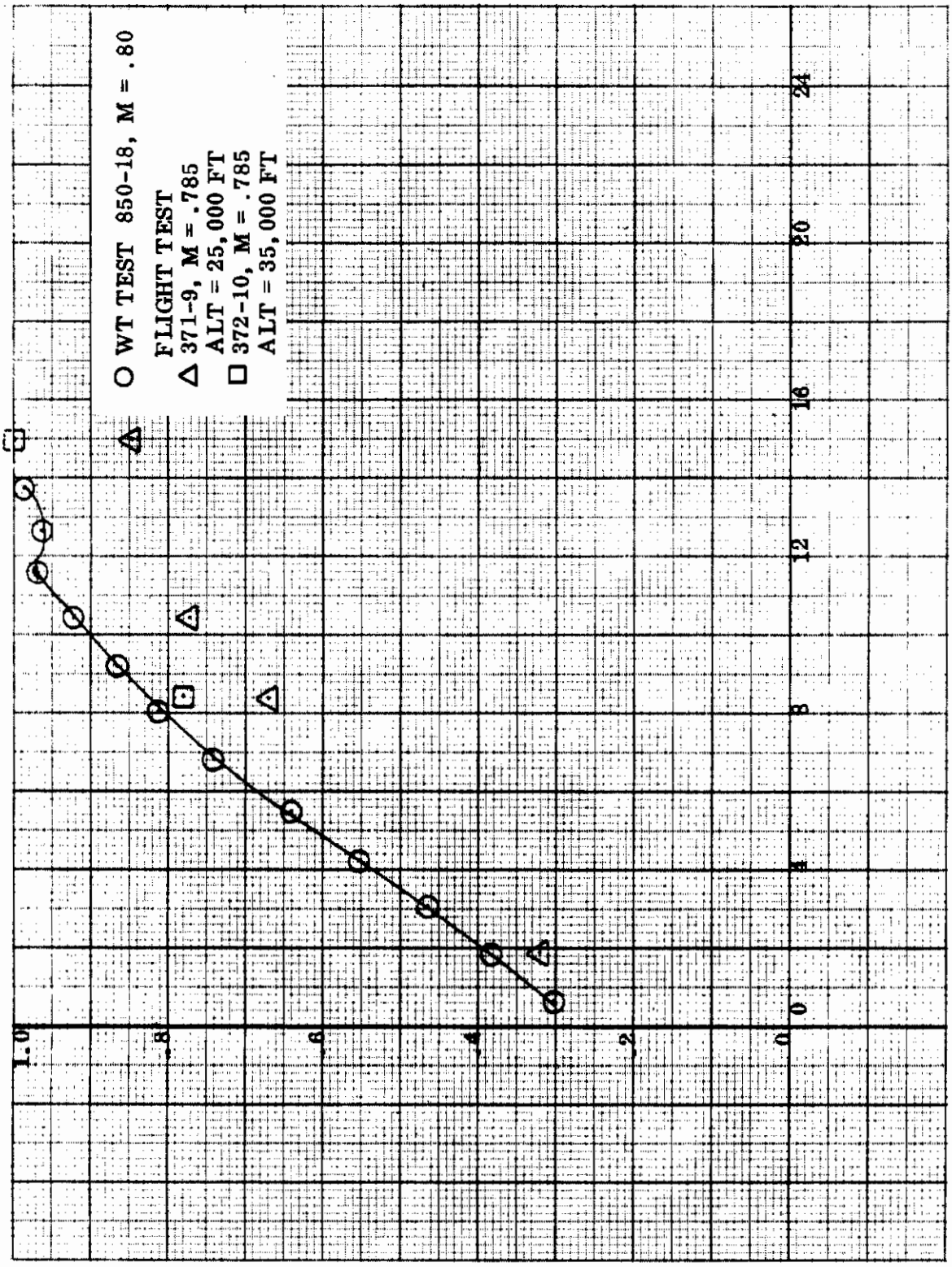

Figure 26. - - - Continued
(d) Leading Edge Flap 8^{o}, Trailing Edge Flap 15^{o}

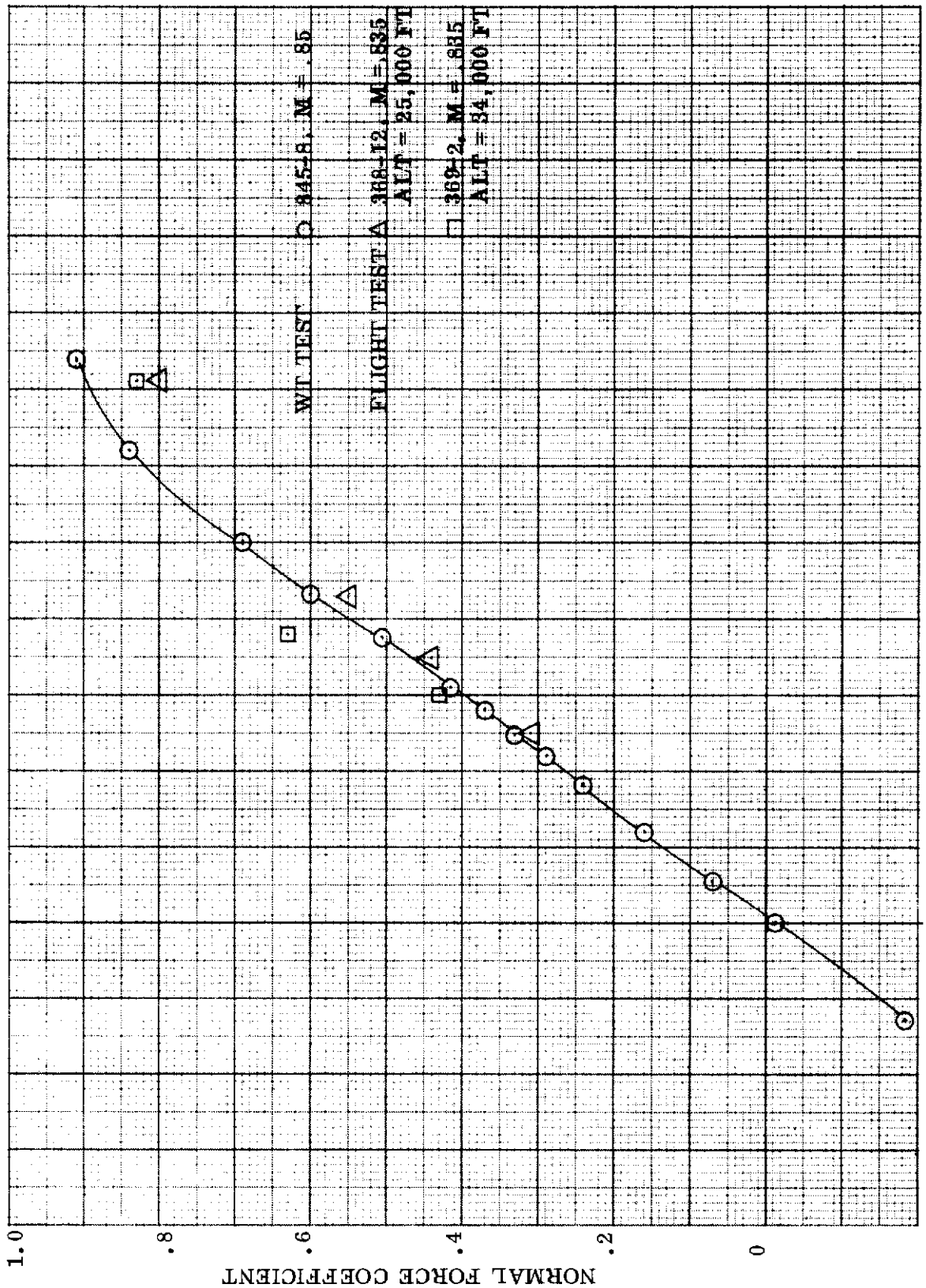

Figure 26. - - - Continued
(e) Leading Edge Flap 20^{o}, Trailing Edge Flap Undeflected

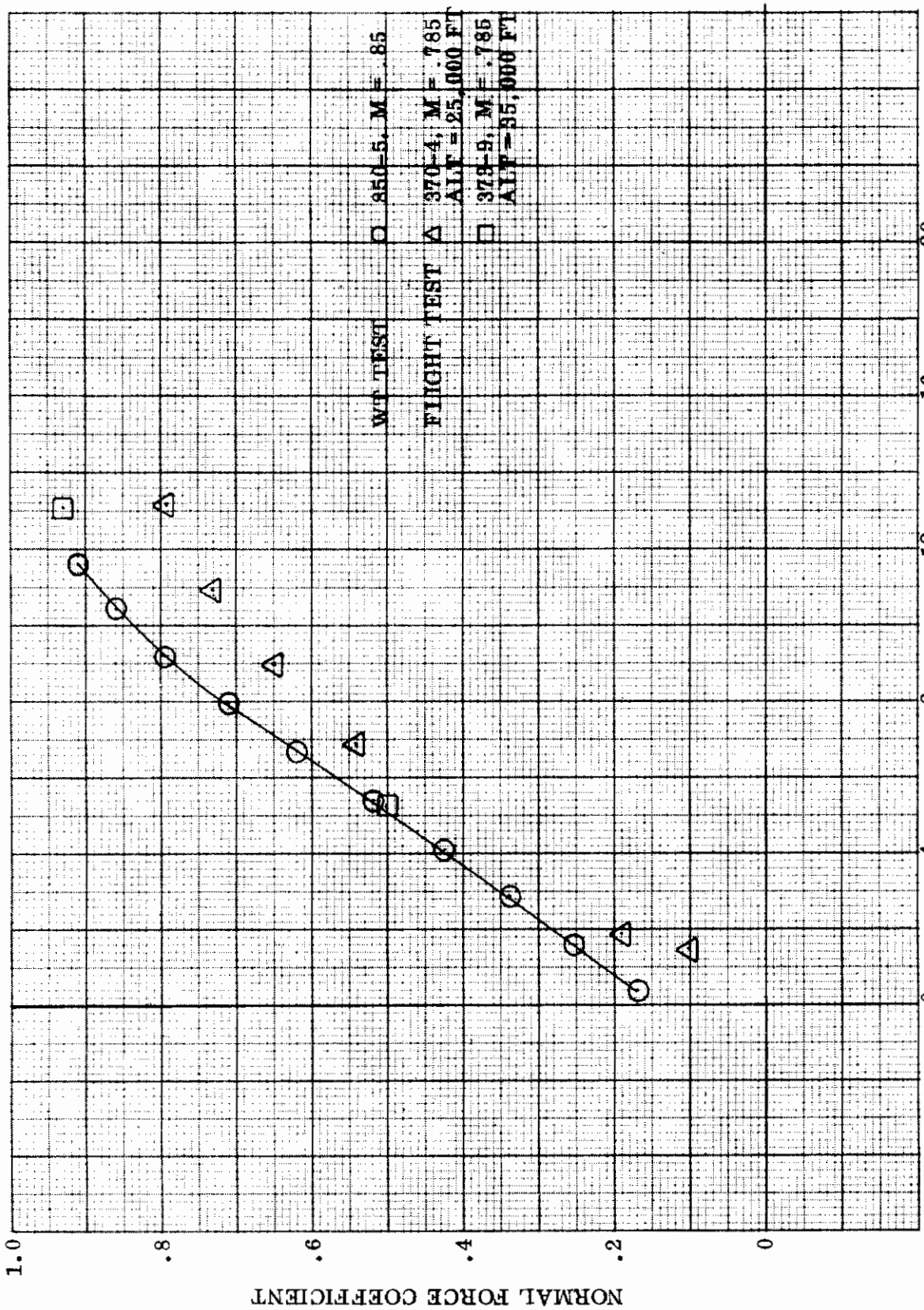

Figure 26. - - - Continued
(f) Leading Edge Flap 20^{o}, Trailing Edge Flap 7.5^{o}

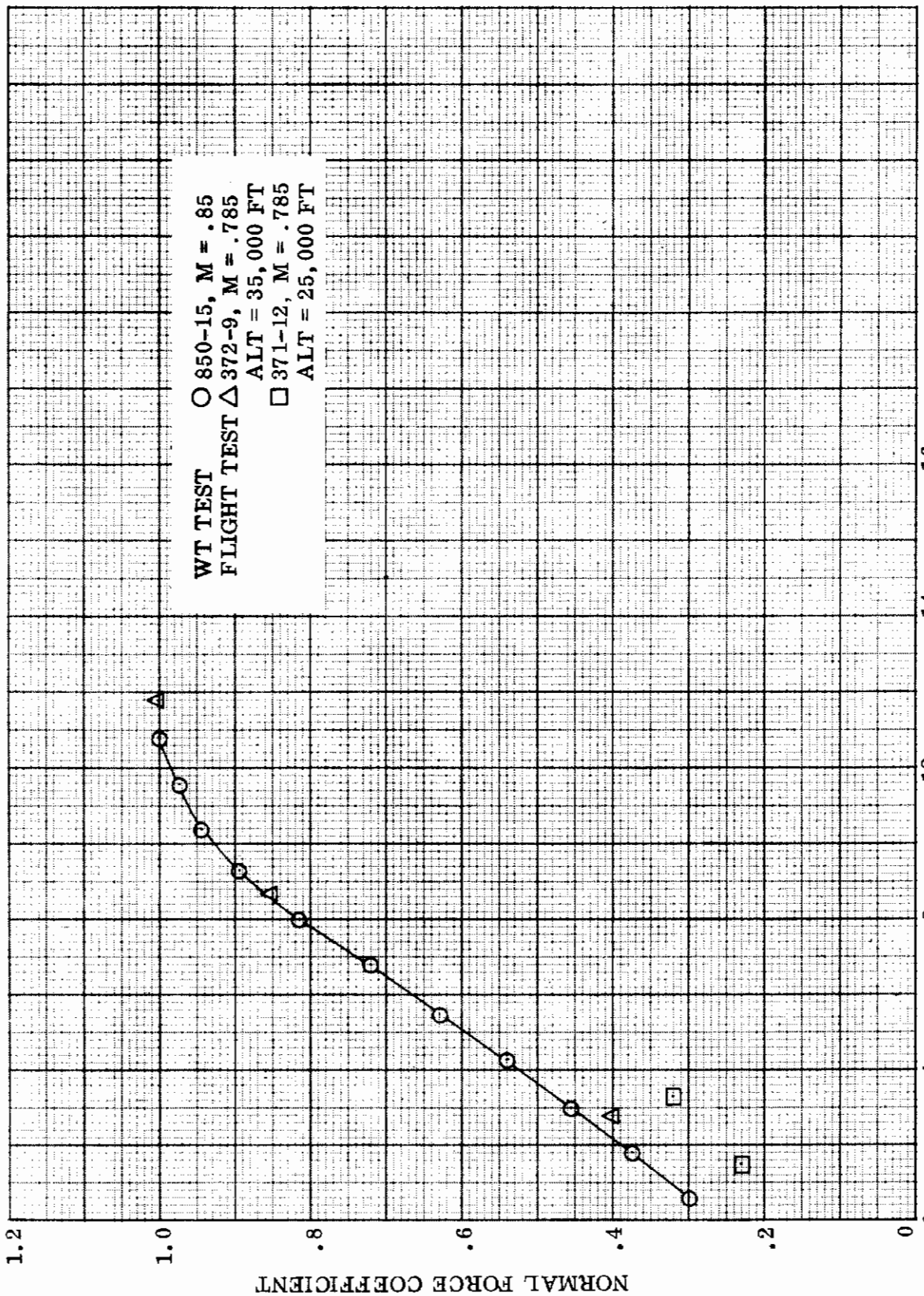

Figure 26. - - - Concluded
(g) Leading Edge Flap 20^{o}, Trailing Edge Flap 15^{o}

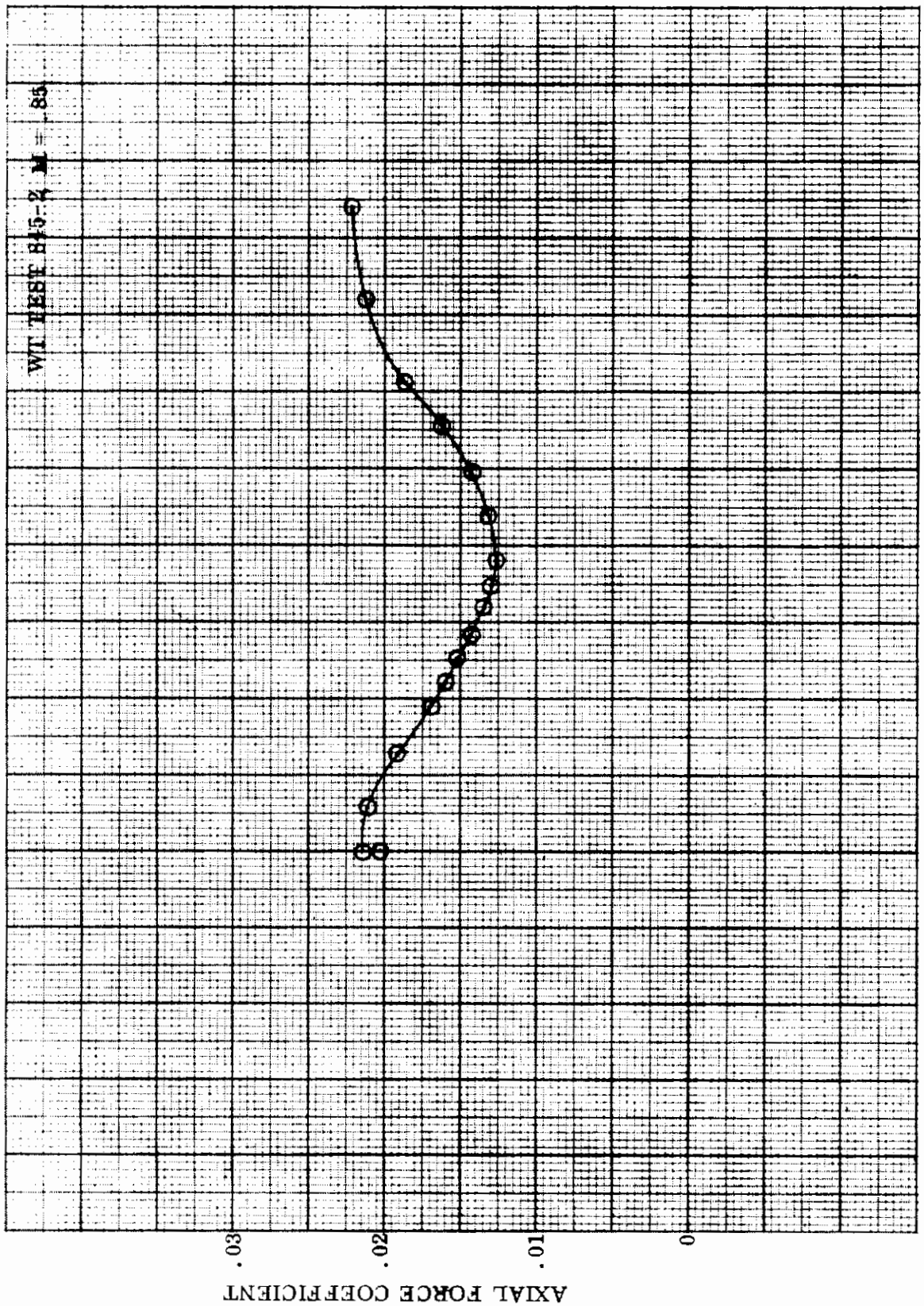

Figure 27. Variation of Axial Force Coefficient with Angle of Attack
(a) Leading Edge Flap and Trailing Edge Flap Undeflected

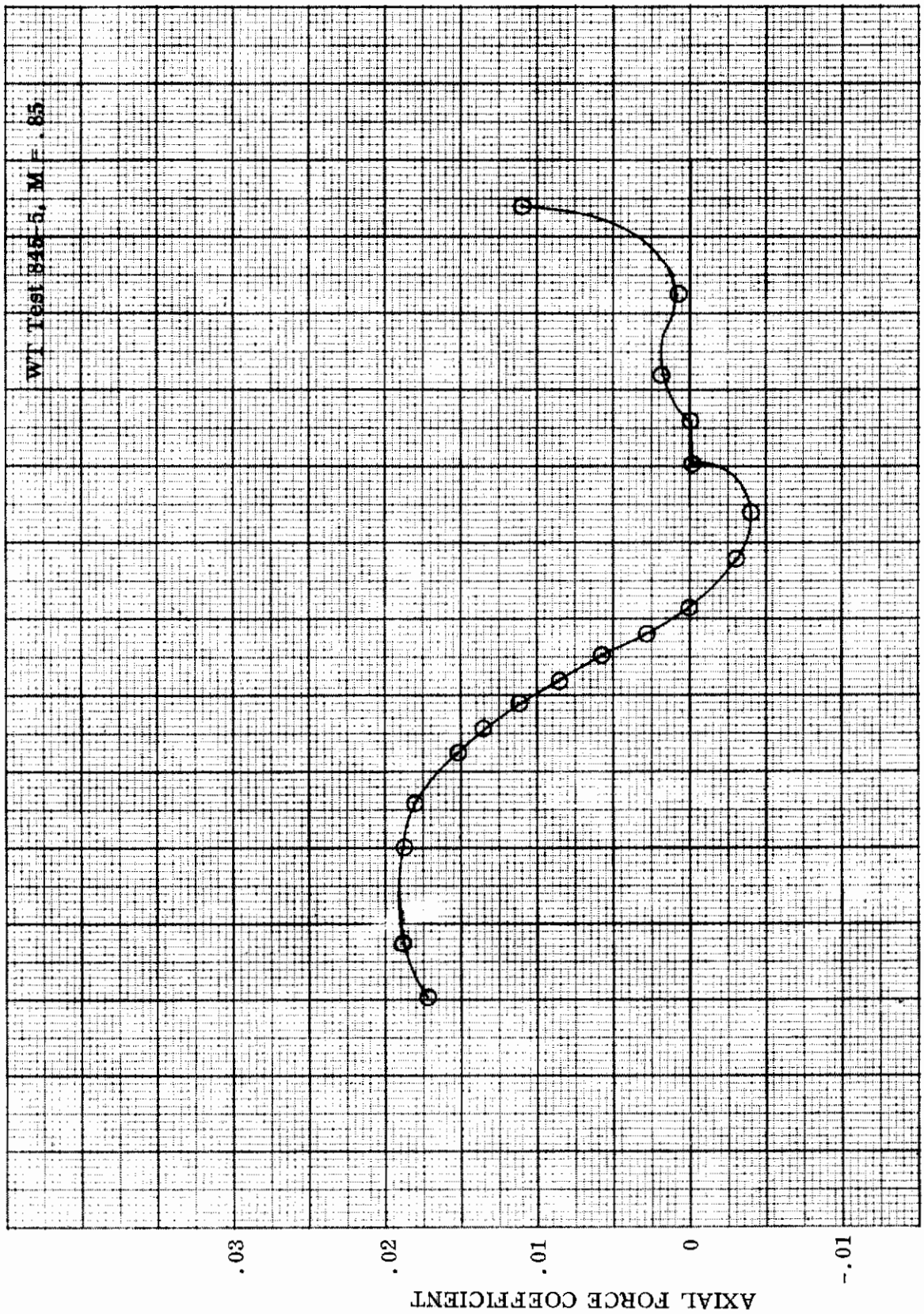

Figure 27. - - - Continued
(b) Leading Edge Flap 8°, Trailing Edge Flap Undeflected

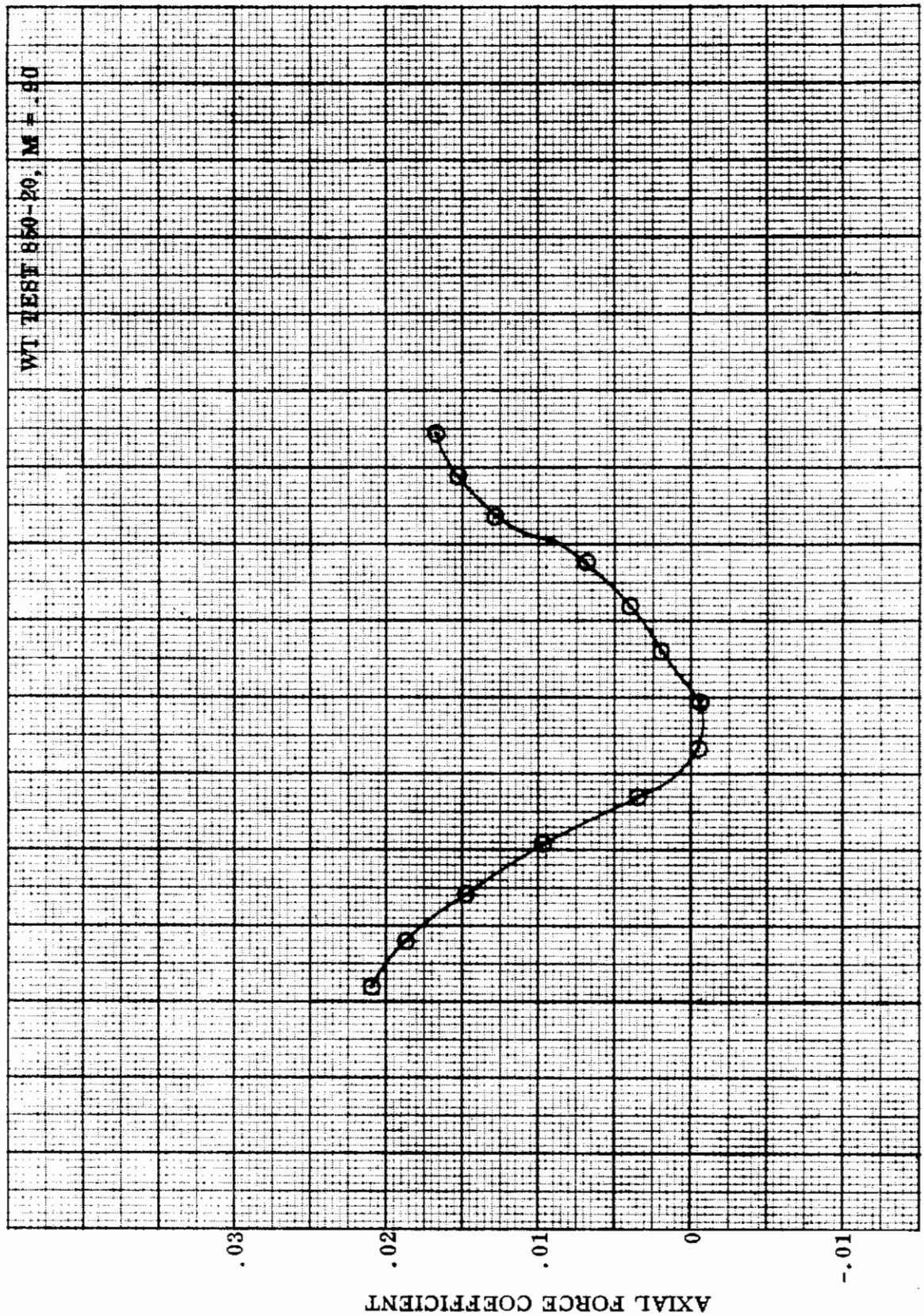

Figure 27. - - - Continued
(c) Leading Edge Flap 8^{o}, Trailing Edge Flap 7.5^{o}

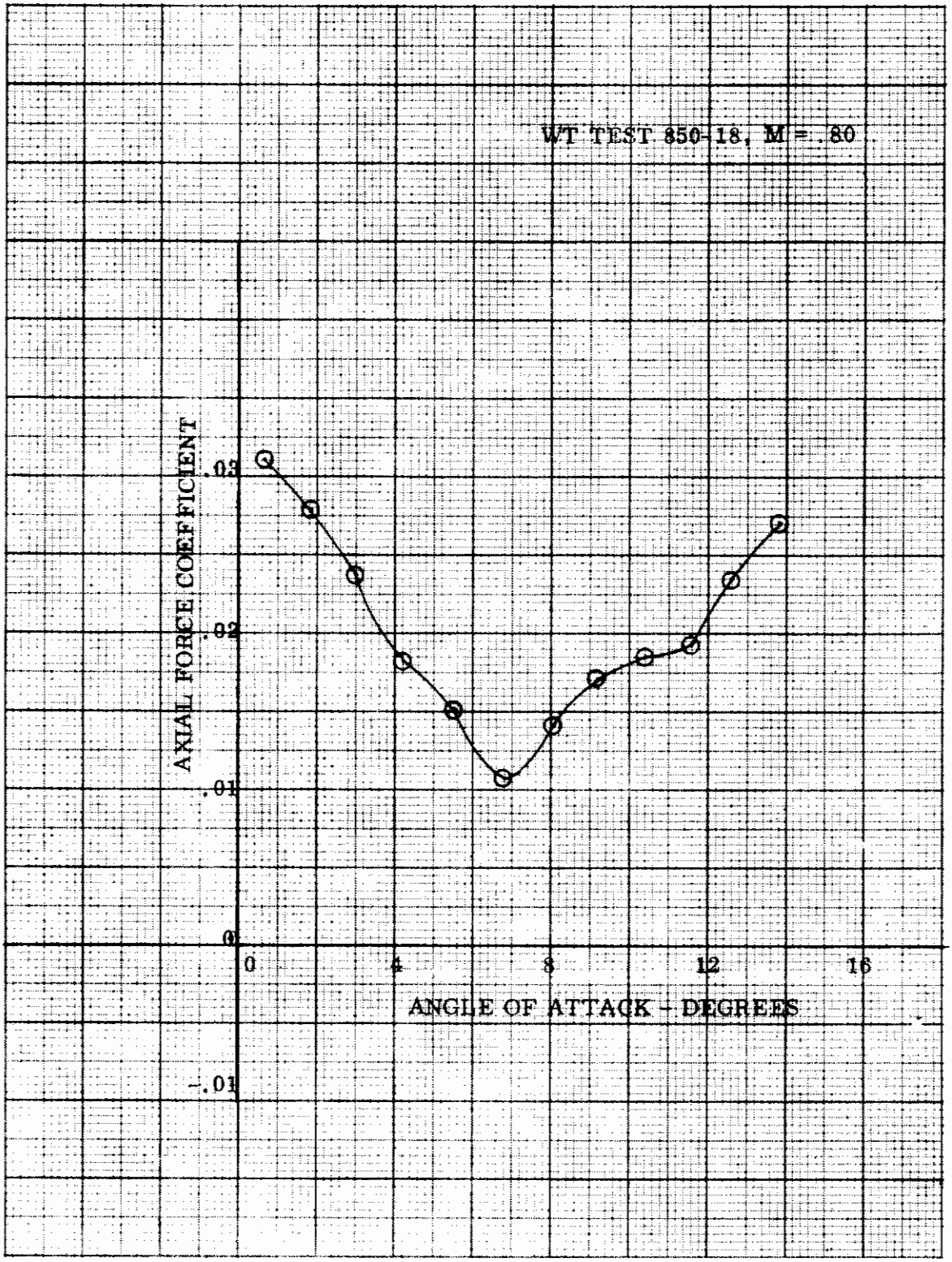

Figure 27. - - - Continued
(d) Leading Edge Flap 8°, Trailing Edge Flap 15°

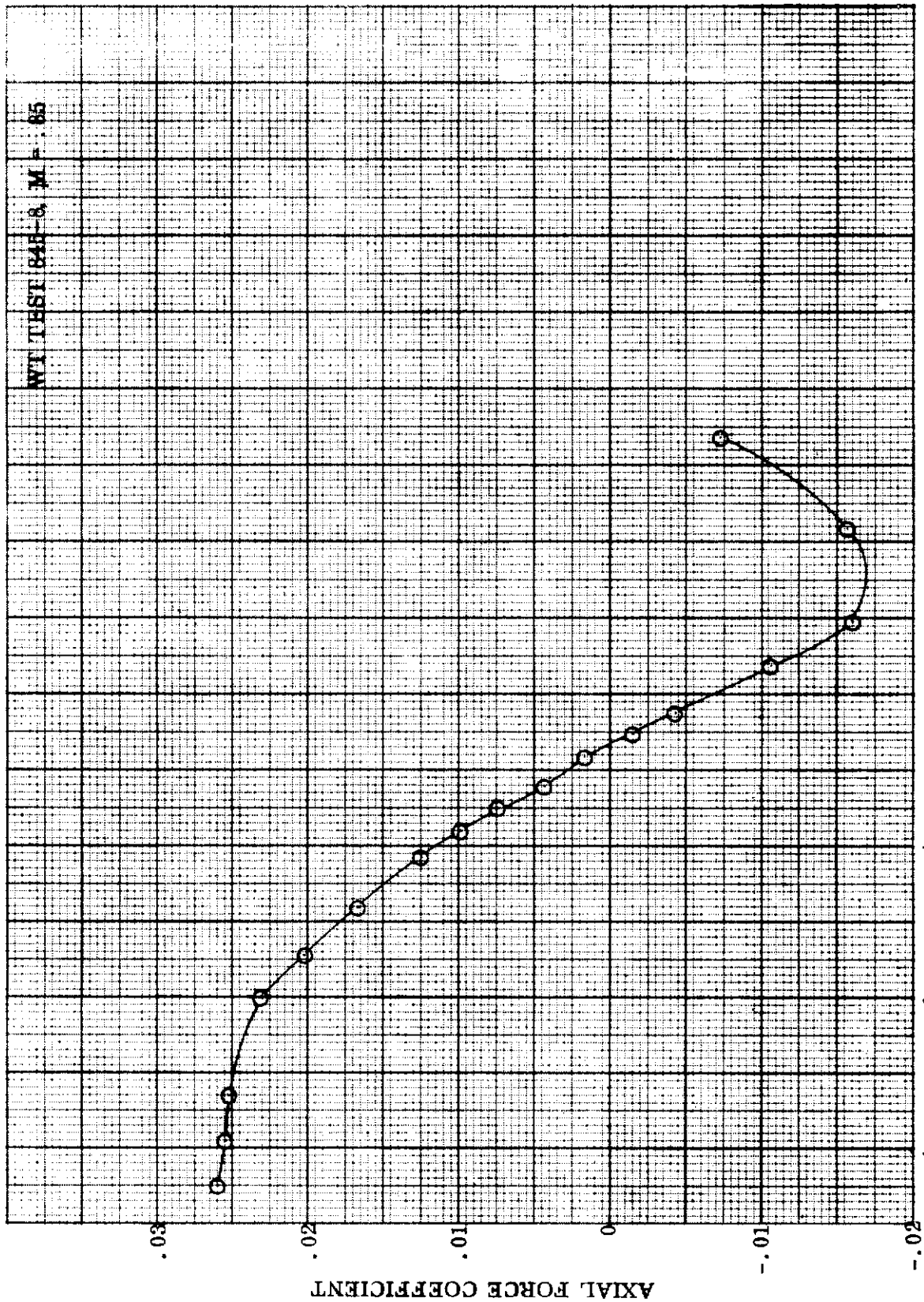

Figure 27. - - - Continued
(e) Leading Edge Flap 20°, Trailing Edge Flap Undeflected

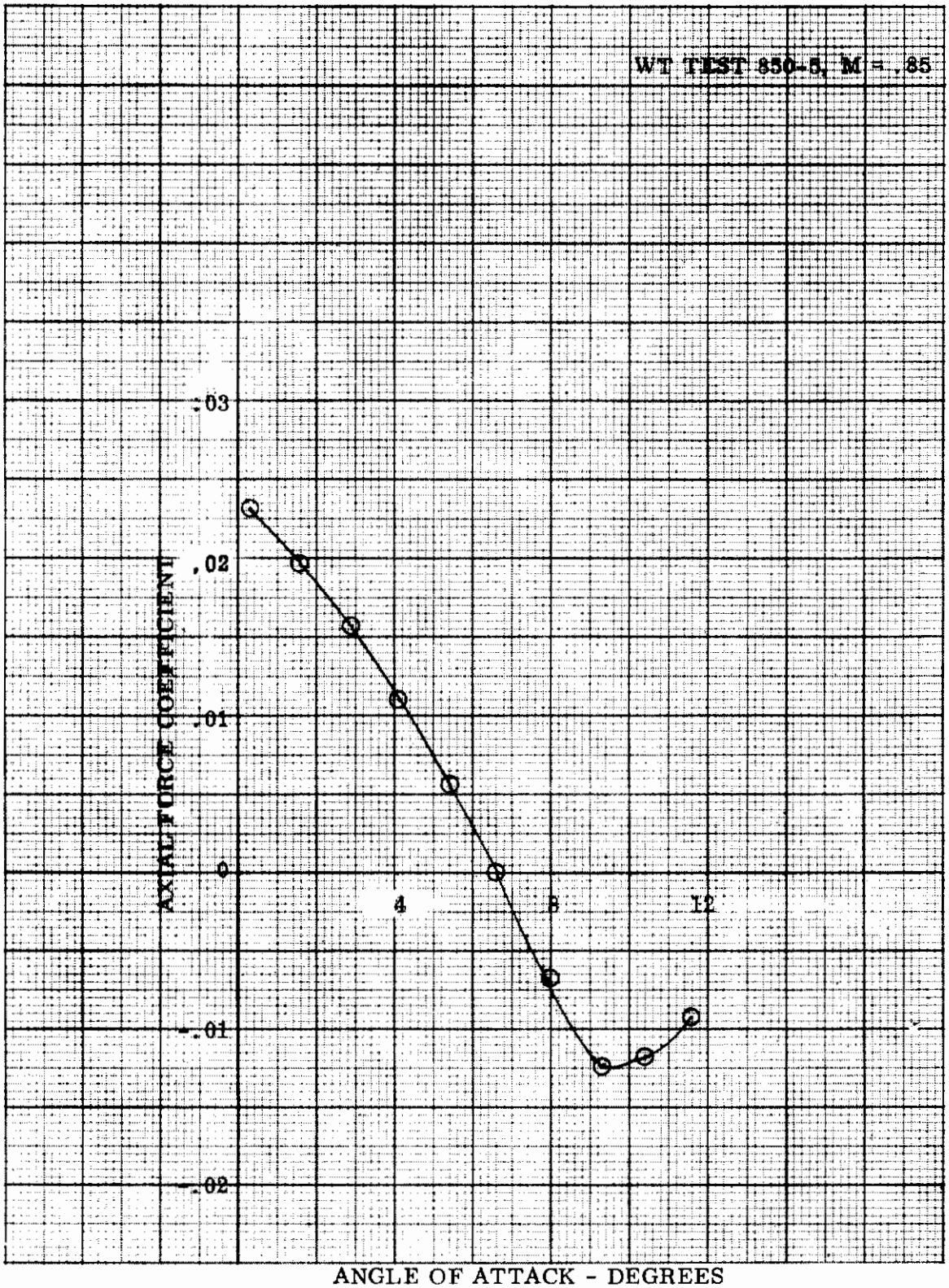

Figure 27. - - - Continued
(f) Leading Edge Flap 20°, Trailing Edge Flap 7.5°

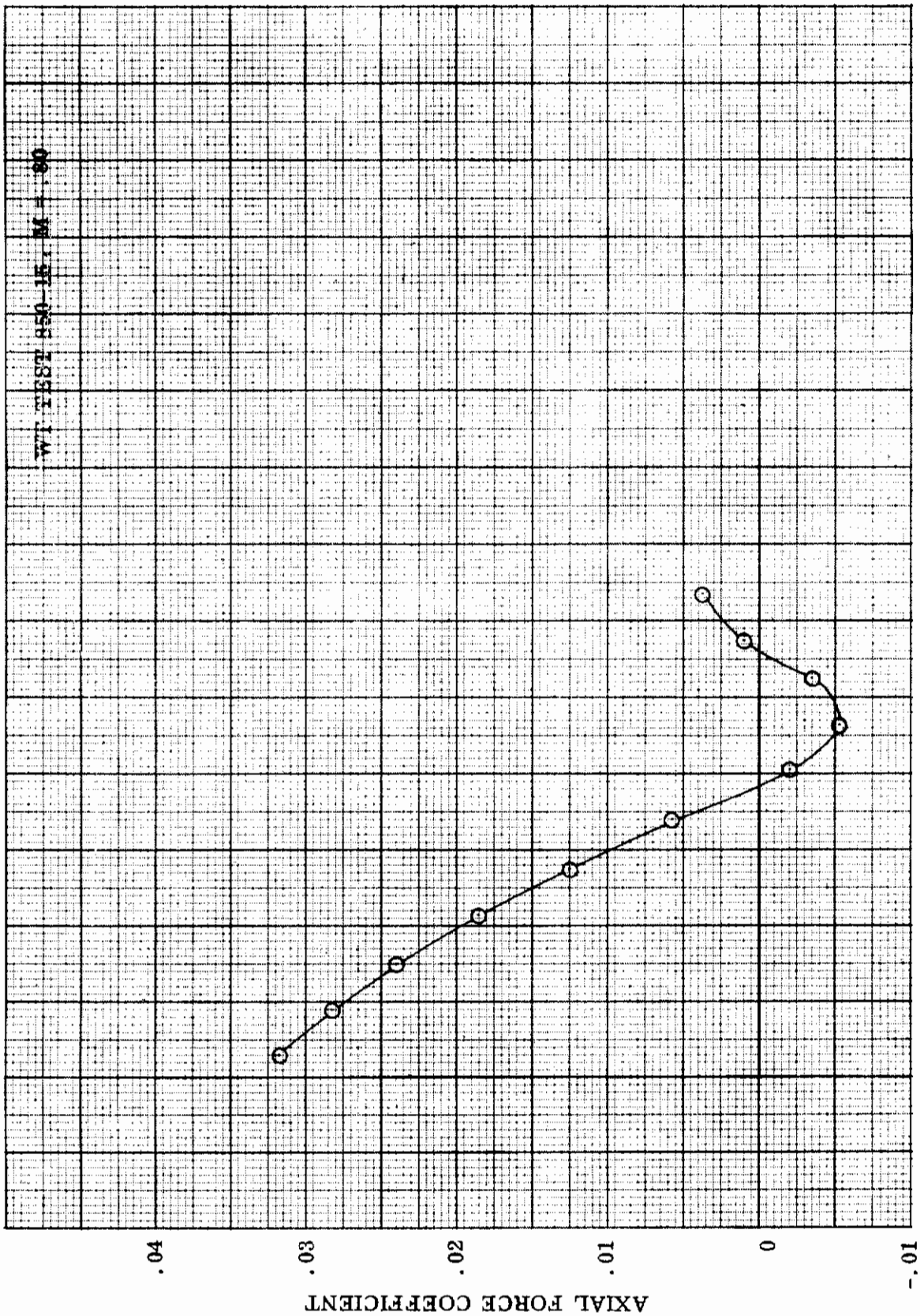

Figure 27. - - - Concluded
(g) Leading Edge Flap 20°, Trailing Edge Flap 15°

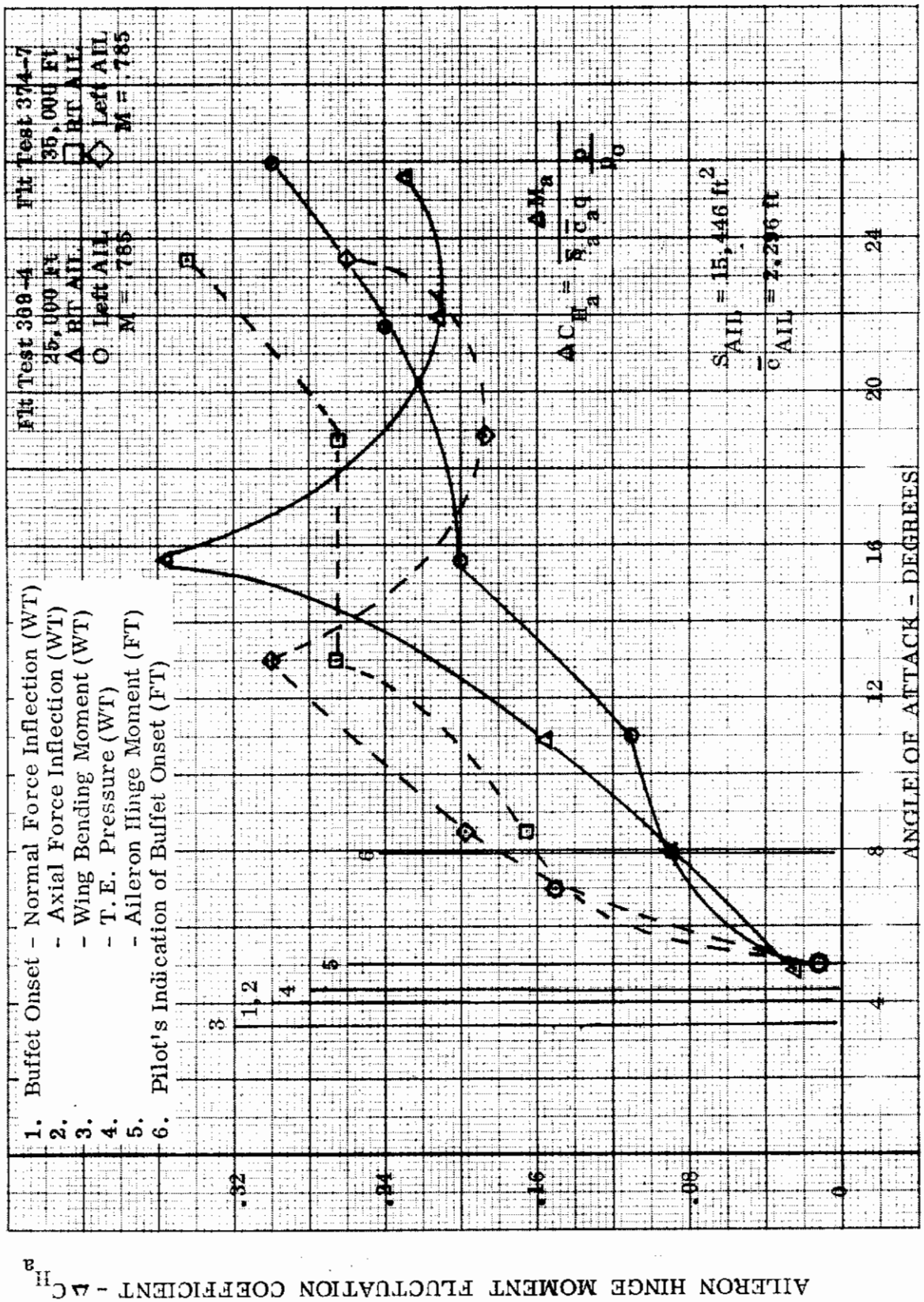

Figure 28. Variation of Aileron Hinge Moment Fluctuation Coefficient with Angle of Attack

(a) Leading Edge Flap and Trailing Edge Flap Undeflected

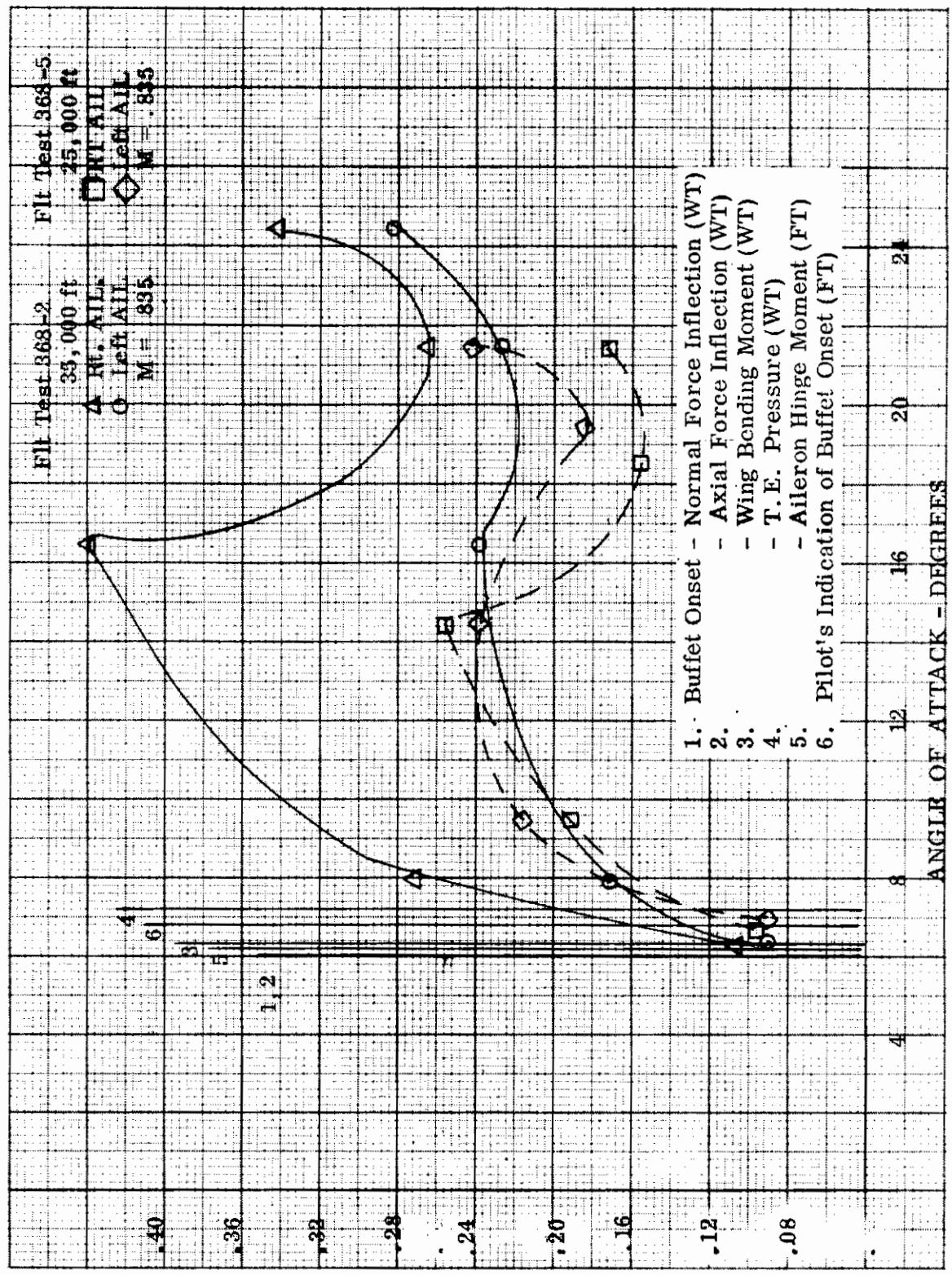

Figure 28. - - - Continued
(b) Leading Edge Flap 8^{o}, Trailing Edge Flap Undeflected

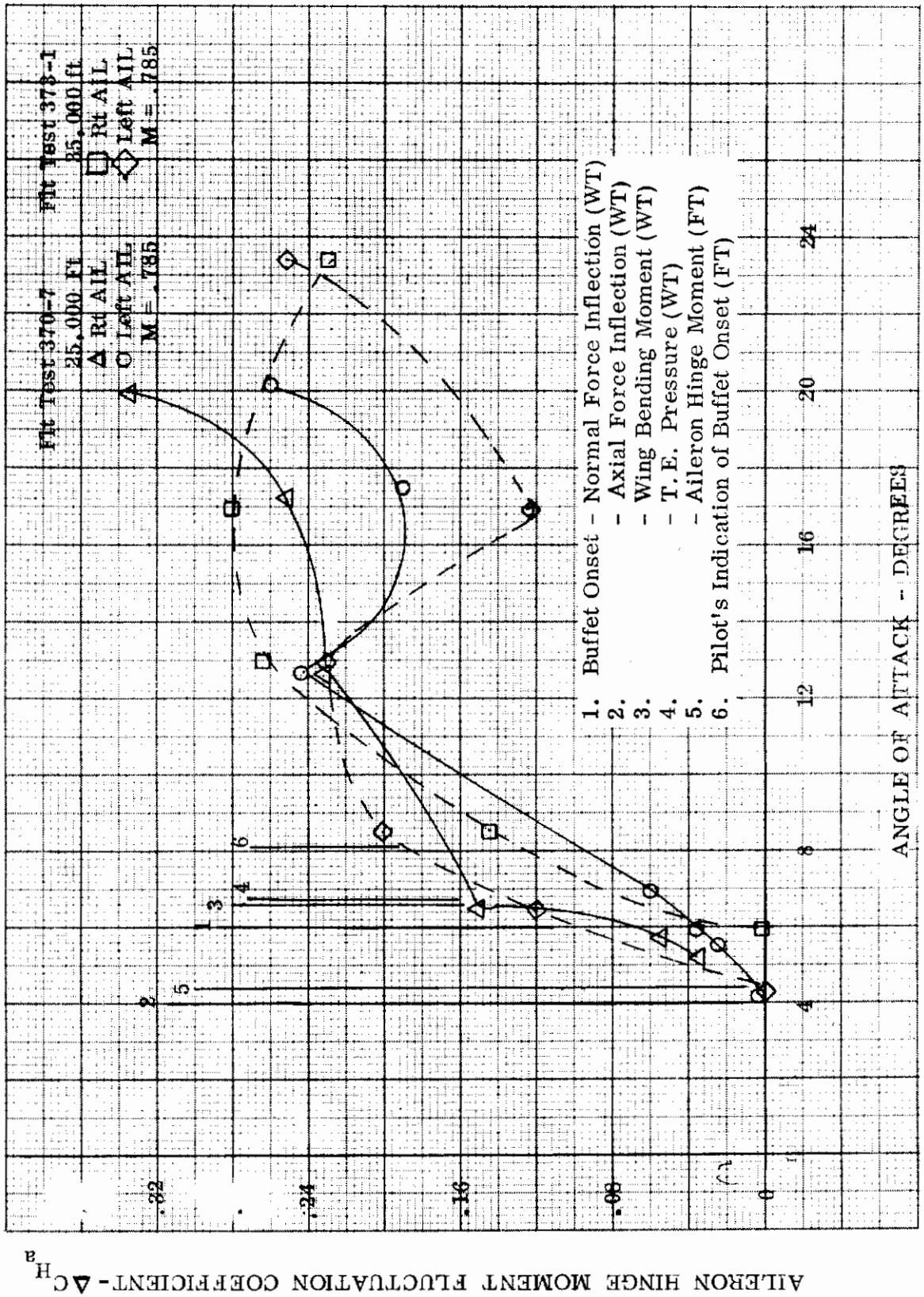

Figure 28. - - - Continued
(c) Leading Edge Flap 8°, Trailing Edge Flap 7.5°

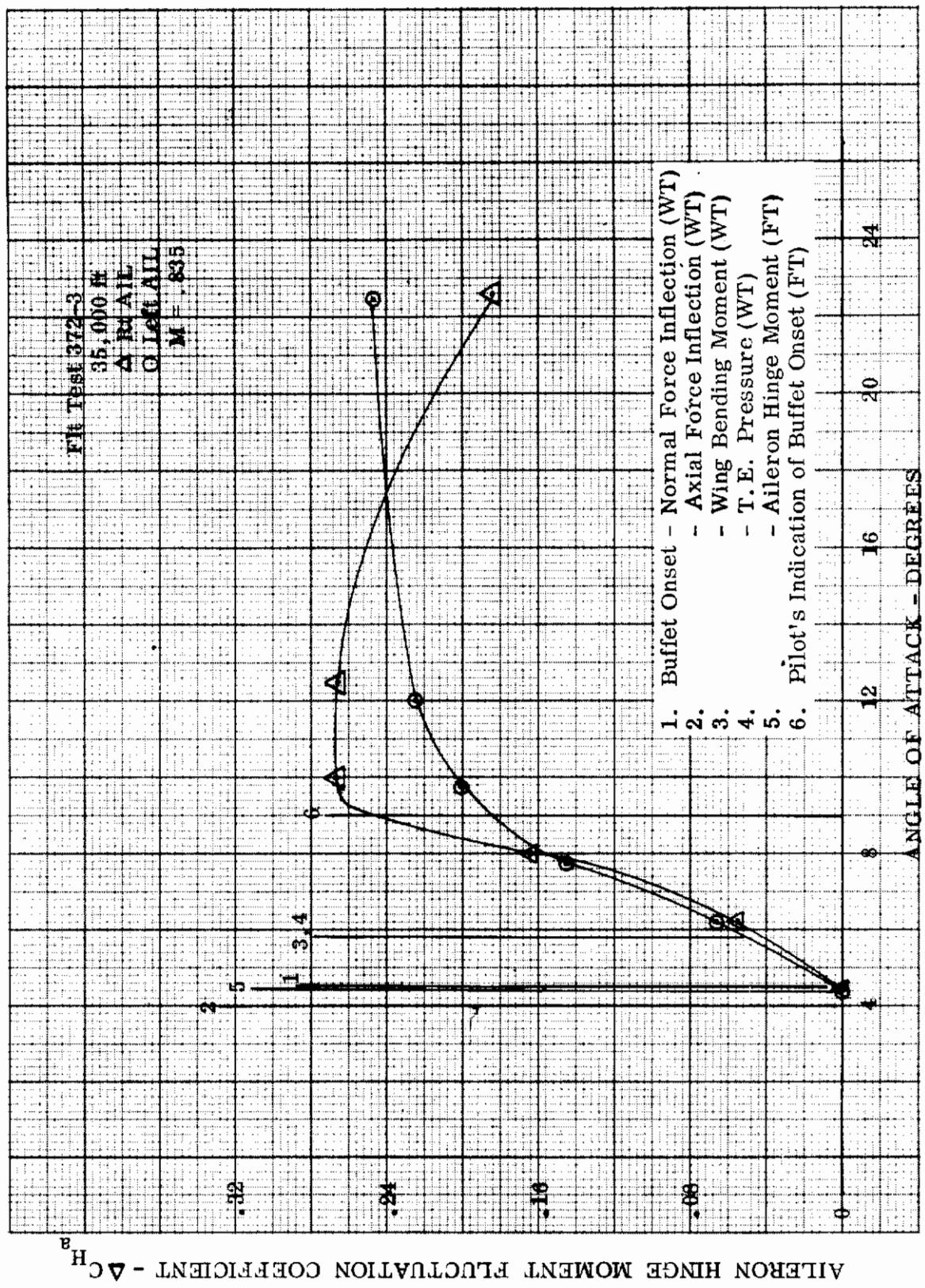

Figure 28. - - - Continued
(d) Leading Edge Flap 8°, Trailing Edge Flap 15°

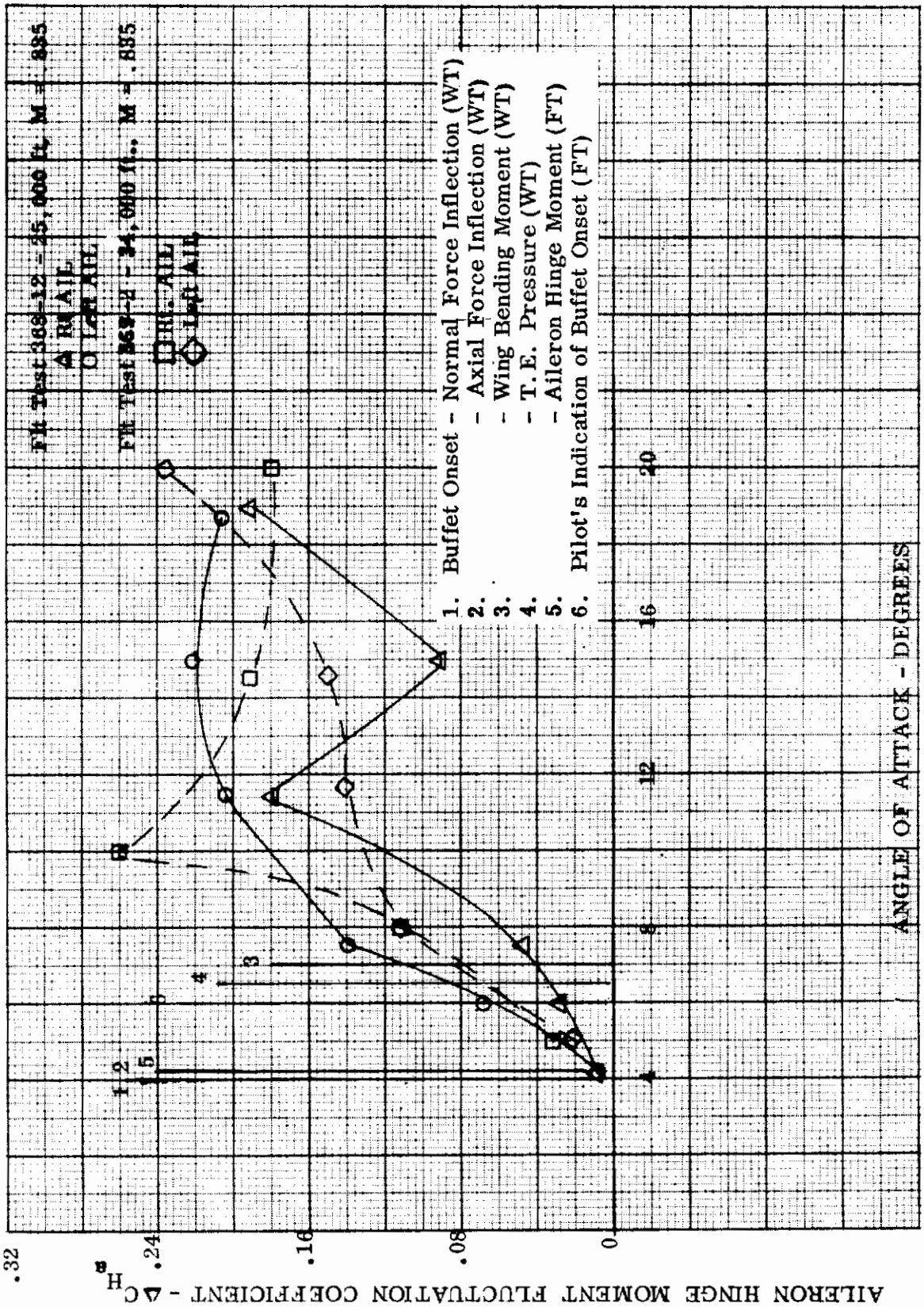

Figure 28. - - - Continued
(e) Leading Edge Flap 20°, Trailing Edge Flap Undeflected

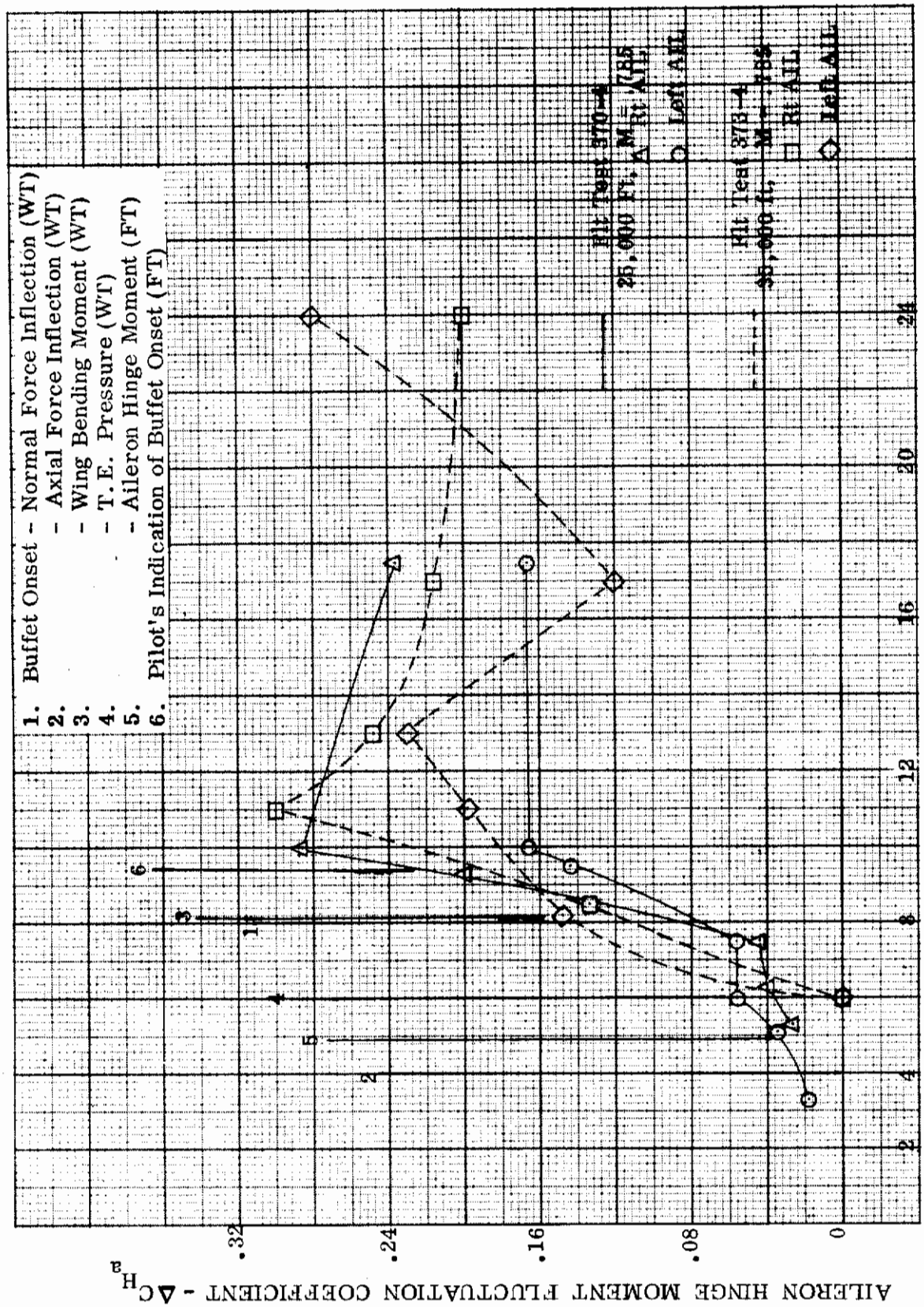

Figure 28. - - - Continued
(f) Leading Edge Flap 20°, Trailing Edge Flap 7.5°

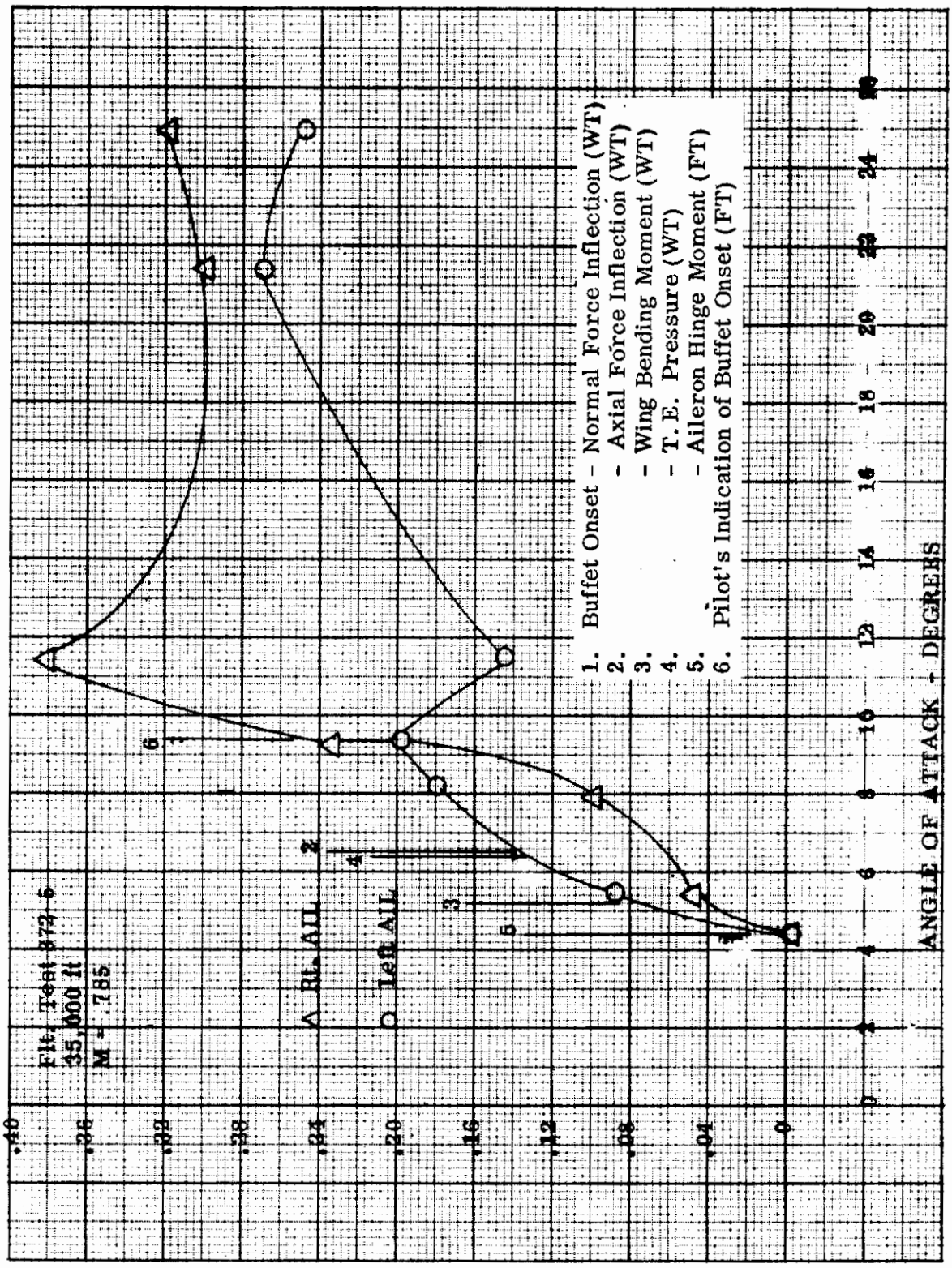

Figure 28. - - - Concluded
(g) Leading Edge Flap 20°, Trailing Edge Flap 15°

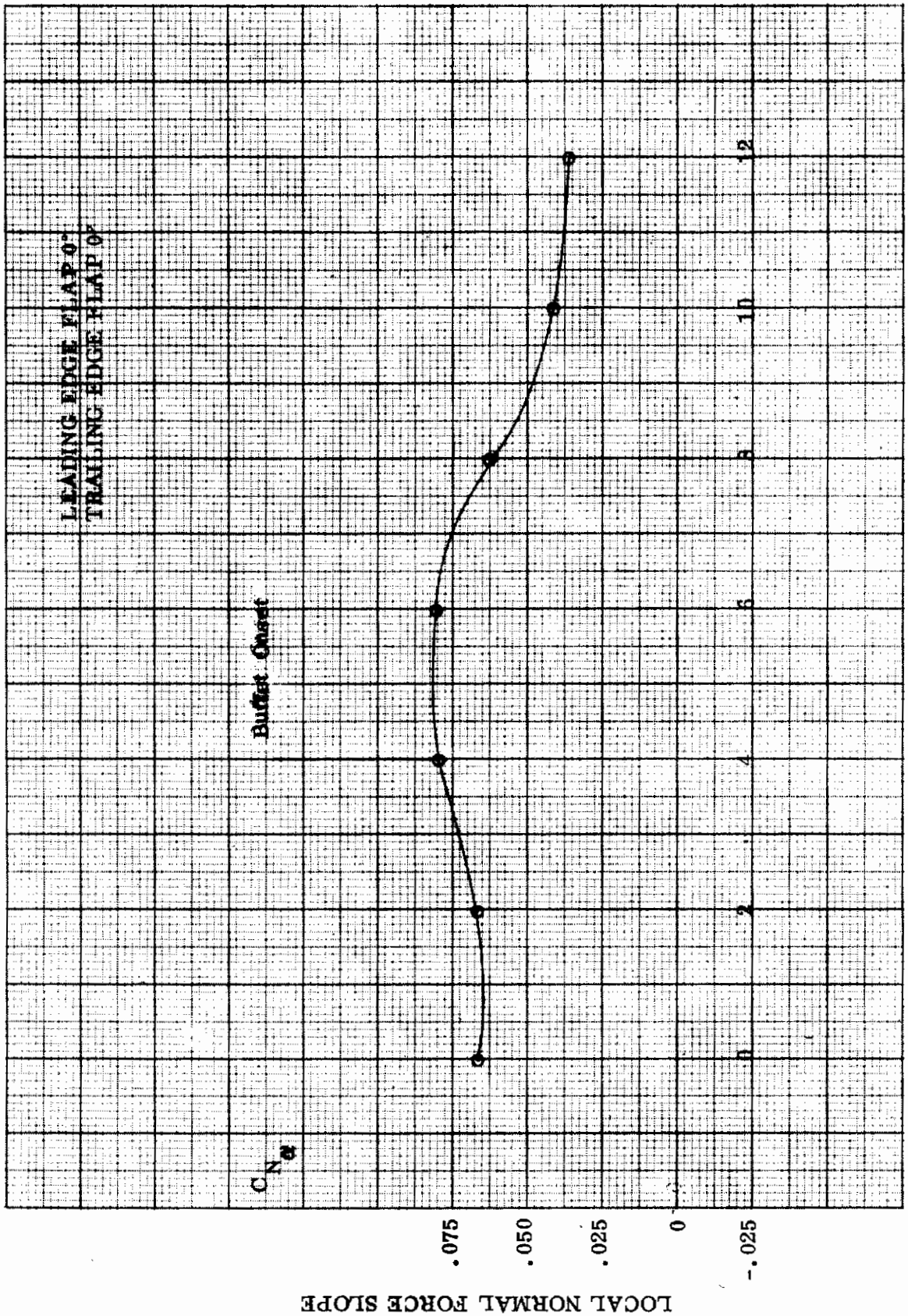

Figure 29. Local Normal Force Curve Slope Variation with Angle of Attack
(a) Leading Edge Flap and Trailing Edge Flap Undeflected

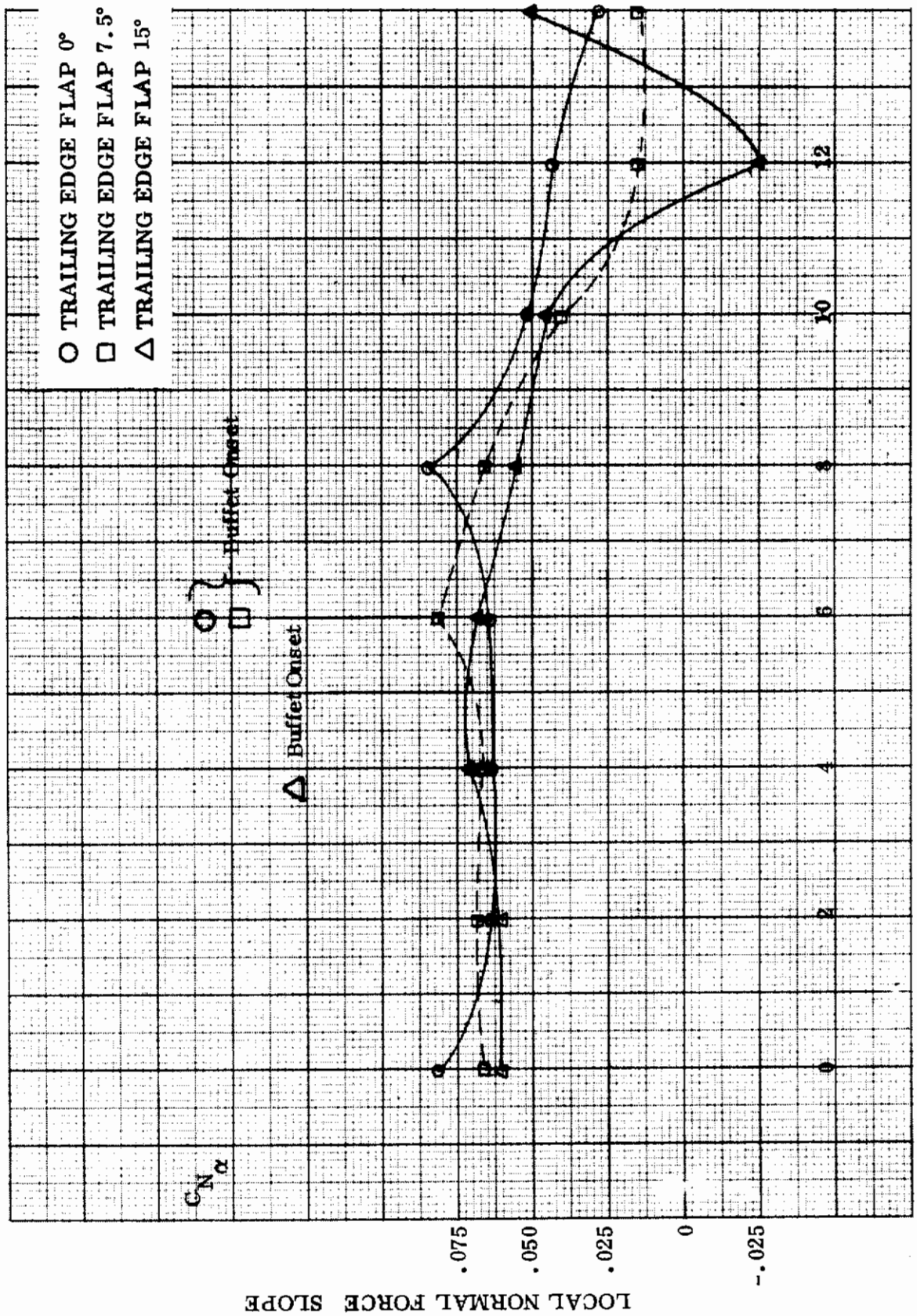

Figure 29. - - - Continued
(b) Leading Edge Flap 8°, Trailing Edge Flap Deflected

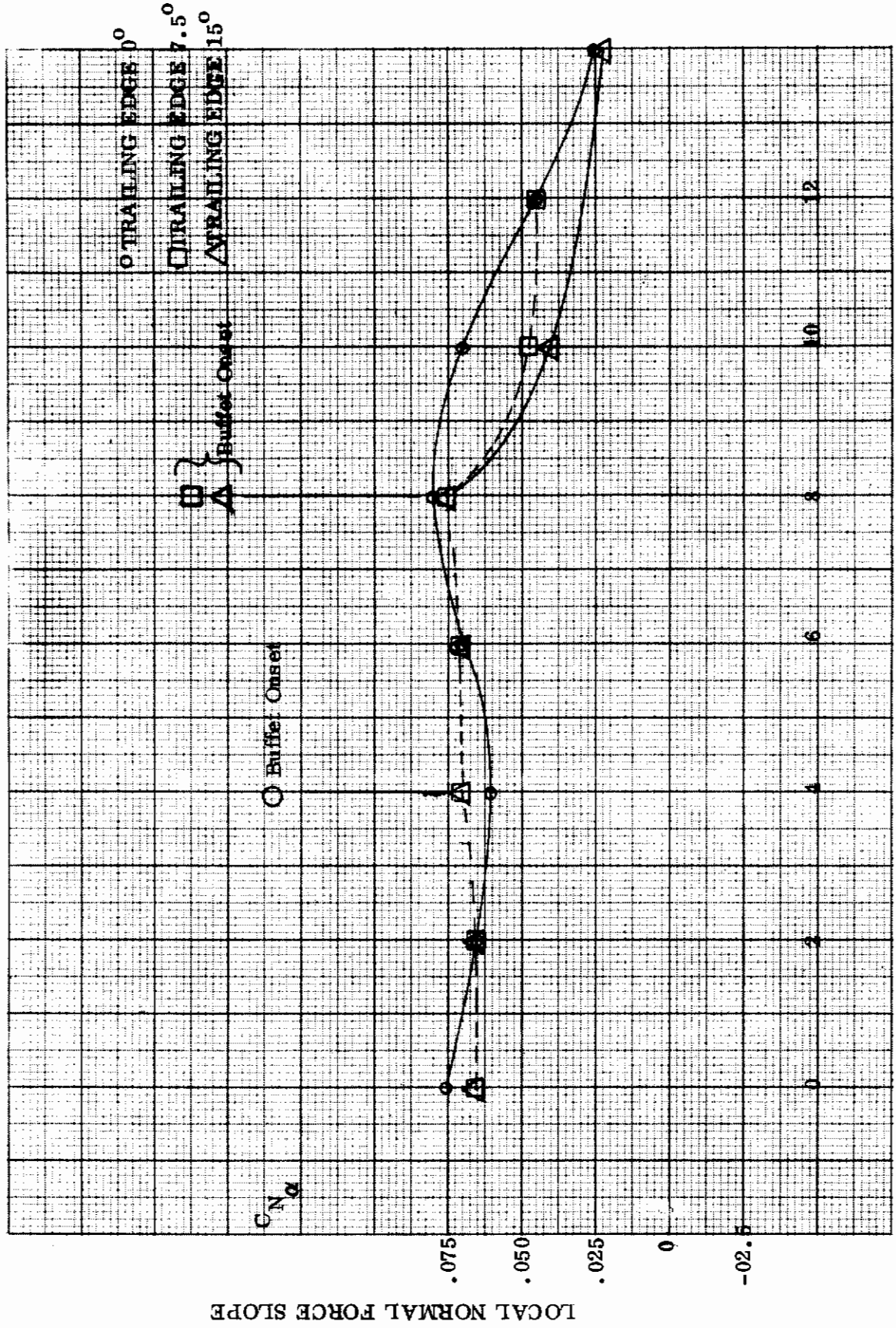

Figure 29. - - - Concluded
(c) Leading Edge Flap 20^o, Trailing Edge Flap Deflected

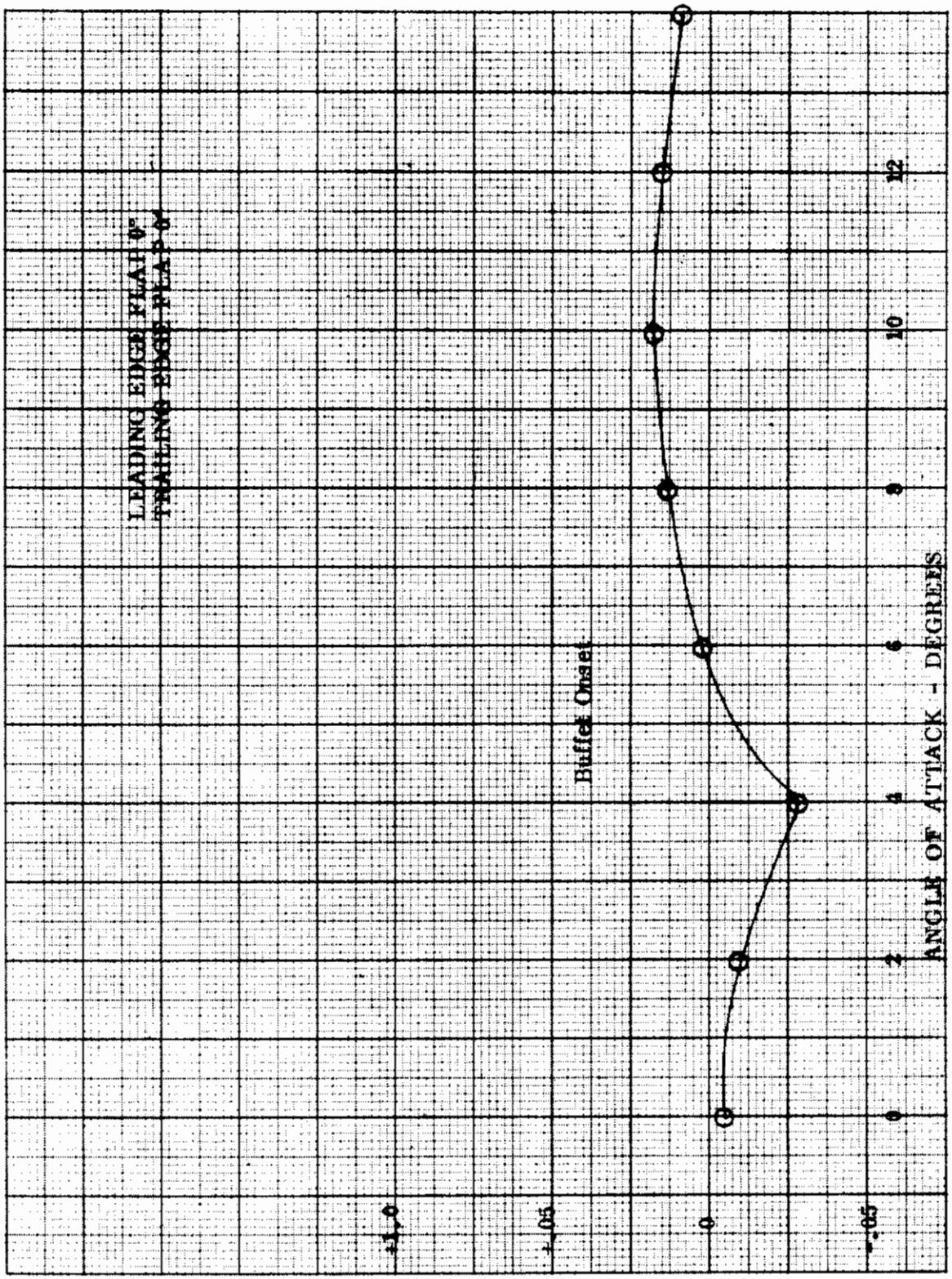

Figure 30. Local Chord Force Curve Slope Variation with Angle of Attack
(a) Leading Edge Flap and Trailing Edge Flap Undeflected

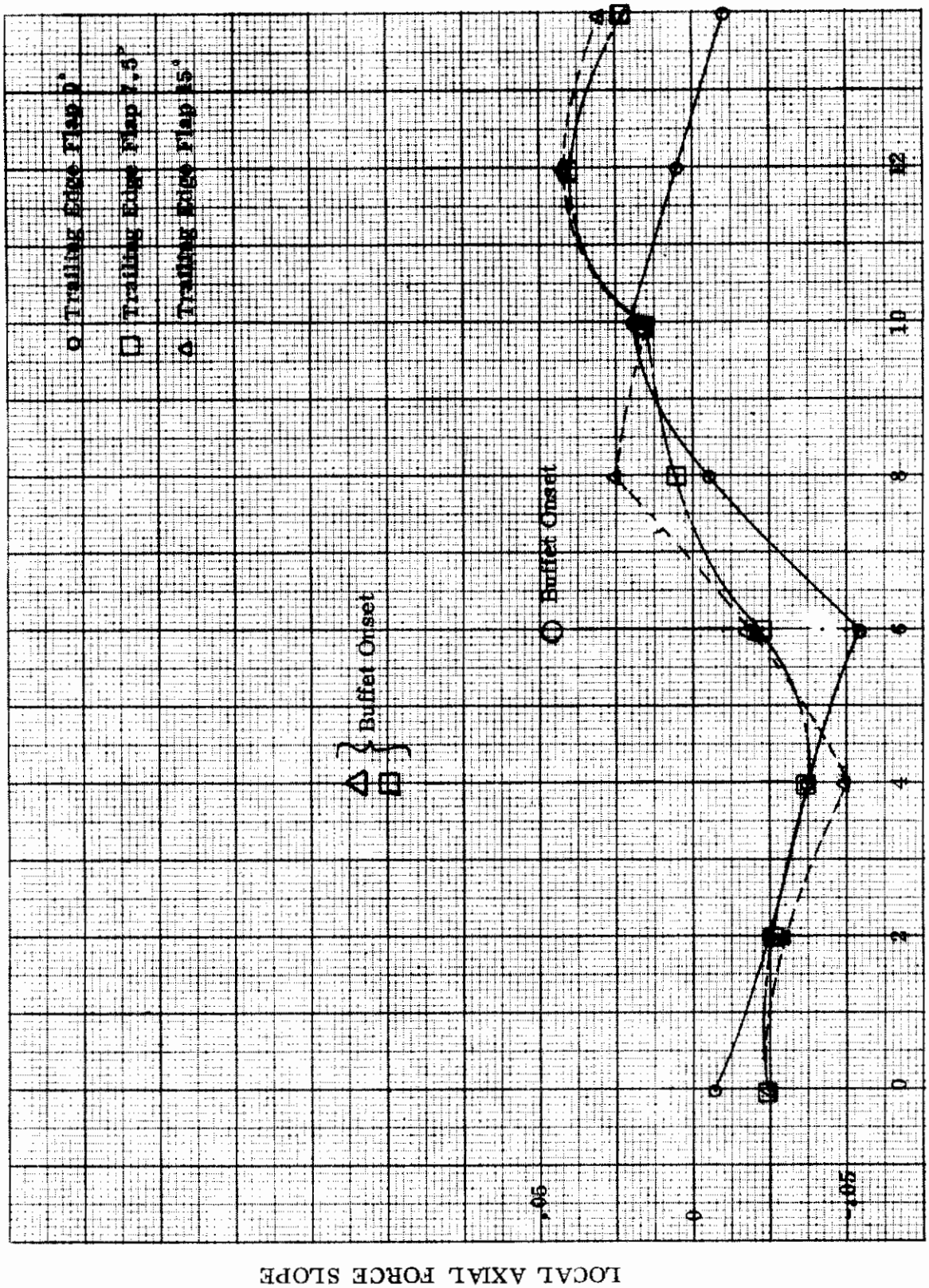

Figure 30. - - - Continued
(b) Leading Edge Flap 8°, Trailing Edge Flap Deflected

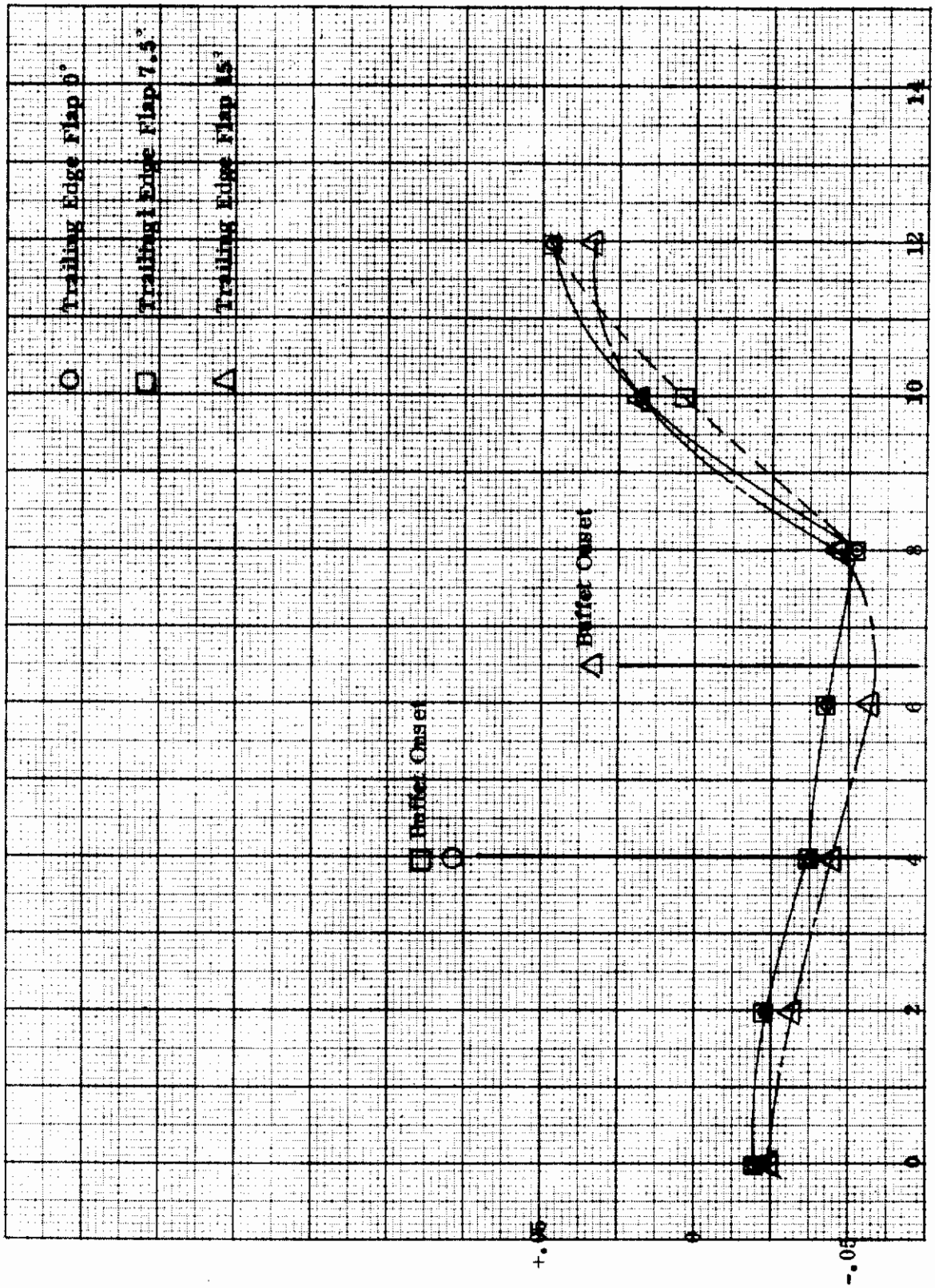

Figure 30. - - - Concluded
(c) Leading Edge Flap 20°, Trailing Edge Flap Deflected

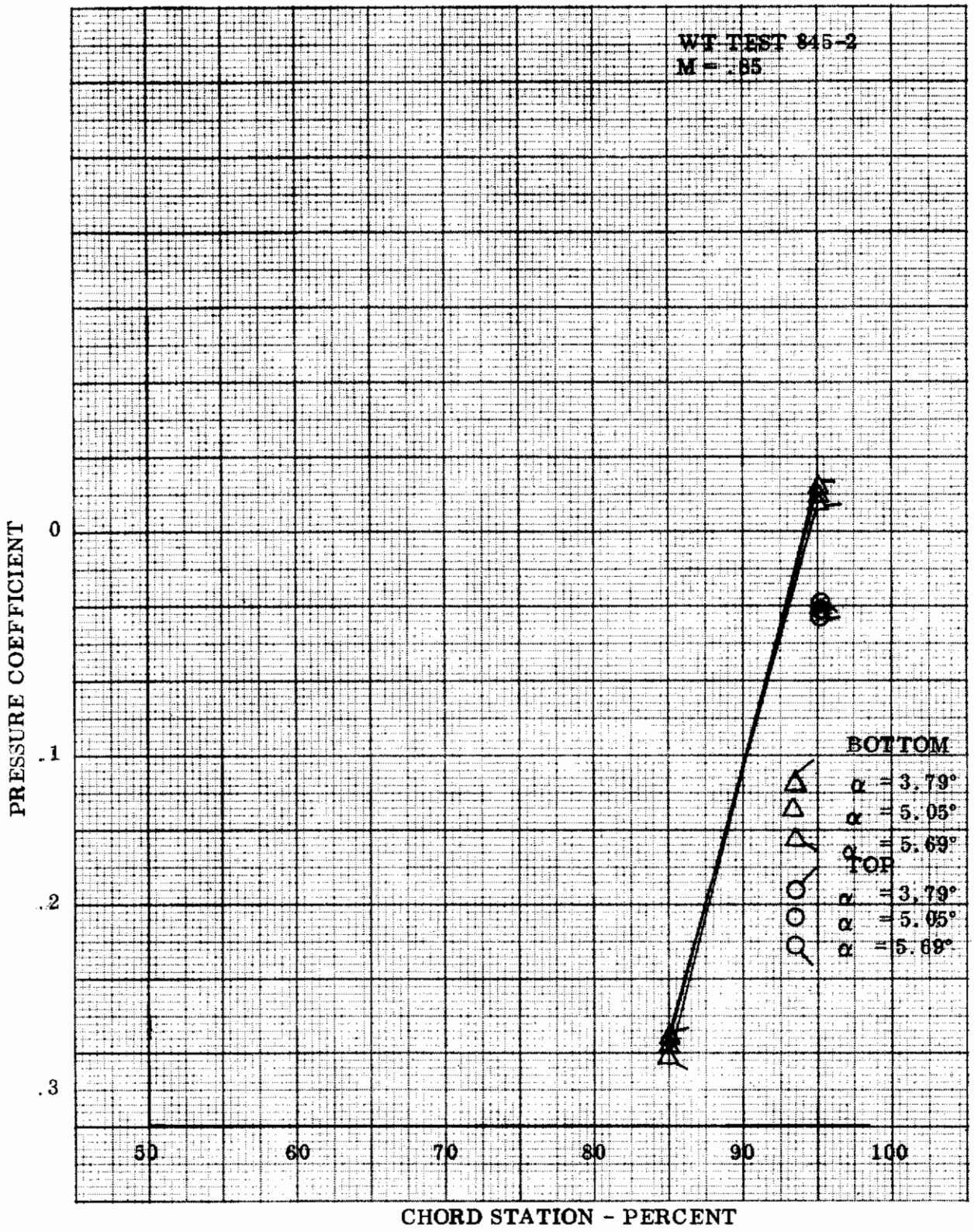

Figure 31. Chordwise Pressure Distribution below Mach Buffet, Near Mach Buffet Onset, and above Onset of Mach Buffet. Wing Station 95
(a) Leading Edge Flap and Trailing Edge Flap Undeflected

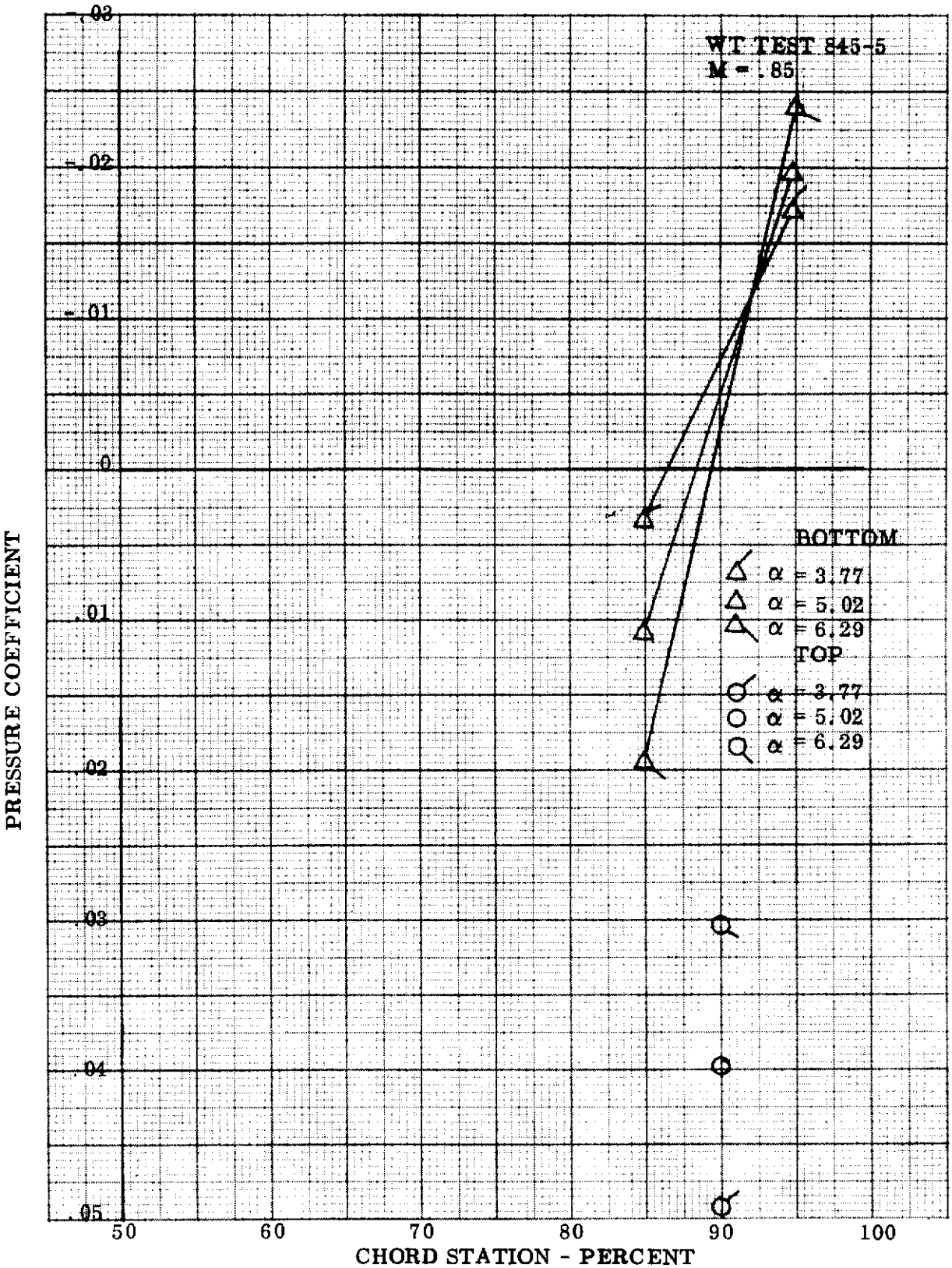

Figure 31. - - - Continued
(b) Leading Edge Flap 8°, Trailing Edge Flap Undeflected

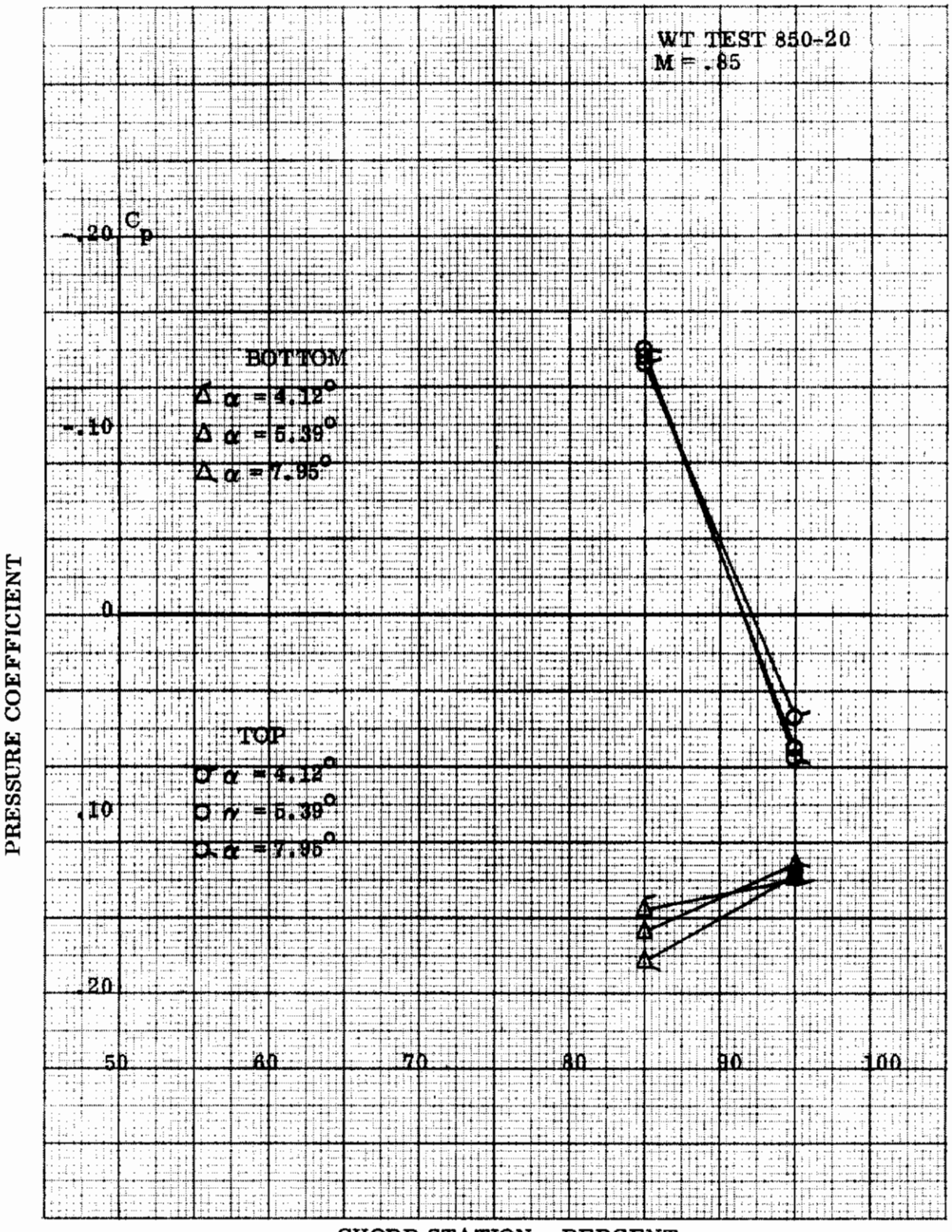

Figure 31. - - - Continued
(c) Leading Edge Flap 8°, Trailing Edge Flap 7.5°

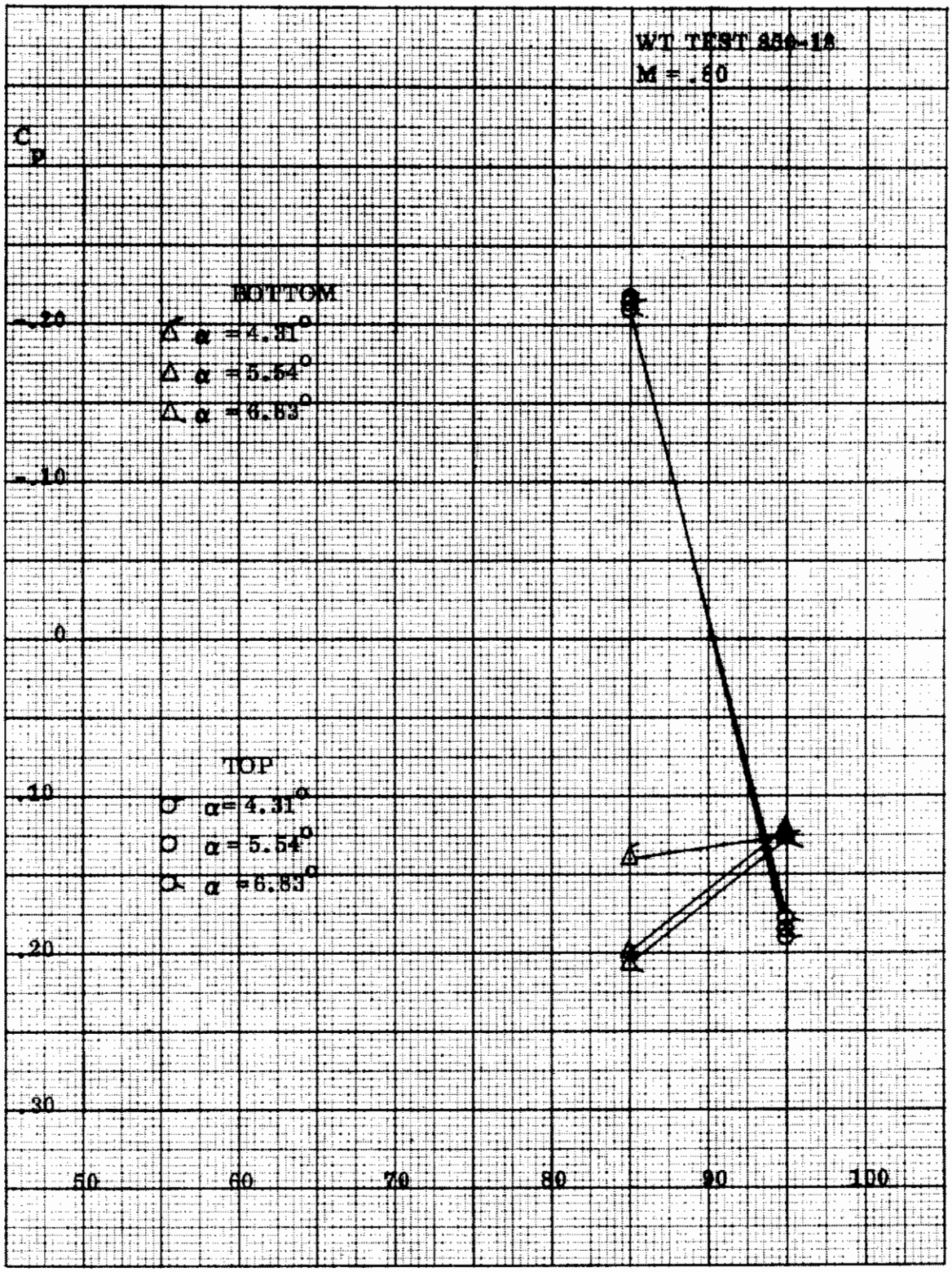

Figure 31. - - - Continued
(d) Leading Edge Flap 8°, Trailing Edge Flap 15°

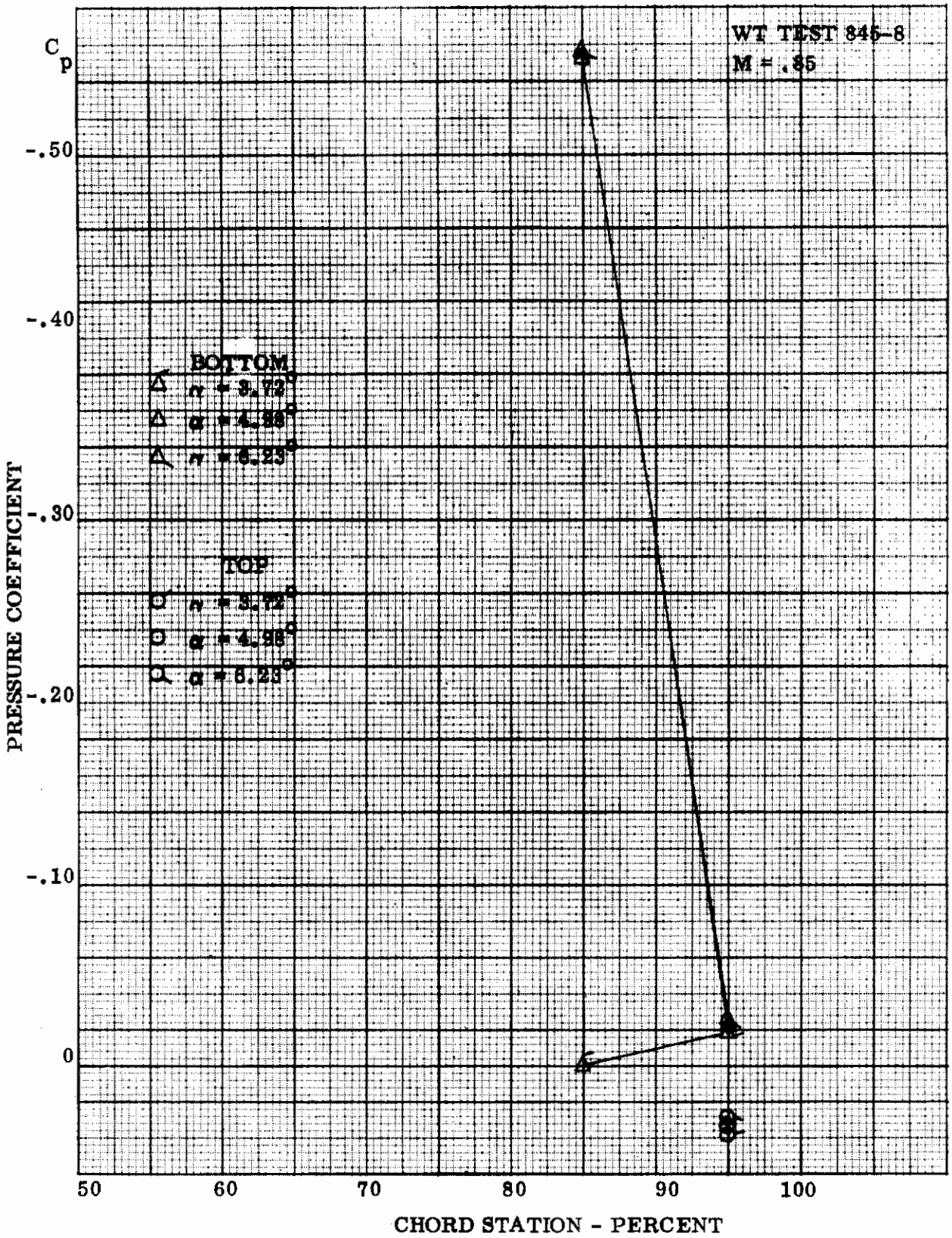

Figure 31. - - - Continued
(e) Leading Edge Flap 20°, Trailing Edge Flap Undeflected

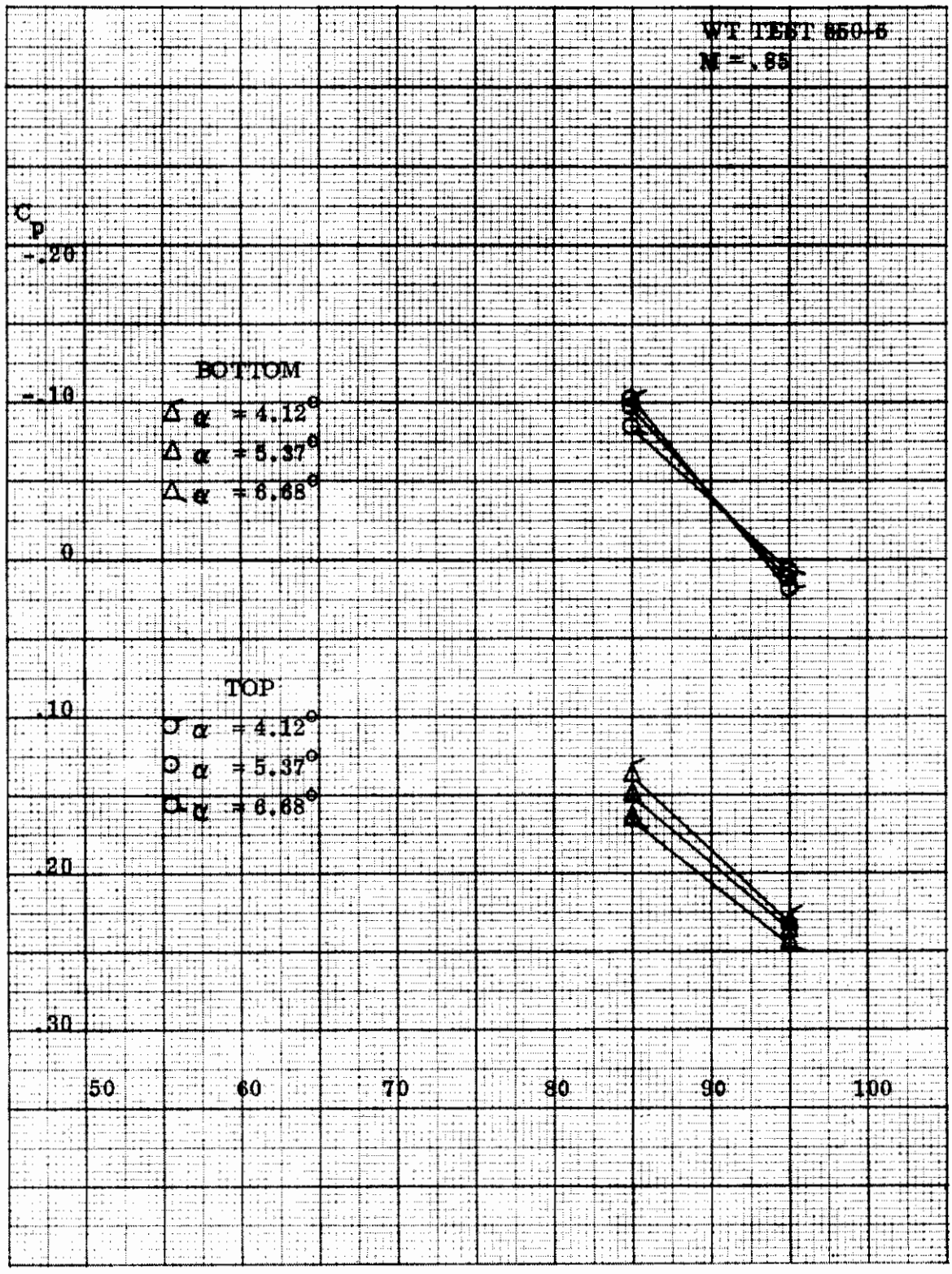

Figure 31. - - - Continued
(f) Leading Edge Flap 20°, Trailing Edge Flap 7.5°

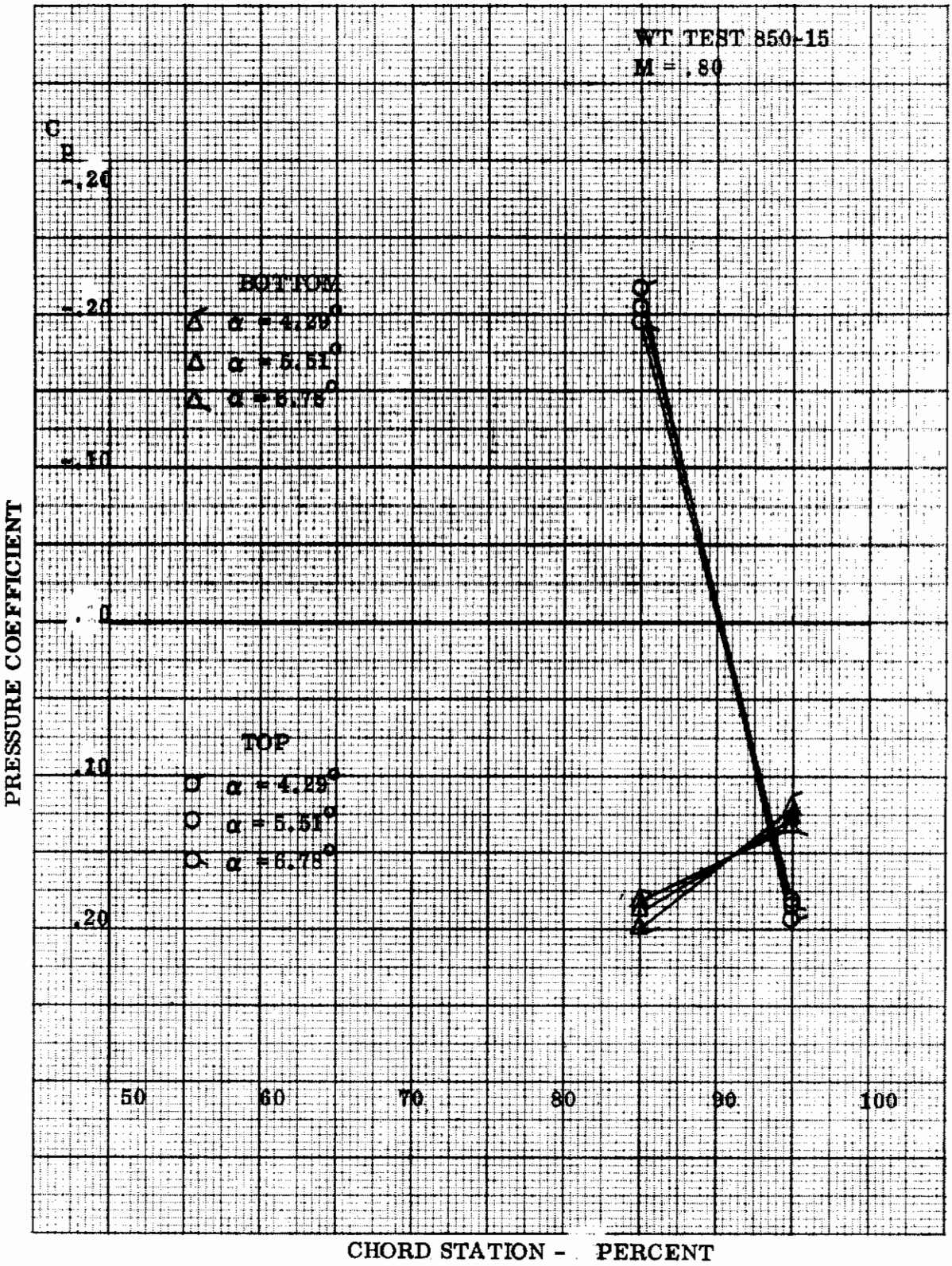

Figure 31. - - - Concluded
(g) Leading Edge Flap 20°, Trailing Edge Flap 15°

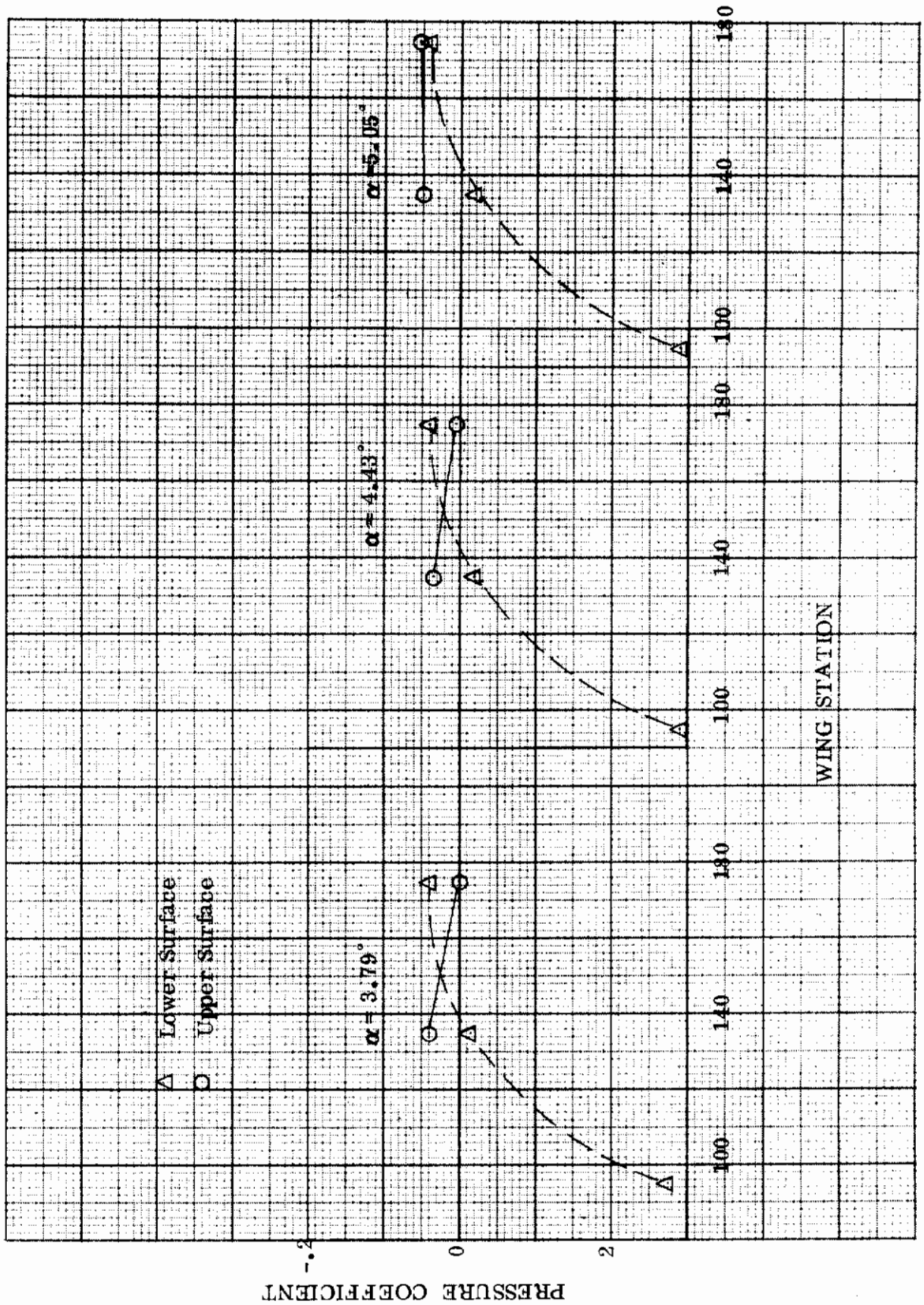

Figure 32. Spanwise Pressure Distribution below Mach Buffet, near Onset of Mach Buffet, and above Cnset of Mach Buffet. 85% Chord.
(a) Leading Edge Flap and Trailing Edge Flap Undeflected

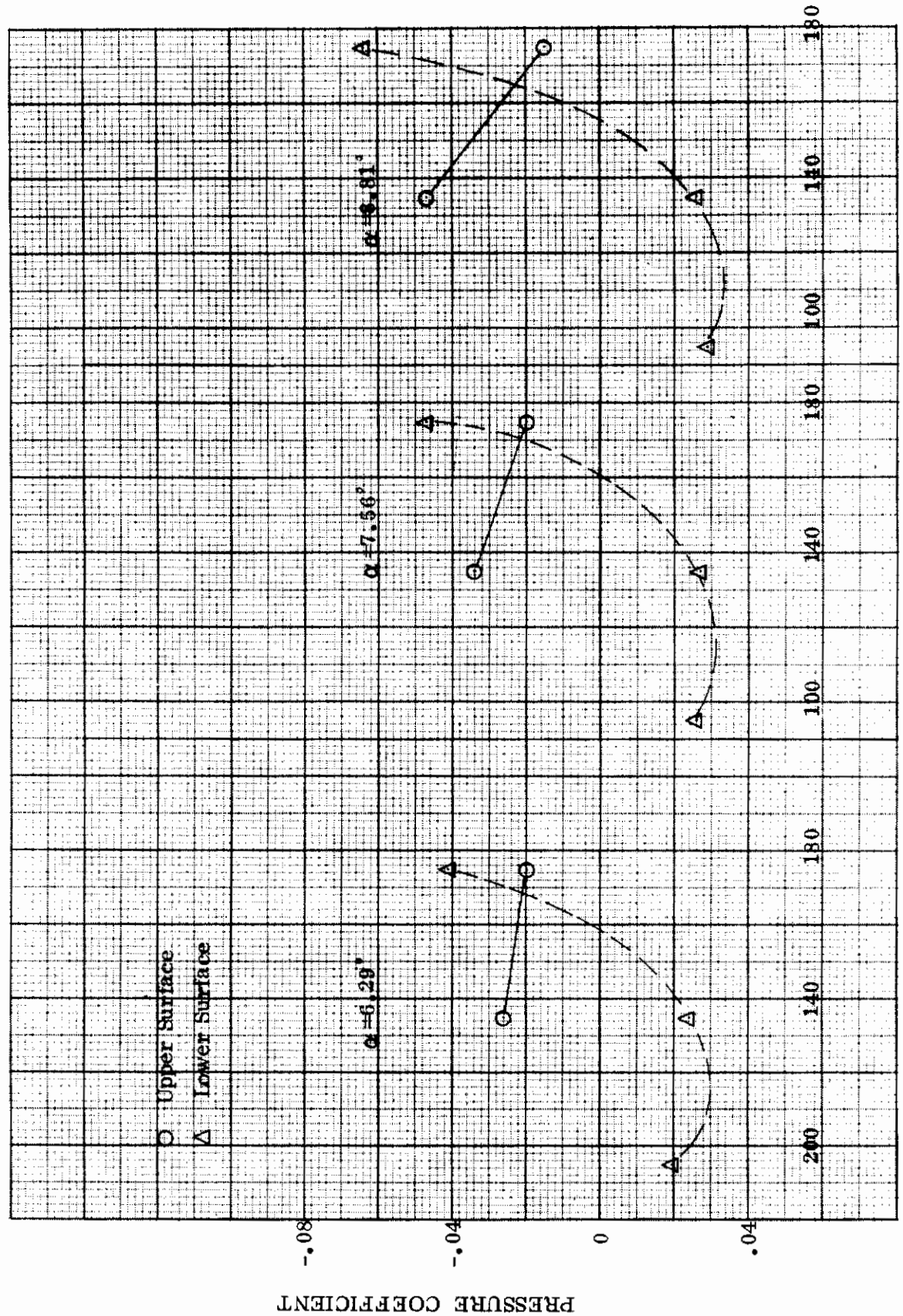

Figure 32. - - - Continued
(b) Leading Edge Flap 8°, Trailing Edge Flap Undeflected

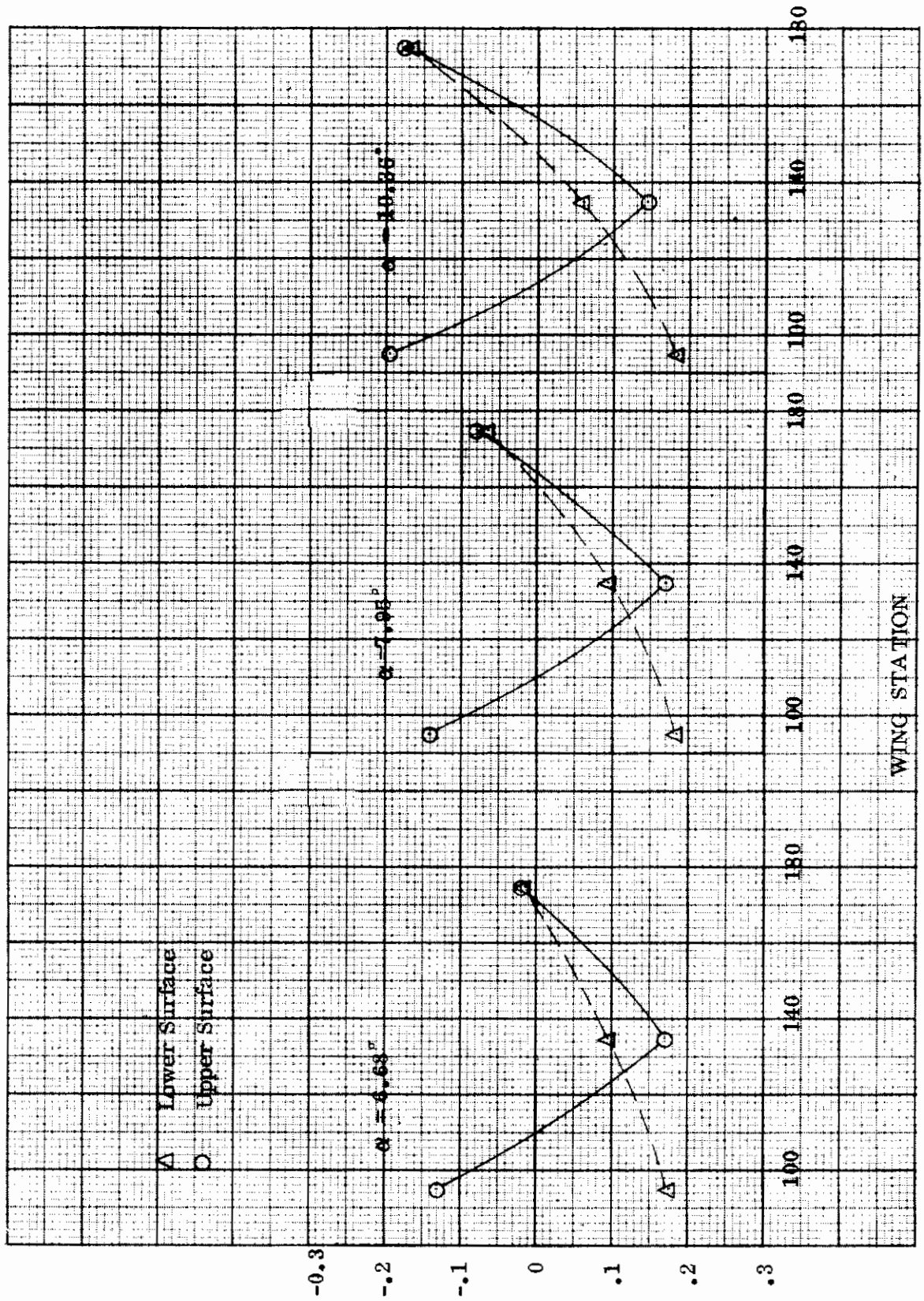

Figure 32. - - - Continued
(c) Leading Edge Flap 8°, Trailing Edge Flap 7.5°

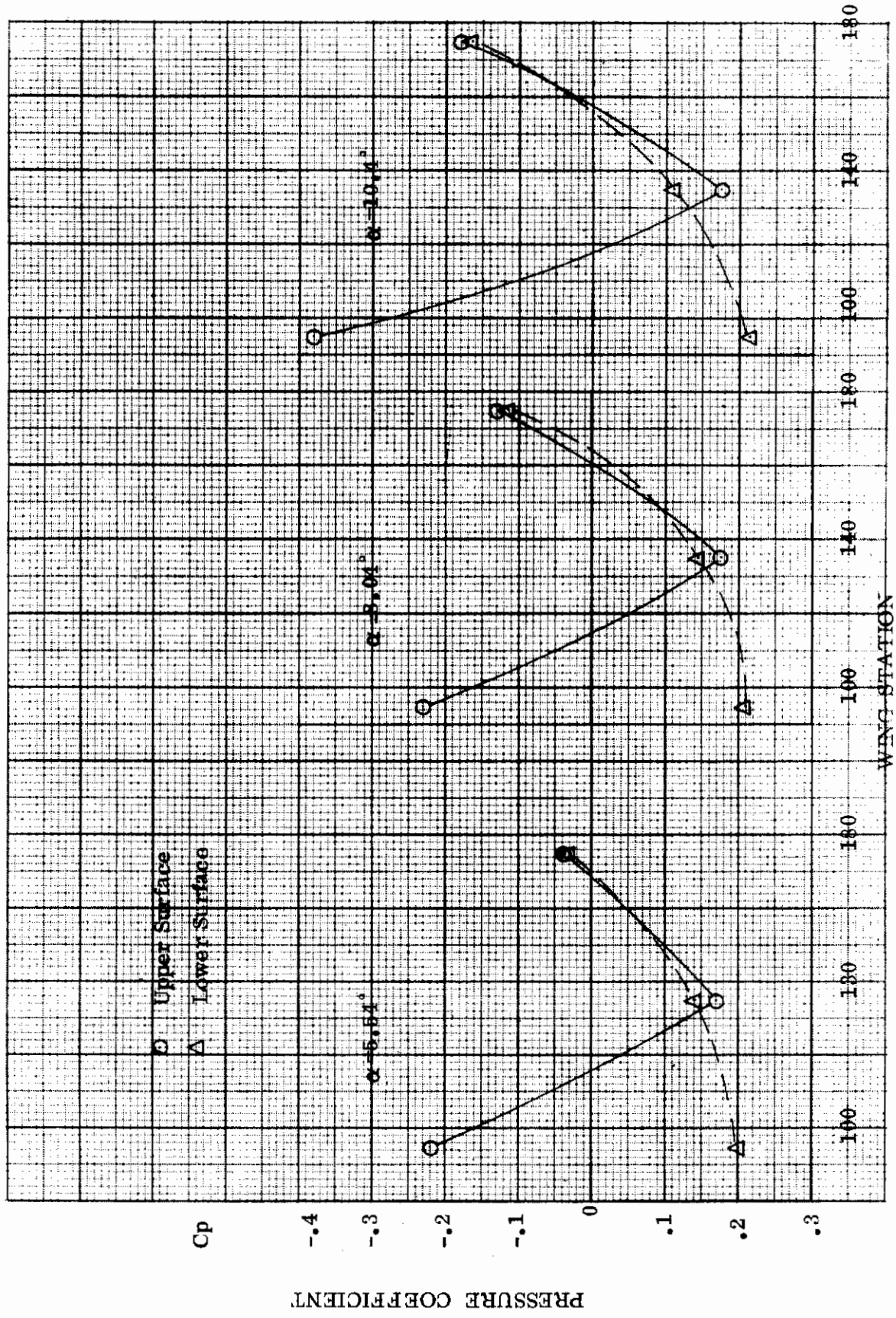

Figure 32. - - - Continued
(d) Leading Edge Flap 8°, Trailing Edge Flap 15°

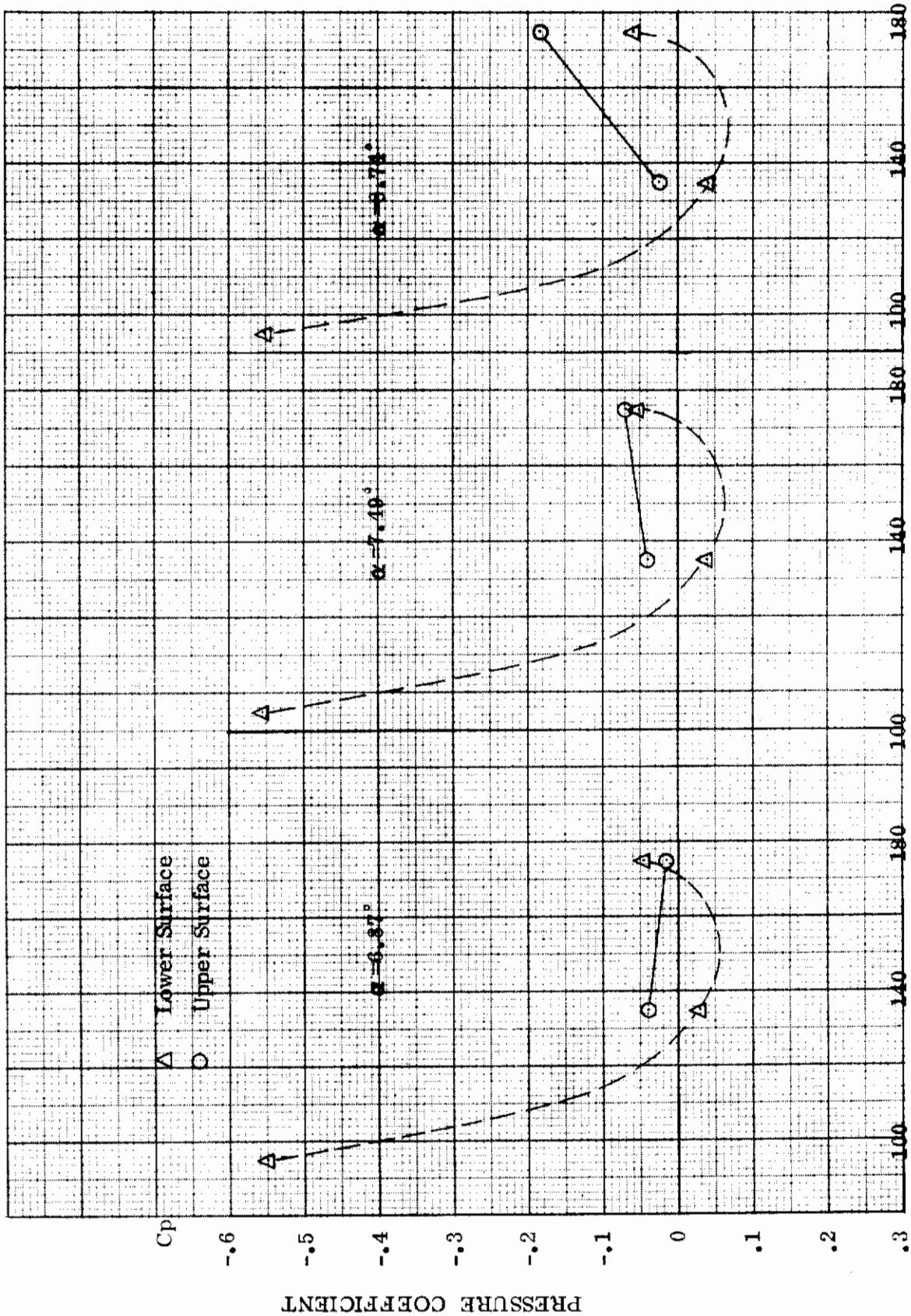

Figure 32. - - - Continued
(e) Leading Edge Flap 20°, Trailing Edge Flap Undeflected

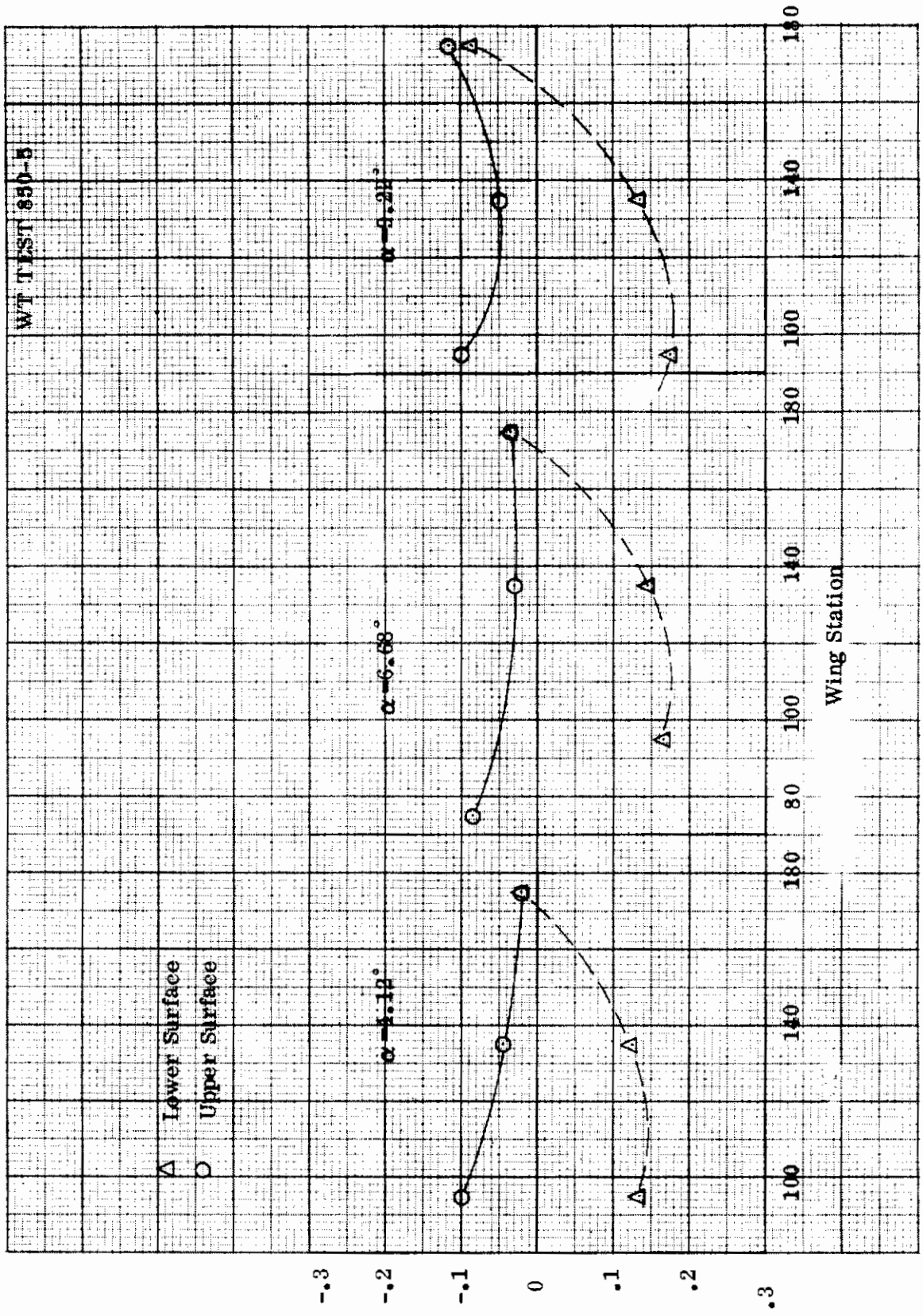

Figure 32. - - - Continued
(f) Leading Edge Flap 20°, Trailing Edge Flap 7.5°

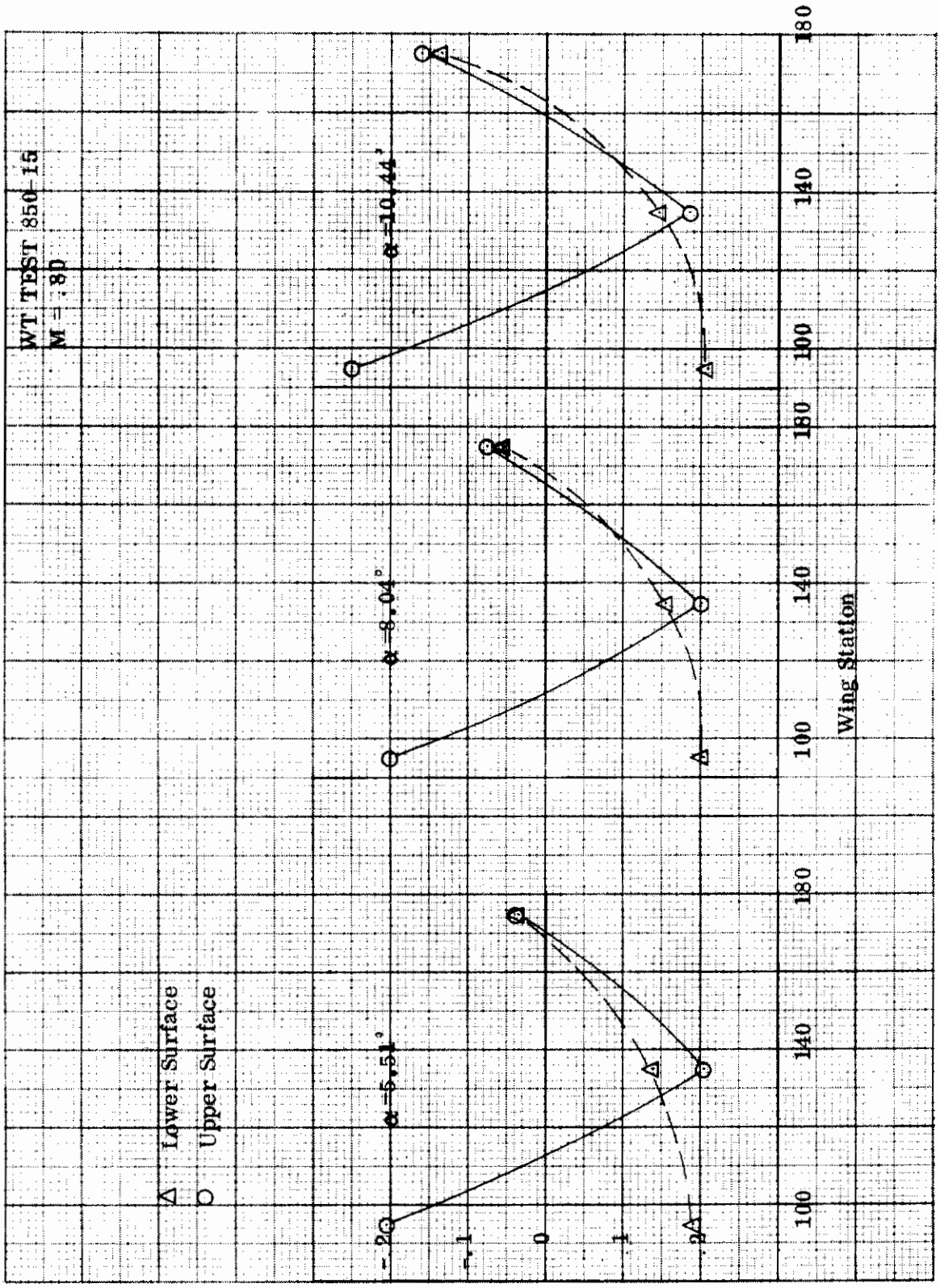

Figure 32. - - - Concluded
(g) Leading Edge Flap 20^{o}, Trailing Edge Flap 15^{o}

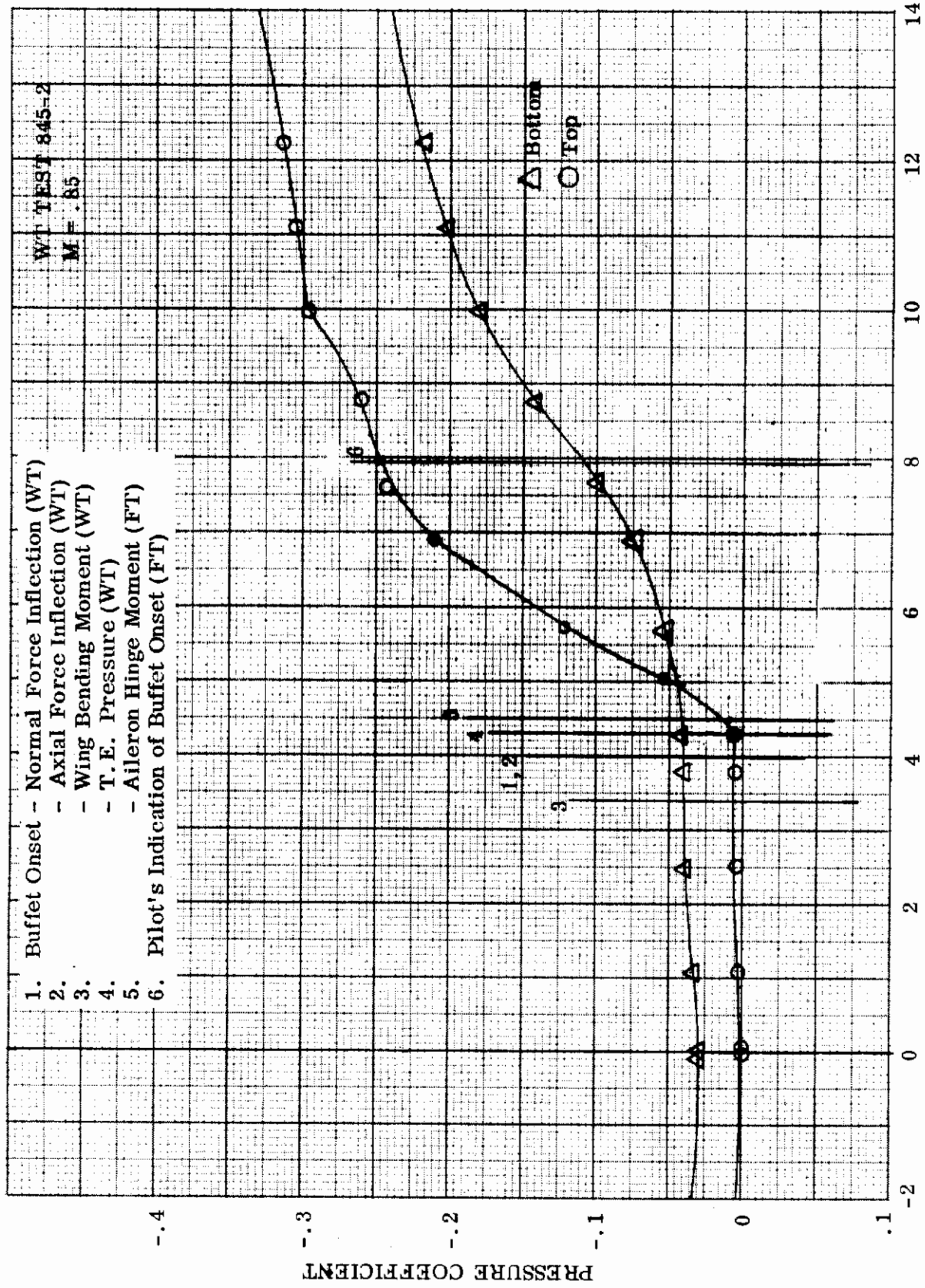

Figure 33. Outboard Trailing Edge Pressure Variation with Angle of Attack at Wing Station 175 at 85% Chord

(a) Leading Edge Flap and Trailing Edge Flap Undeflected

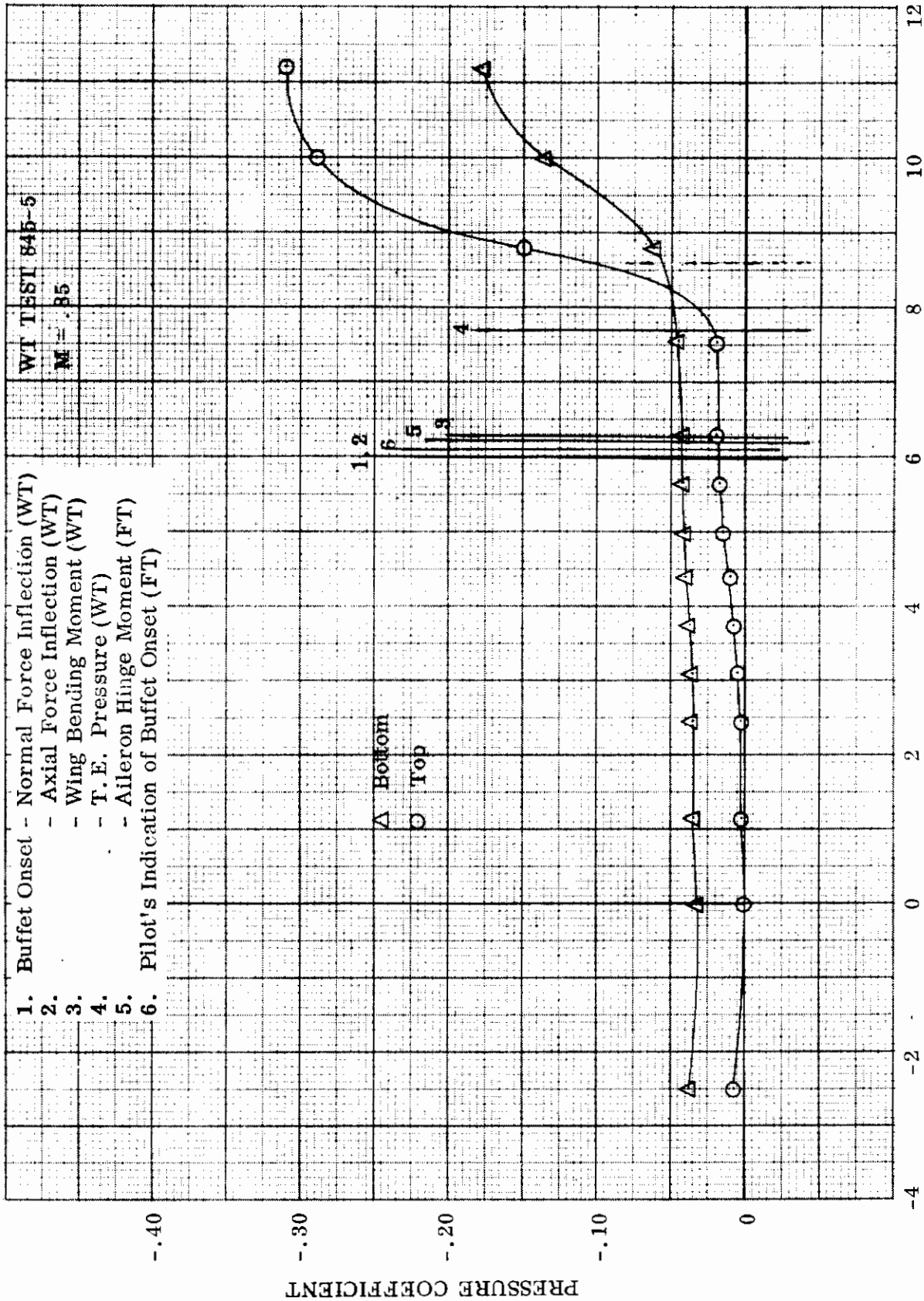

Figure 33. - - - Continued
(b) Leading Edge Flap 8°, Trailing Edge Flap Undeflected

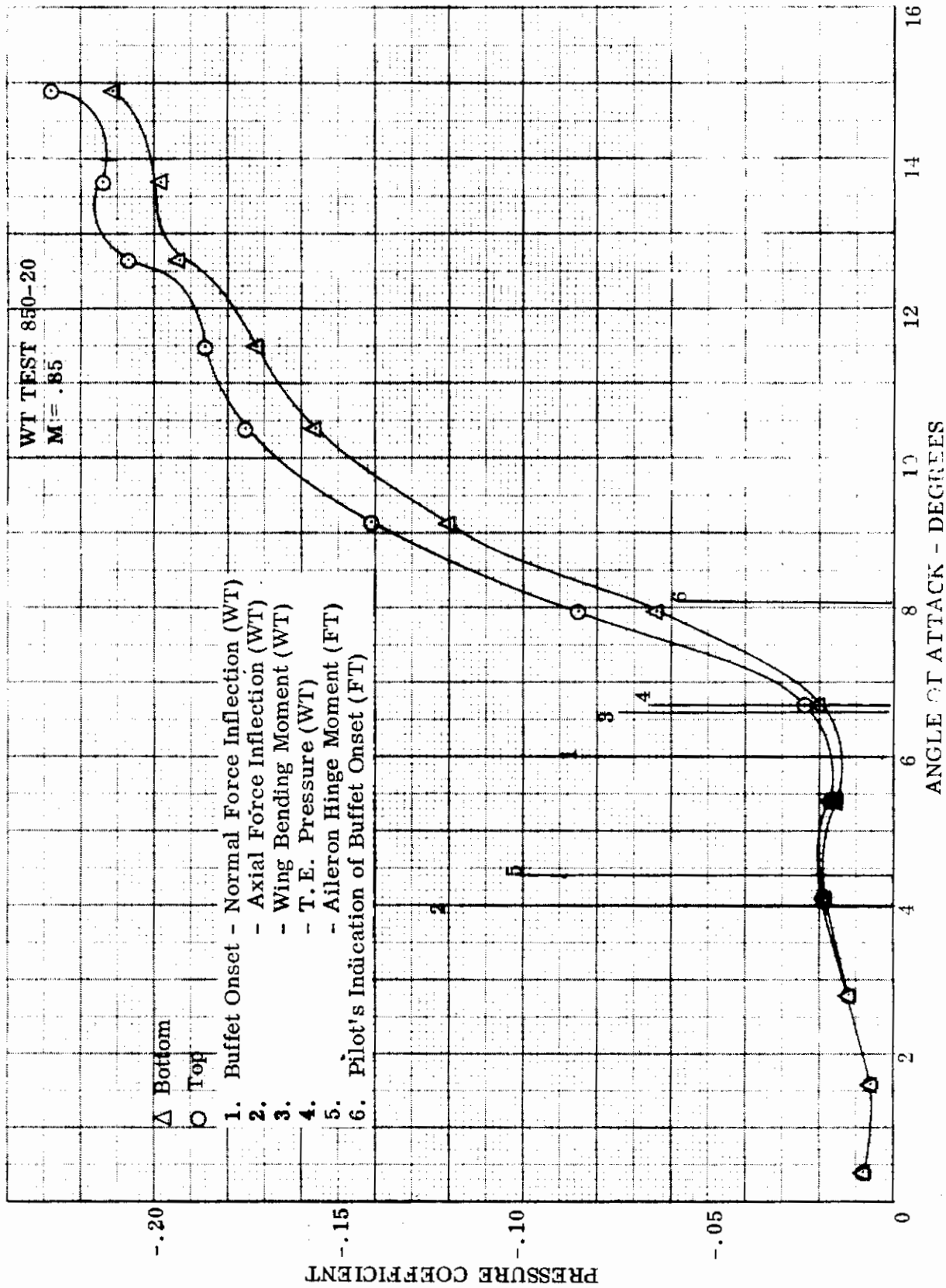

Figure 33. - - - Continued
(c) Leading Edge Flap 8^{o}, Trailing Edge Flap 7.5^{o}

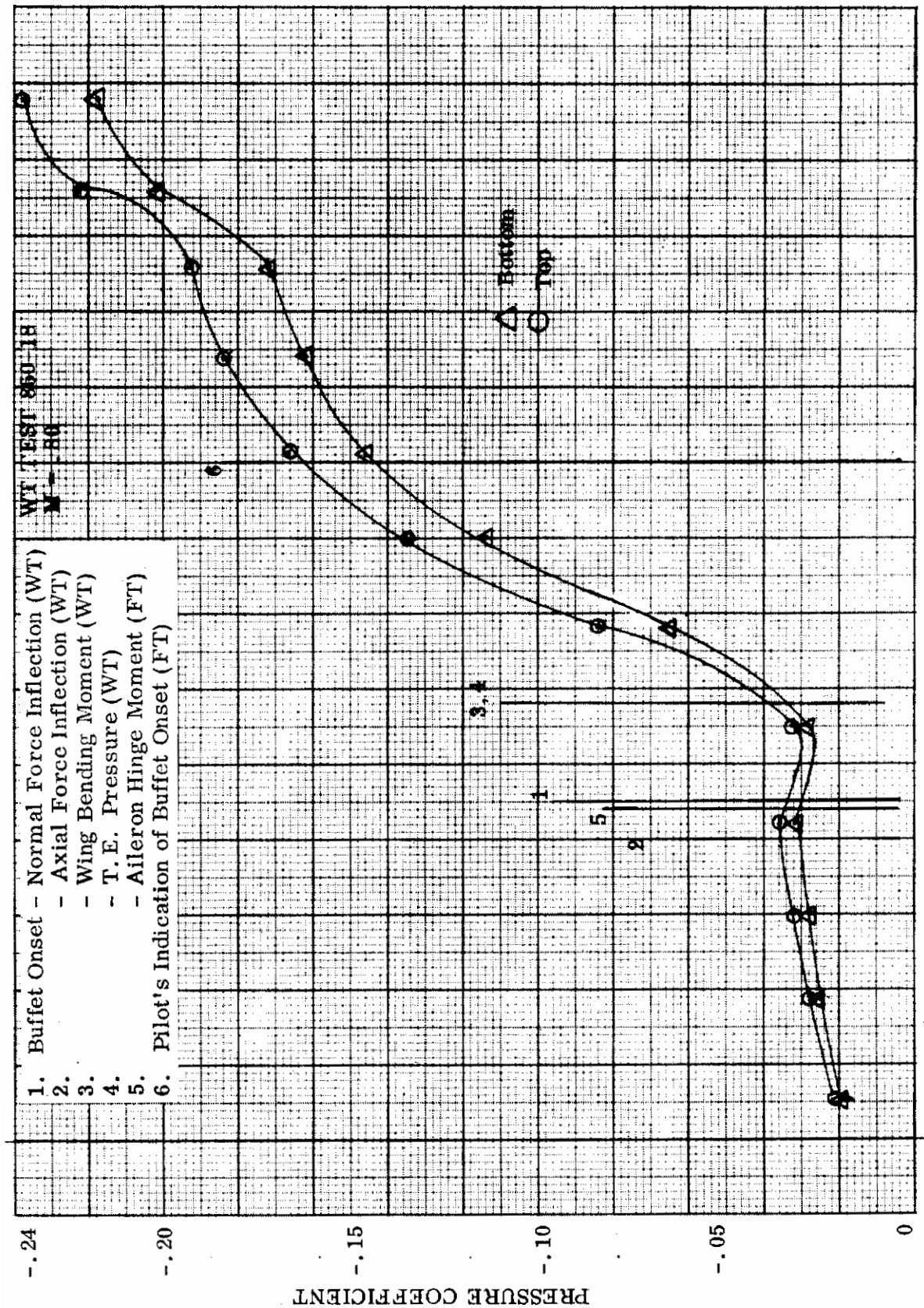

Figure 33. - - - Continued
(d) Leading Edge Flap 8°, Trailing Edge Flap 15°

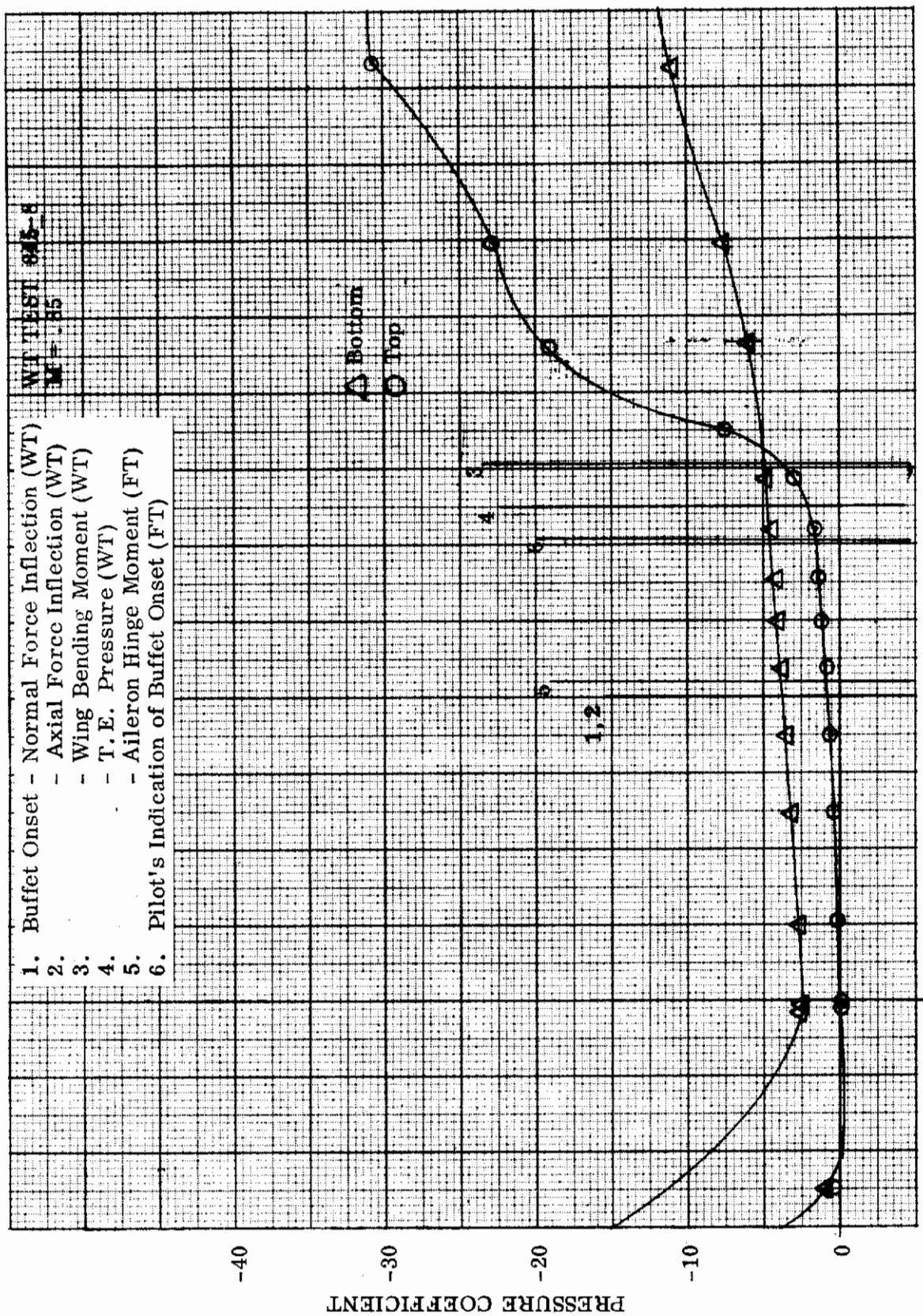

Figure 33. - - - - Continued
(e) Leading Edge Flap 20^{0}, Trailing Edge Flap Undeflected

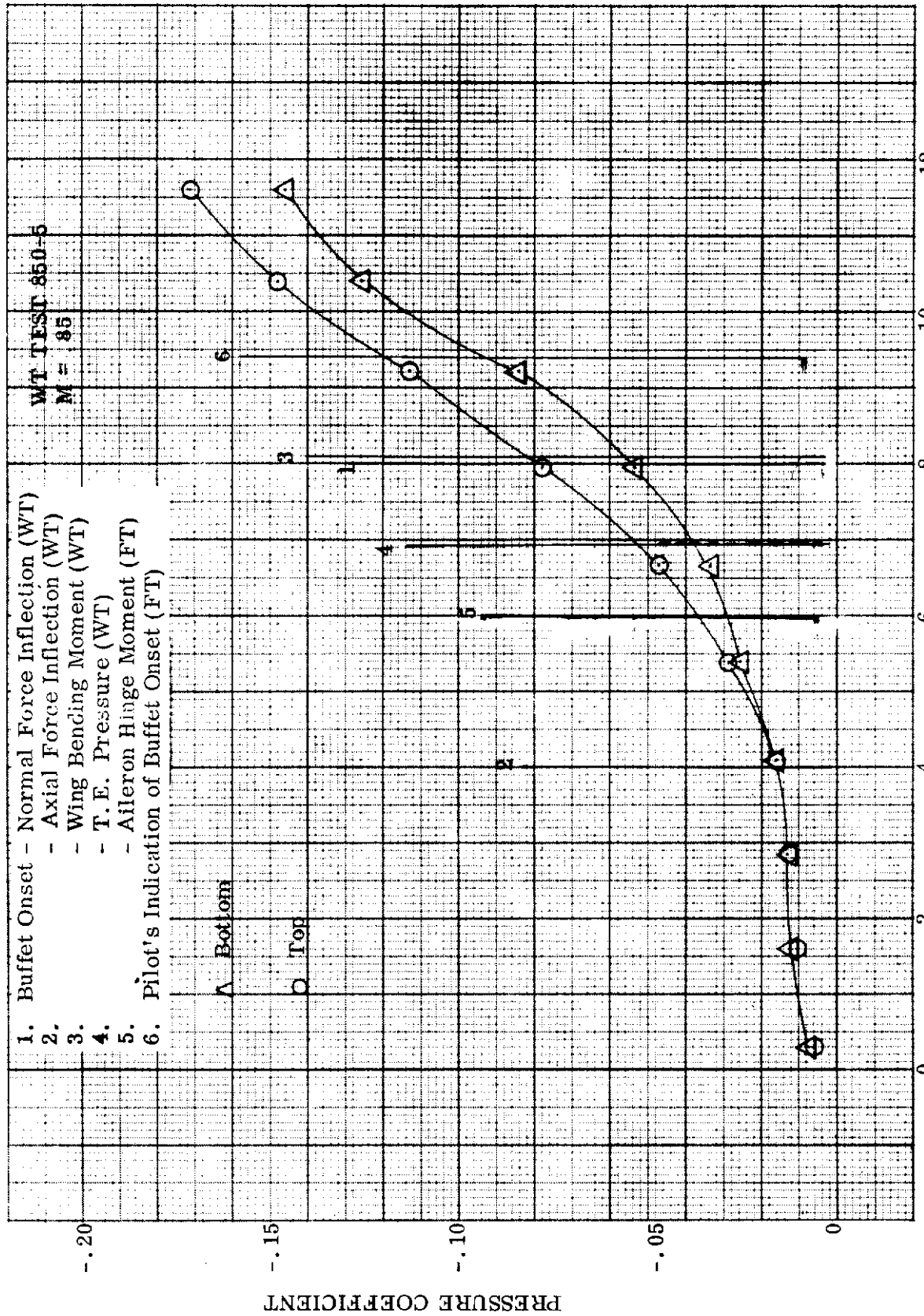

Figure 33. - - - Continued
(f) Leading Edge Flap 20°, Trailing Edge Flap 7.5°

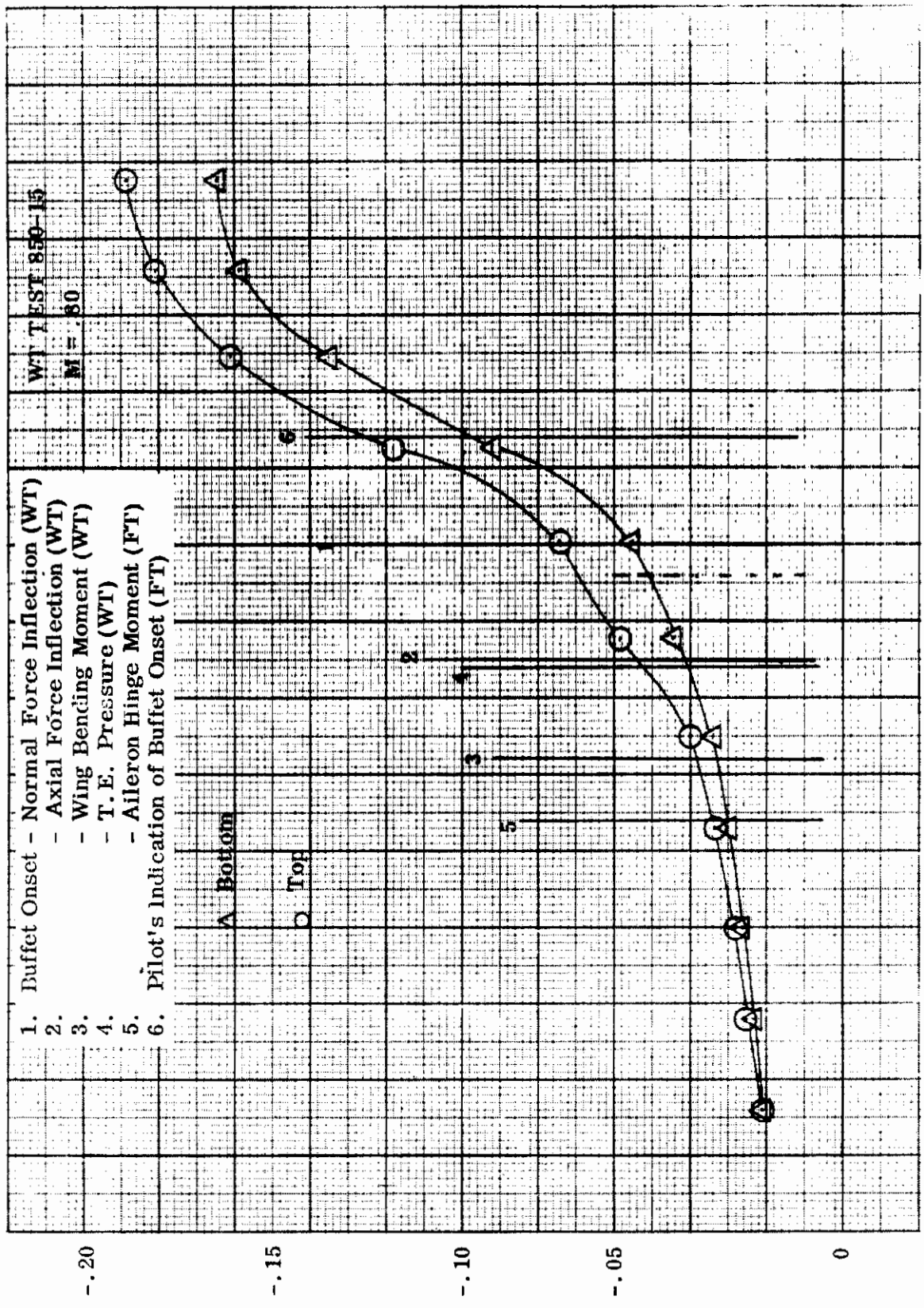

Figure 33. - - - Concluded
(g) Leading Edge Flap 20°, Trailing Edge Flap 15°

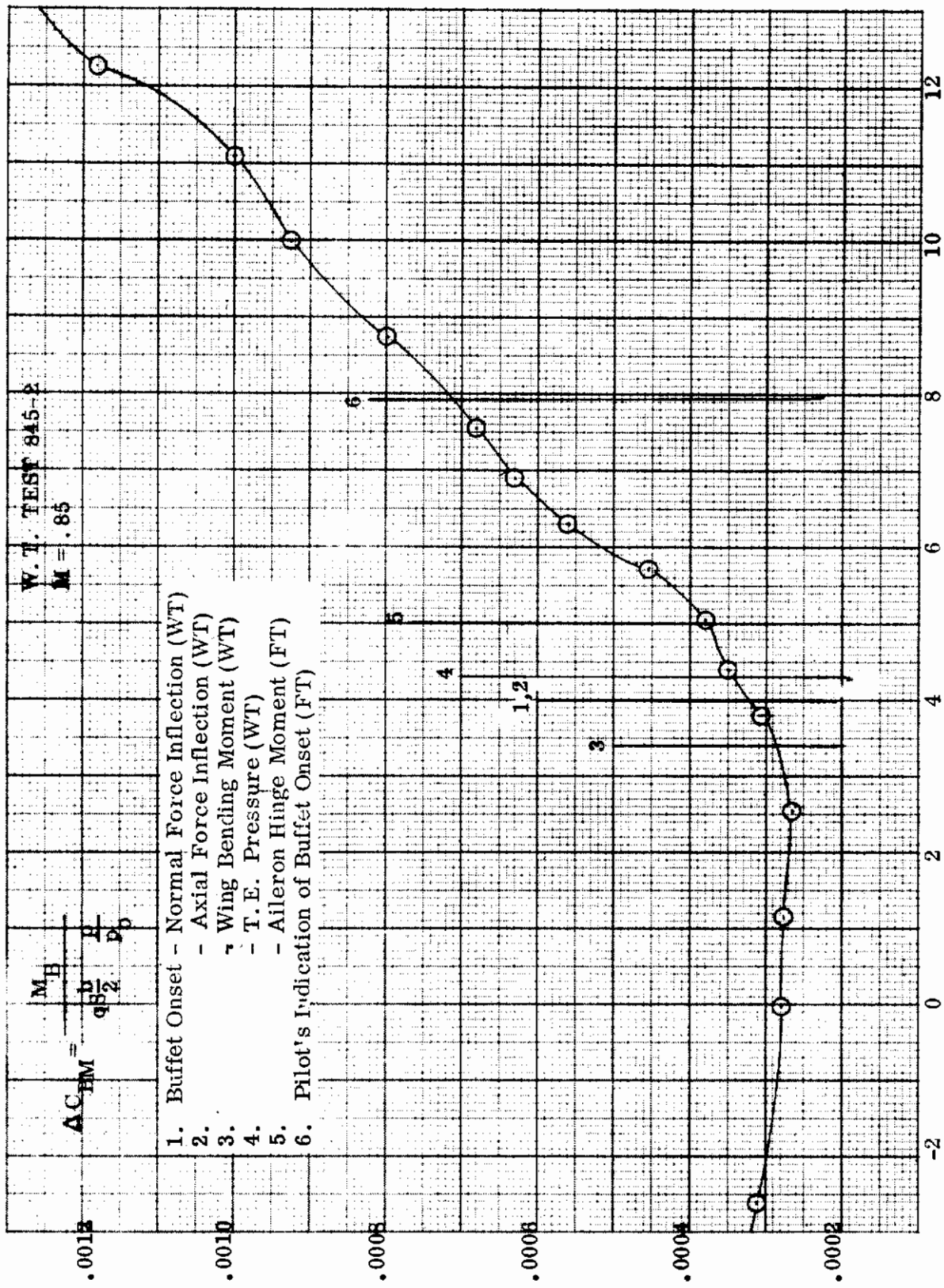

Figure 34. Variation of Coefficient of Wing Root-Mean-Square Bending Moment Fluctuations with Angle of Attack

(a) Leading Edge Flap and Trailing Edge Flap Undeflected

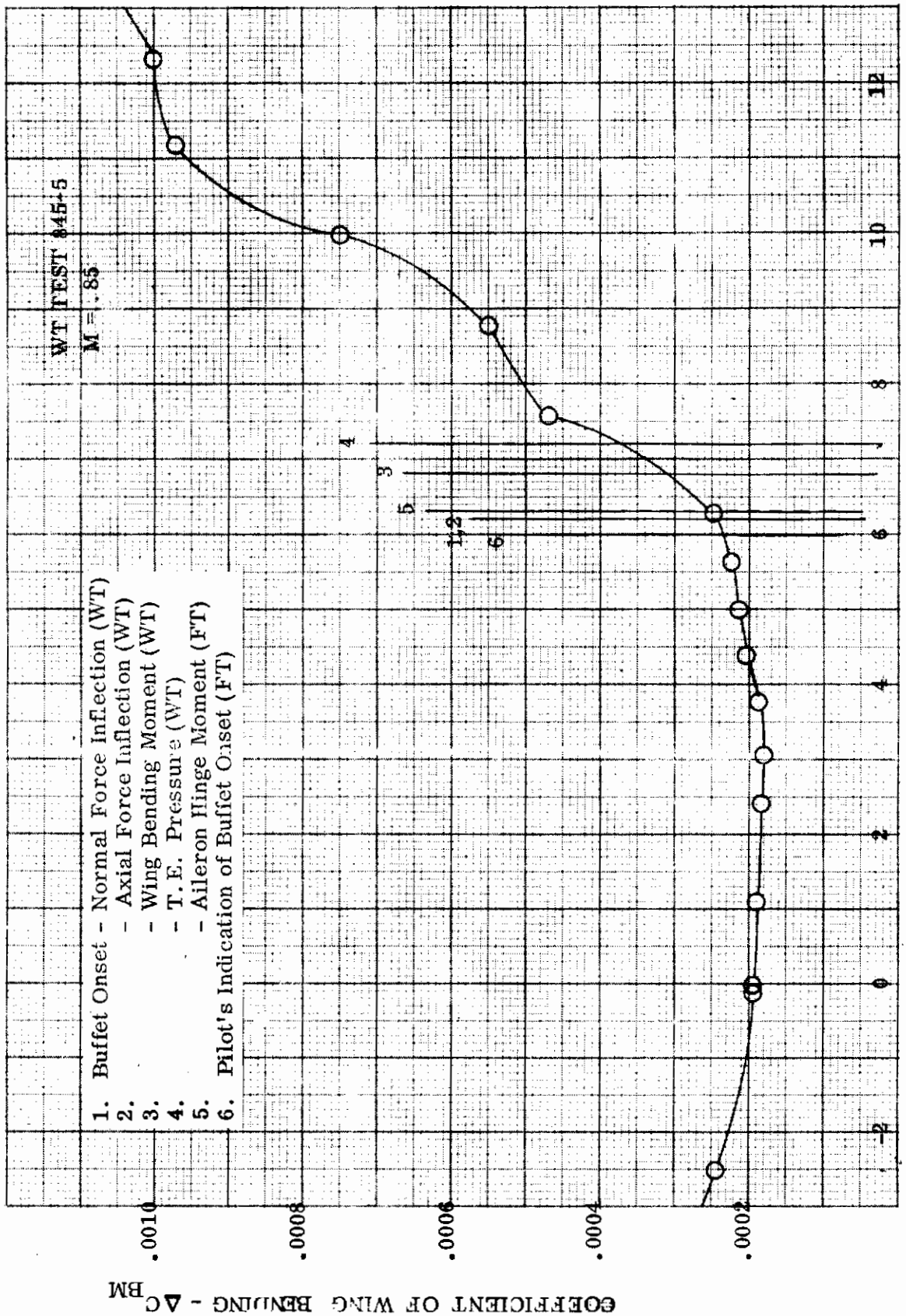

Figure 34. - - - Continued
(b) Leading Edge Flap 8°, Trailing Edge Flap Undeflected

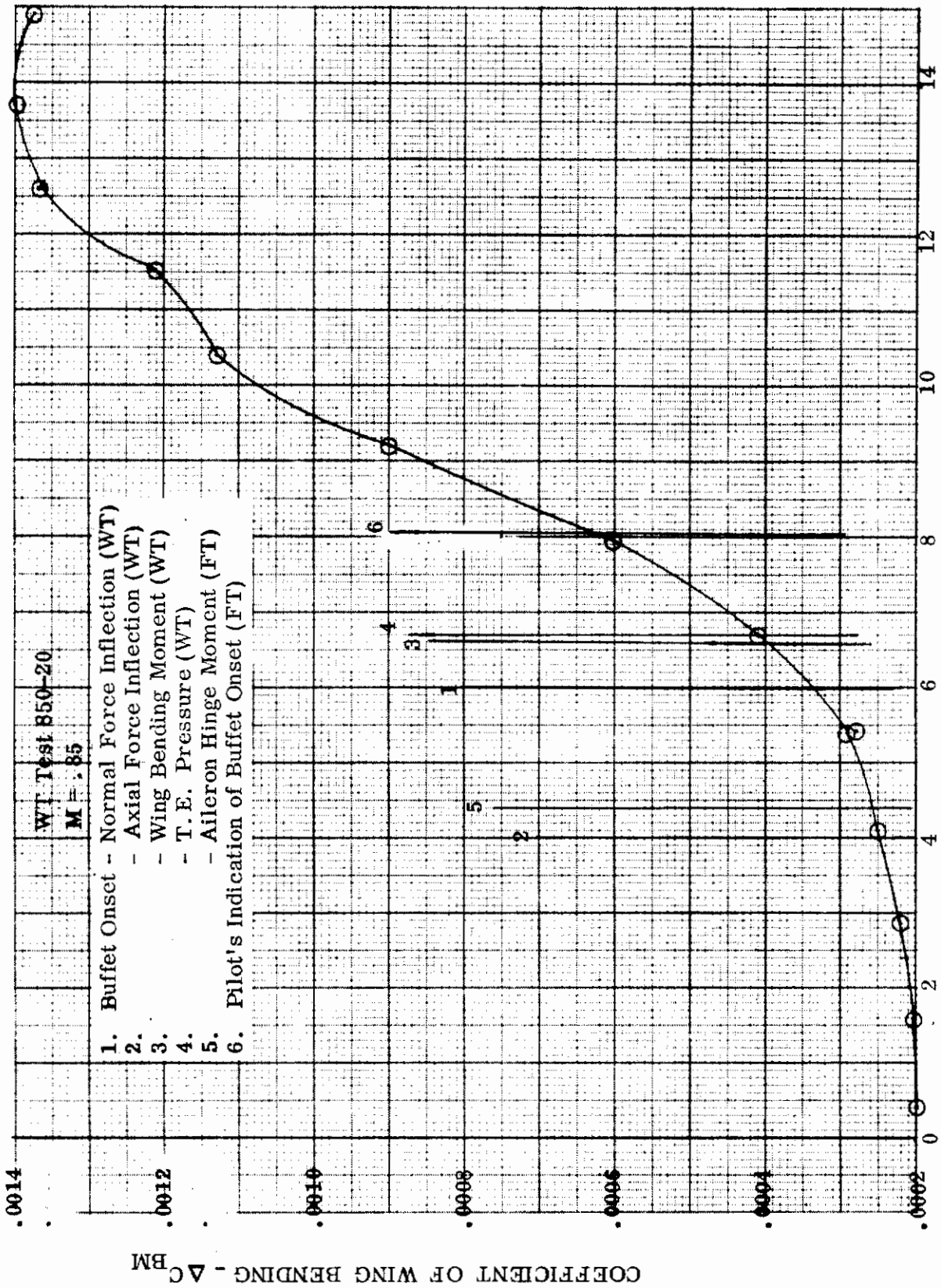

Figure 34. - - - Continued
(c) Leading Edge Flap 8^{o}, Trailing Edge Flap 7.5^{o}

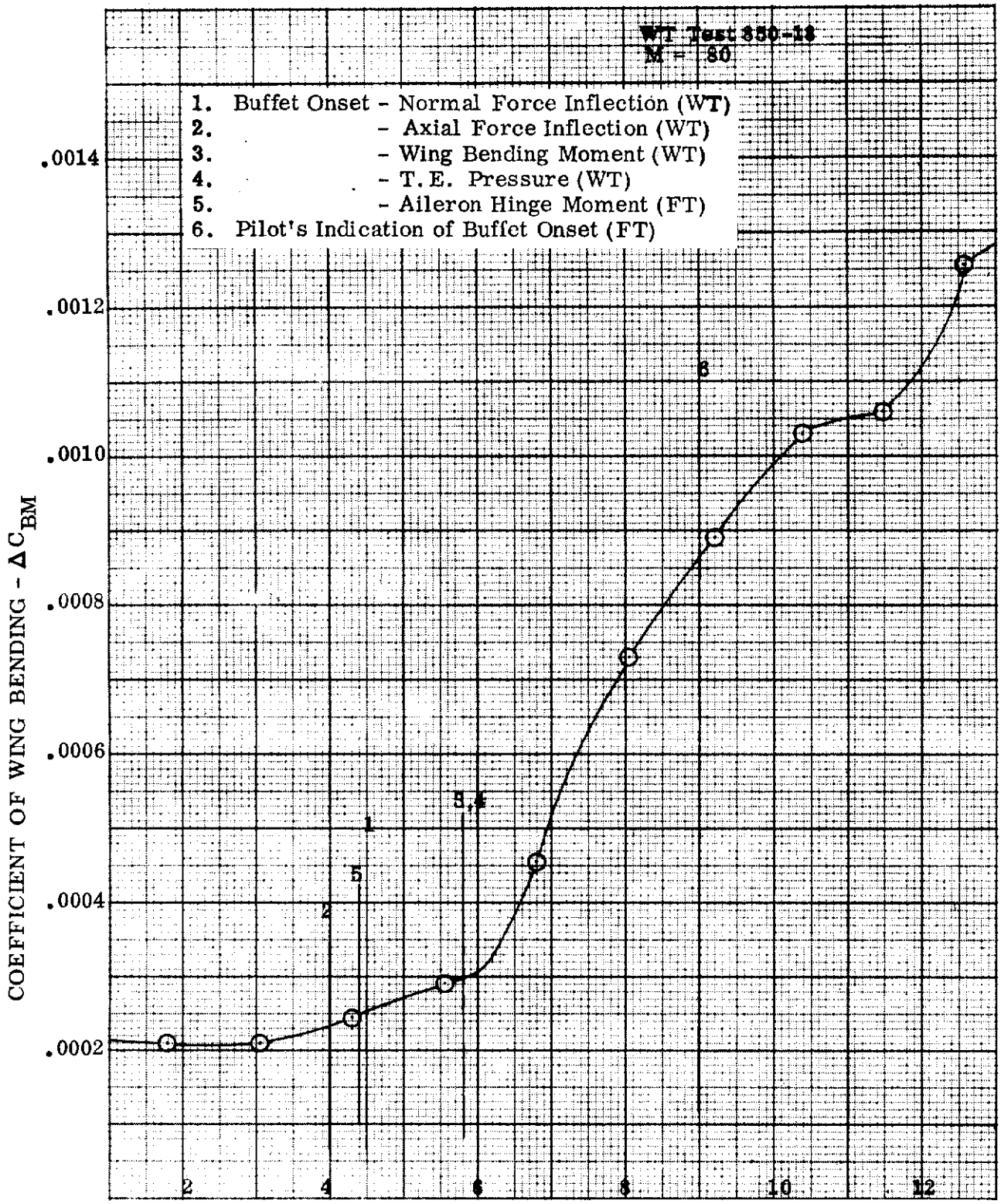

Figure 34. - - - Continued
(d) Leading Edge Flap 8°, Trailing Edge Flap 15°

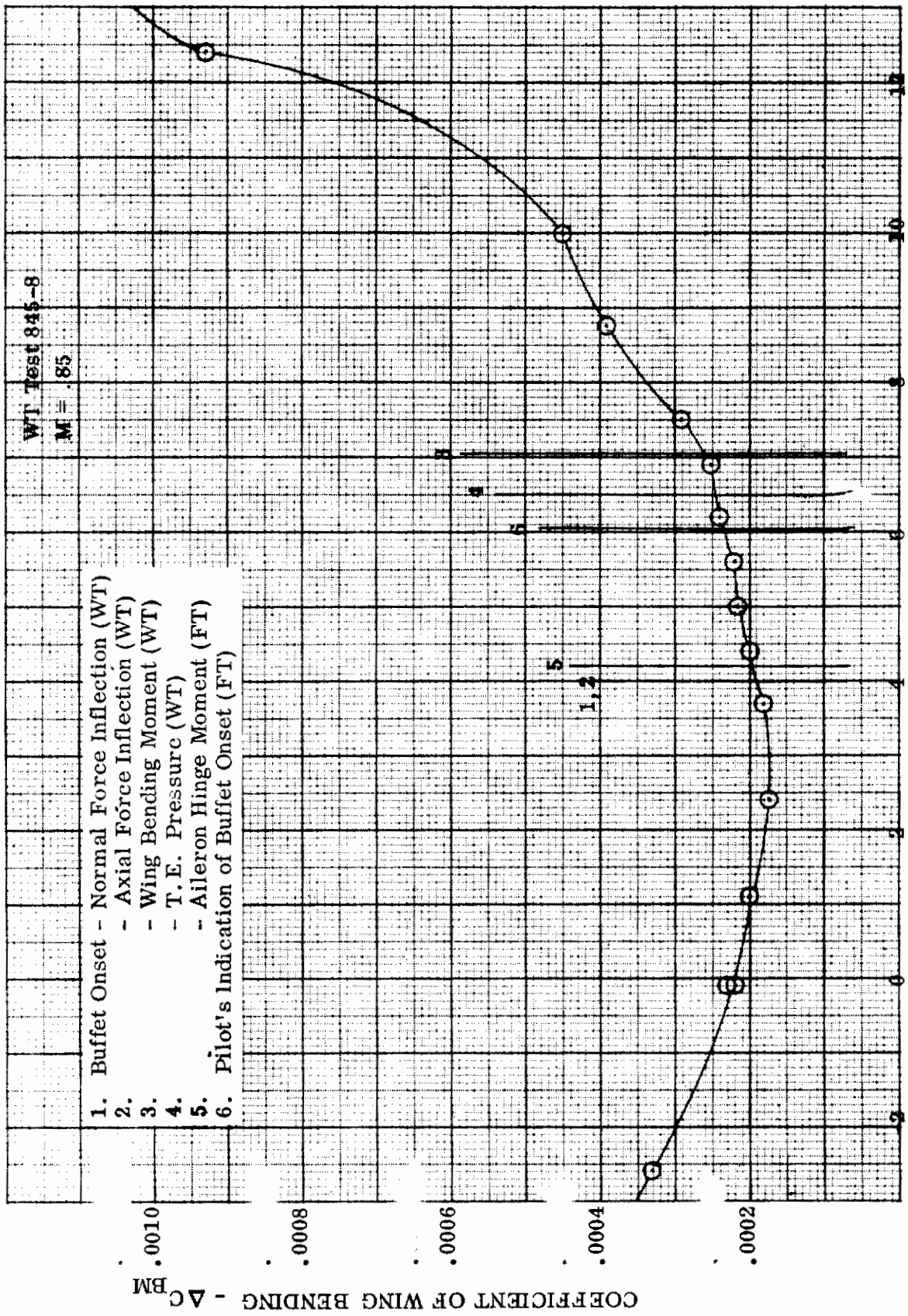

Figure 34. - - - Continued
(e) Leading Edge Flap 20°, Trailing Edge Flap Undeflected

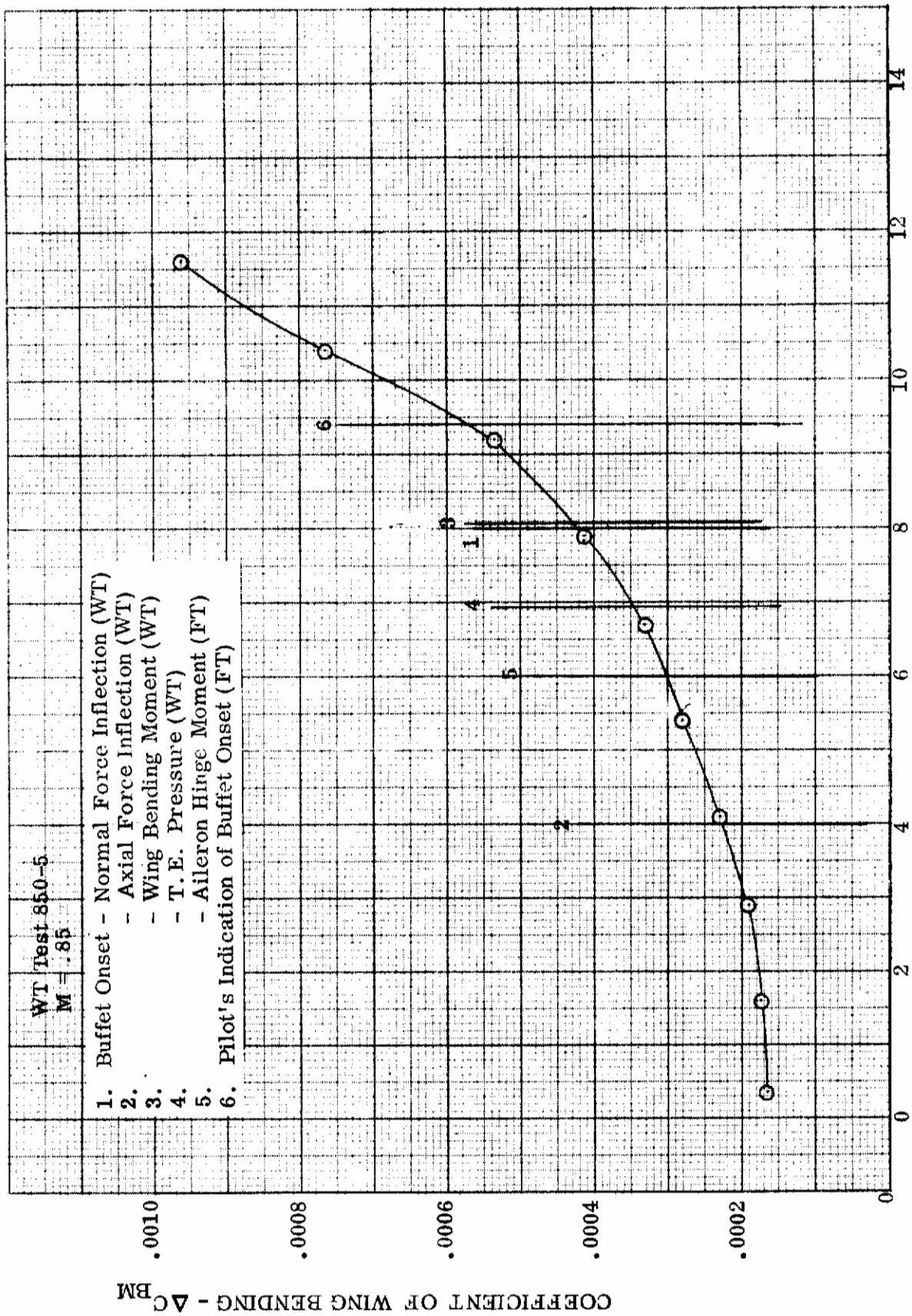

Figure 34. - - - Continued
(f) Leading Edge Flap 20°, Trailing Edge Flap 7.5°

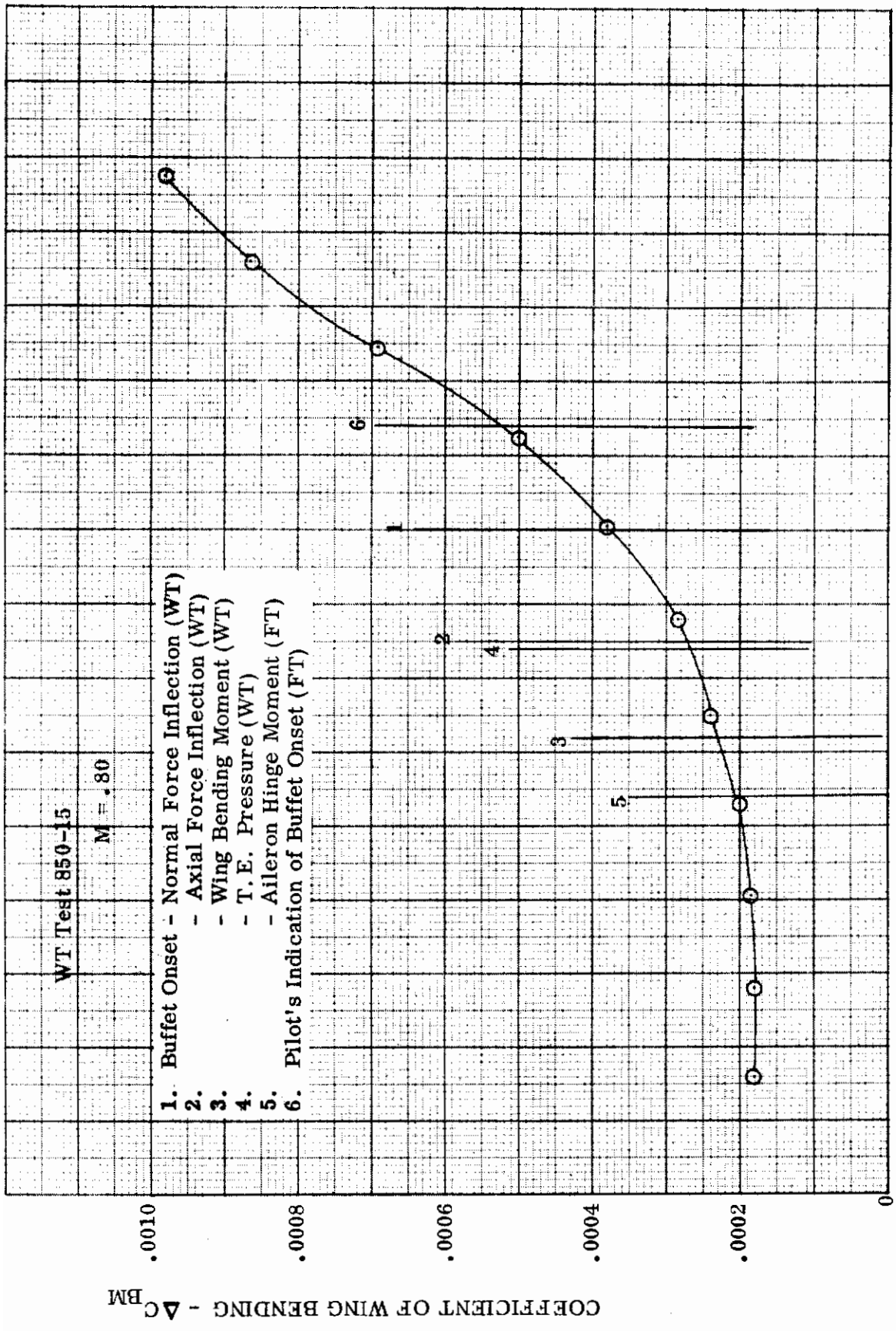

Figure 34. - - - Concluded
(g) Leading Edge Flap 20^{o}, Trailing Edge Flap 15^{o}

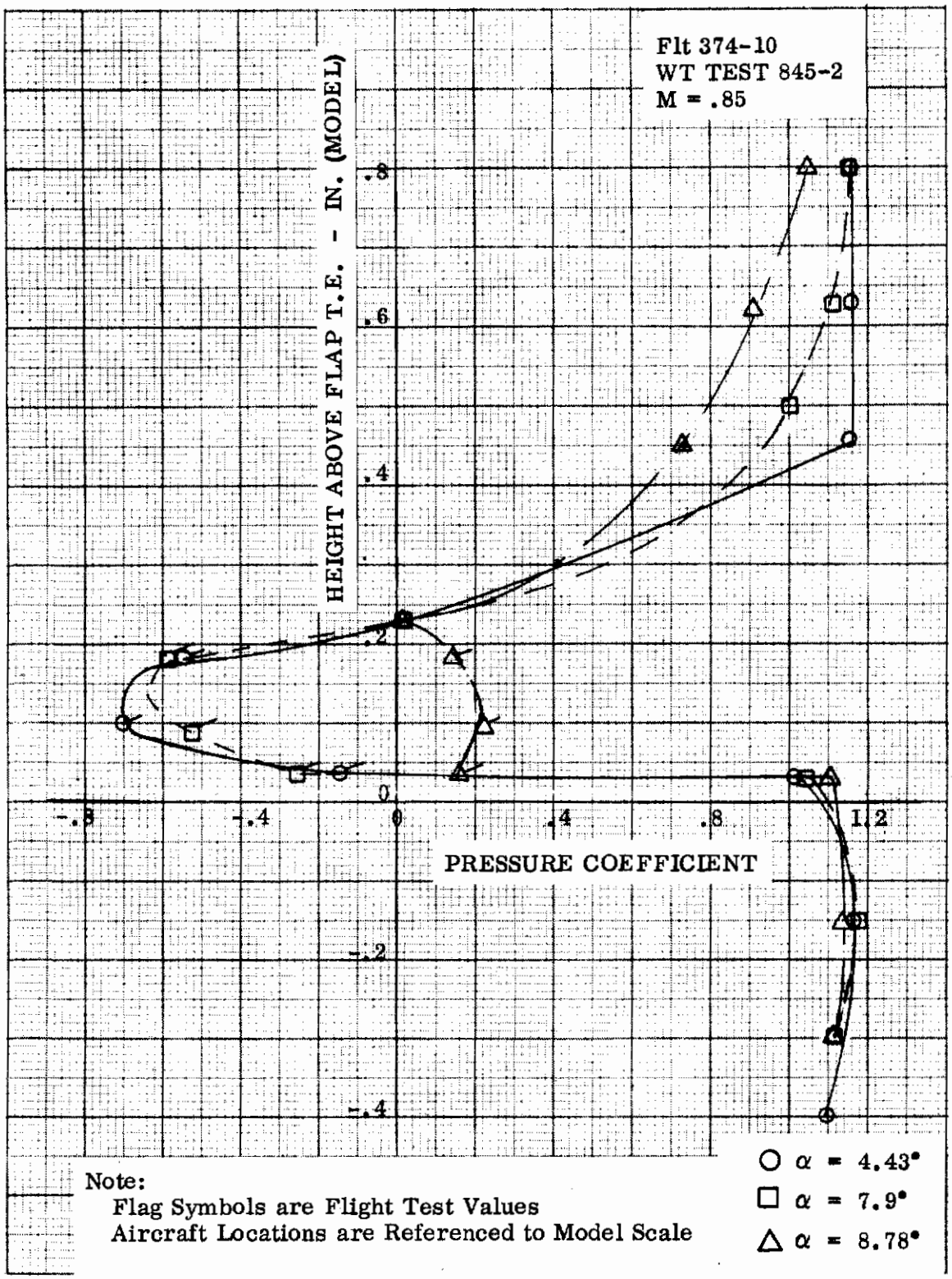

Figure 35. Boundary Layer Pressure Distribution below Mach Buffet, near Onset of Mach Buffet, and above the Onset of Mach Buffet
(a) Leading Edge Flap and Trailing Edge Flap Undeflected

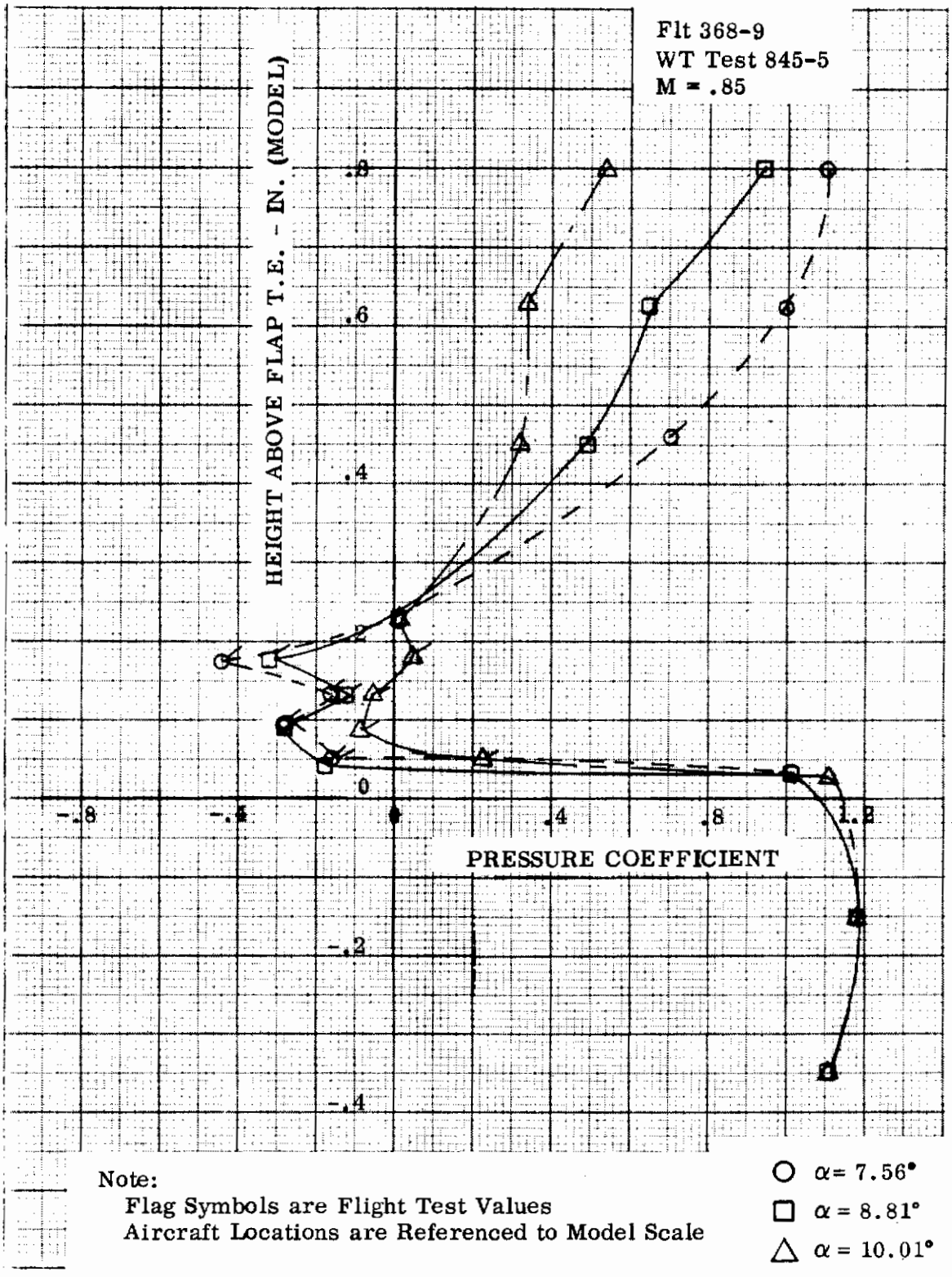

Figure 35. - - - Continued
(b) Leading Edge Flap 8°, Trailing Edge Flap Undeflected

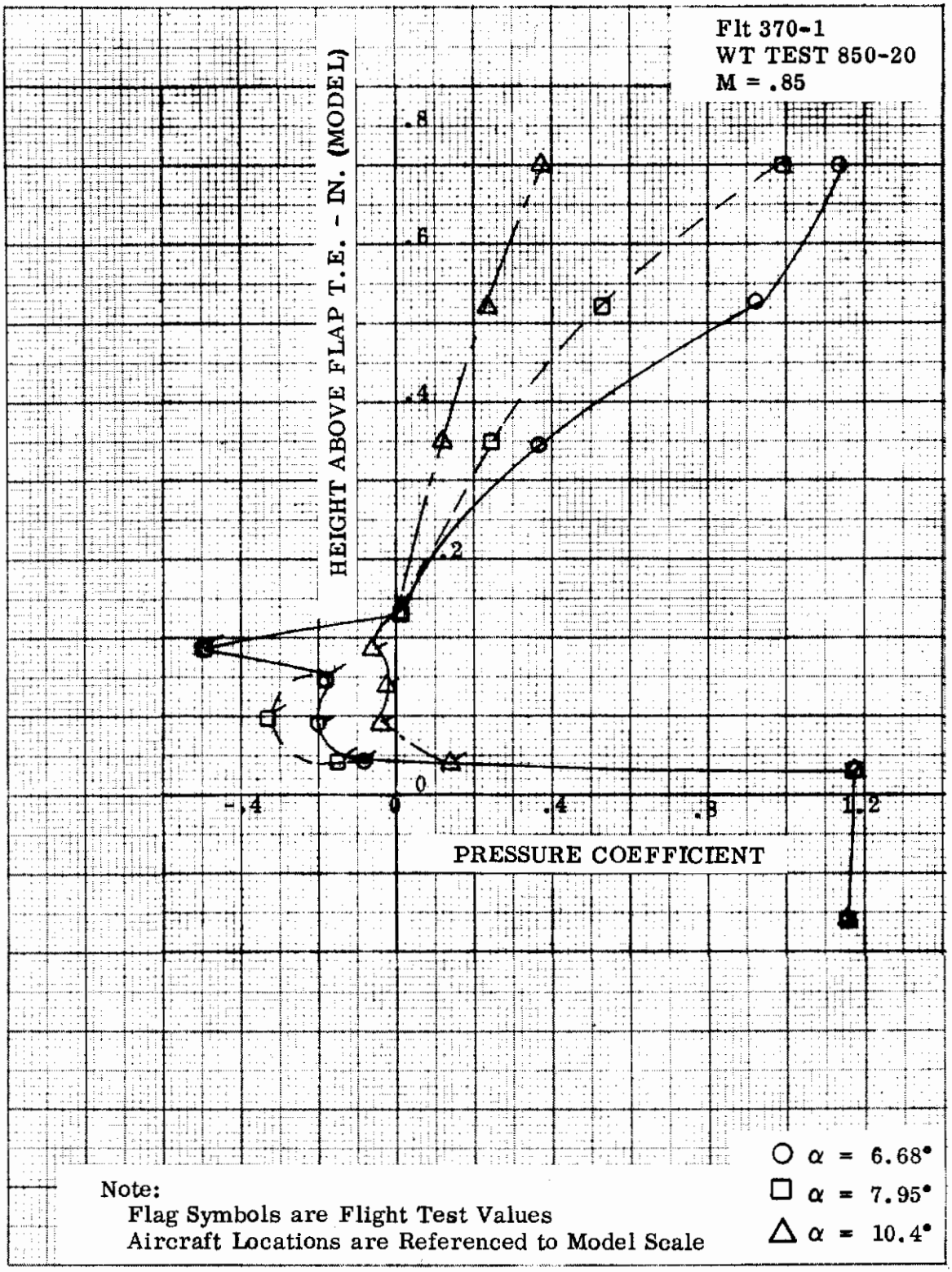

Figure 35. - - - Continued
(c) Leading Edge Flap 8°, Trailing Edge Flap 7.5°

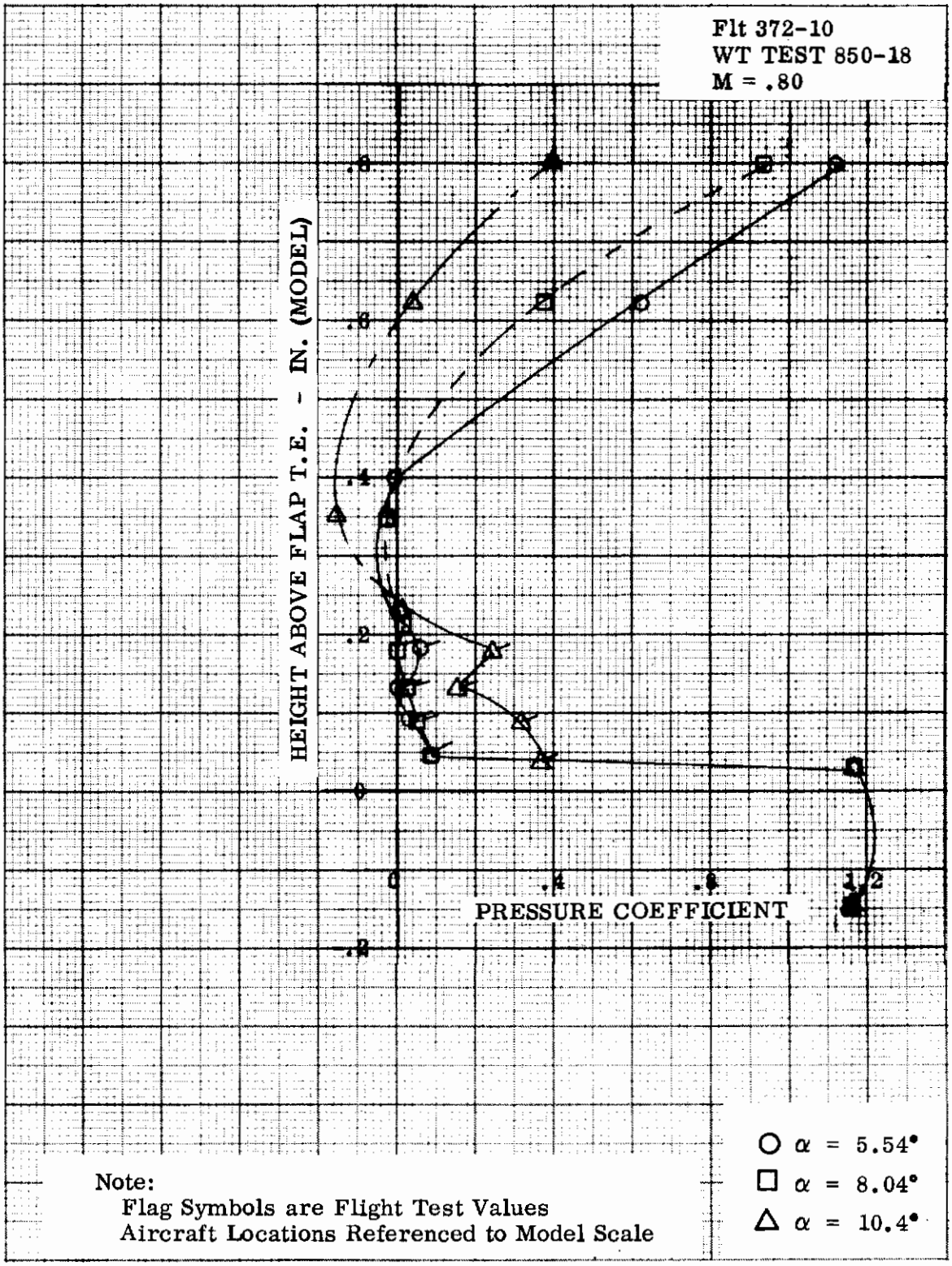

Figure 35. - - - Continued
(d) Leading Edge Flap 8°, Trailing Edge Flap 15°

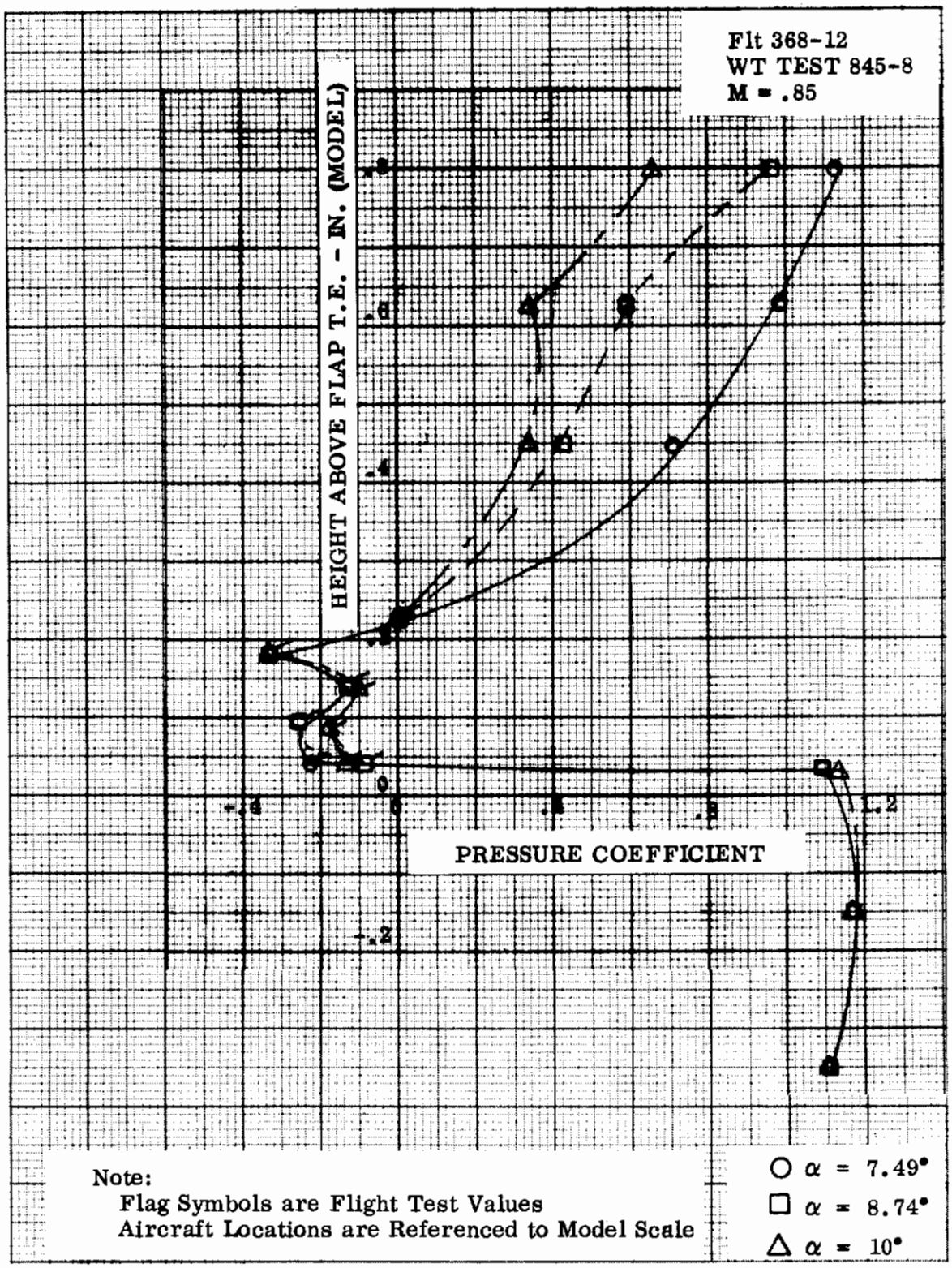

Figure 35. - - - Continued
(e) Leading Edge Flap 20°, Trailing Edge Flap Undeflected

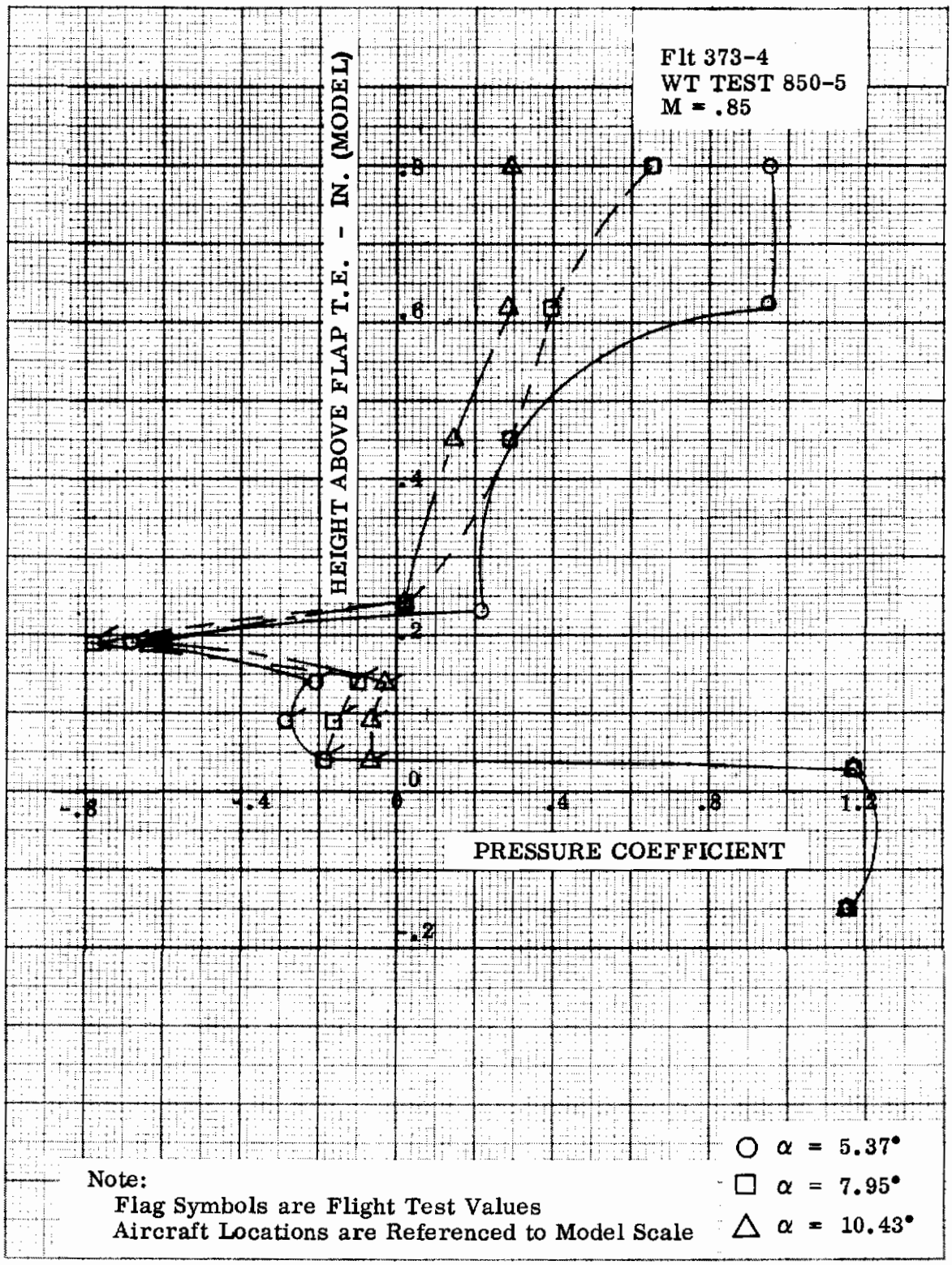

Figure 35. - - - Continued
(f) Leading Edge Flap 20°, Trailing Edge Flap 7.5°

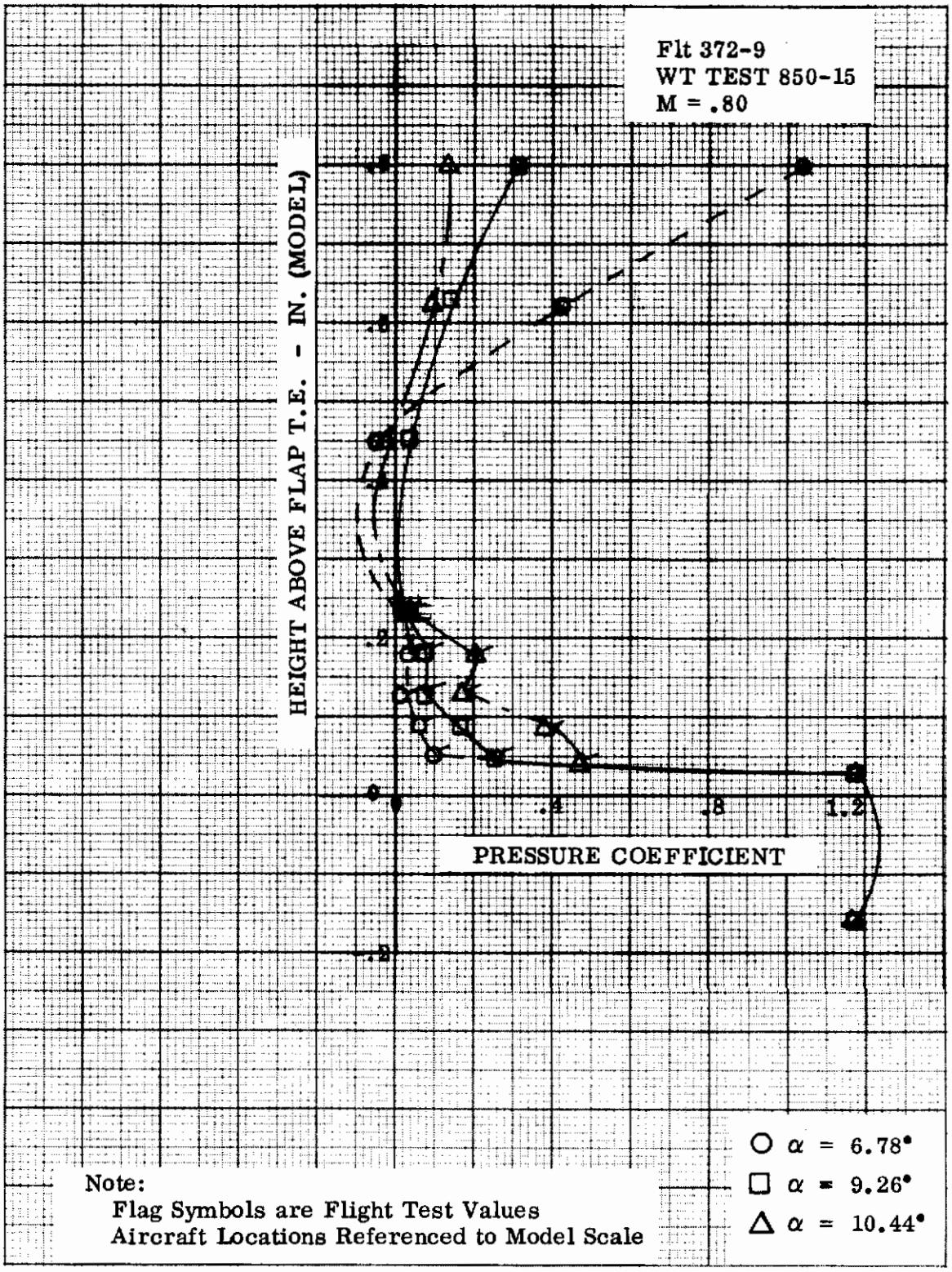

Figure 35. - - - Concluded
(g) Leading Edge Flap 20°, Trailing Edge Flap 15°

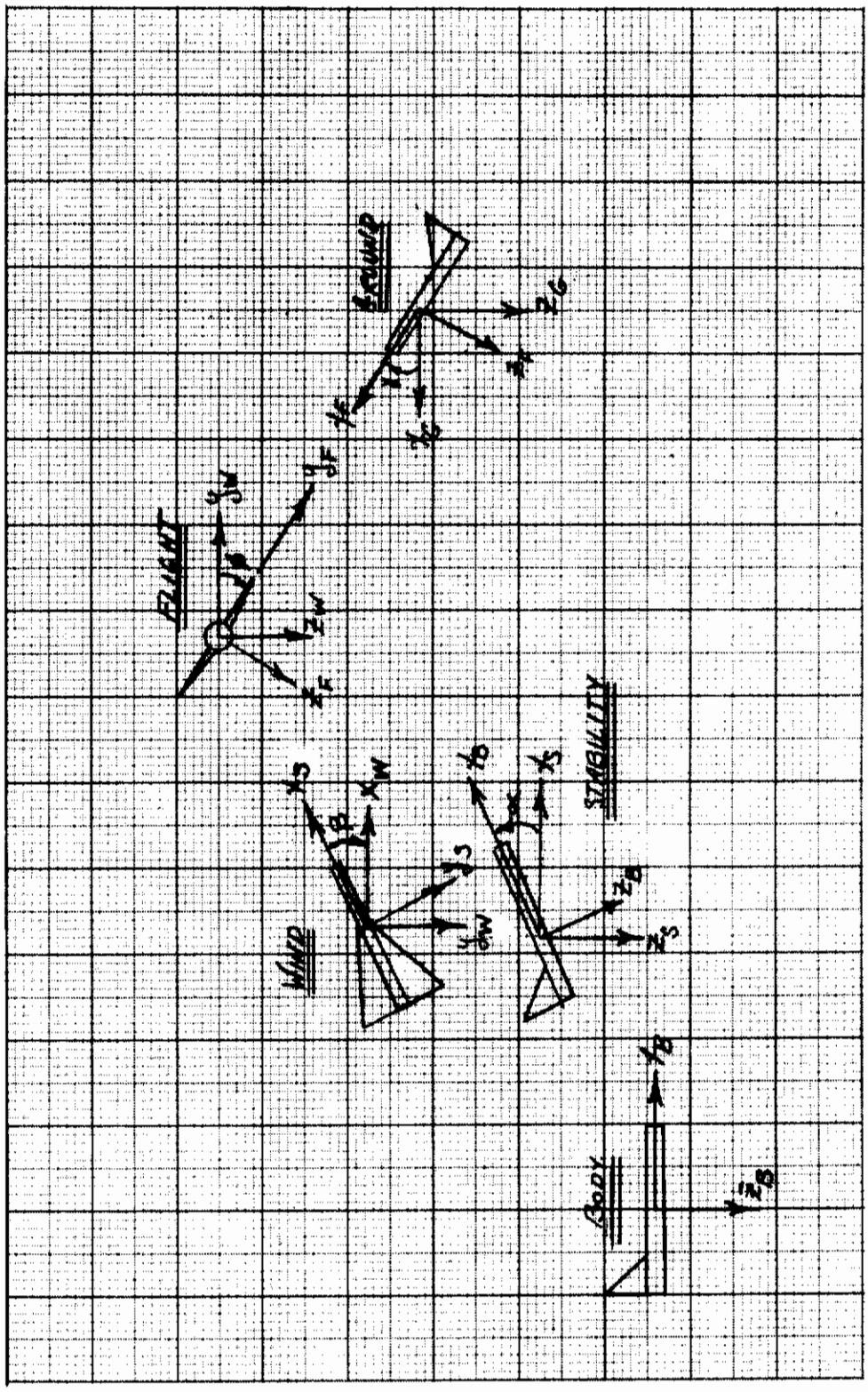

Figure 36. Axes Transformation: Body, Stability, Wind, Flight, Ground

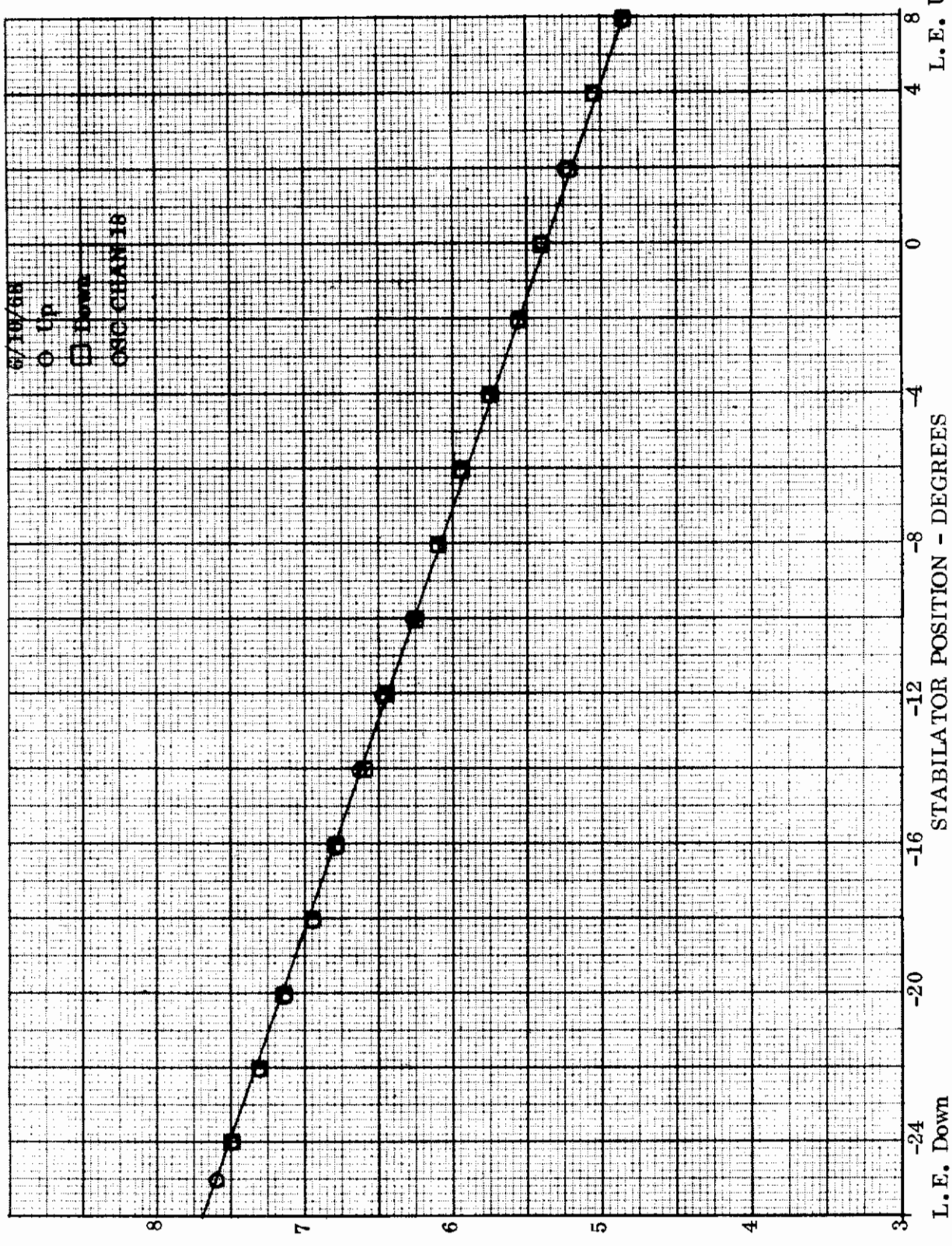

Figure 37. Airplane Stabilator Position. Flight Test Calibration Curve No. 51063165

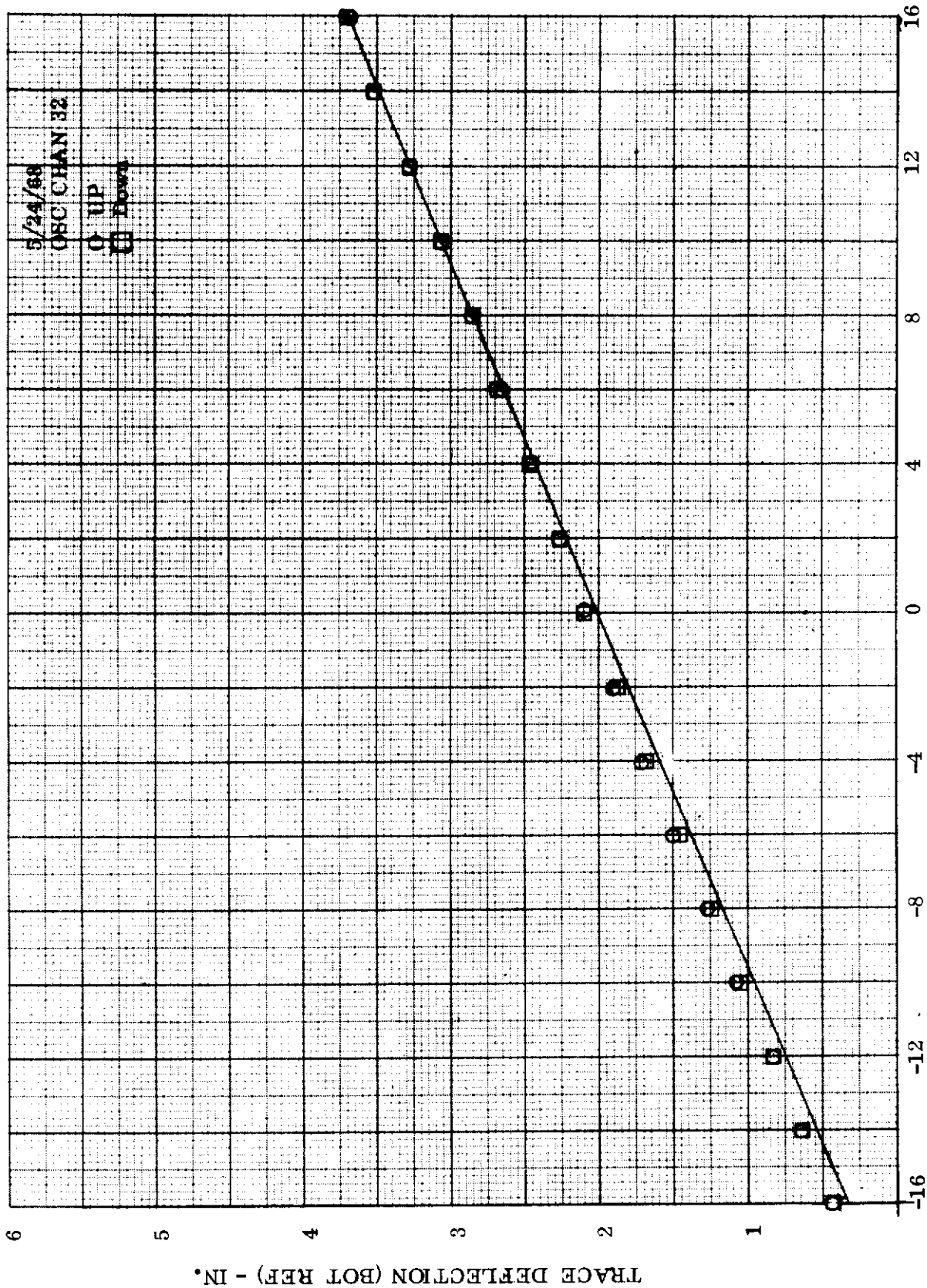

Figure 38. Right Wing Aileron Position. Flight Test Calibration Curve No. 51063011

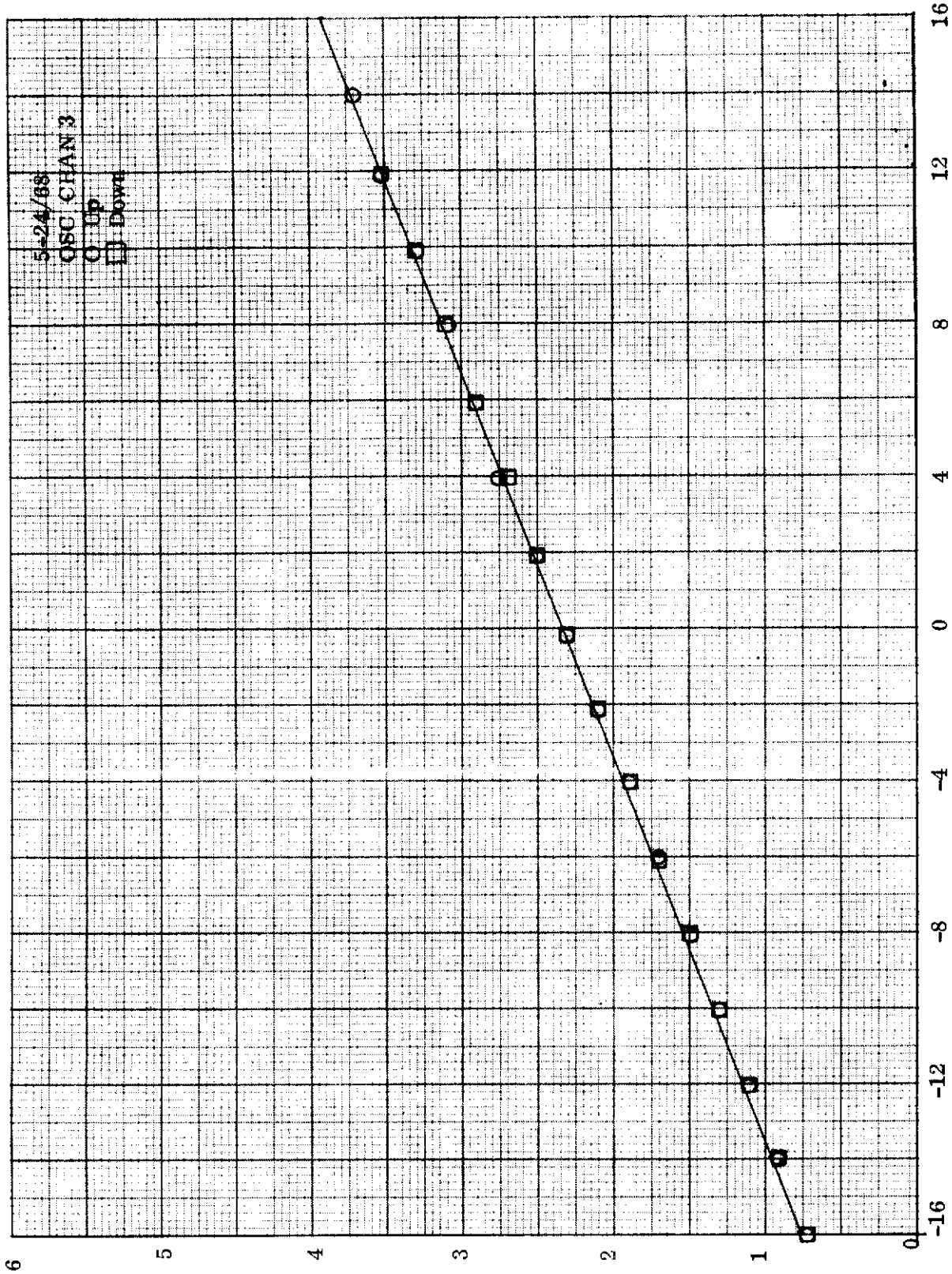

Figure 39. Left Wing Aileron Position. Flight Test Calibration Curve No. 51063034

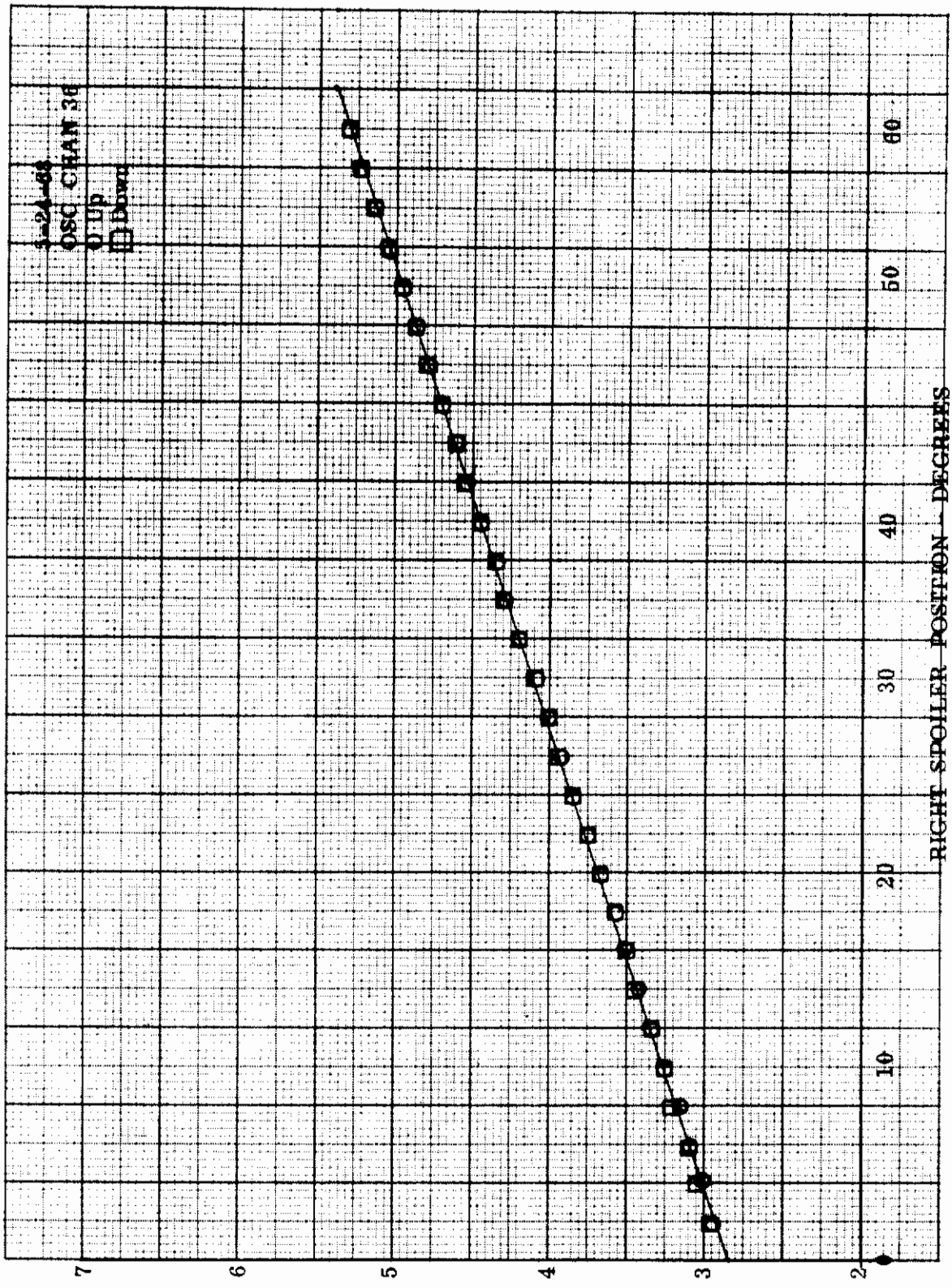

Figure 40. Right Wing Spoiler Position. Flight Test Calibration Curve No. 51063057

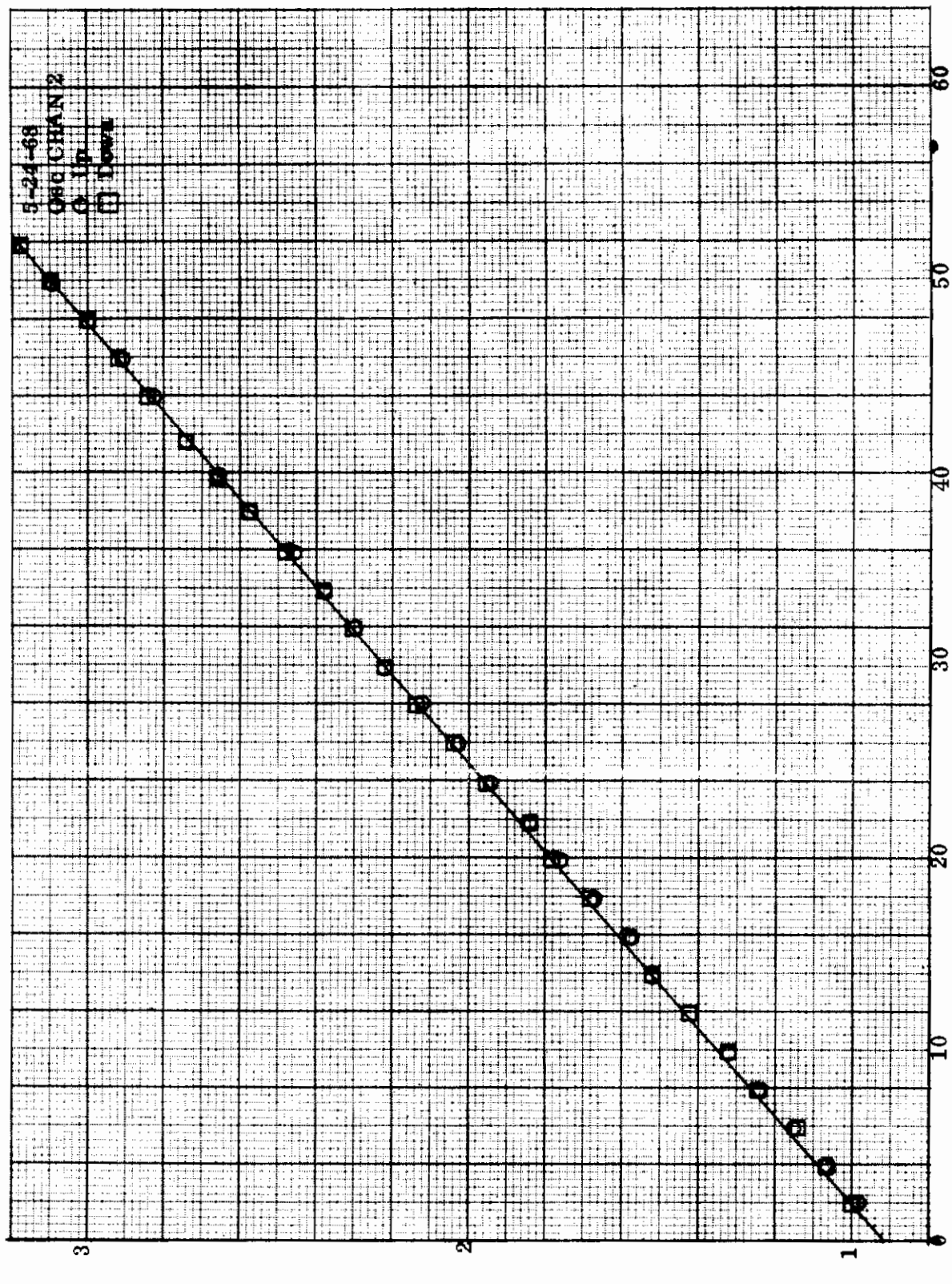

Figure 41. Left Wing Spoiler Position. Flight Test Calibration Curve No. 51063087

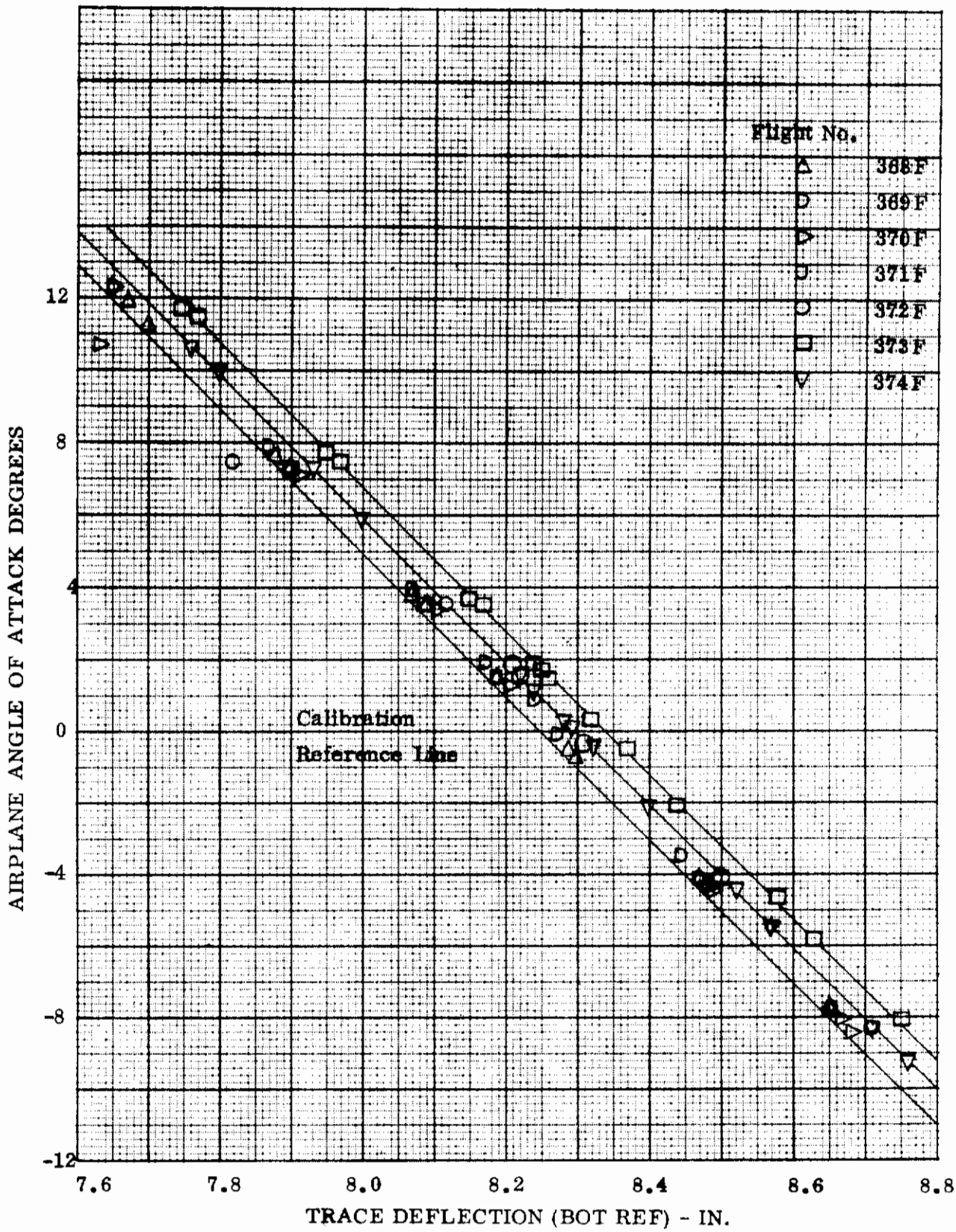

Figure 42. Airplane Angle of Attack Calibration Curve for F-105F-3 Flights No. 368 to 374

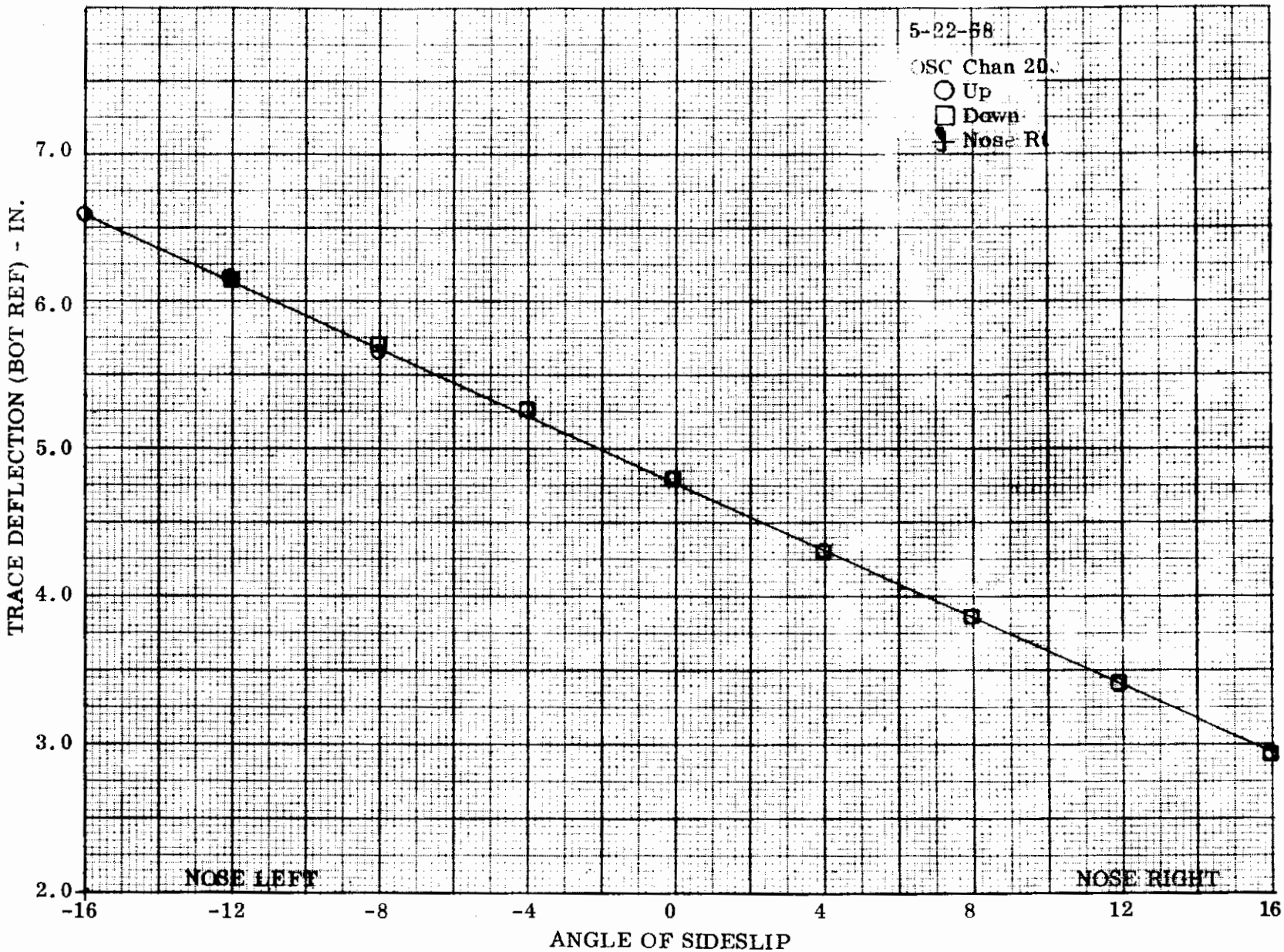

Figure 43. Airplane Angle of Sideslip Calibration Curve. Flight Test Calibration Curve No. 50363045

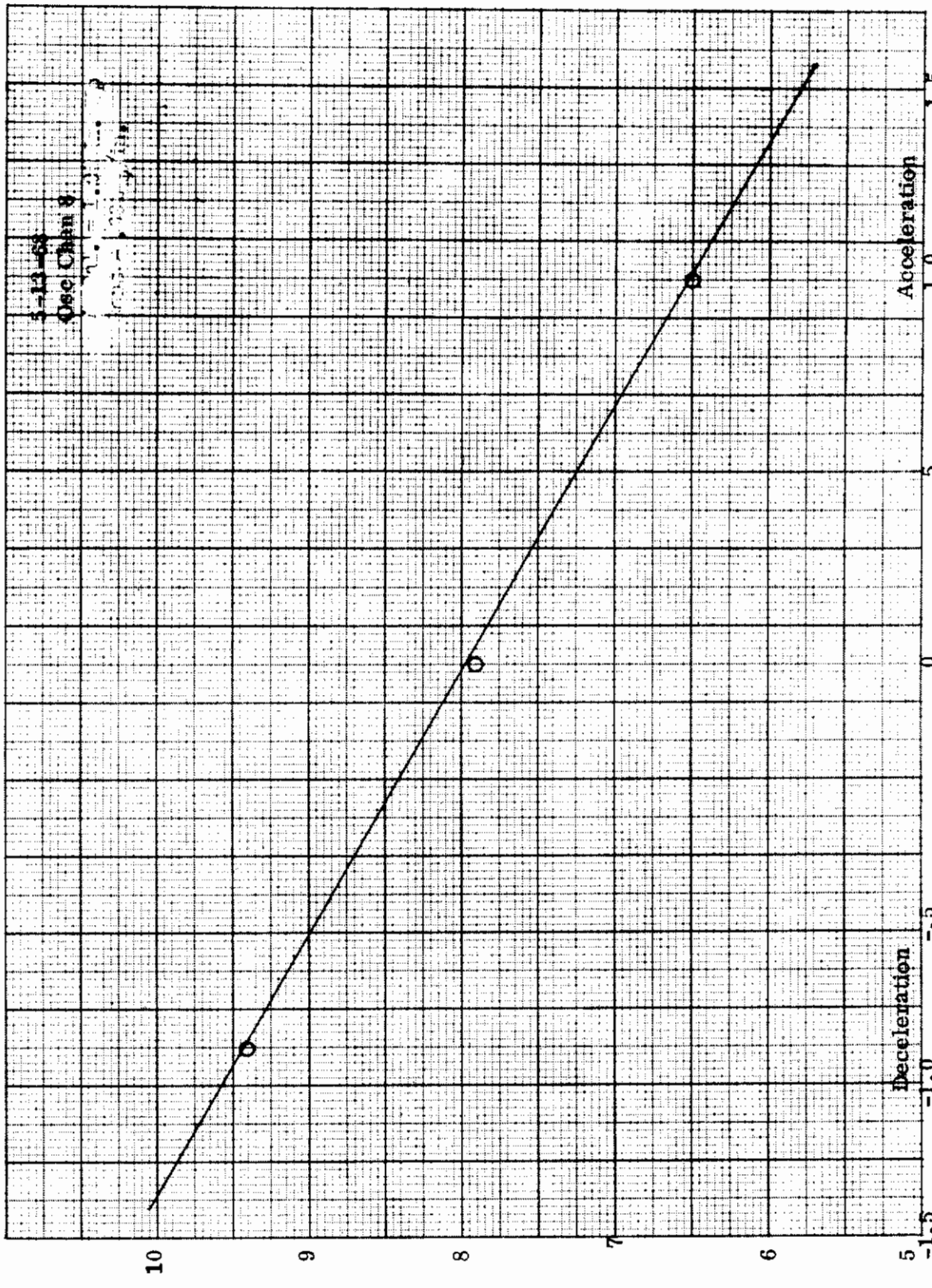

Figure 44. Airplane Longitudinal Acceleration Calibration Curve. Flight Test Calibration Curve No. 51263033

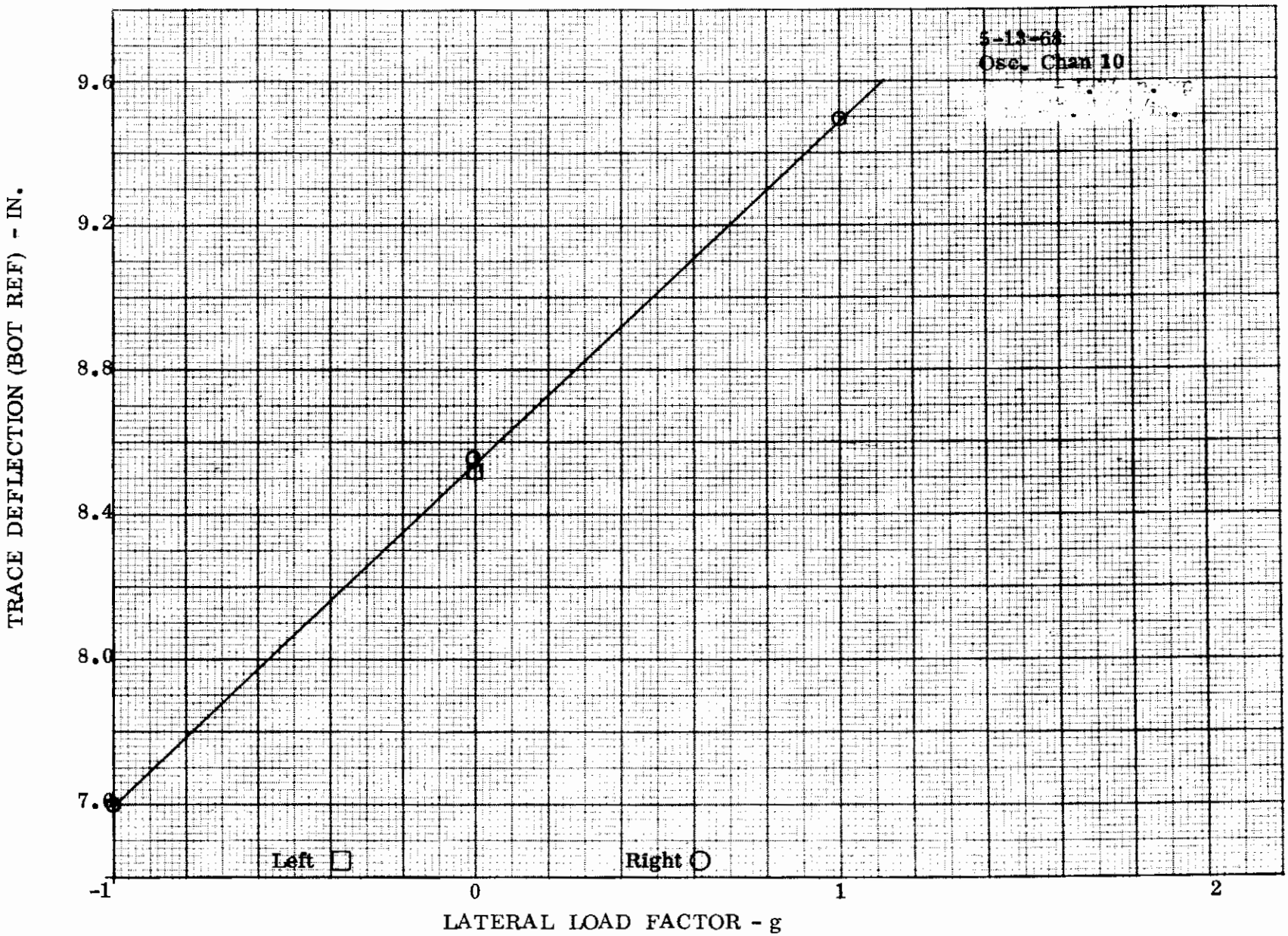

Figure 45. Airplane Lateral Acceleration Calibration Curve. Flight Test Calibration Curve No. 51263018

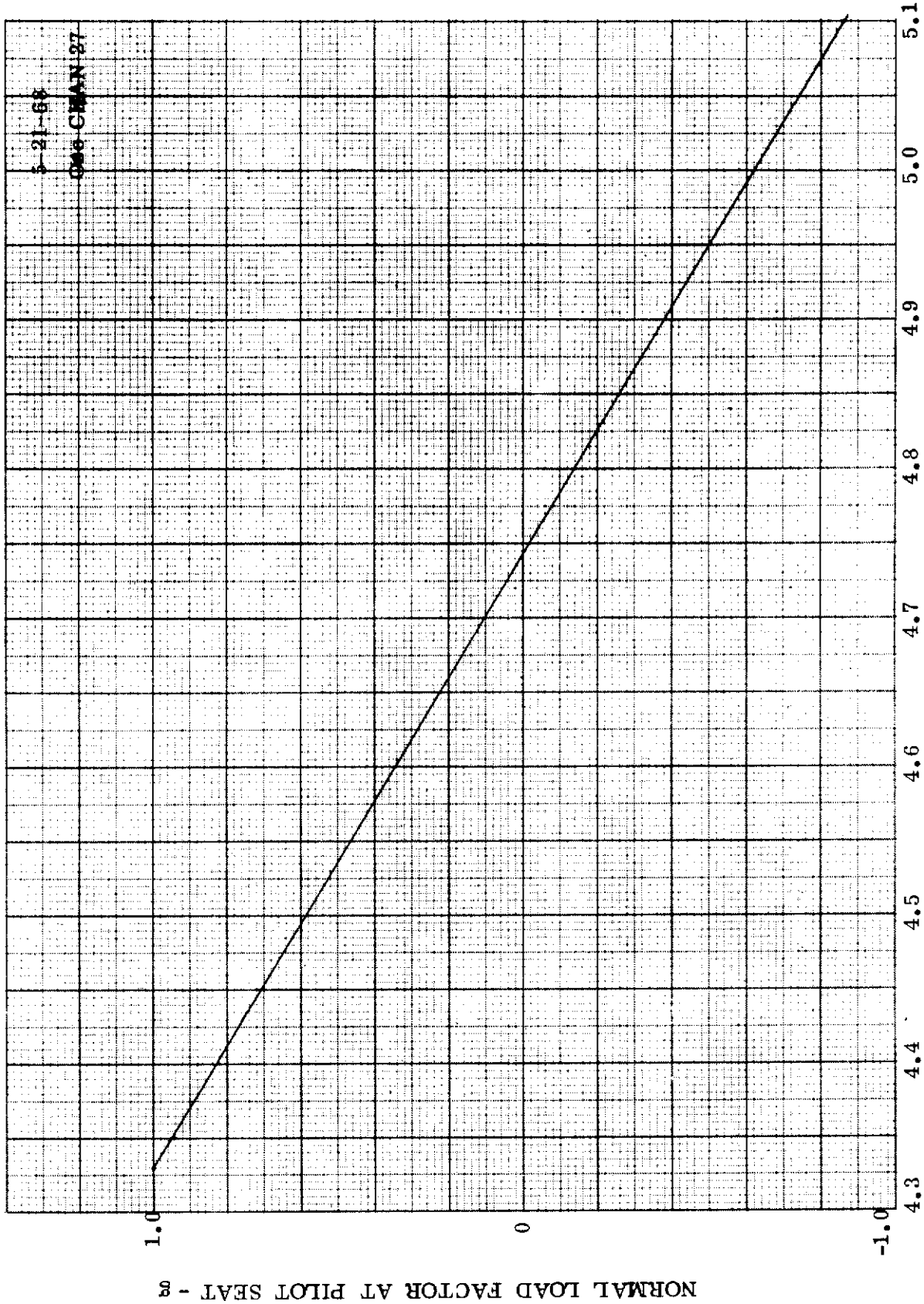

Figure 46. Normal Acceleration at the Pilot's Seat. Flight Test Calibration Curve No. 51263075

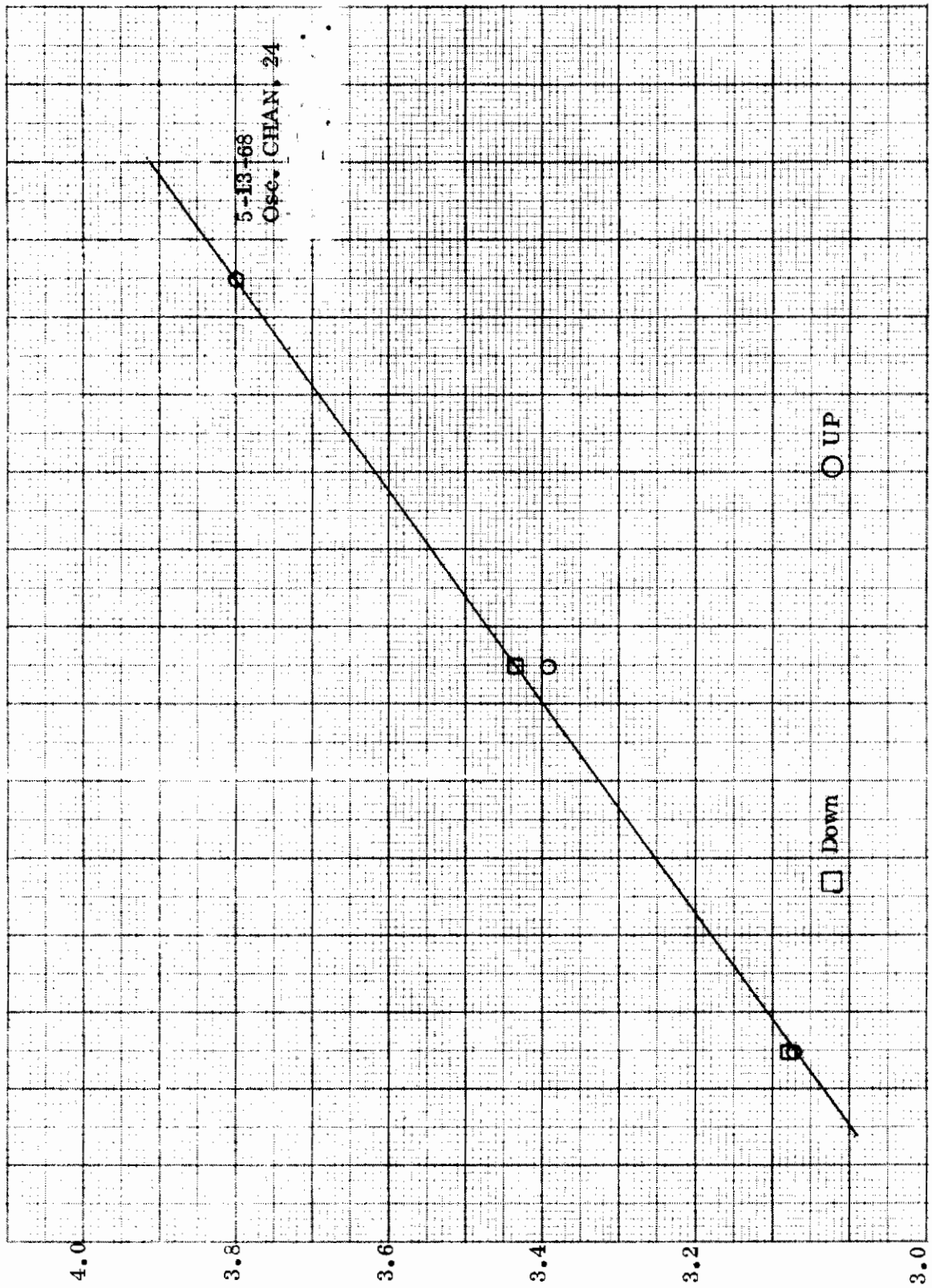

Figure 47. Calibration Curve for Right Wing Tip Accelerometer. Flight Test Calibration Curve No. 51263078

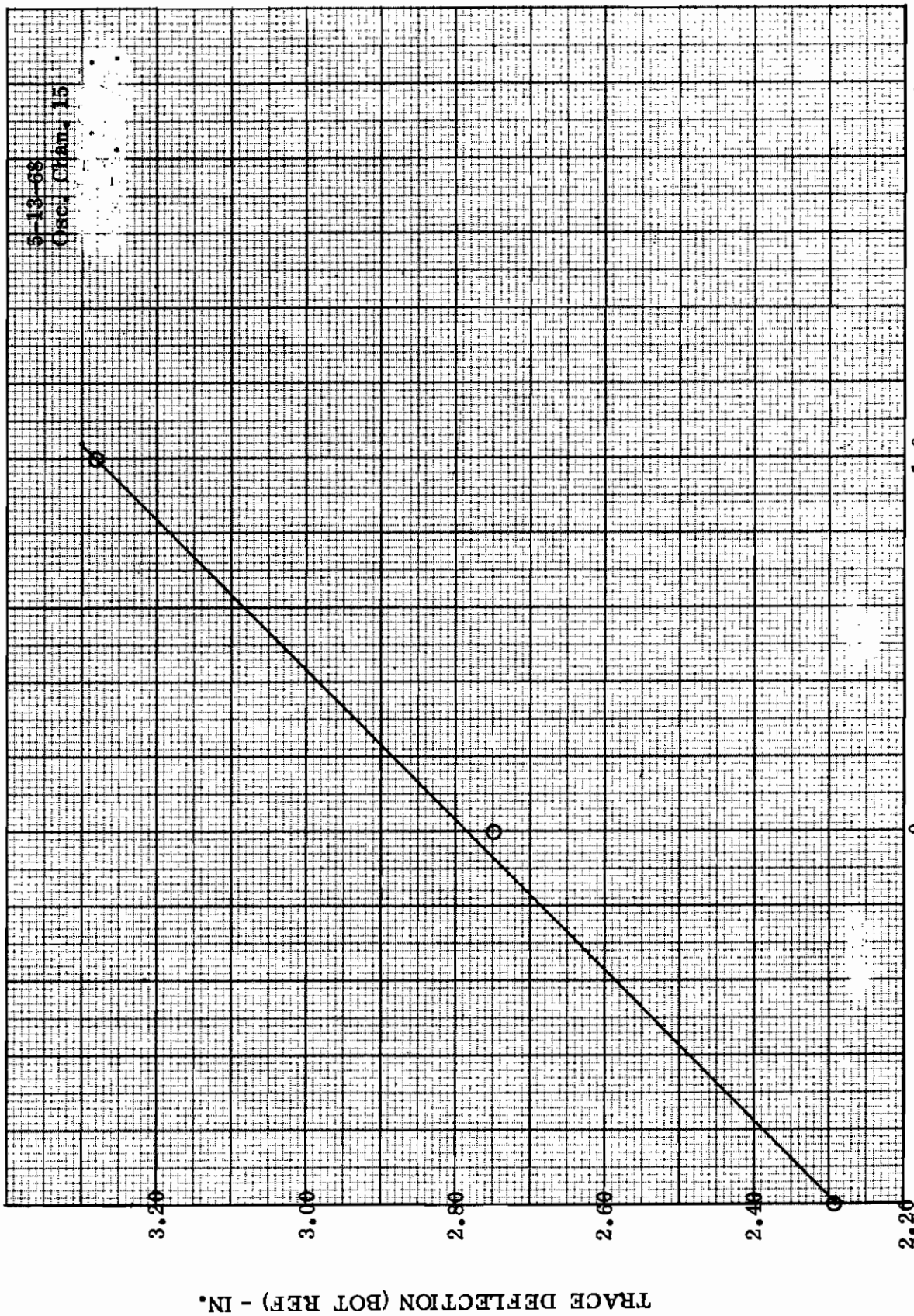

Figure 48. Calibration Curve for Left Wing Tip Accelerometer. Flight Test Calibration Curve No. 5126:

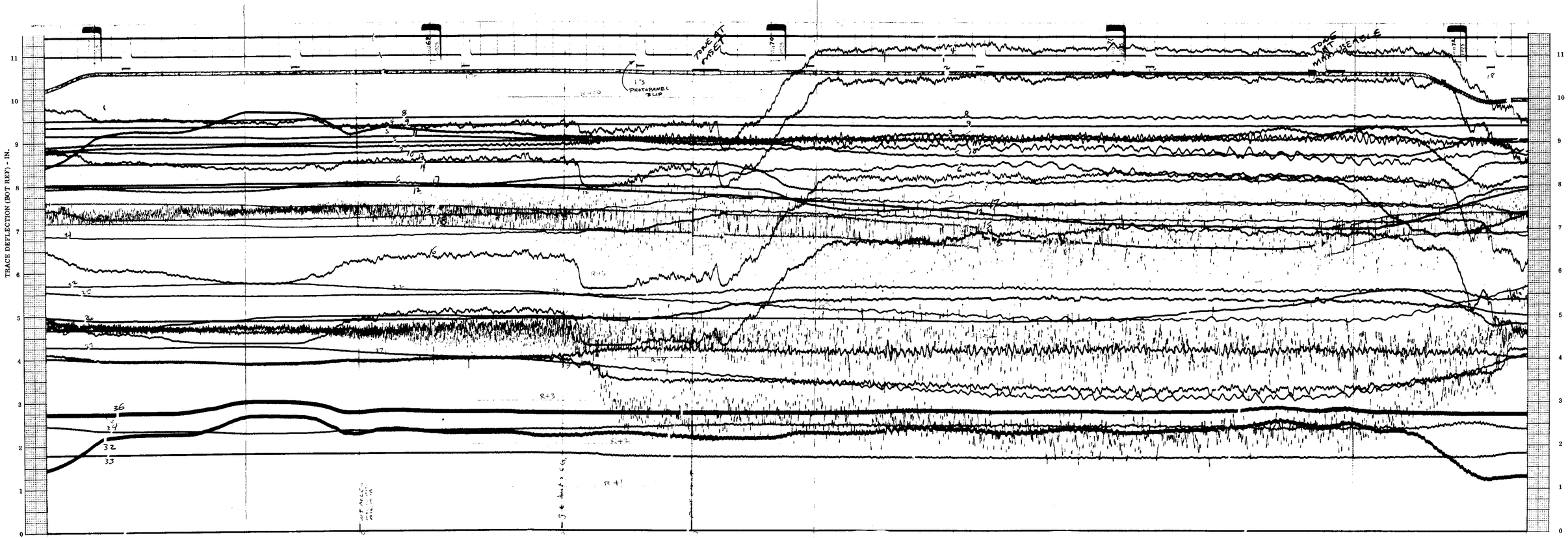

Figure 49. Typical Portion of Oscillograph Record.
Flight Test No. 369, Run No. 4

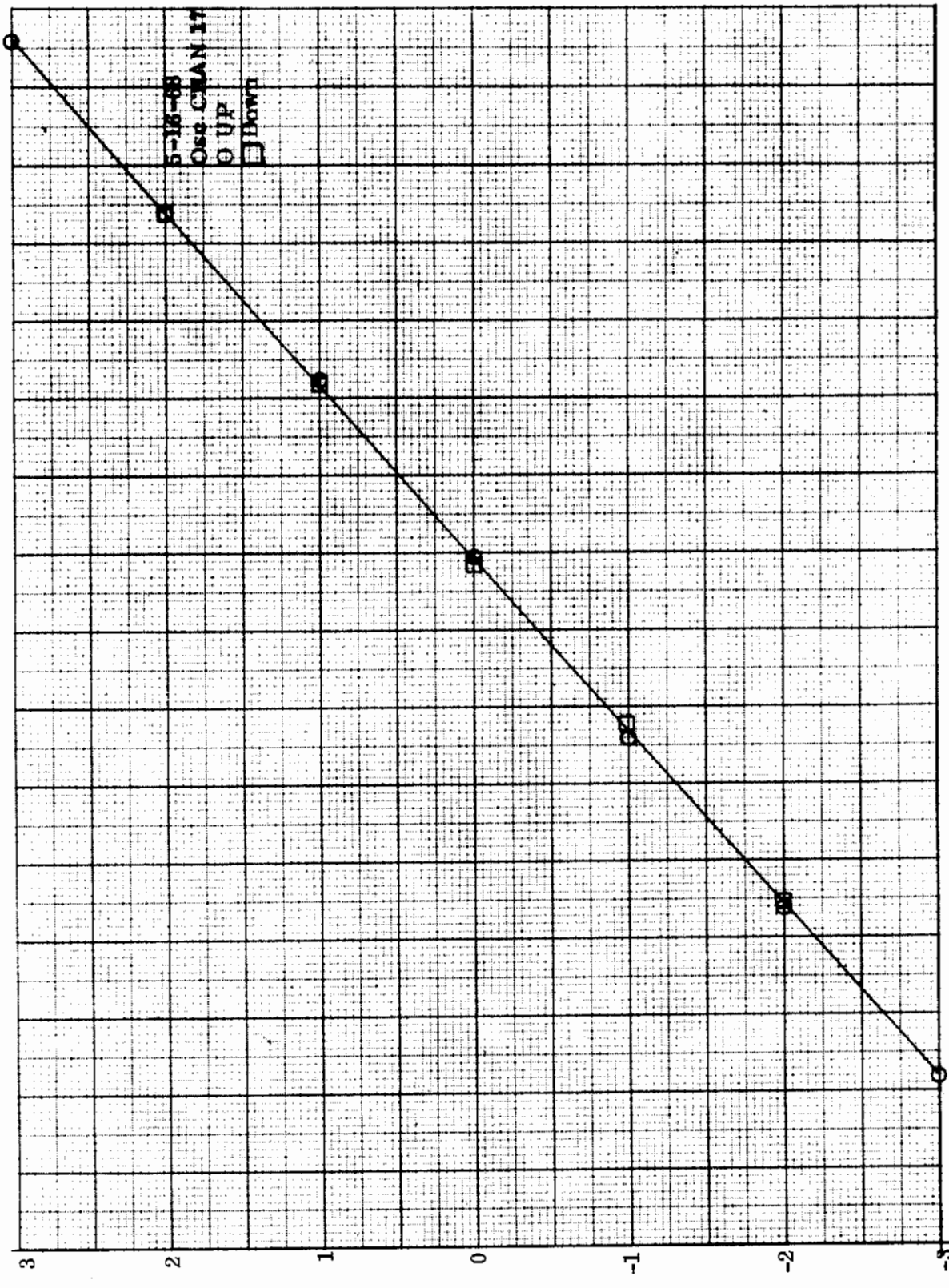

Figure 50. Calibration Curve for Pressure Transducer to Top Surface Static Pressure Port. Wing Station 95, at 95% Chord. Flight Test Calibration Curve No. 50663039

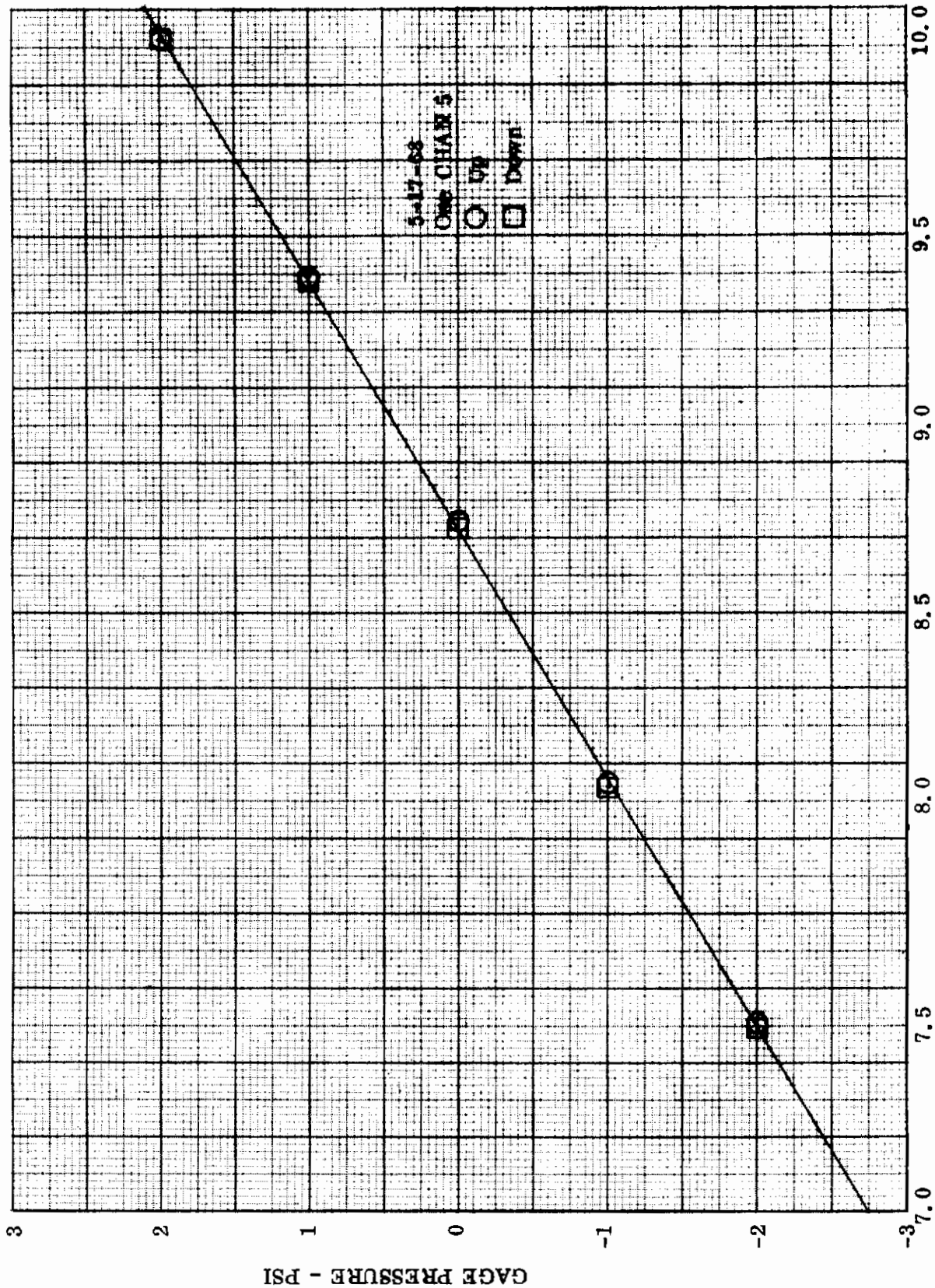

Figure 51. Calibration Curve for Pressure Transducer to Bottom Surface Static Pressure Port. Wing Station 95 at 95% Chord. Flight Test Calibration Curve No. 50663043

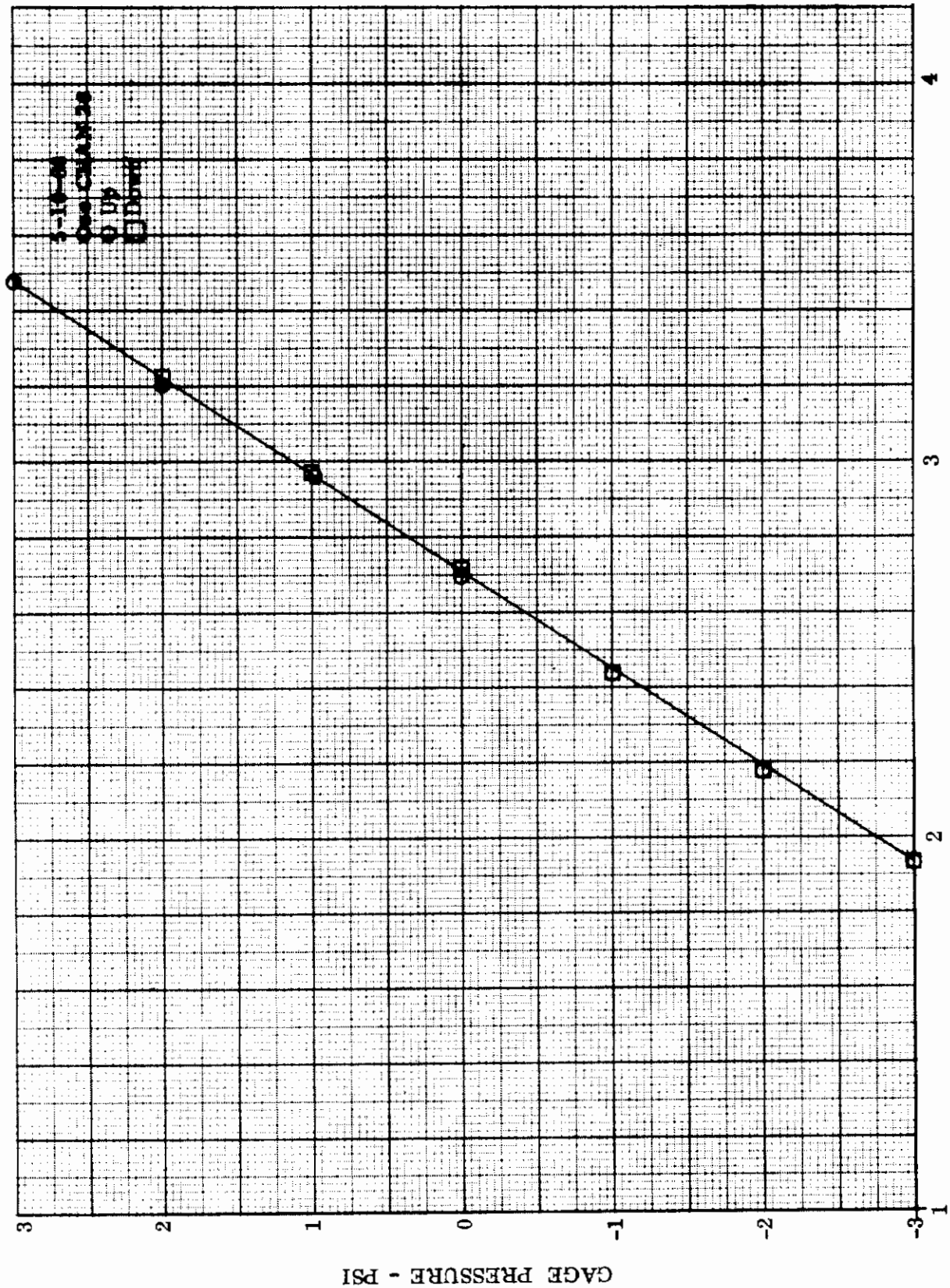

Figure 52. Calibration Curve for Pressure Transducer to Bottom Surface Static Pressure Port. Wing Station 135 at 95% Chord. Flight Test Calibration Curve No. 50663046

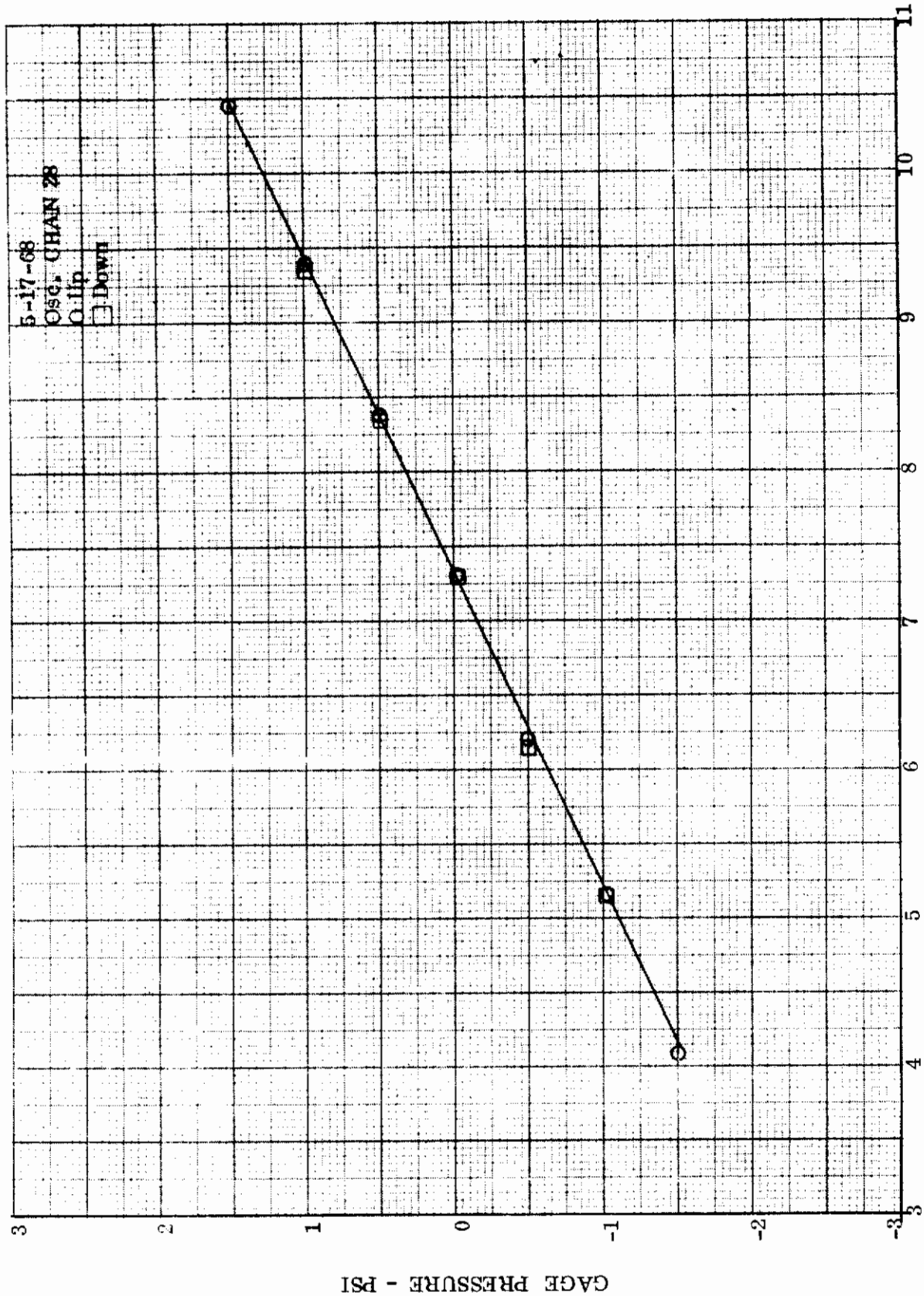

Figure 53. Calibration Curve for Pressure Transducer to Top Surface Static Pressure Port. Wing Station 175 at 95% Chord. Flight Test Calibration Curve No. 50663041

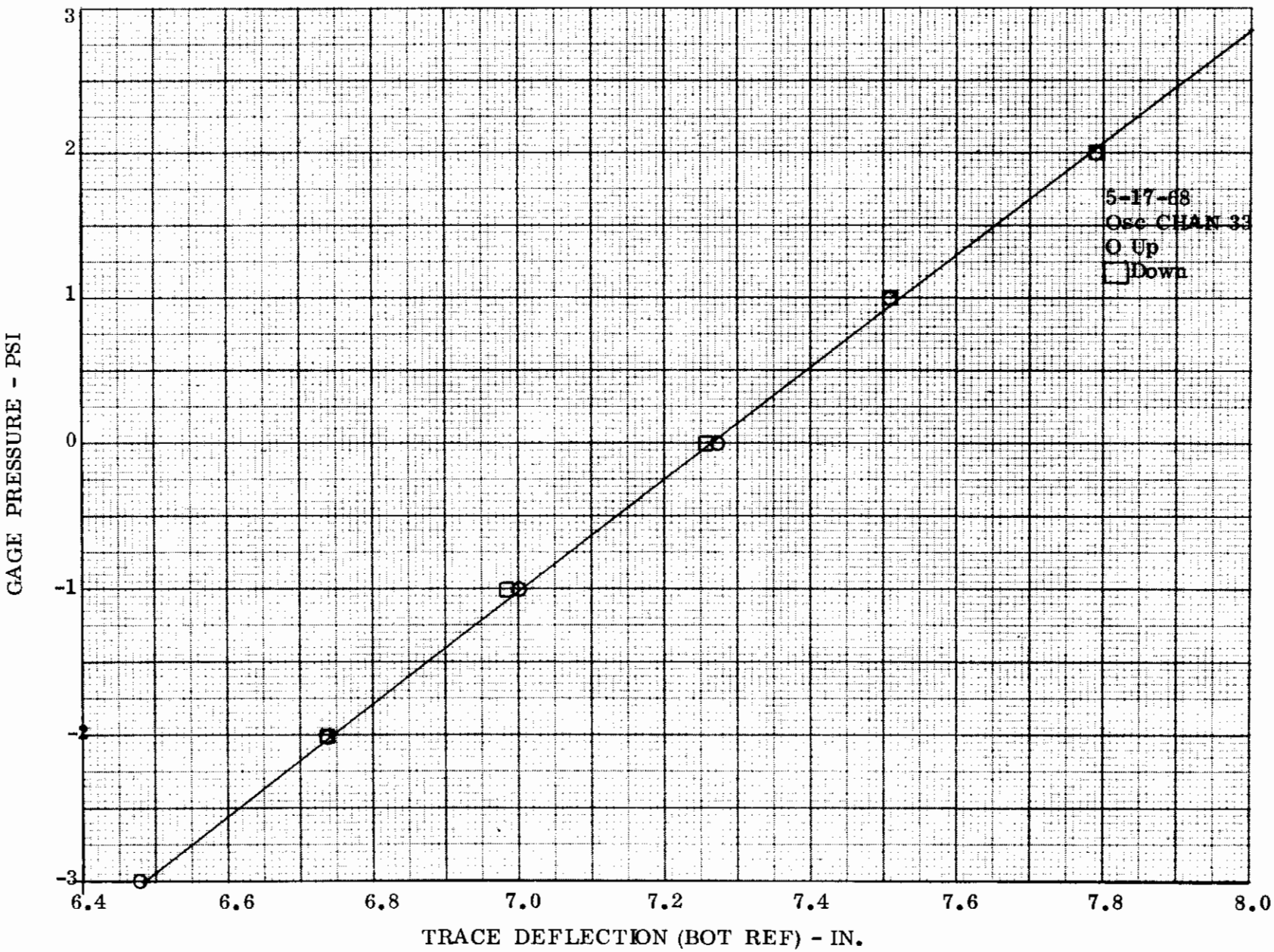

Figure 54. Calibration Curve for Pressure Transducer to Bottom Surface Static Pressure Port. Wing Station 175 at 95% Chord. Flight Test Calibration Curve No. 50663047

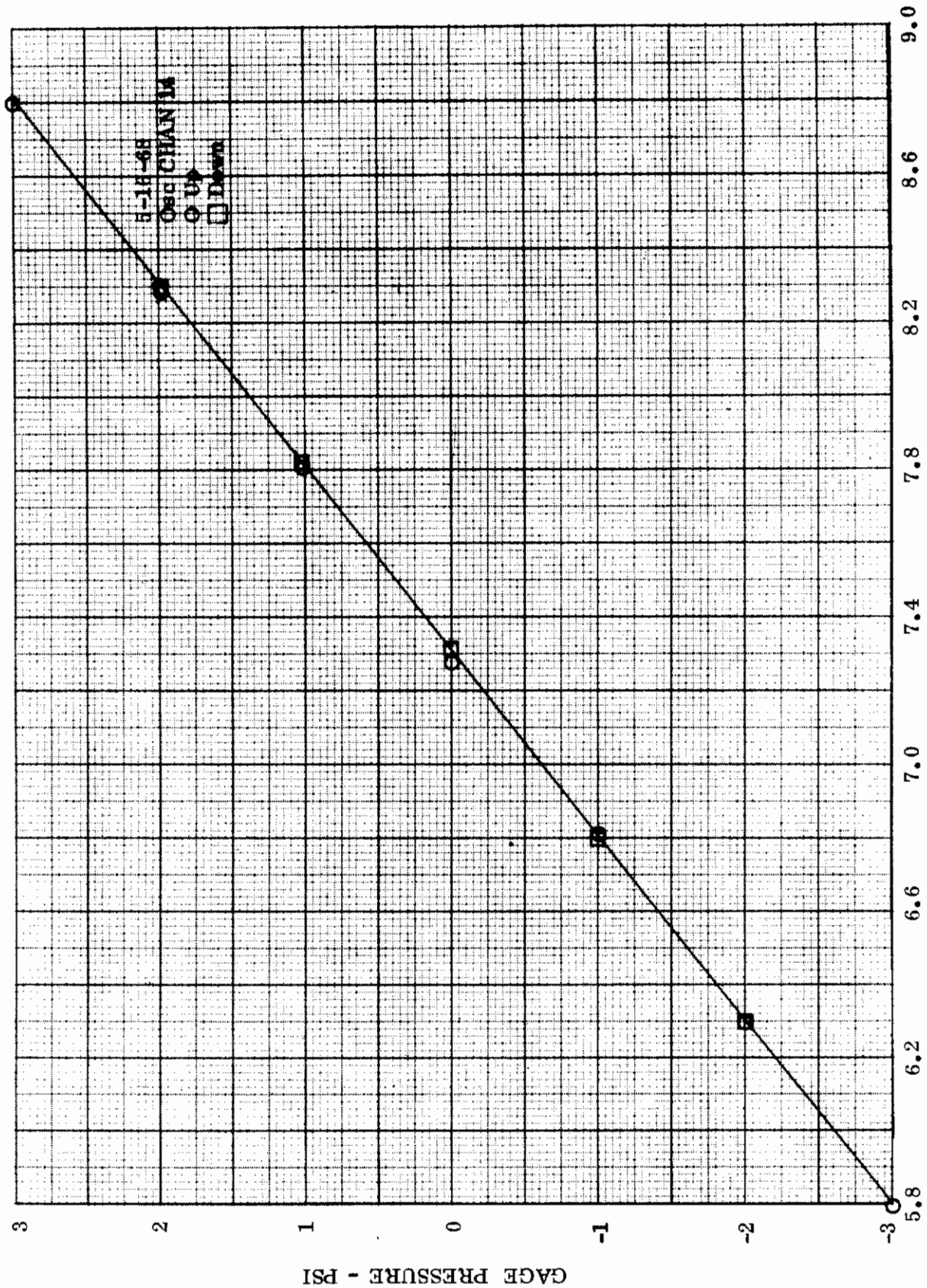

Figure 55. Calibration Curve for Pressure Transducer to Top Surface Static Pressure Port. Wing Station 95 at 85% Chord. Flight Test Calibration Curve No. 50663040

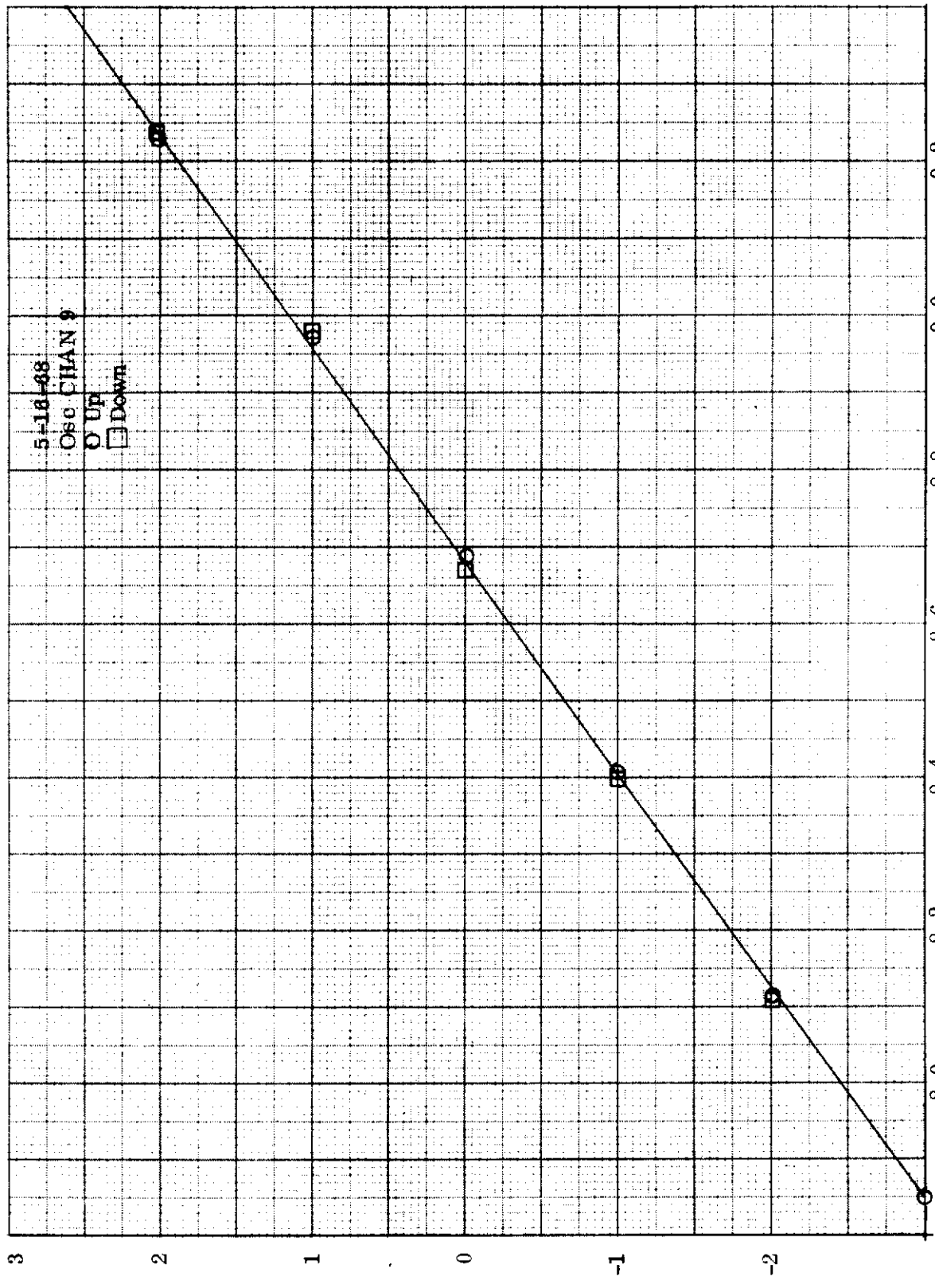

Figure 56. Calibration Curve for Pressure Transducer to Bottom Surface Static Pressure Port. Wing Station 95 at 85% Chord. Flight Test Calibration Curve No. 50663042

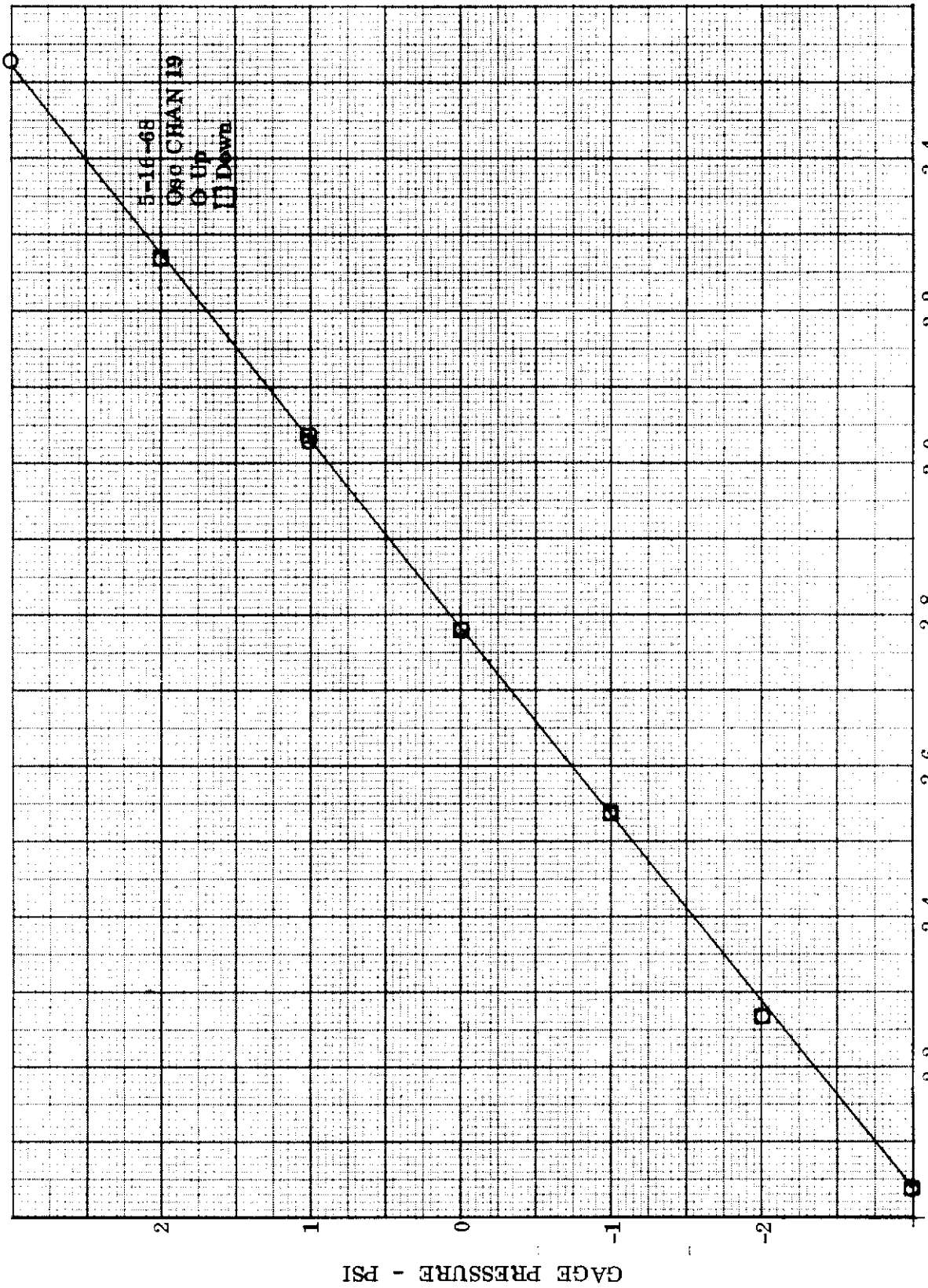

Figure 57. Calibration Curve for Pressure Transducer to Top Surface Static Pressure Port. Wing Station 135 at 85% Chord. Flight Test Calibration Curve No. 50663044

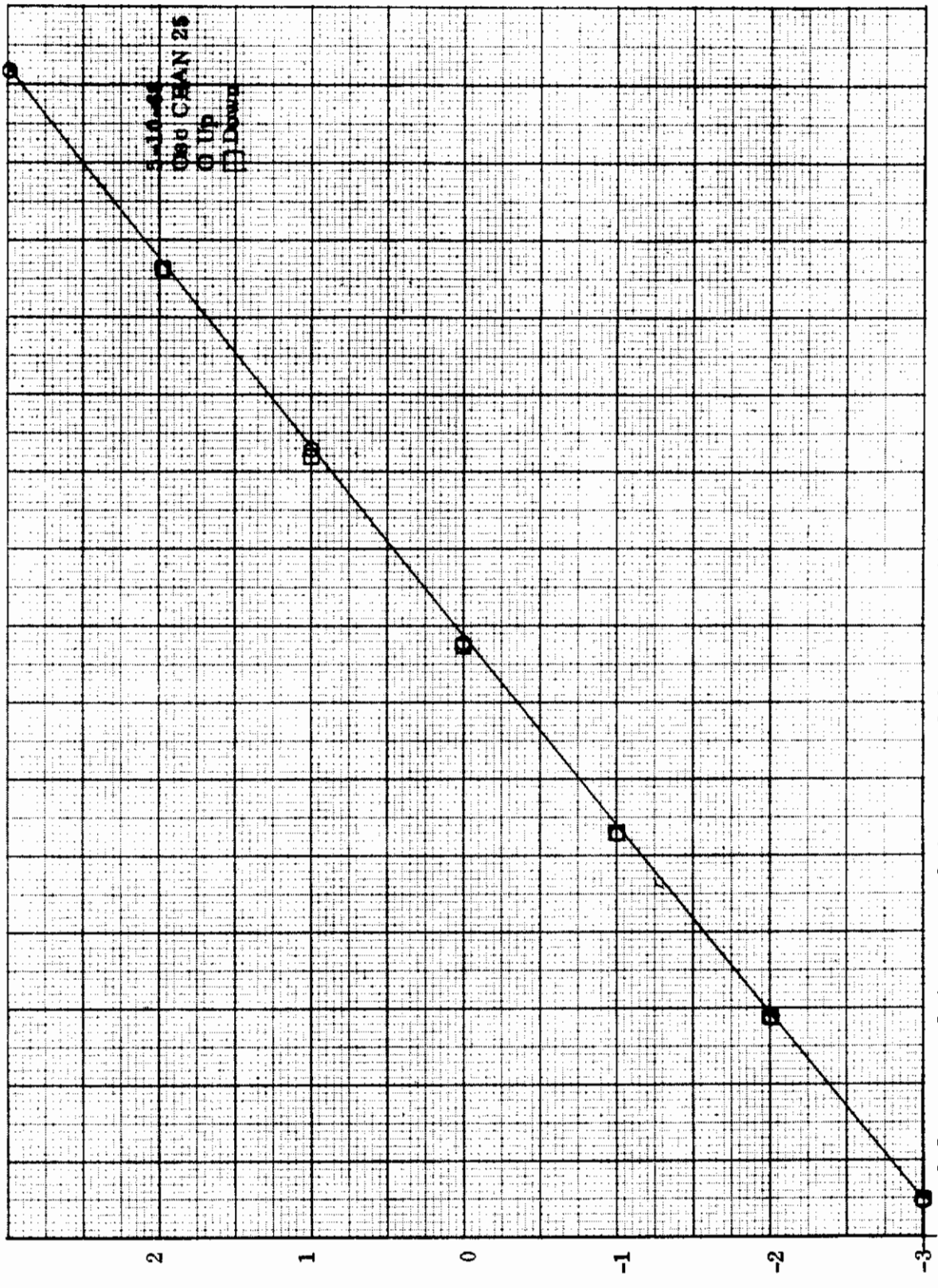

Figure 58. Calibration Curve for Pressure Transducer to Bottom Surface Static Pressure Port. Wing Station 135 at 85% Chord. Flight Test Calibration Curve No. 50663045

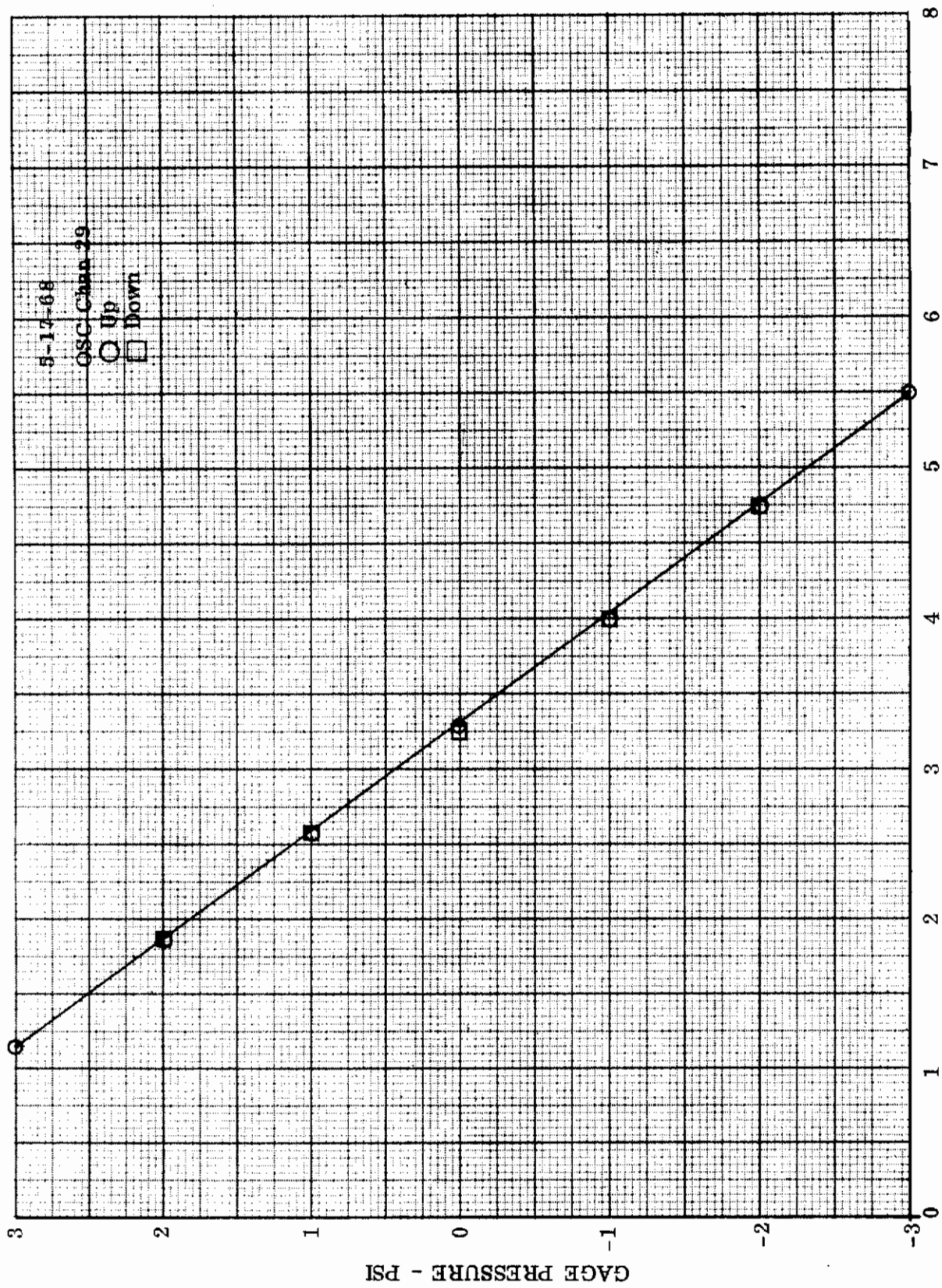

Figure 59. Calibration Curve for Pressure Transducer to Top Surface Static Pressure Port. Wing Station 175 at 85% Chord. Flight Test Calibration Curve No. 50663038

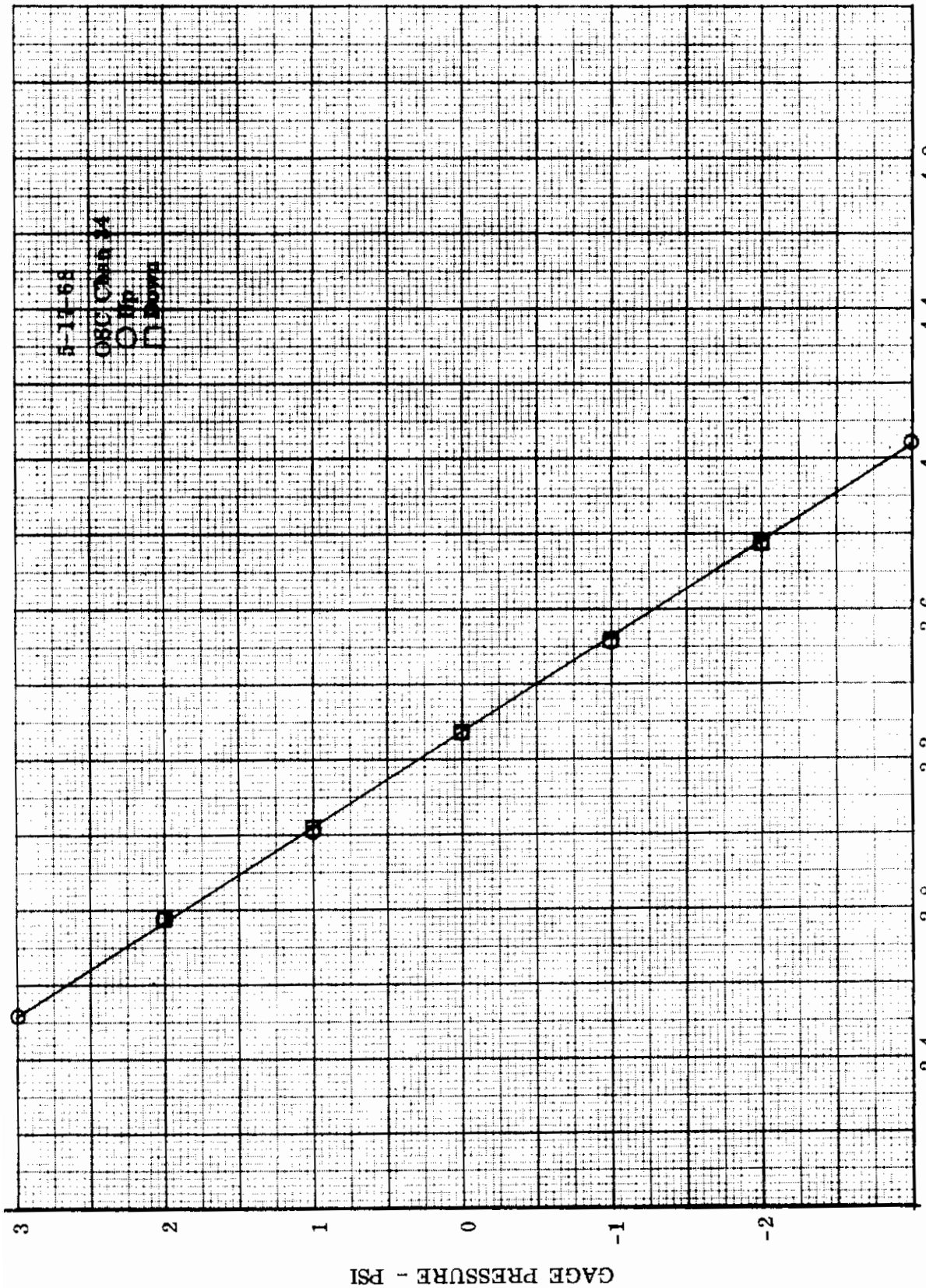

Figure 60. Calibration Curve for Pressure Transducer to Bottom Surface Static Pressure Port. Wing Station 175 at 85% Chord. Flight Test Calibration Curve No. 50663037

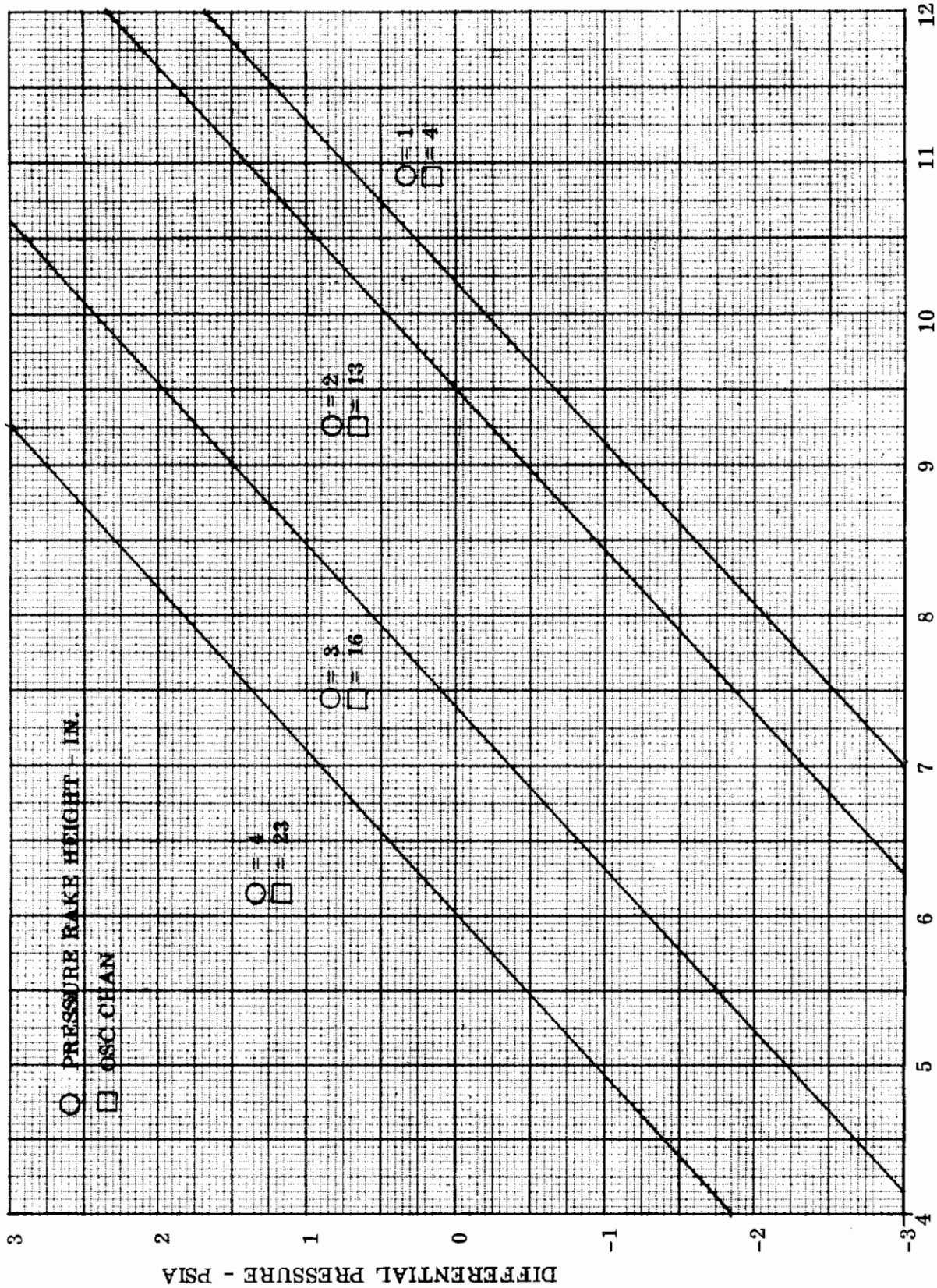

Figure 61. Calibration Curve for Pressure Transducer to Total Pressure Tubes on Boundary Layer Rake. Wing Station 105. Flight Test Calibration Curve No. 50663036G

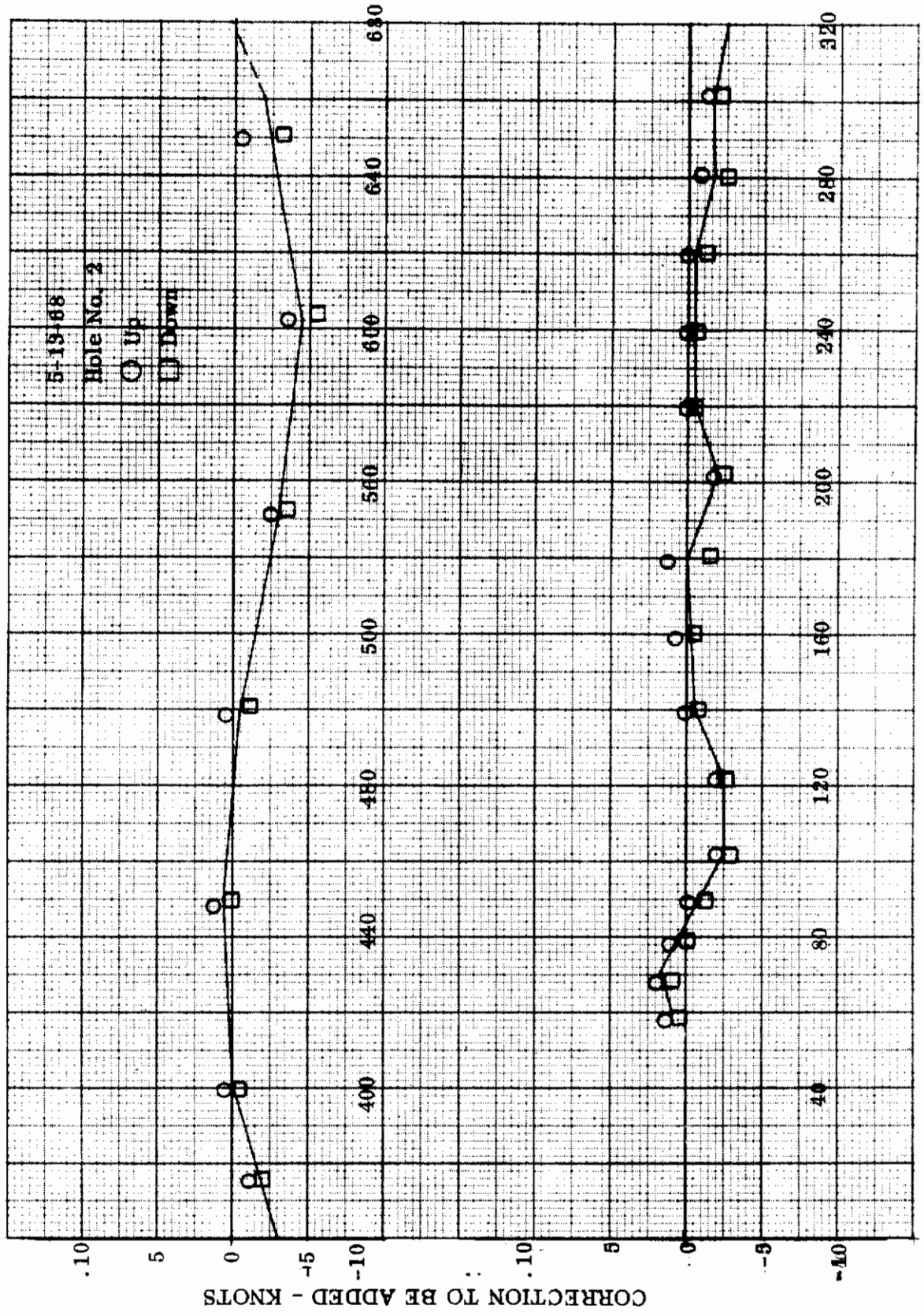

Figure 62. Airspeed Calibration Curve to Correct for Instrument Error. Flight Test Calibration Curve No. 10163025

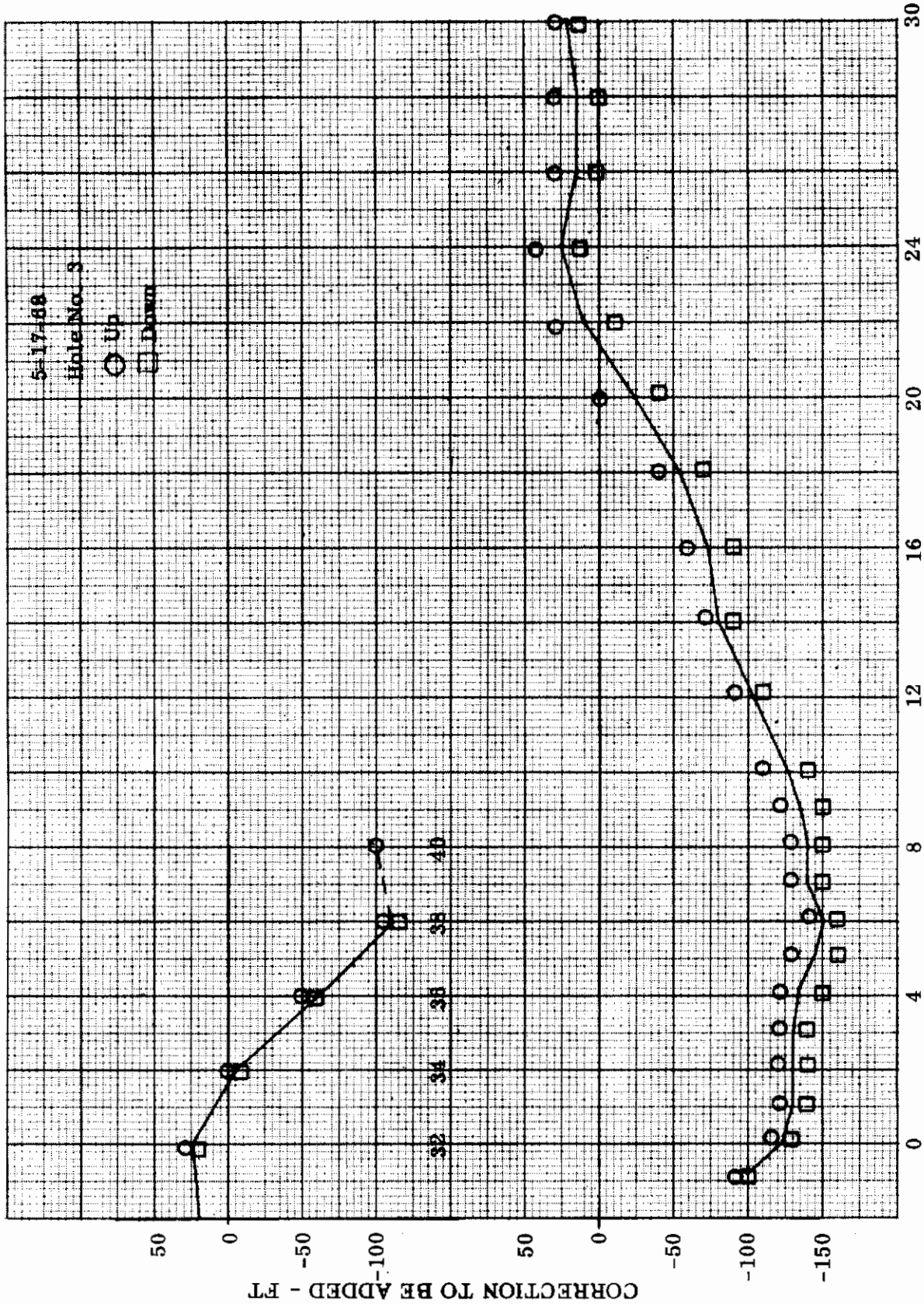

Figure 63. Altimeter Calibration Curve to Correct for Instrument Error.
Flight Test Calibration Curve No. 10263029

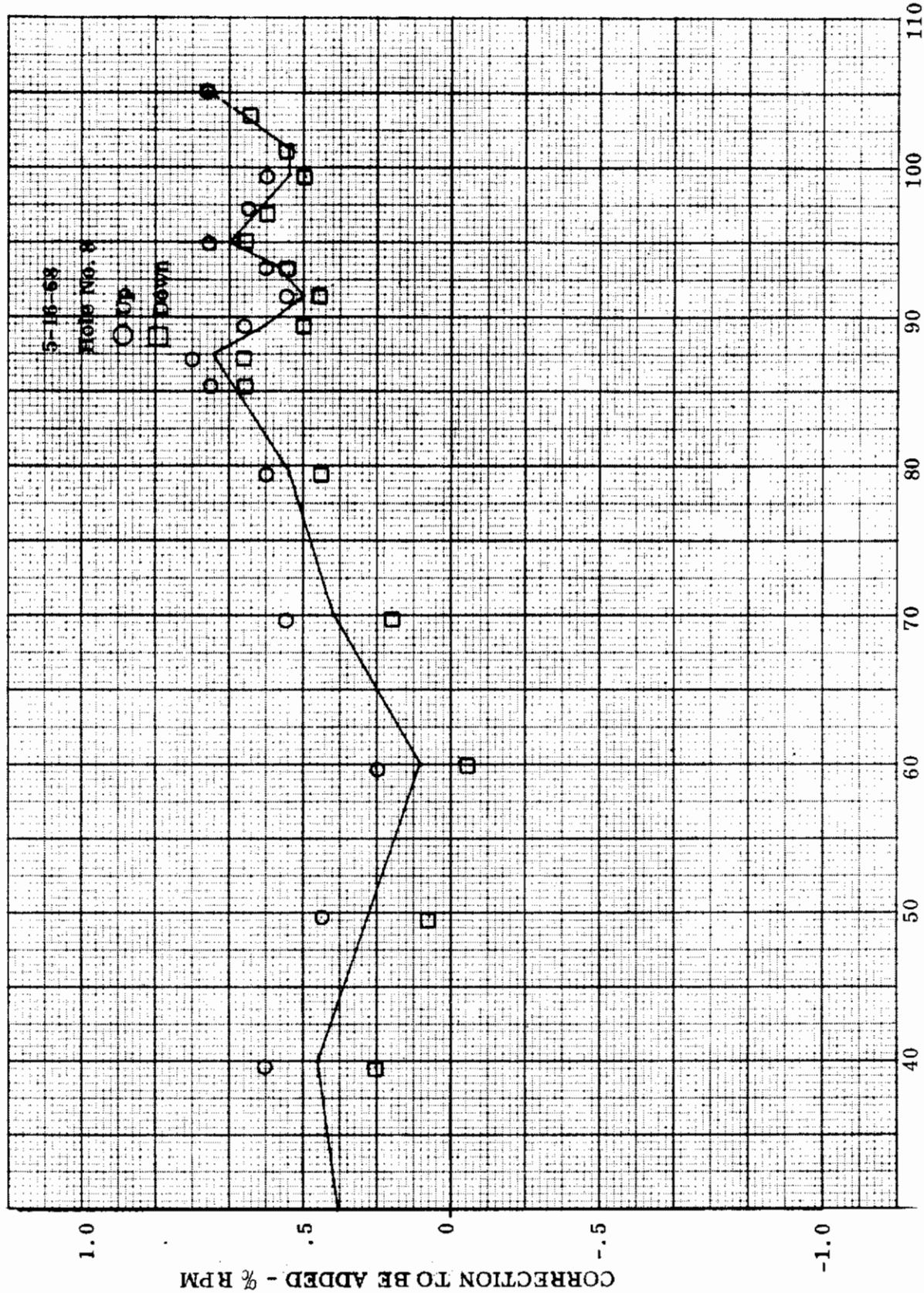

Figure 64. Tachometer Correction Curve for Rotor Speed, Low Pressure Side.
Flight Test Calibration Curve No. 10563017

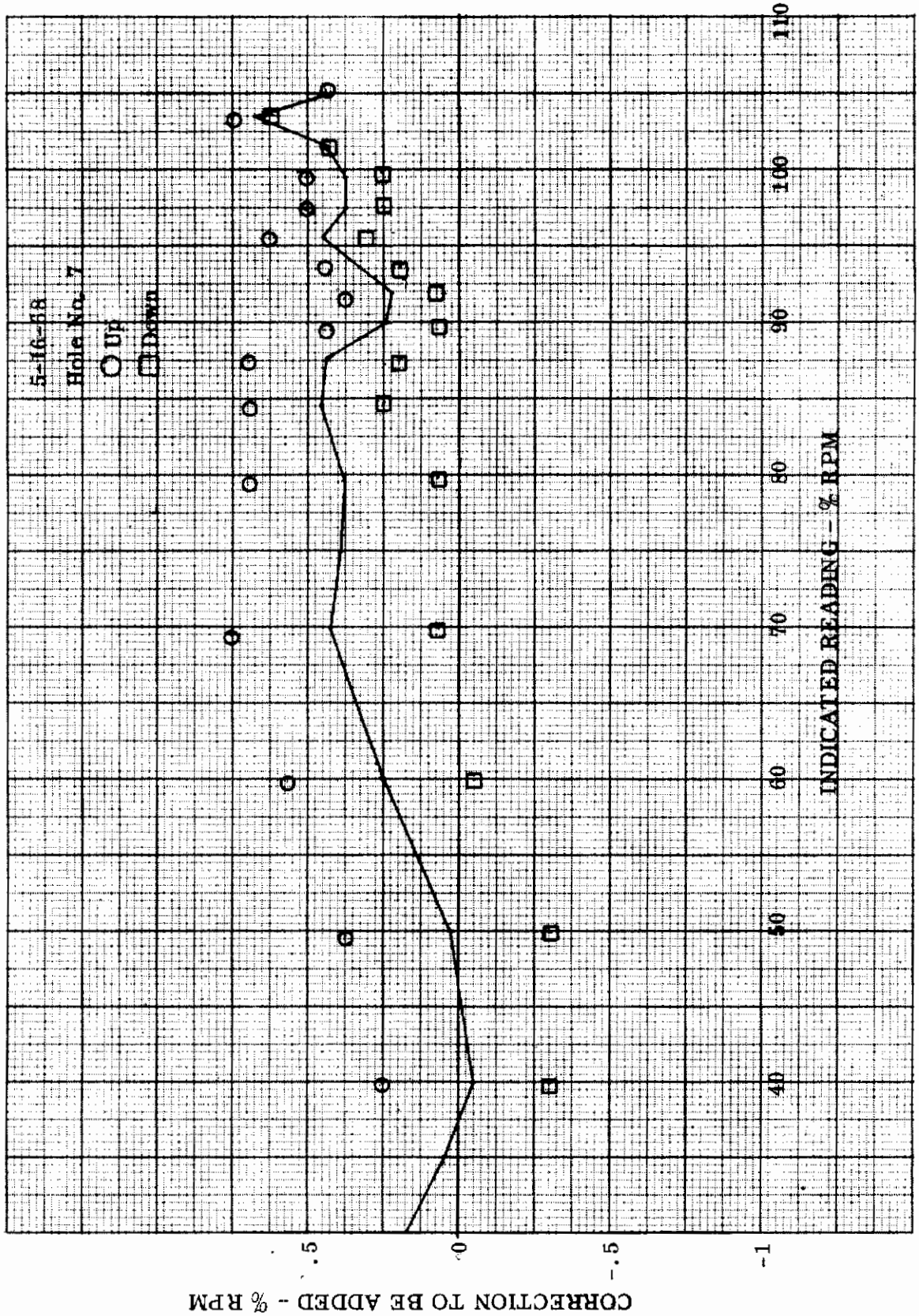

Figure 65. Tachometer Correction Curve for Rotor Speed, High Pressure Side.
Flight Test Calibration Curve No. 10563018

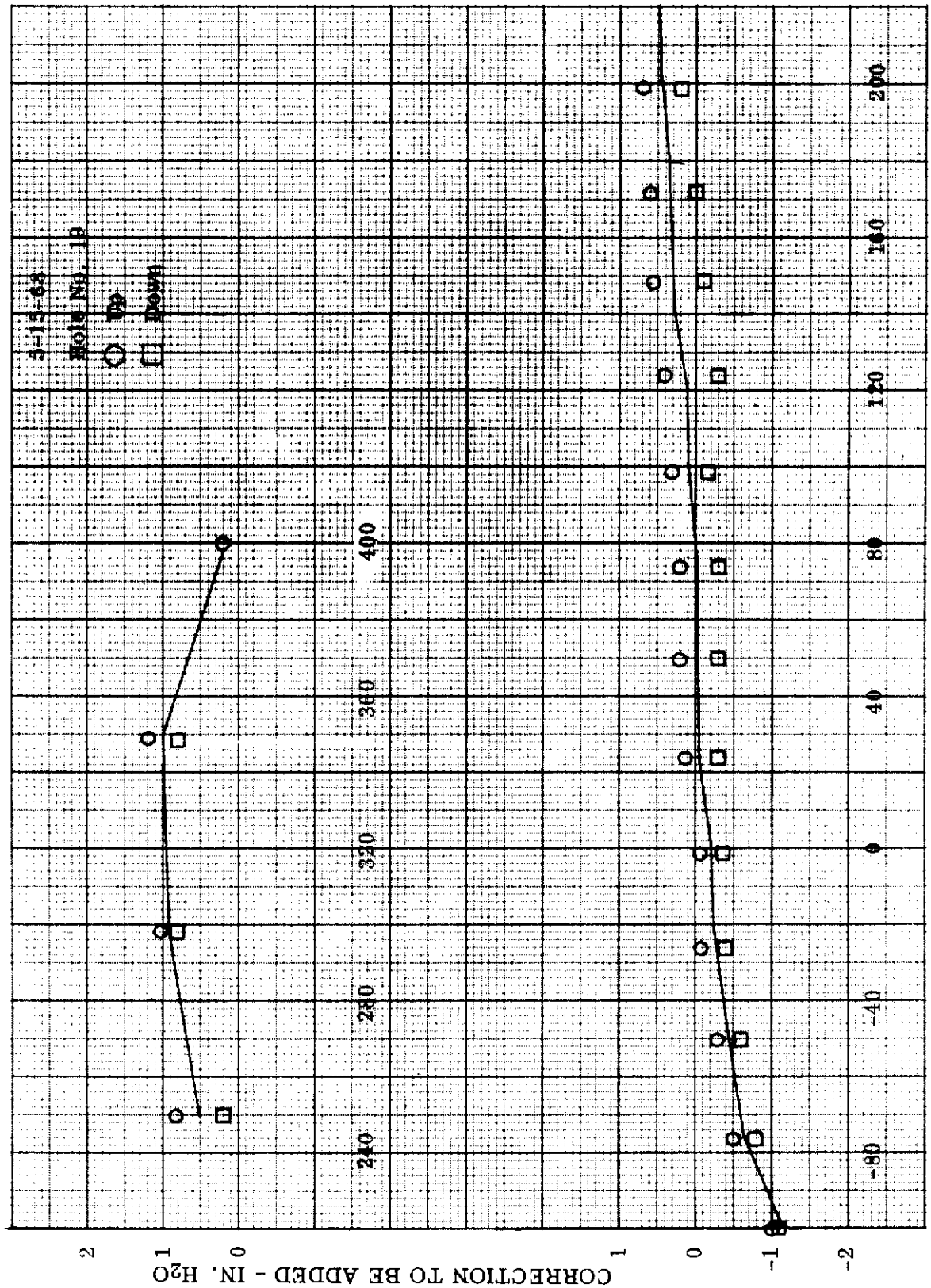

Figure 66. Differential Pressure Correction Curve for Primary Inlet Ducts, Right Side. Flight Test Calibration Curve No. 10763096

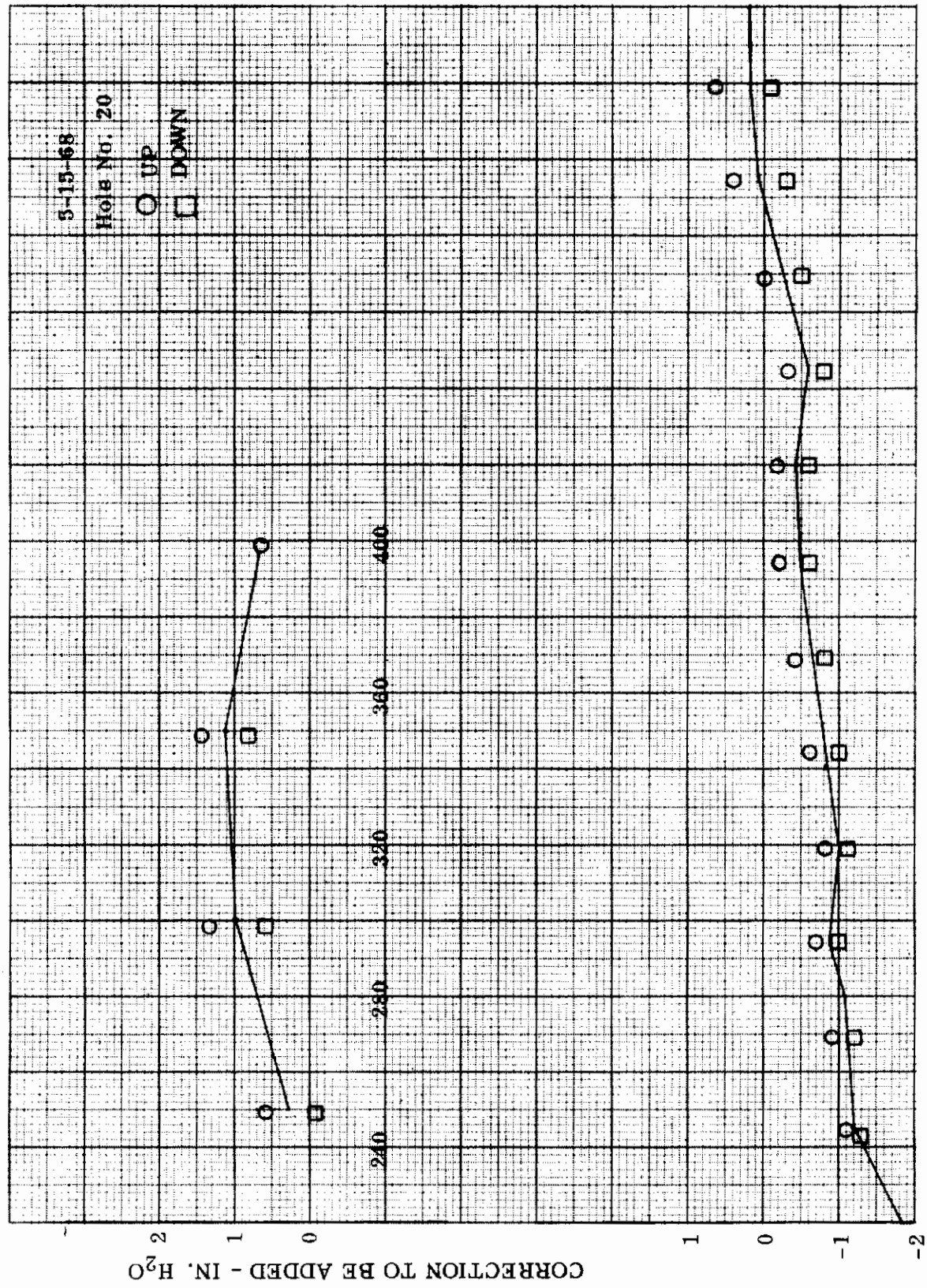

Figure 67. Differential Pressure Correction Curve for Primary Inlet Duct, Center Probe.
Flight Test Calibration Curve No. 10763097

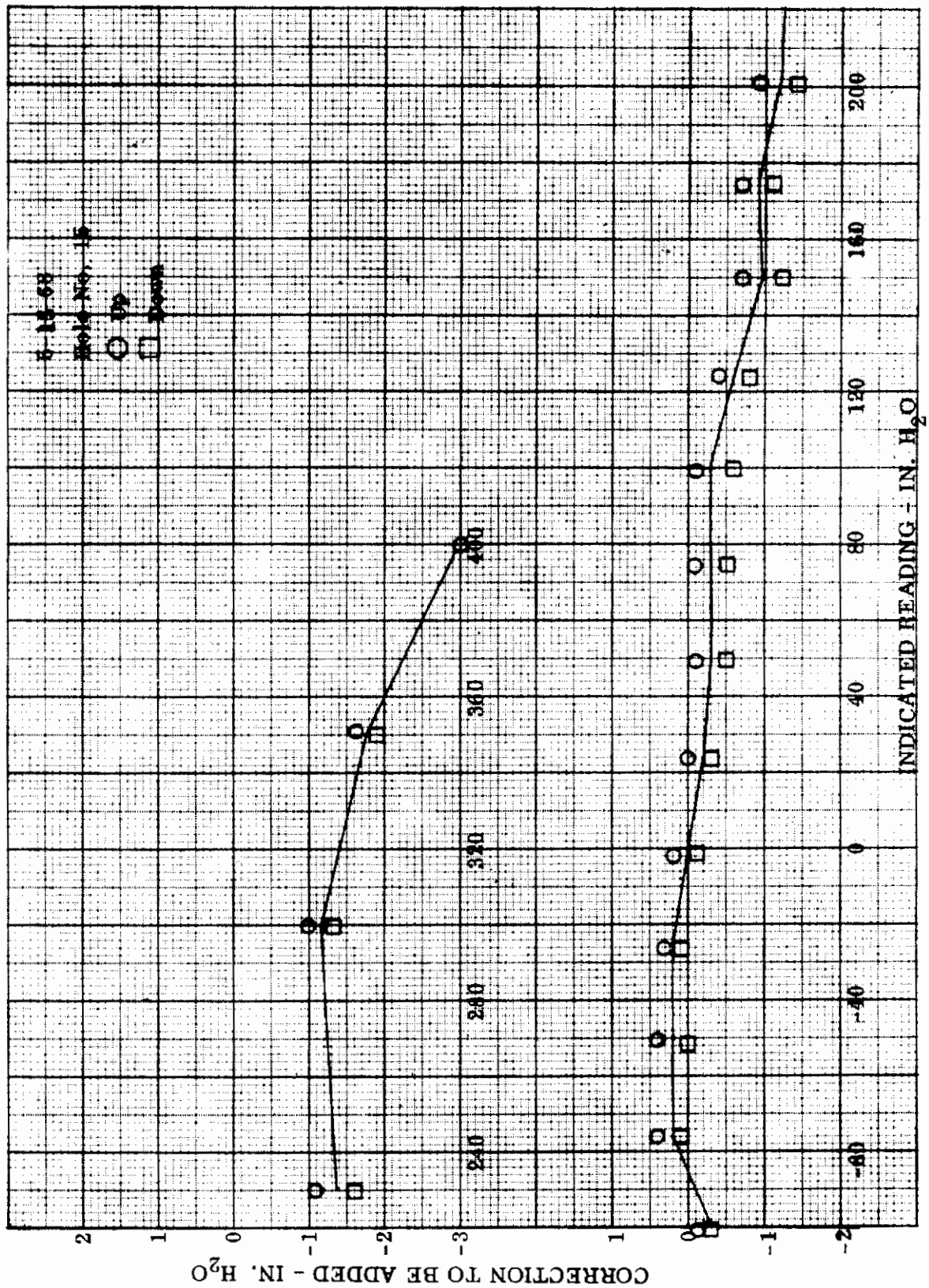

Figure 68. Differential Pressure Correction Curve for Primary Inlet Duct, Left Side. Flight Test Calibration Curve No. 10763095

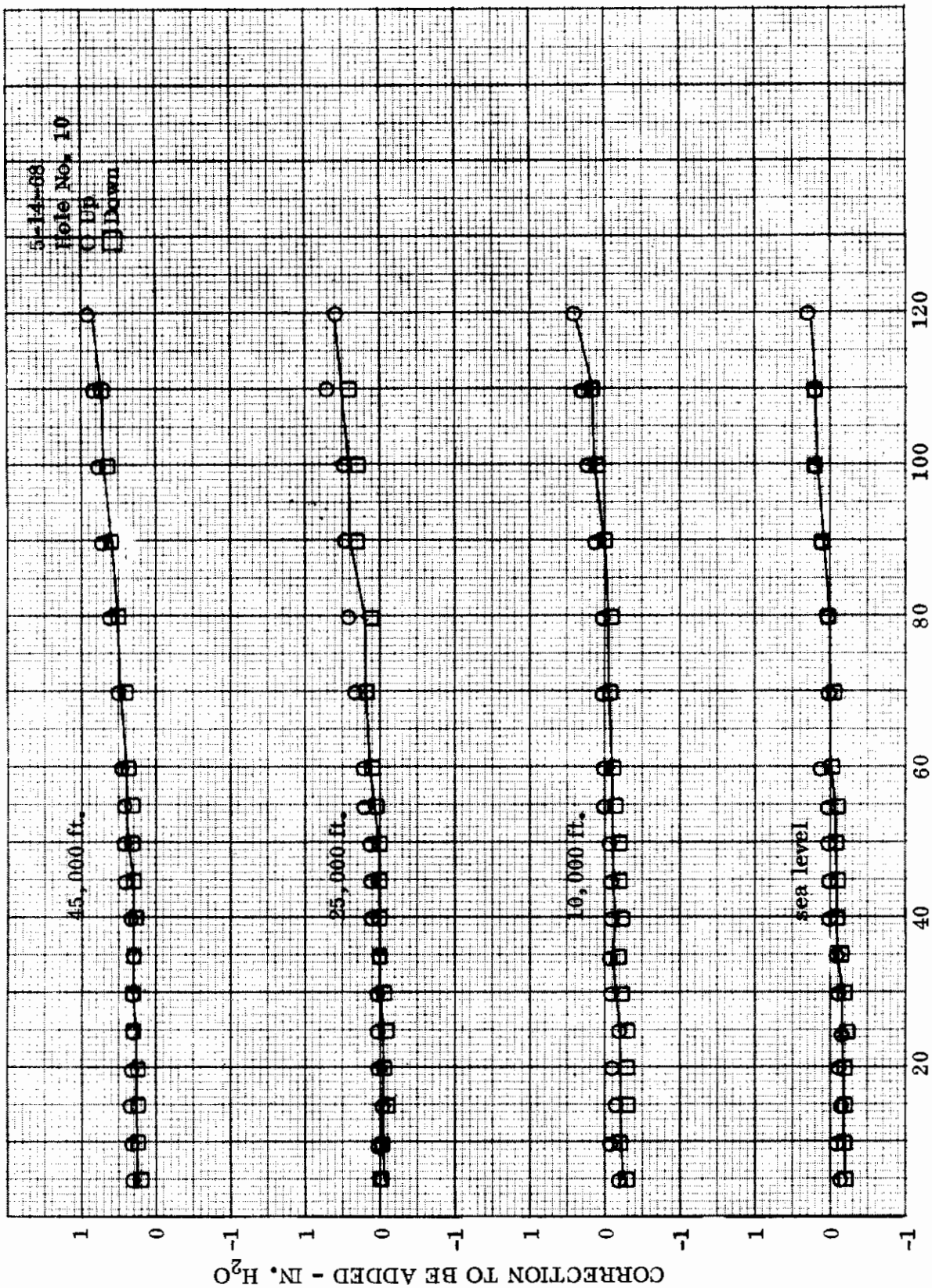

Figure 69. Pressure Reading Correction Curve for Total Pressure at Turbine Discharge.
Flight Test Calibration Curve No. 10663019

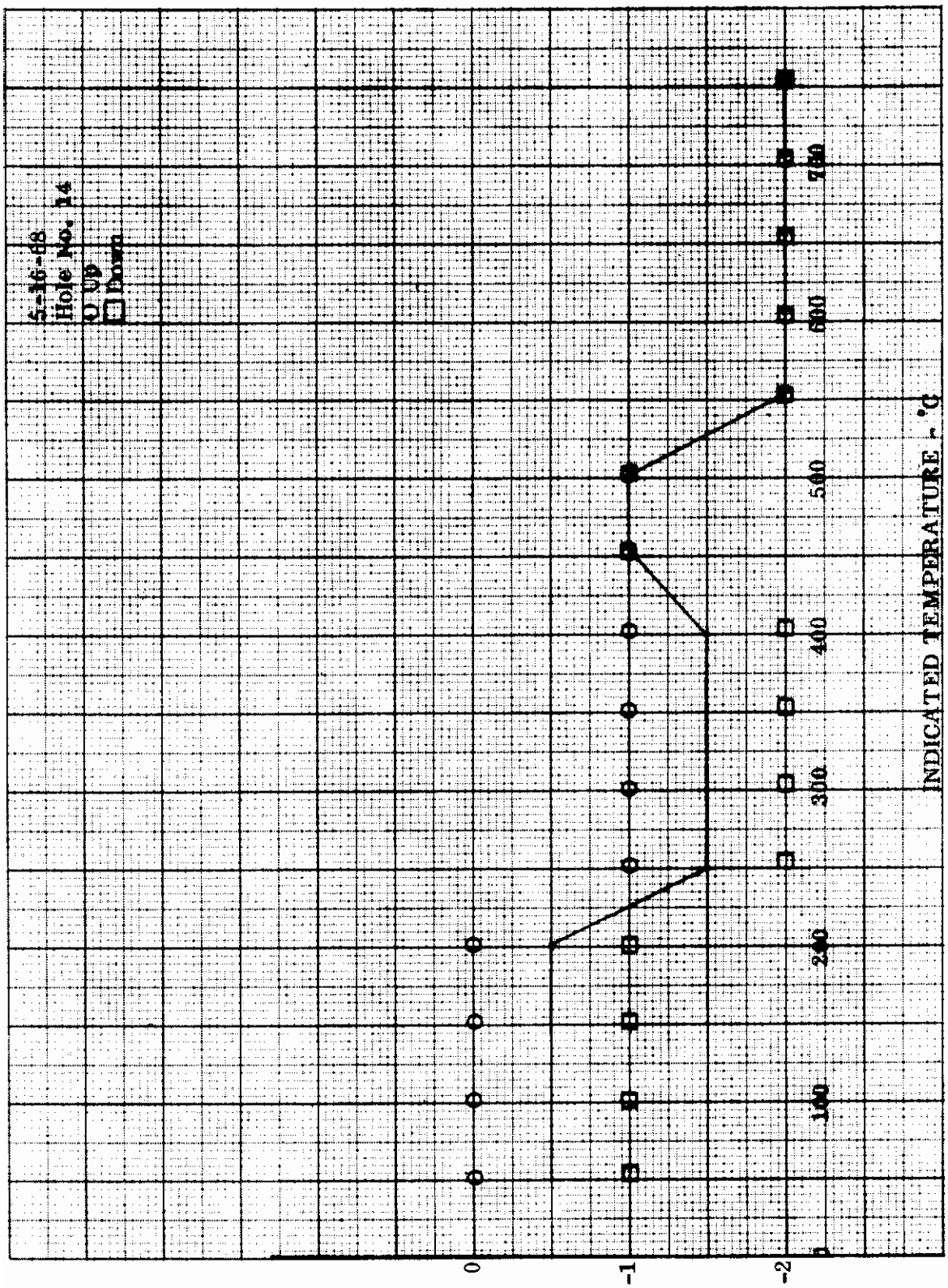

Figure 70. Temperature Correction Curve for Temperature Readings at Turbine Discharge.
Flight Test Calibration Curve No. 10863032

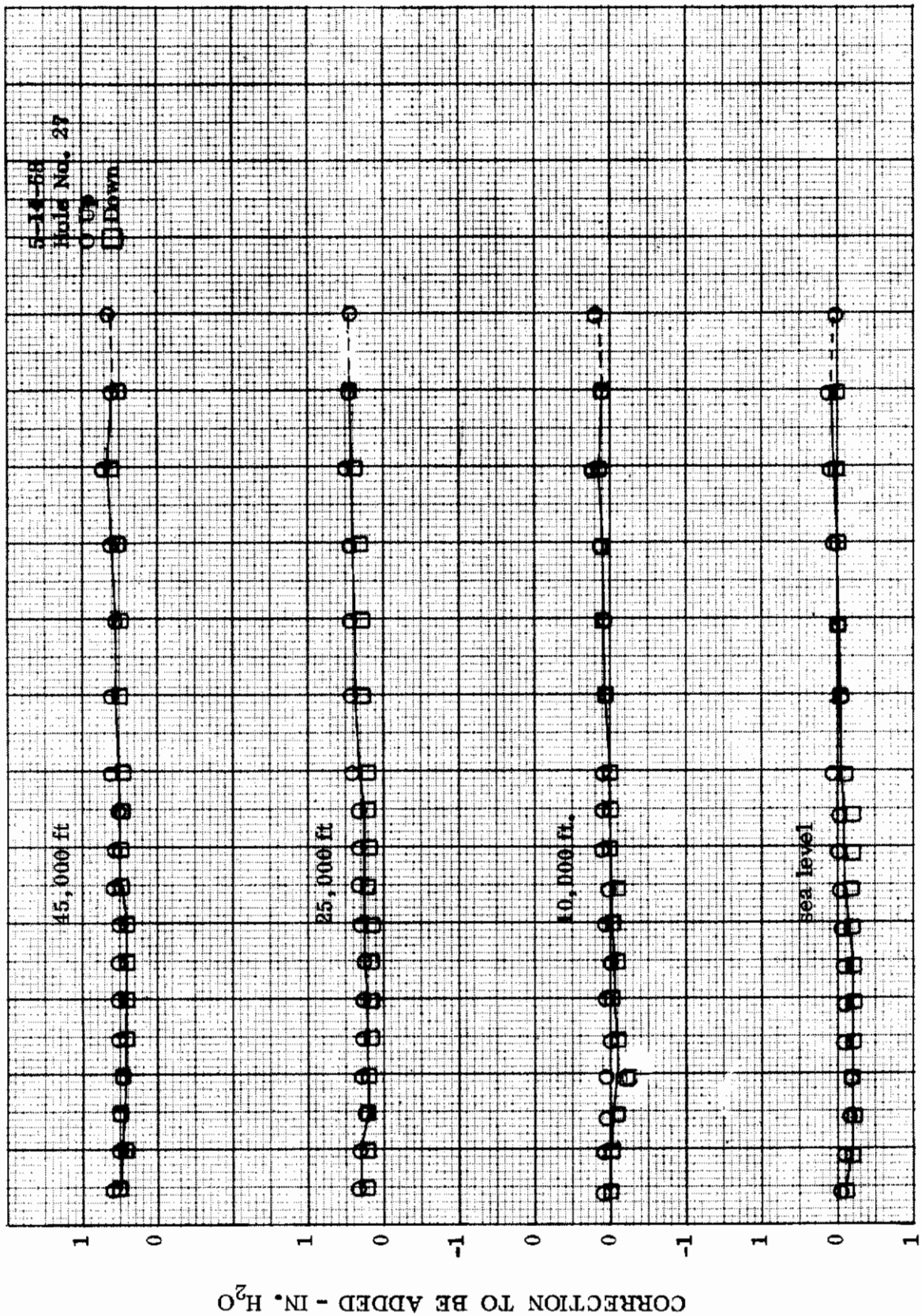

Figure 71. Total Pressure Reading Correction Curve for Shroud Cooling Scoop.
Flight Test Calibration Curve No. 10663020

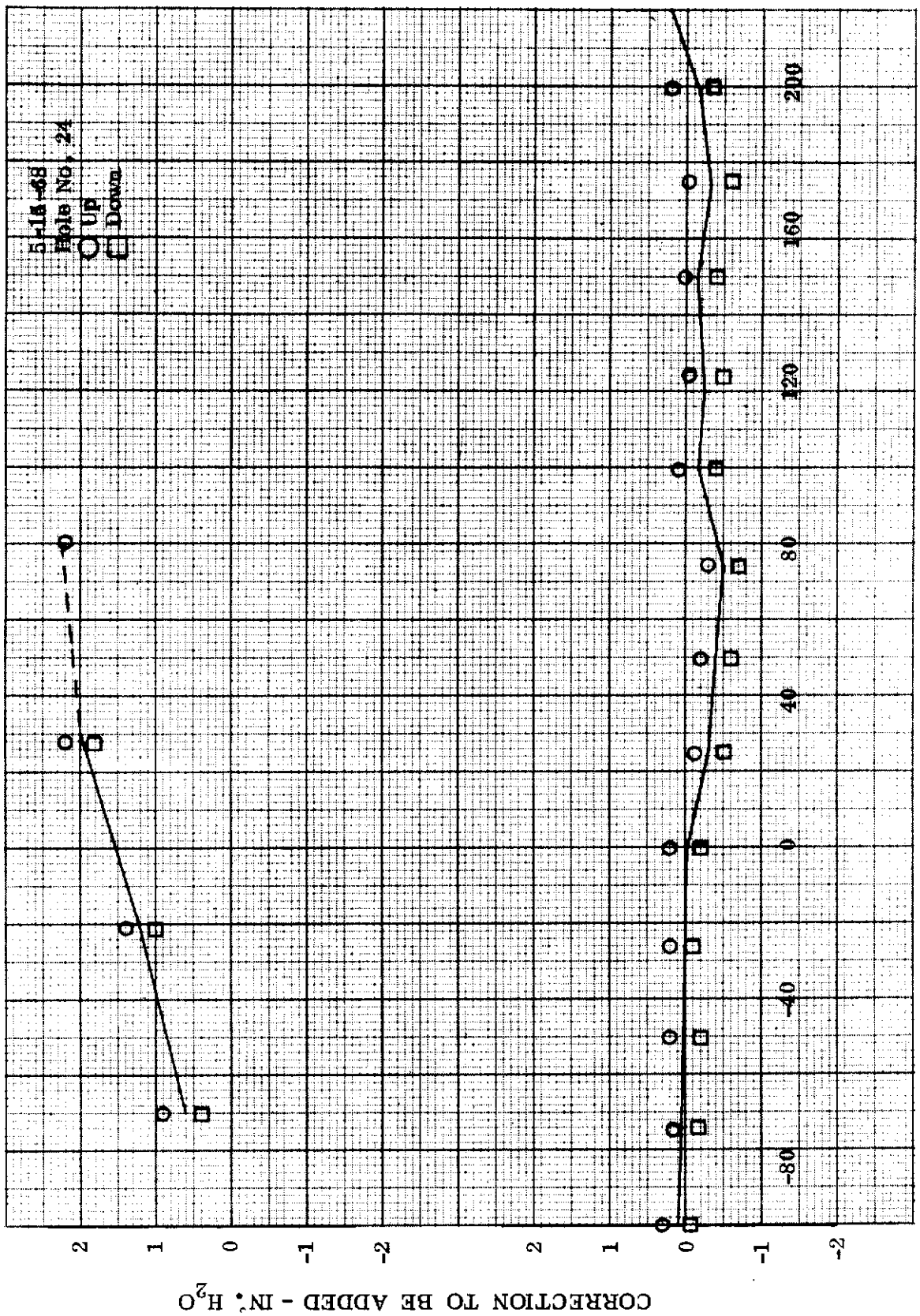

Figure 72. Differential Pressure Reading Correction Curve for Shroud Cooling Scoop.
Flight Test Calibration Curve No. 10763098

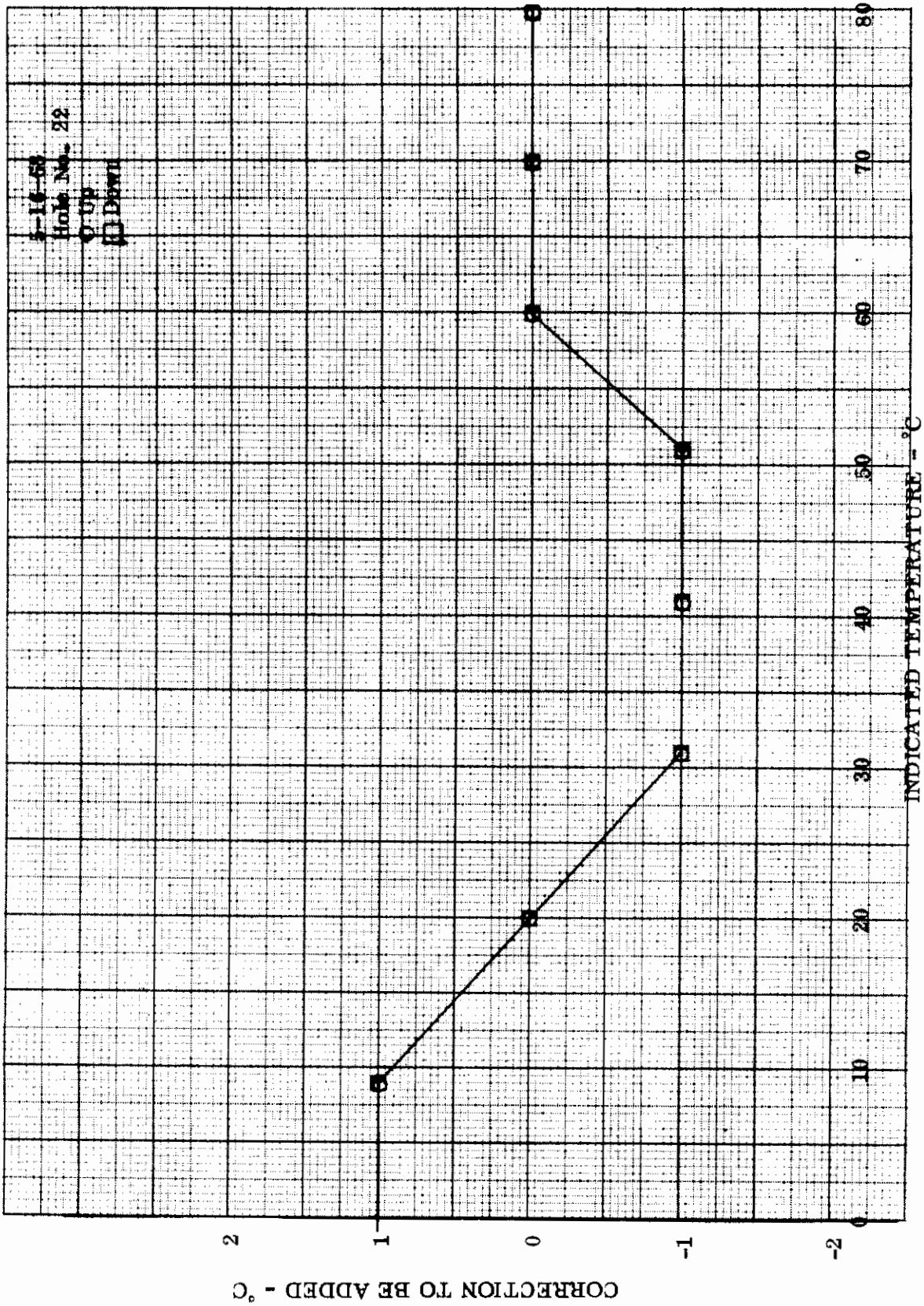

Figure 73. Temperature Reading Correction Curve for Engine Fuel Temperature.
Flight Test Calibration Curve No. 10863033

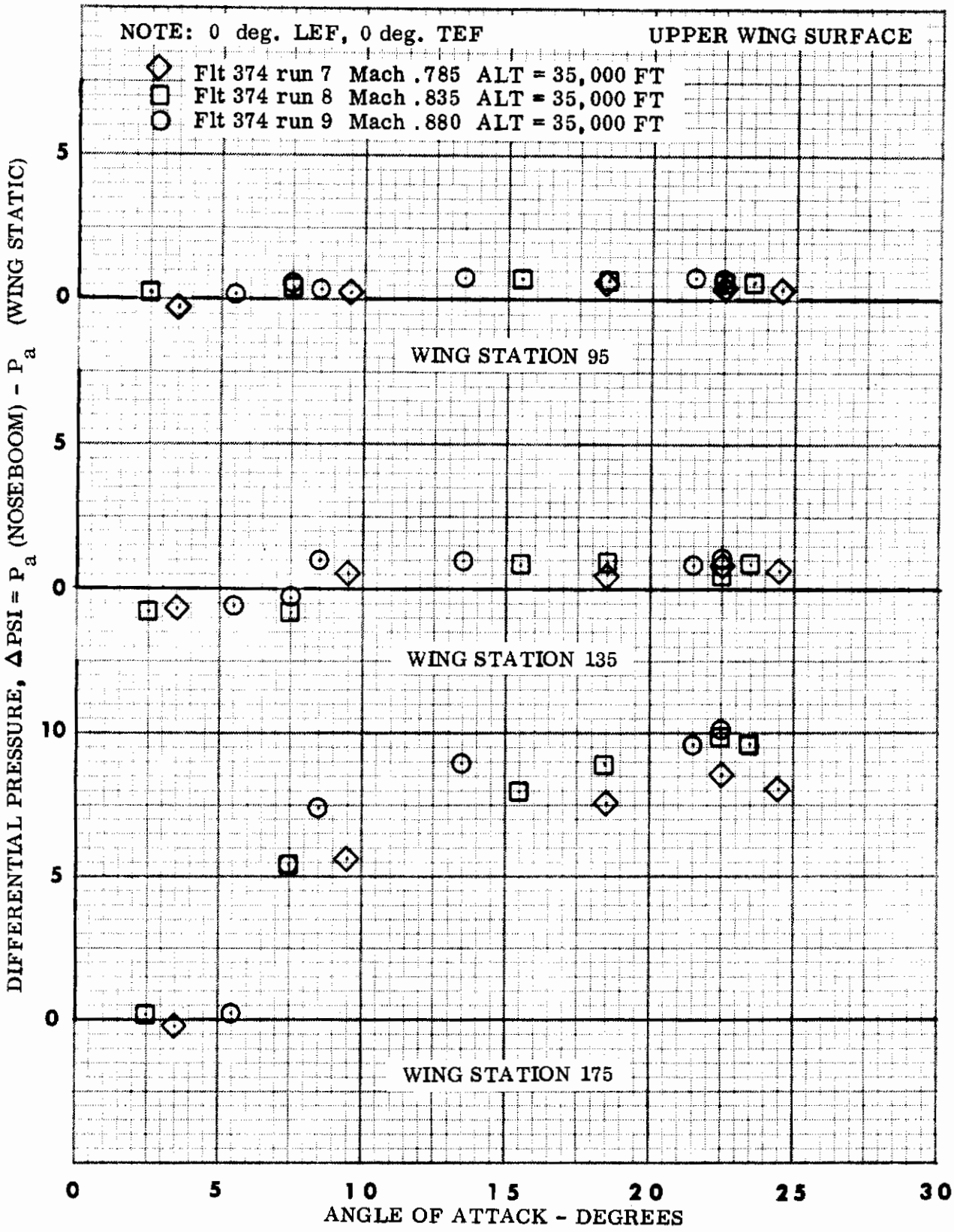

Figure 74. Variation of the Trailing Edge Static Pressure at the Top Surface Pressure Port. Wing Station 175 at 95% Chord

(a) Leading Edge Flap and Trailing Edge Flap Undeflected

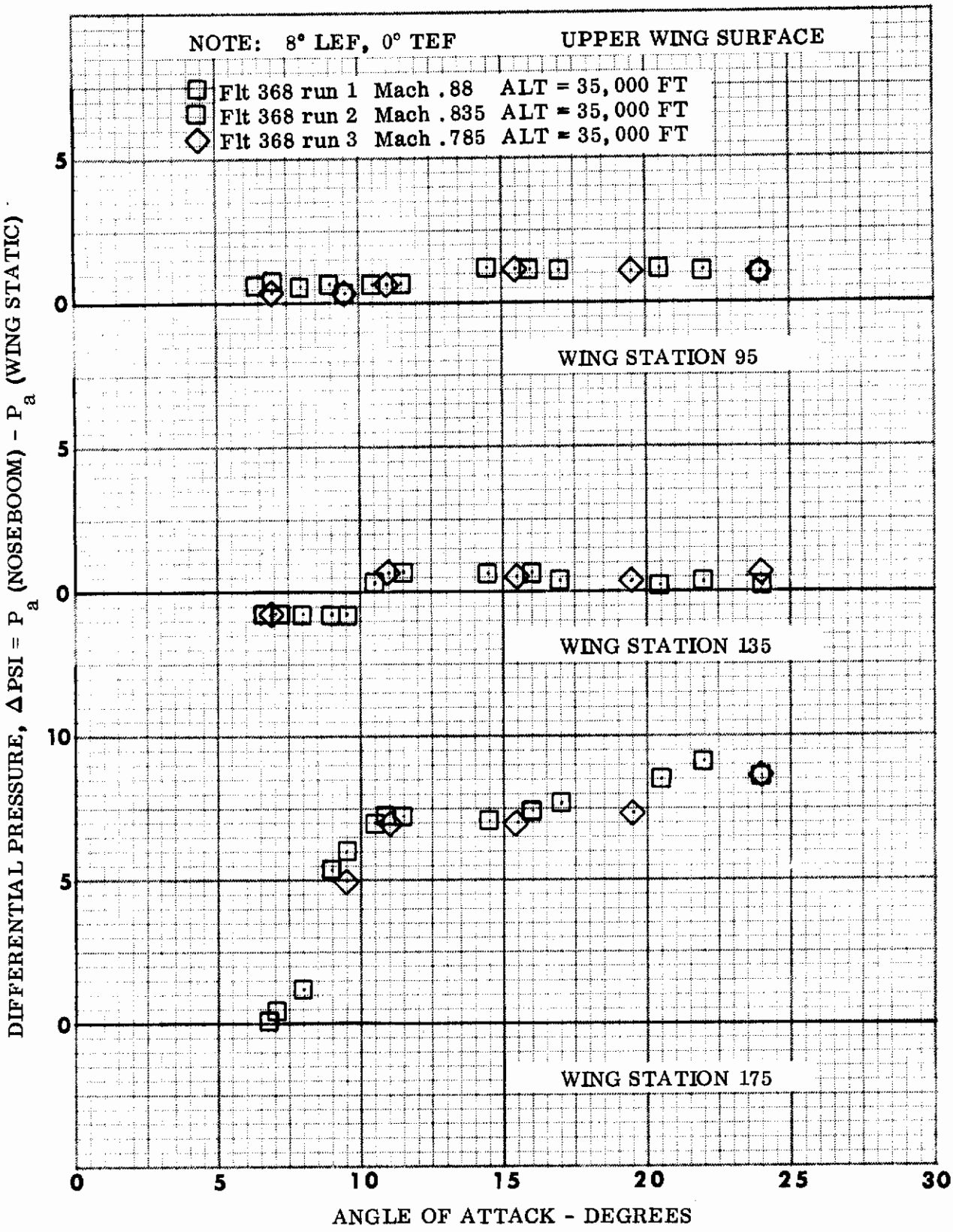

Figure 74. --- Continued
(b) Leading Edge Flap 8°, Trailing Edge Flap Undeflected

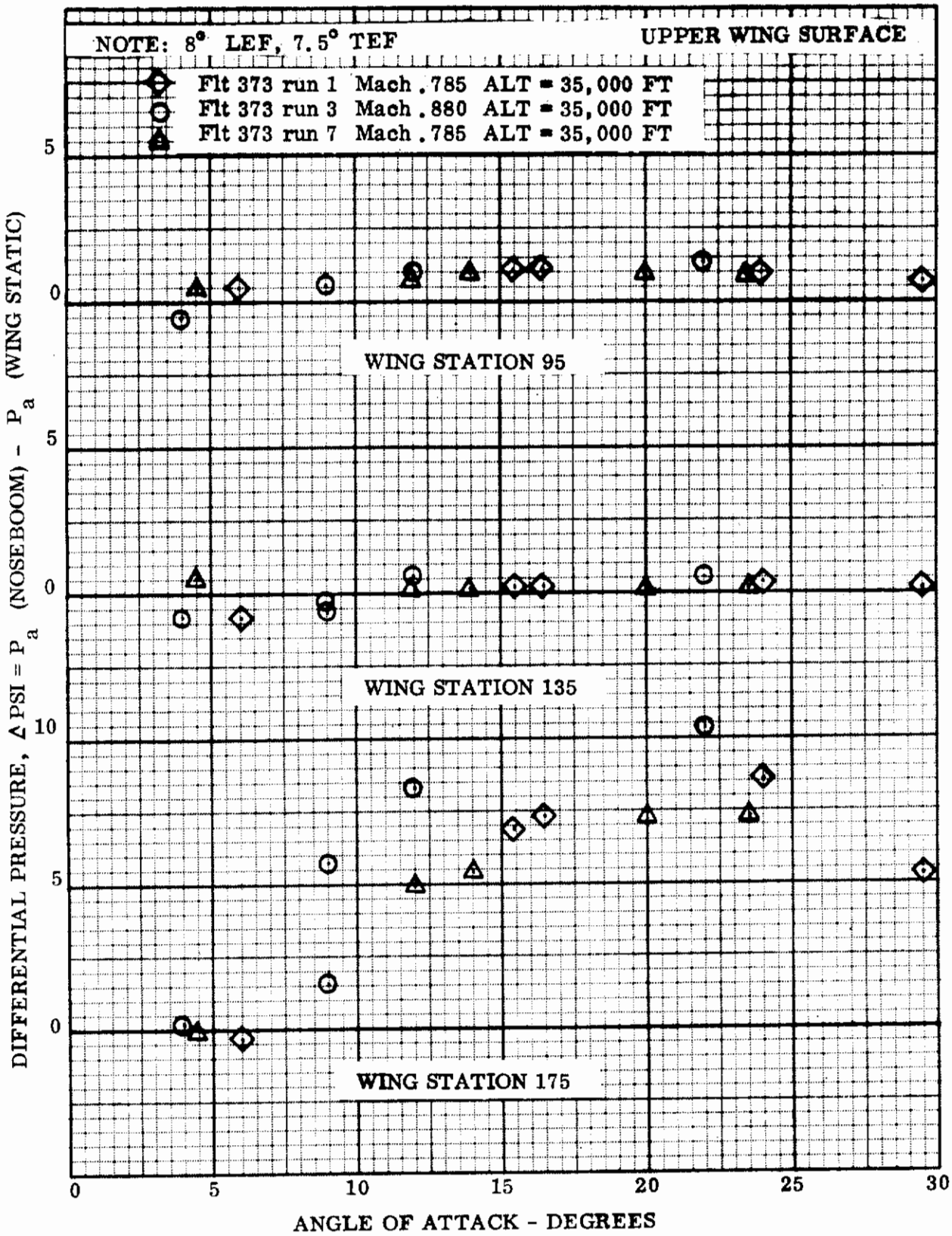

Figure 74. --- Concluded
(c) Leading Edge Flap 8° , Trailing Edge Flap 7.5°

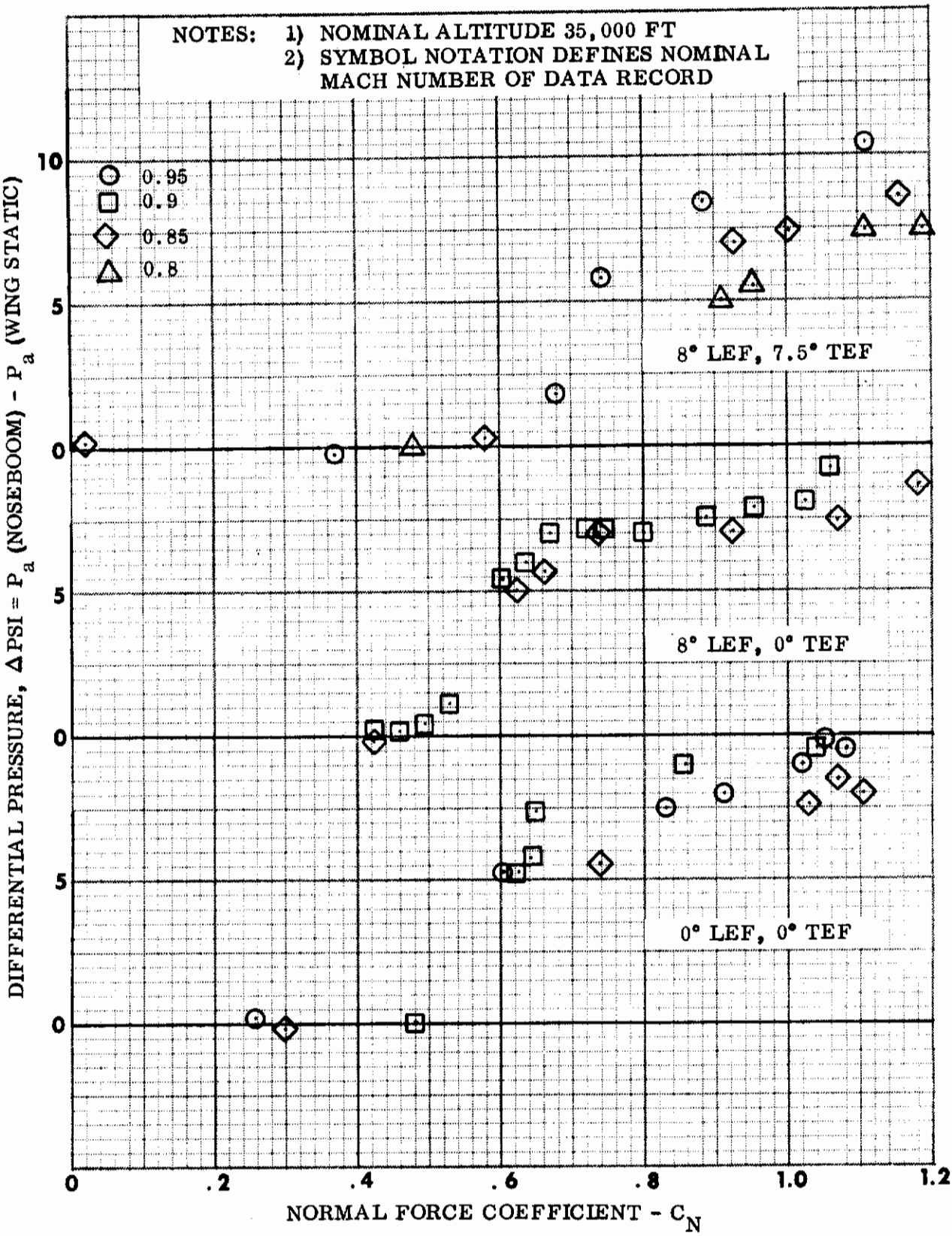

Figure 75. Variation of the Trailing Edge Static Pressure at the Top Surface Pressure Port with Normal Force Coefficient. Wing Station 175 at 95% Chord. Three Flap Configurations

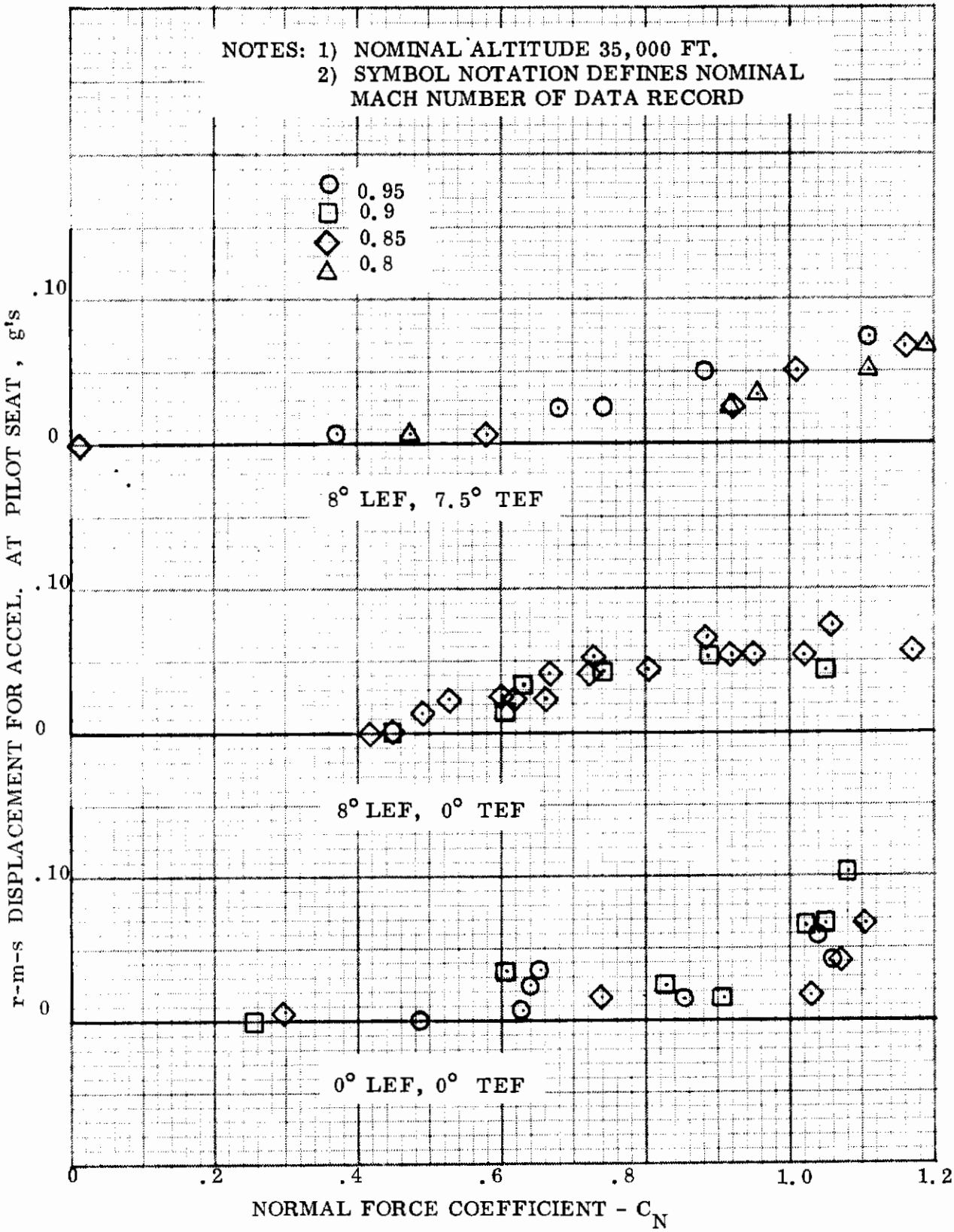

Figure 76. Variation of the Root-Mean-Square Fluctuations for the Normal Acceleration at the Pilot's Seat. Three Flap Configuration
(a) Variation with Normal Force Coefficient

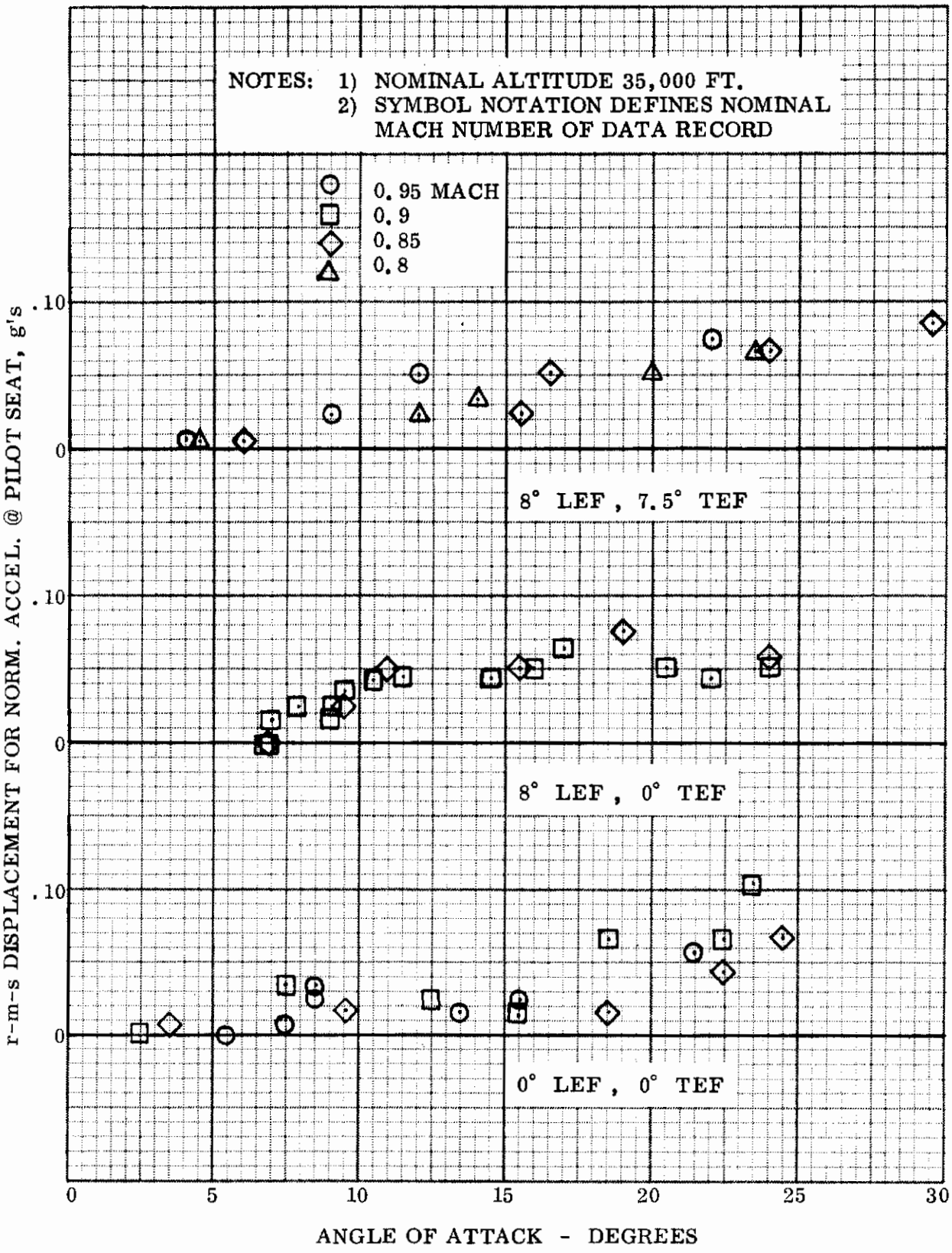

Figure 76. --- Concluded
(b) Variation with Angle of Attack

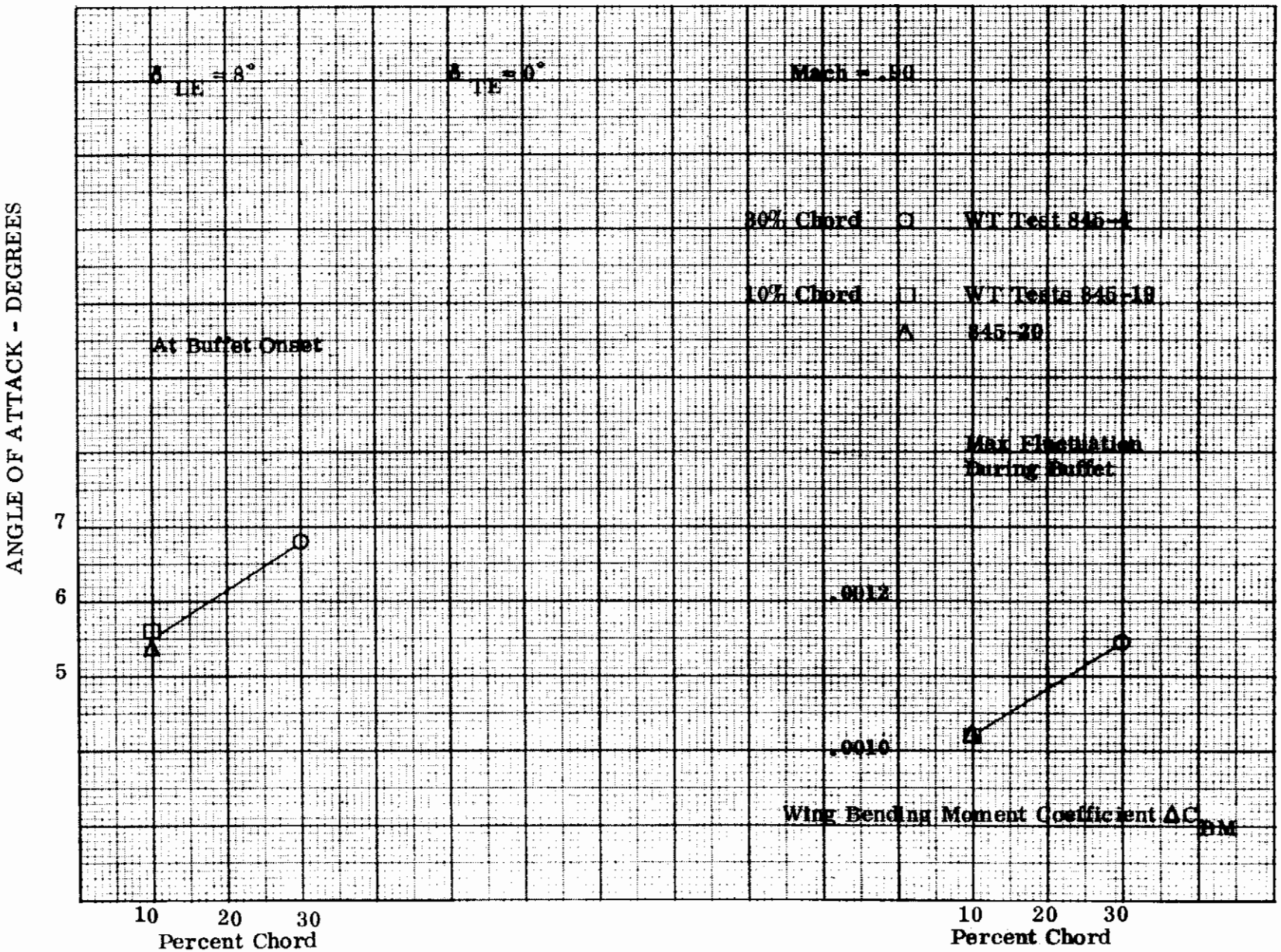

Figure 77. Chordwise Variation of the Boundary Layer **Transition Strip** and Its Effects on the Buffet Onset and Intensity Characteristics

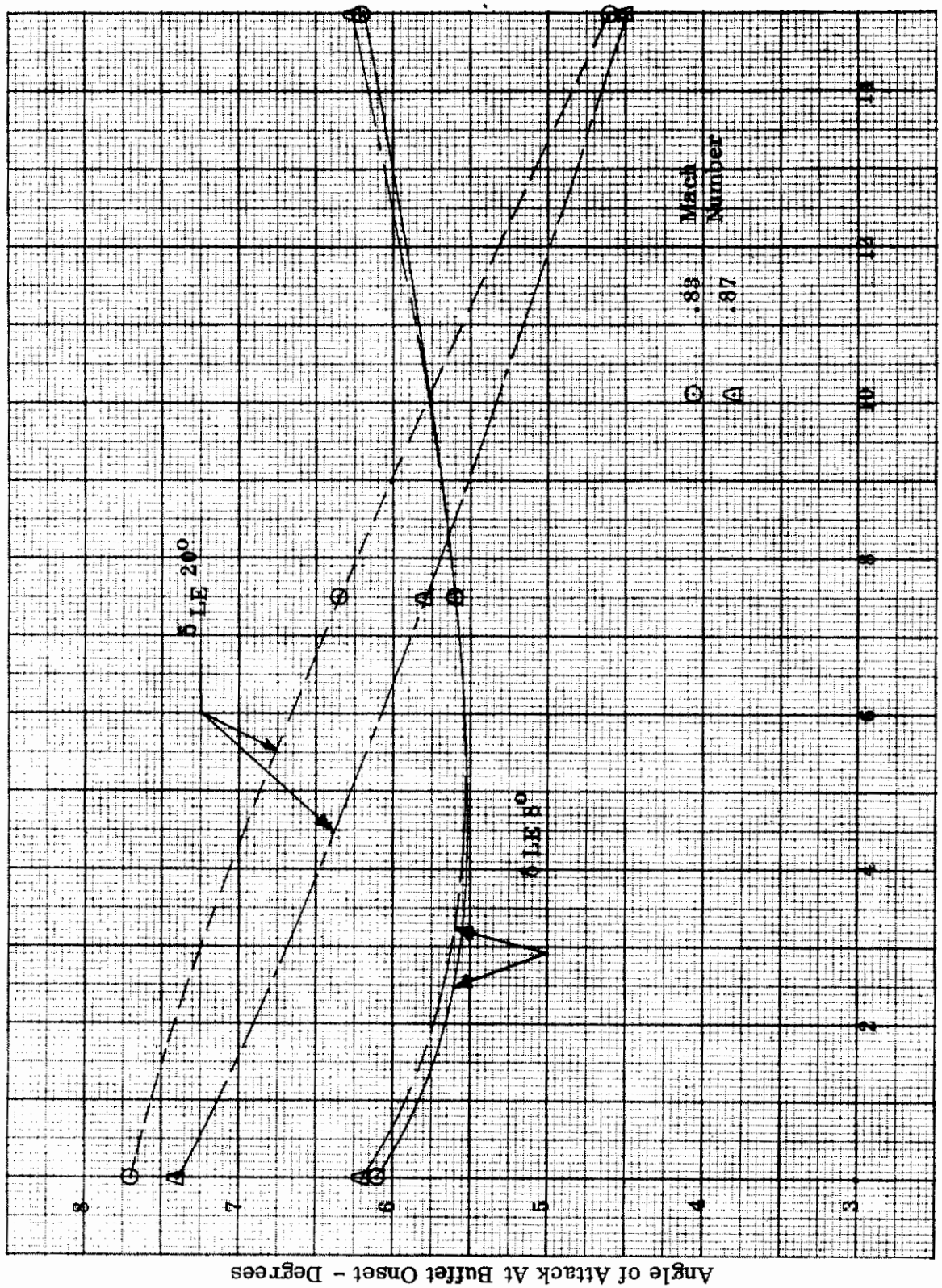

Figure 78. Leading Edge Flap and Trailing Edge Flap Deflection Effects on the Angle of Attack at Buffet Onset

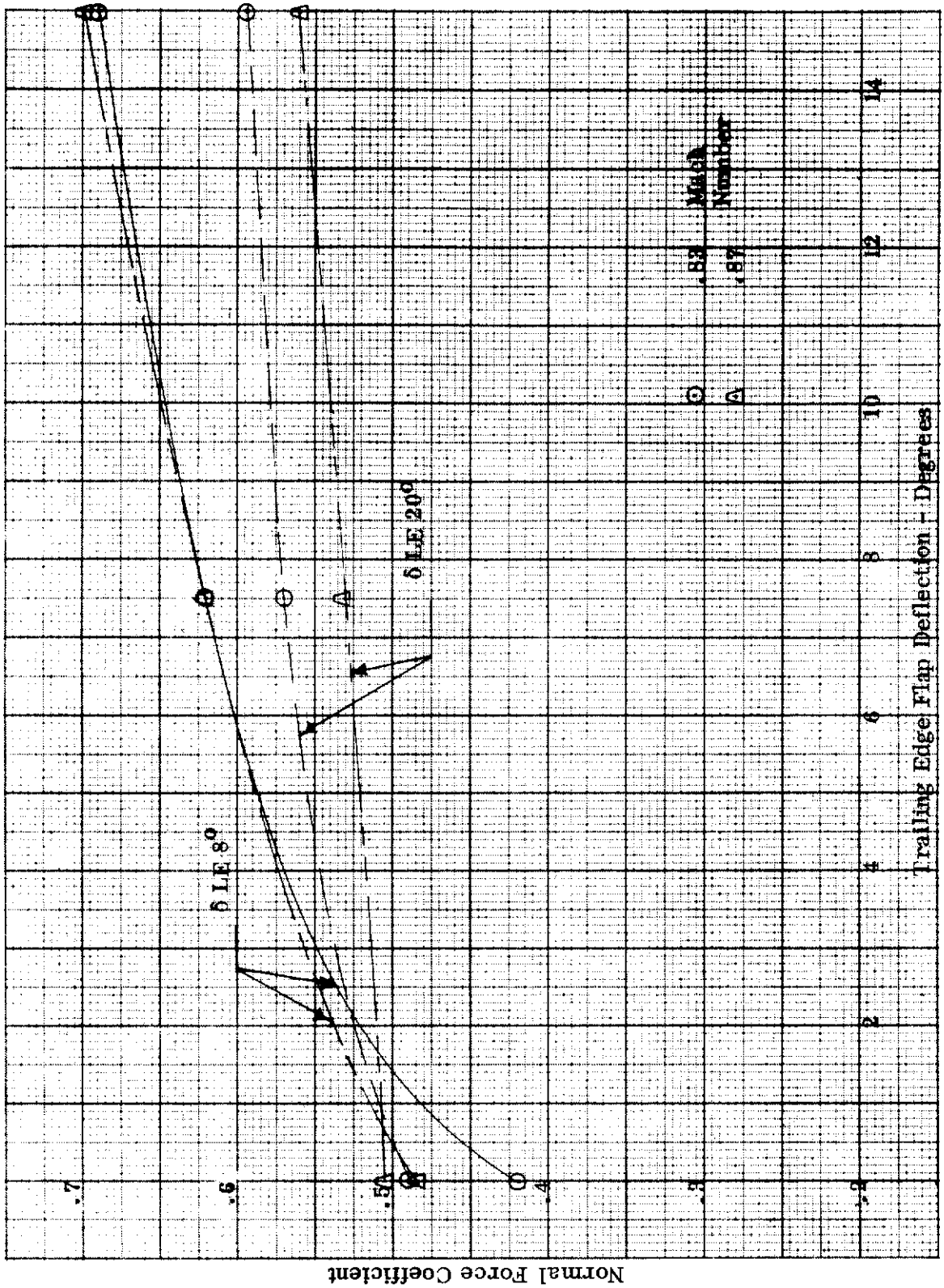

Figure 79. Leading Edge Flap and Trailing Edge Flap Deflection Effects on the Normal Force Coefficient at Buffet Onset

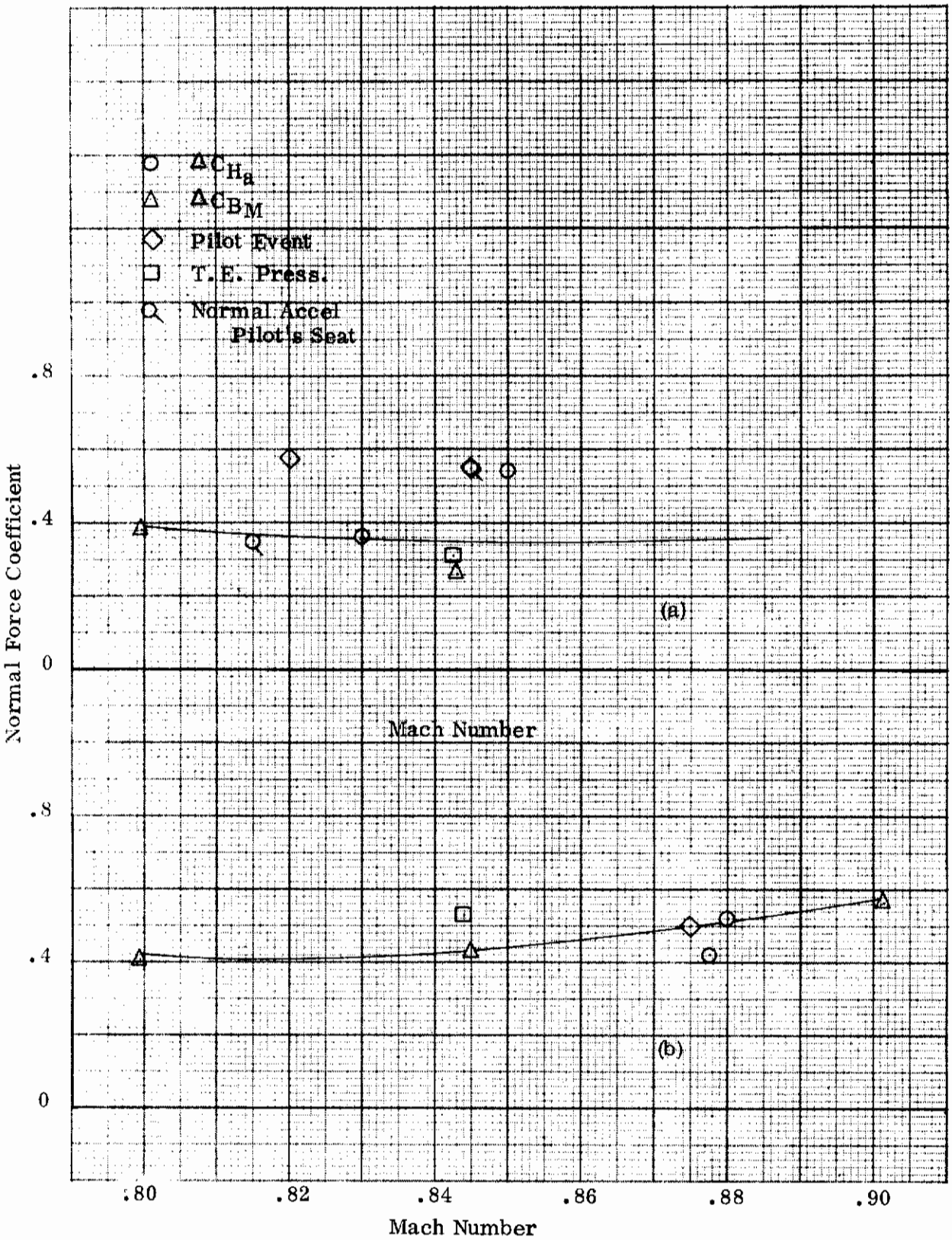

Figure 80. Normal Force Coefficient at Buffet Onset
(a) Leading Edge Flap and Trailing Edge Flap Undeflected
(b) Leading Edge Flap 8°, Trailing Edge Flap Undeflected

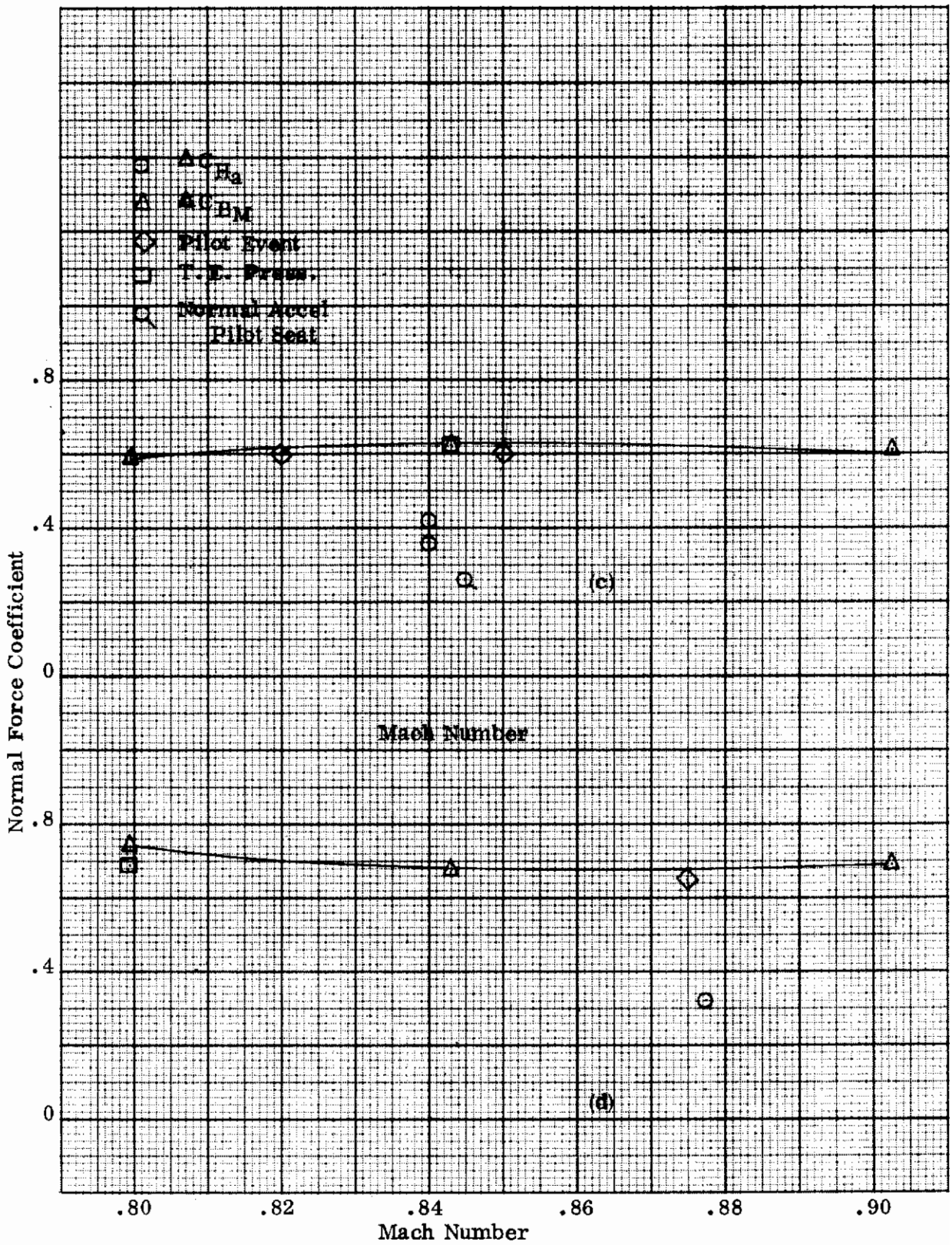

Figure 80. --- Continued

(c) Leading Edge Flap 8^0, Trailing Edge Flap 7.5^o

(d) Leading Edge Flap 8^o, Trailing Edge Flap 15^o

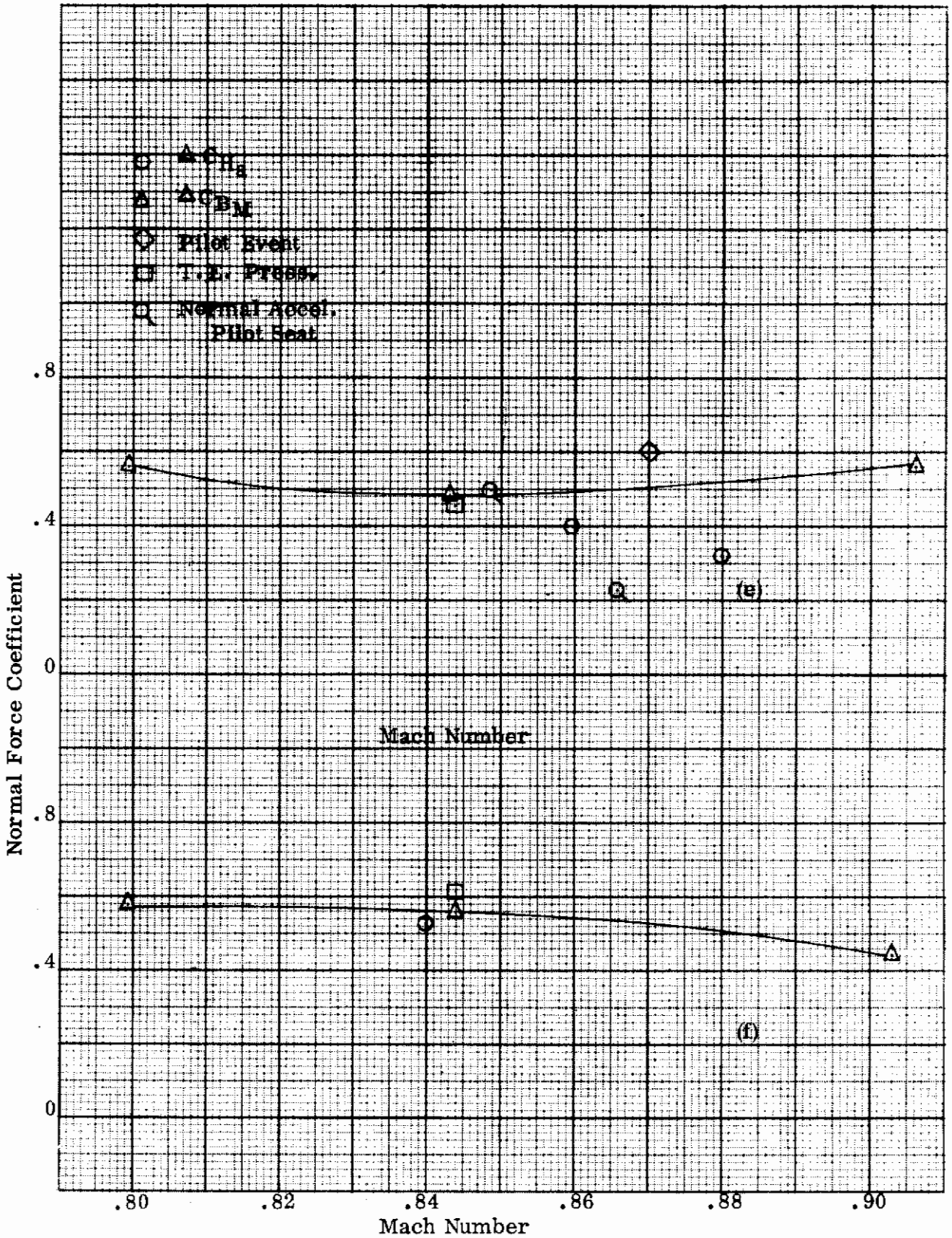

Figure 80. --- Continued
(e) Leading Edge Flap 20°, Trailing Edge Flap Undeflected
(f) Leading Edge Flap 20°, Trailing Edge Flap 7.5°

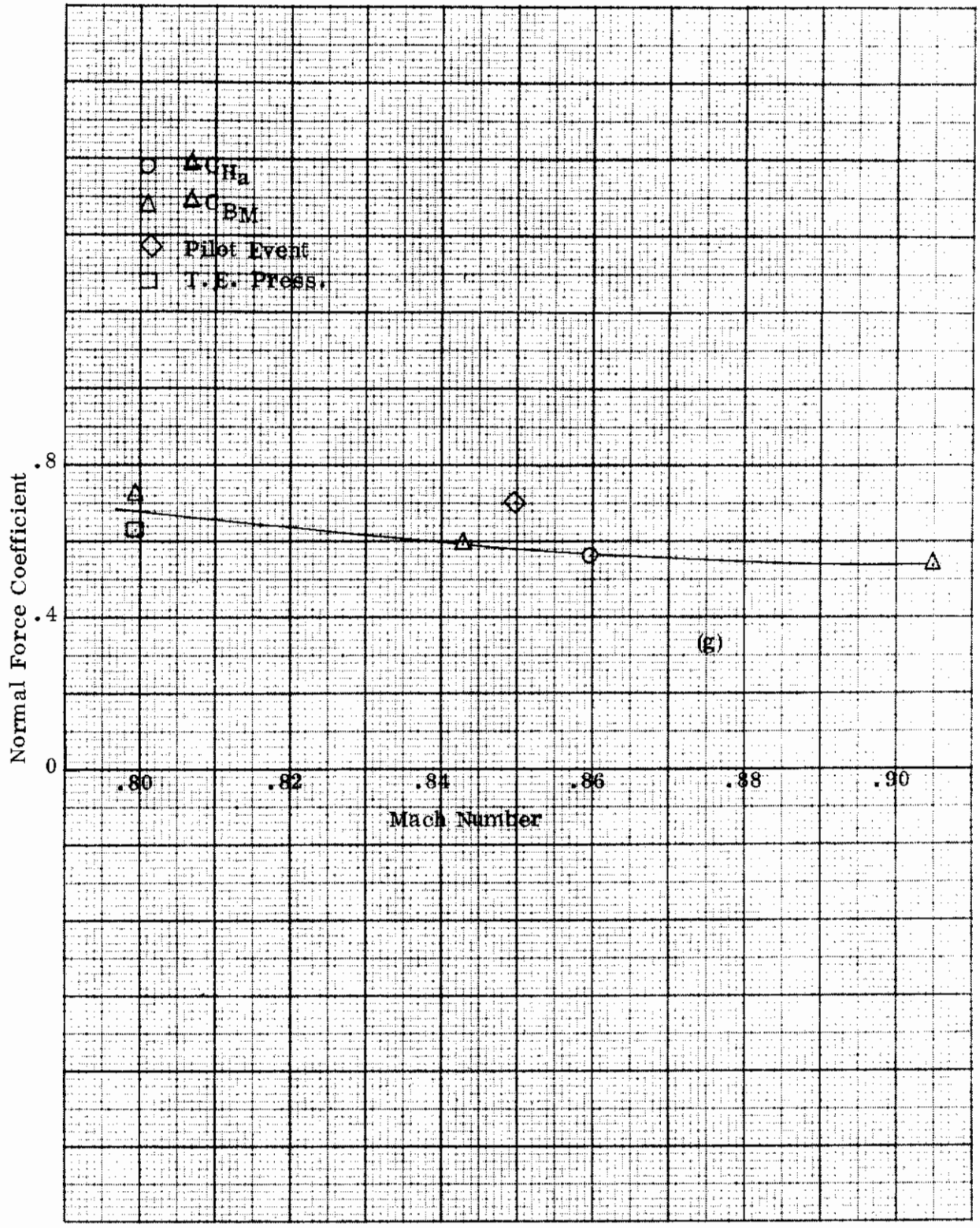

Figure 80. --- Concluded
(g) Leading Edge Flap 20°, Trailing Edge Flap 15°

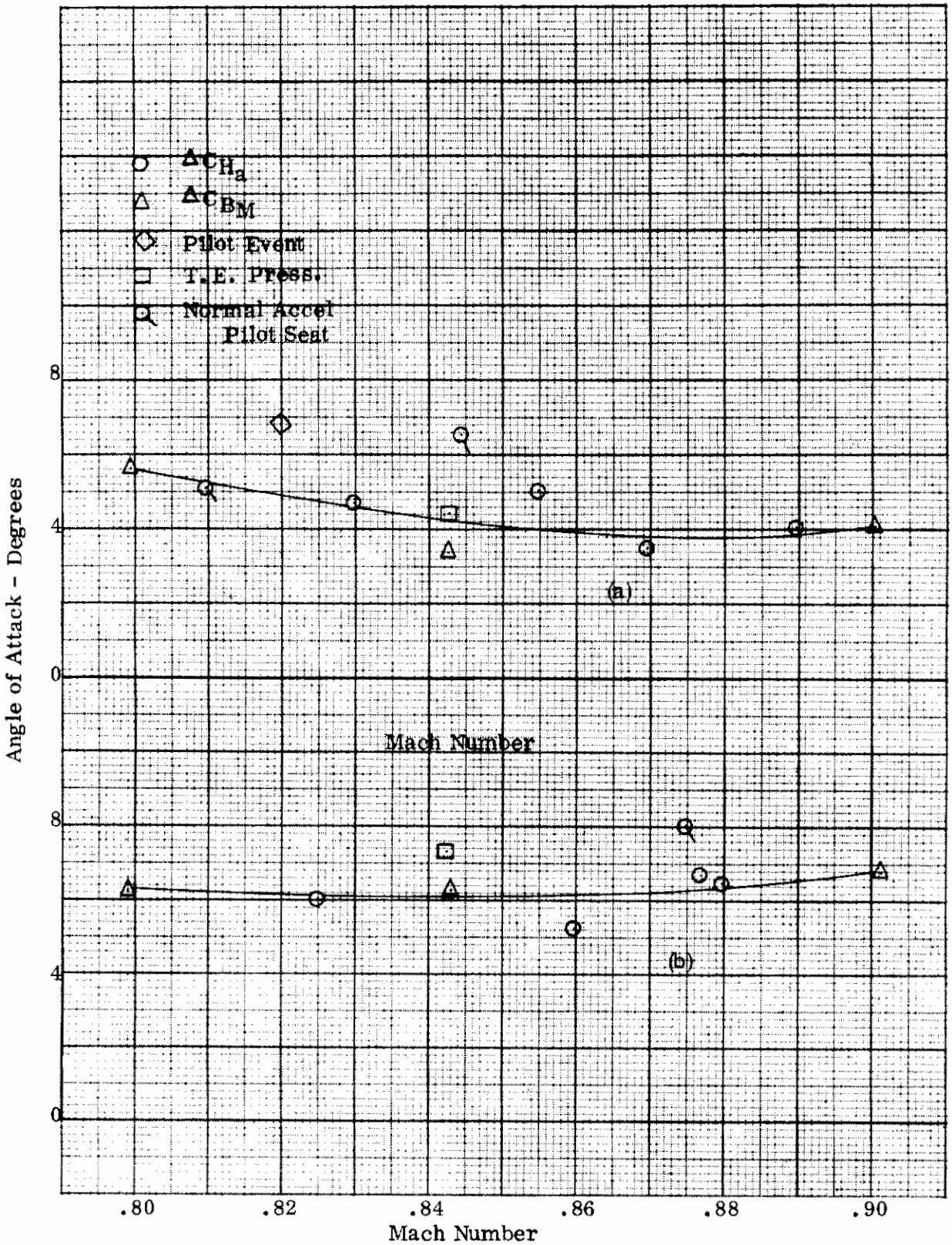

Figure 81. Angle of Attack at Buffet Onset
(a) Leading Edge Flap and Trailing Edge Flap Undeflected
(b) Leading Edge Flap 8°, Trailing Edge Flap Undeflected

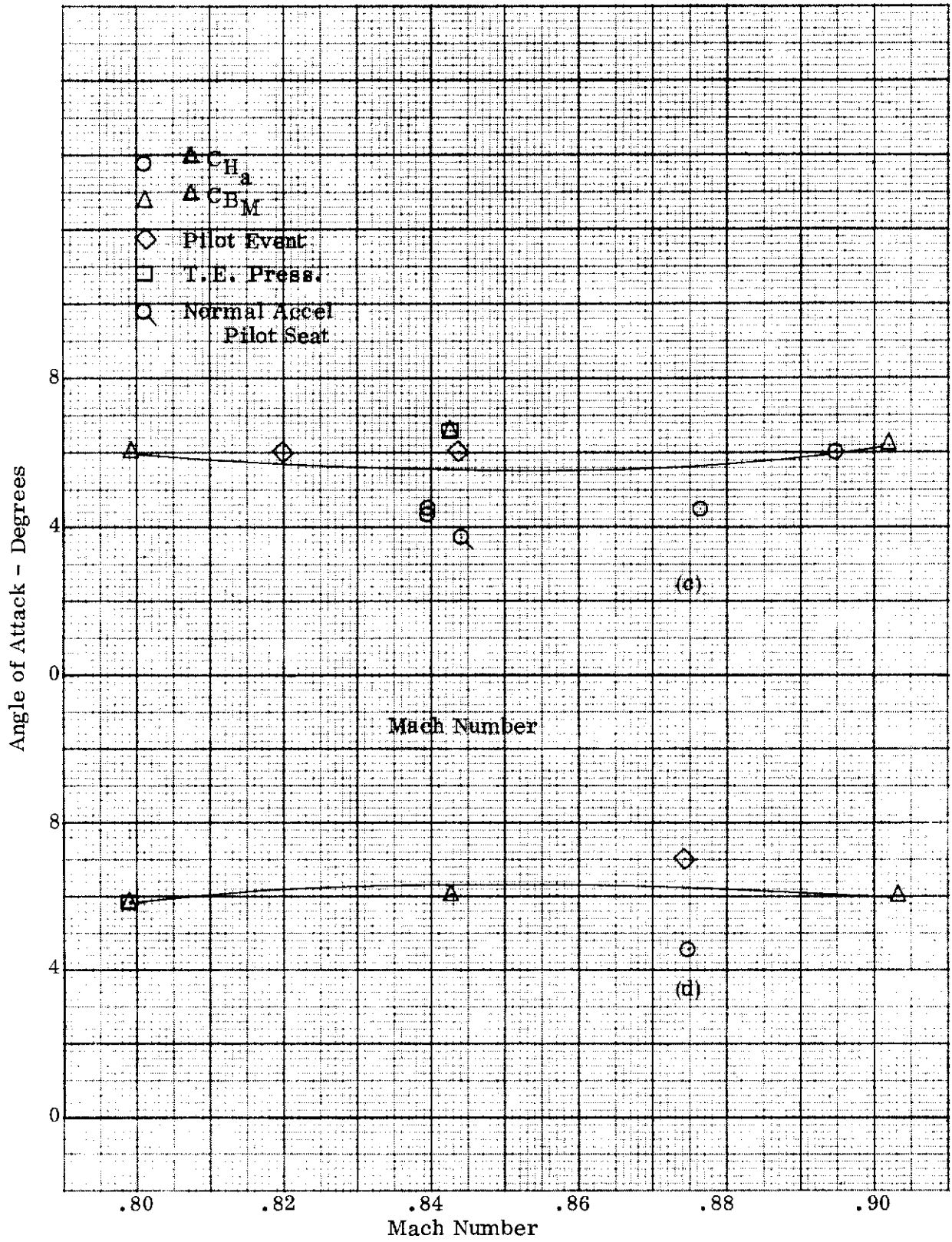

Figure 81 --- Continued
(c) Leading Edge Flap 8°, Trailing Edge Flap 7.5°
(d) Leading Edge Flap 8°, Trailing Edge Flap 15°

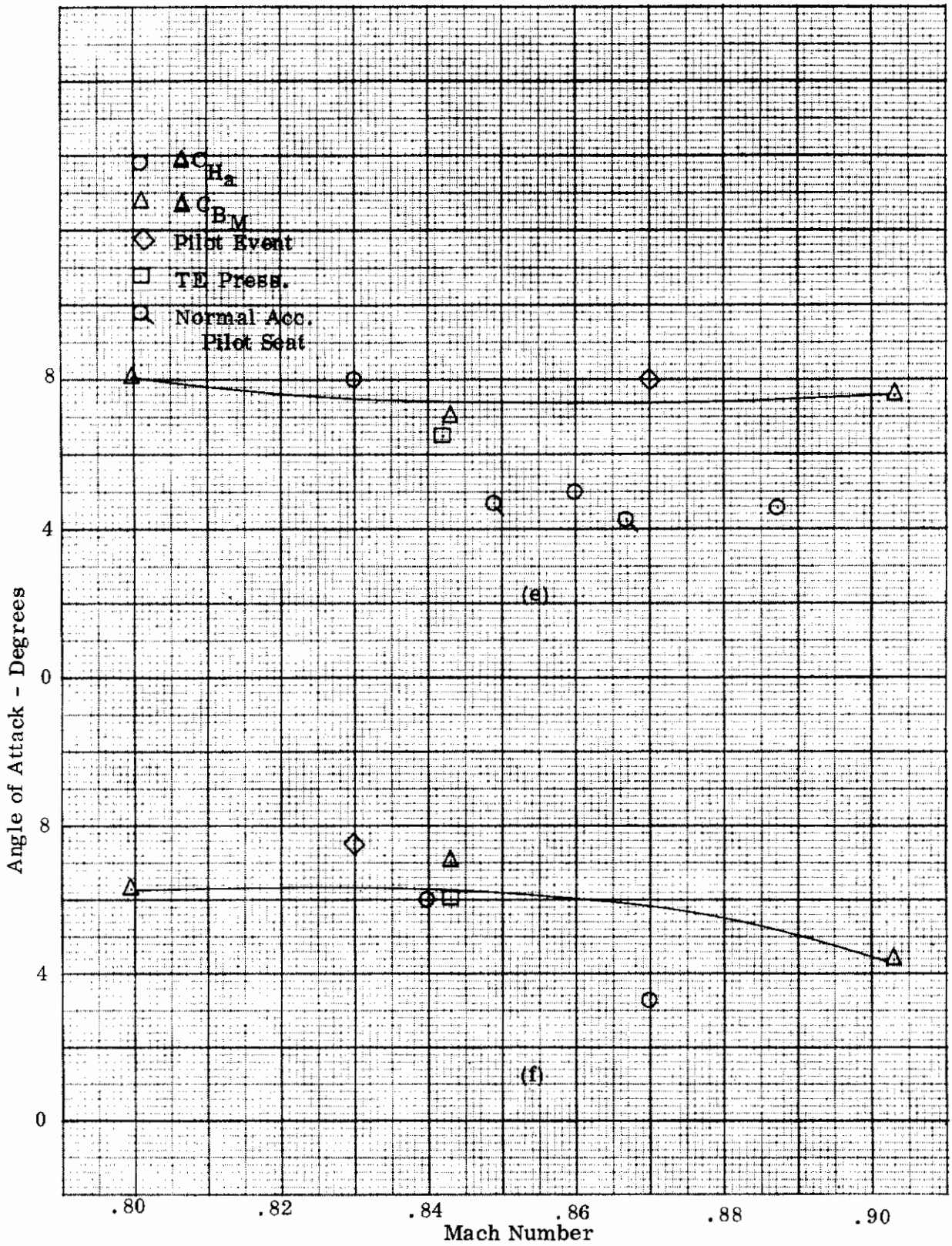

Figure 81 --- Continued
(e) Leading Edge Flap 20°, Trailing Edge Flap Undeflected
(f) Leading Edge Flap 20°, Trailing Edge Flap 7.5°

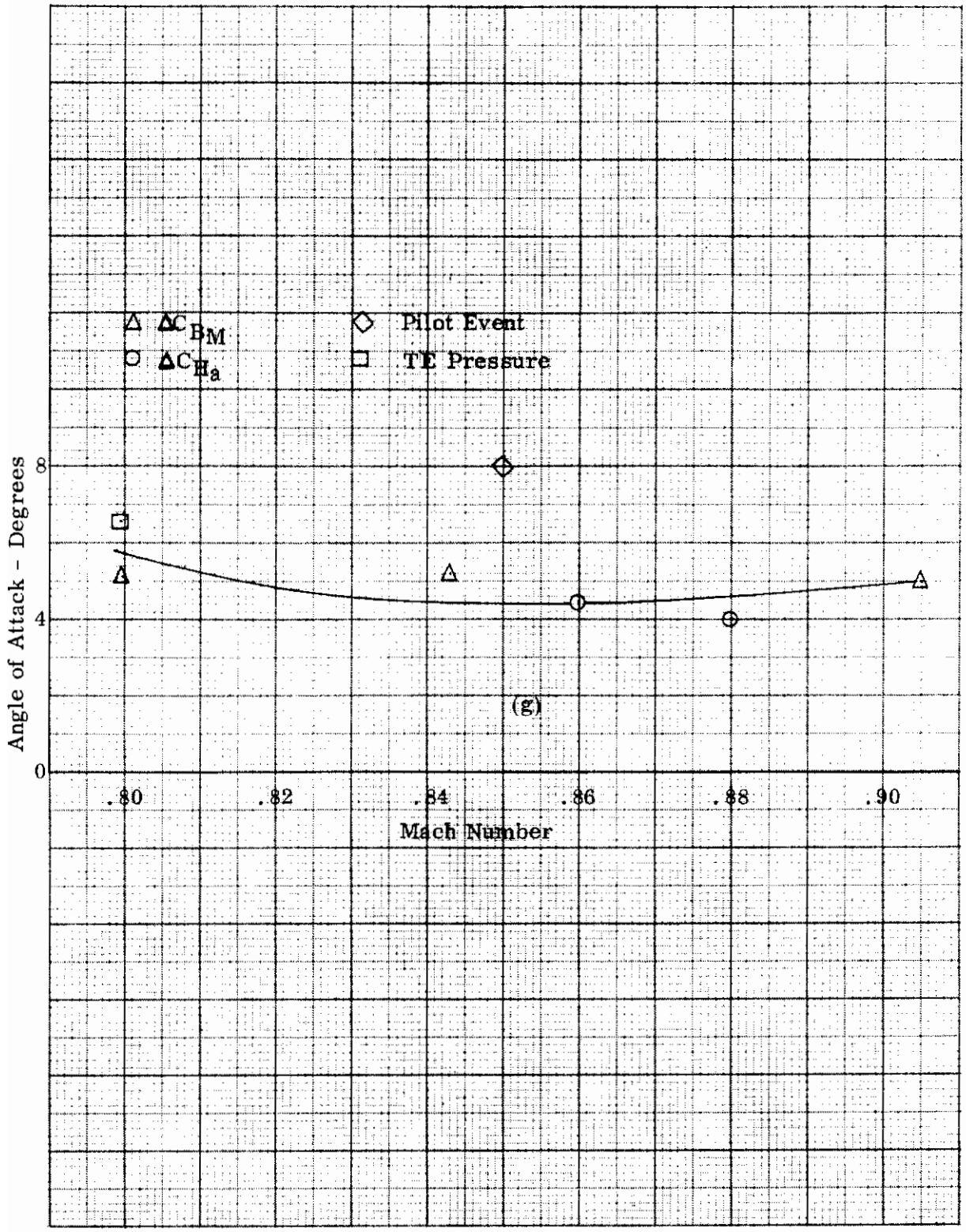

Figure 81 --- Concluded
(g) Leading Edge Flap 20°, Trailing Edge Flap 15°

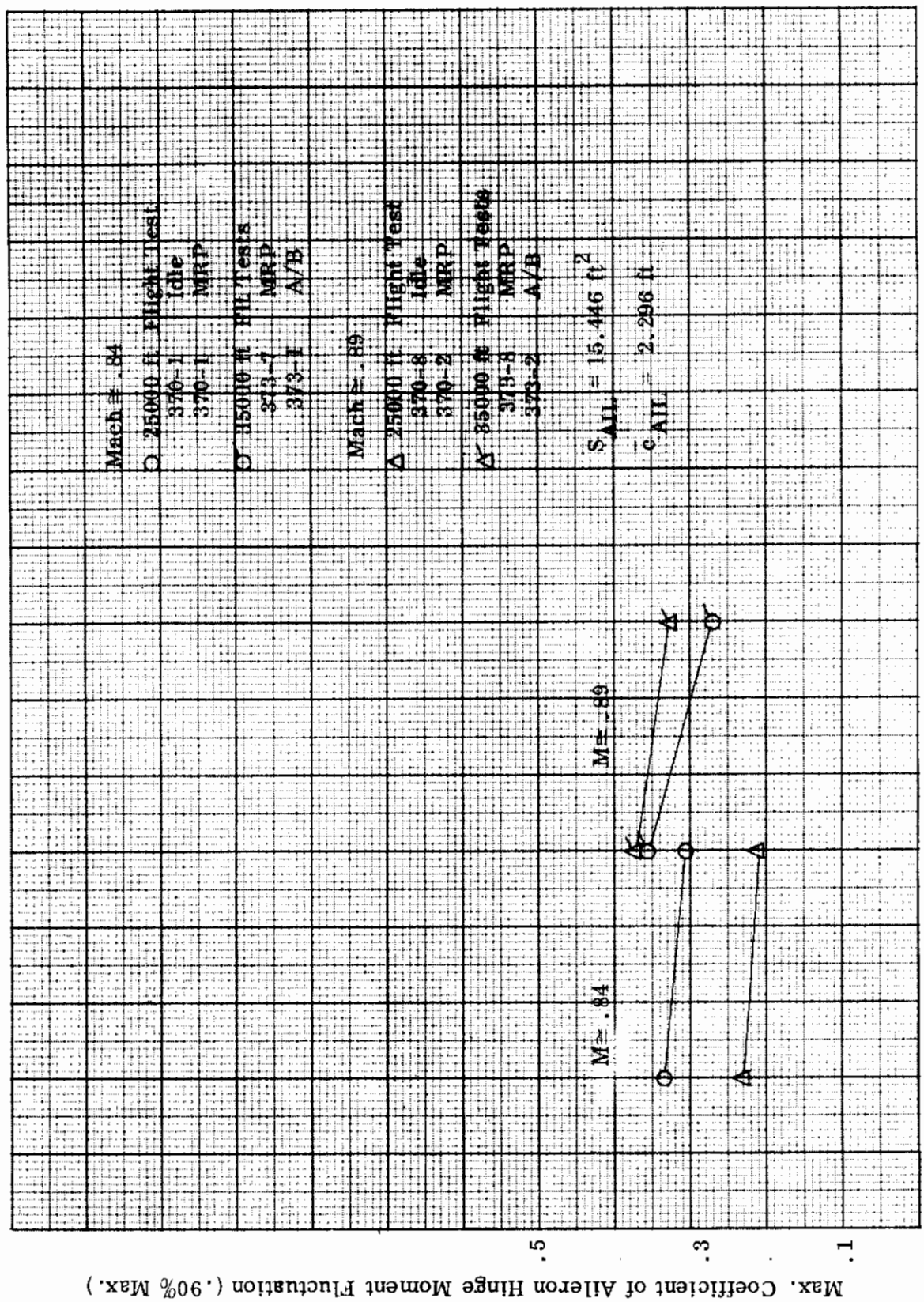

Figure 82. Power Effects on Buffet Intensity of Aileron Hinge Moment Fluctuations Leading Edge Flap 8°, Trailing Edge Flap 7.5°

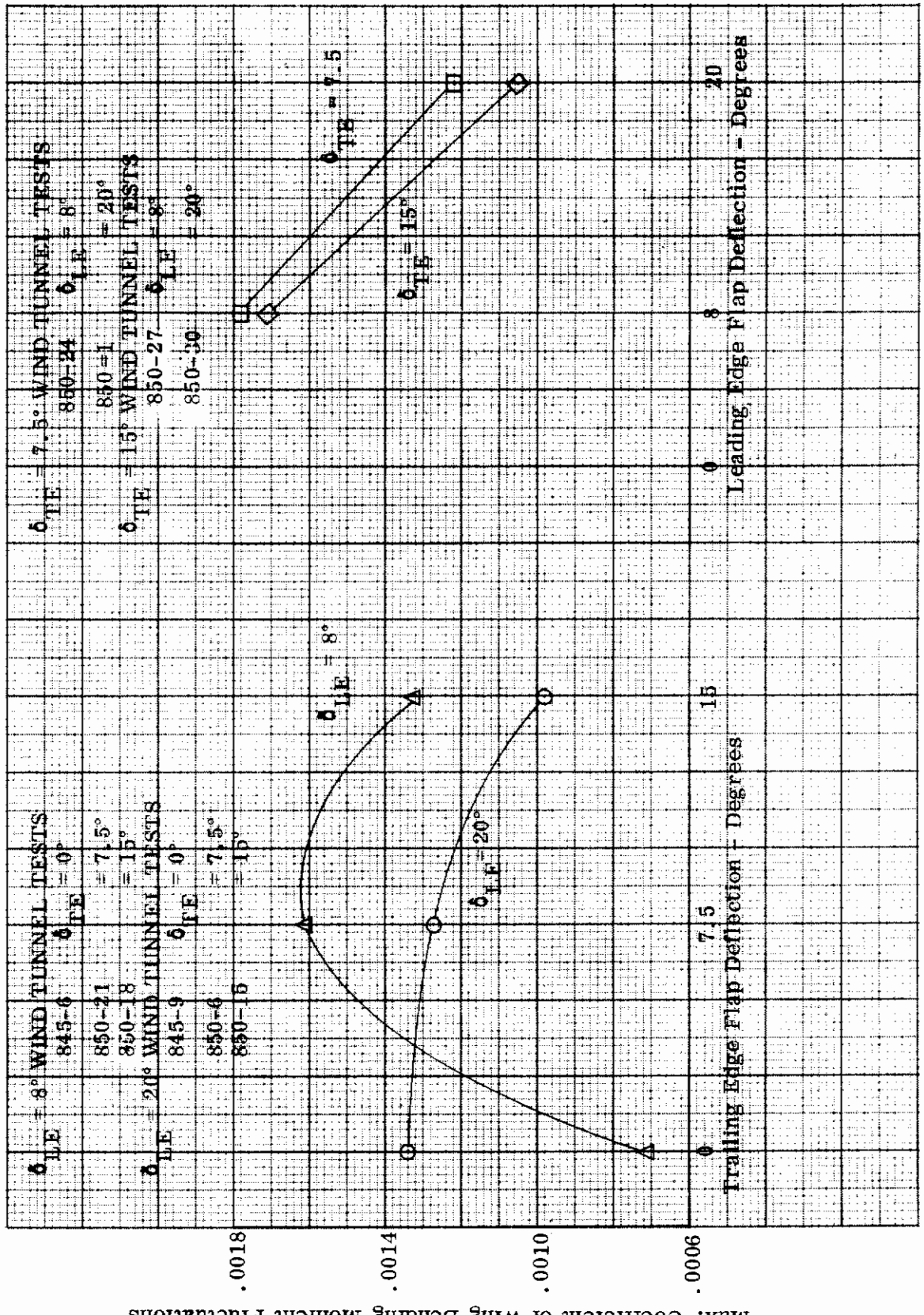

Figure 83. Leading Edge Flap and Trailing Edge Flap Deflection Effects on Buffet Intensity of Wing Bending Moment Fluctuations at M = 0.80

Figure 84. Leading Edge Flap and Trailing Edge Flap Deflection Effects on Buffet Intensity of Aileron Hinge Moment Fluctuations

REFERENCES

1. Breslauer, L., and Tenenbaum, S., Buffet Boundary Characteristics of the F-105B Airplane with 3 Leading Edge Flap Positions, IOC EFTIL No. 4450, Republic Aviation Corporation, 26 December 1958.

2. Old, W., and Tenenbaum, S., A Compilation of F-105B Wing and Vertical Tail Preliminary Chordwise Pressure Distribution Data Acquired during the F-8 Structural Integrity Flight Test Program, IOC EFTIL No. 4458, Republic Aviation Corporation, 6 February 1959.

3. Landau, D., F-105B/D Airplane Aerodynamic Data for Dynamic Motion Studies, Revision A, EAR 406, Republic Aviation Corporation, 24 February 1961.

4. Beeler, DeE., Bellman, D. R., and Saltzman, E. J., Flight Techniques for Determining Airplane Drag at High Mach Numbers, NACA TN 3821, August 1956.

Security Classification

DOCUMENT CONTROL DATA - R & D

(Security classification of title, body of abstract and indexing annotation must be entered when the overall report is classified)

1. ORIGINATING ACTIVITY (Corporate author)	2a. REPORT SECURITY CLASSIFICATION
Fairchild Hiller Corporation Republic Aviation Division Farmingdale, New York 11735	Unclassified 2b. GROUP

3. REPORT TITLE

F-105F TRANSONIC BUFFET STUDY AND EFFECT OF MANEUVERING FLAPS

4. DESCRIPTIVE NOTES (Type of report and inclusive dates)

R&D Final Technical Report (29 March 1968 to 1 April 1969)

5. AUTHOR(S) (First name, middle initial, last name)

Milton Margolin
Jung G. Chung

6. REPORT DATE	7a. TOTAL NO. OF PAGES	7b. NO. OF REFS
7 July 1969	230	4

8a. CONTRACT OR GRANT NO.	9a. ORIGINATOR'S REPORT NUMBER(S)
F33657-68-C-1057 b. PROJECT NO.	FHR 3649-1
c. d.	9b. OTHER REPORT NO(S) (Any other numbers that may be assigned this report) AFFDL-TR-69-37

10. DISTRIBUTION STATEMENT

Distribution of this document is unlimited.

11. SUPPLEMENTARY NOTES	12. SPONSORING MILITARY ACTIVITY
	Air Force Flight Dynamics Laboratory Wright-Patterson AFB, Ohio 45433

13. ABSTRACT

A flight test investigation was made using a Republic F-105F aircraft to obtain data related to high subsonic-transonic buffet and the effects of utilizing a maneuvering flap. Flight tests were made at nominal altitudes of 25,000 feet and 35,000 feet. At each altitude, data was collected at three Mach numbers from level flight to maximum usable lift. A related investigation was made using a 1/22-scale model of the F-105F aircraft in the NASA Langley High-Speed Wind Tunnel. The wind tunnel tests were made at three Mach numbers (0.80, 0.85, and 0.90) and data was obtained from zero angle-of-attack to the strain gage balance limits.

Flight test results compare readily to wind tunnel data. The boundary layer profiles between flight test and wind tunnel are quite similar. The angles of attack at buffet onset are also comparable.

Selection of the leading edge flap and trailing edge flap deflection may be made on the basis of the greatest normal force coefficient at buffet onset, but the final criterion will be the level of buffet intensity apparent to the pilot. This level may be varied with the leading edge flap deflection.

DD FORM 1 NOV 65 1473

Security Classification

Security Classification

14. KEY WORDS	LINK A		LINK B		LINK C	
	ROLE	WT	ROLE	WT	ROLE	WT
Aerodynamic Coefficients						
Aerodynamic Drag						
Angle of Attack						
Bending Moments						
Boundary Layer Flow						
Boundary Layer Separation						
Buffet						
Drag						
Dynamic Characteristics						
F-105F Aircraft						
Flaps						
Flight Tests						
Flow Characteristics						
Mach Buffet						
Maneuvering Flap						
Pressure Distribution						
Transonic Buffet						
Tufts						
Wind Tunnel Model						

Security Classification